Government of the People's Republic of Bangladesh
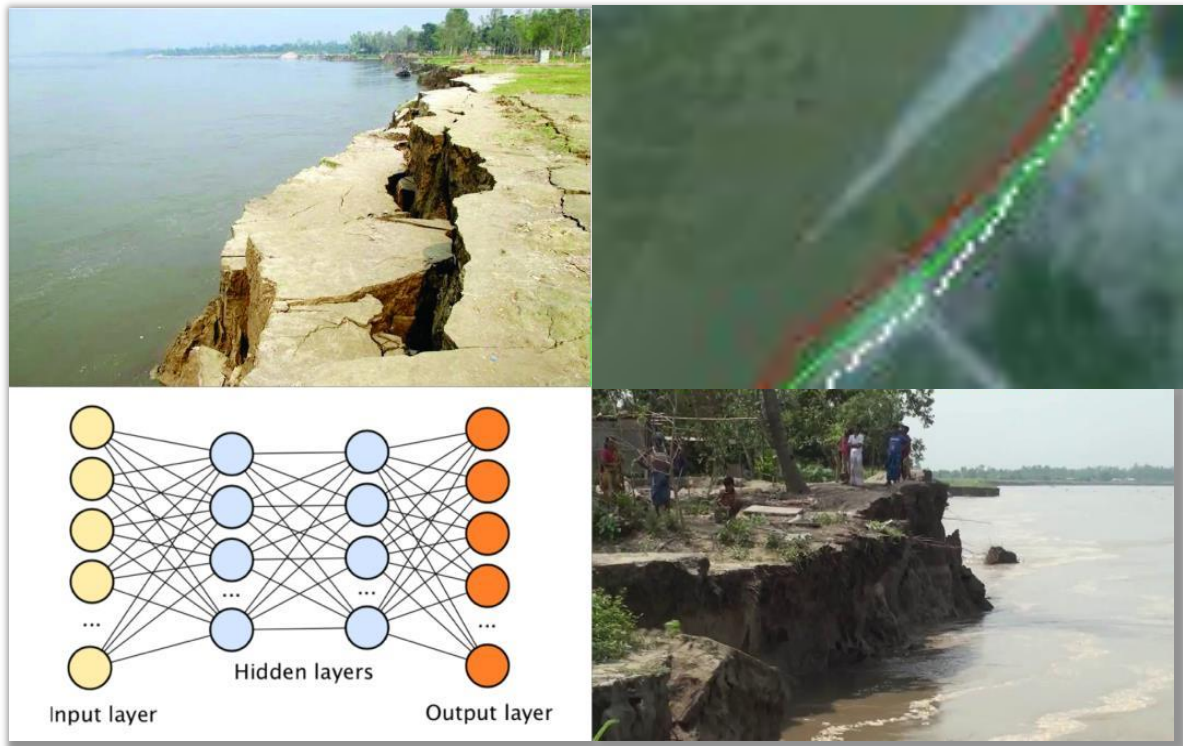## Ministry of Water Resources
Water Resources Planning Organization (WARPO)

Research on River Bank Erosion Dynamics using Numerical Modeling and Deep Learning Techniques

Final Report
June, 2021

**Water Resources
Planning Organization**

**Dept. of Water Resources
Engineering, BUET**

Government of the People's Republic of Bangladesh

Ministry of Water Resources

Water Resources Planning Organization (WARPO)

Research on River Bank Erosion Dynamics using Numerical Modeling and Deep Learning Techniques

Authors:

Dr. Md. Mostafa Ali, Professor, DWRE, BUET

Dr. Hasan Zobeyer, Professor, DWRE, BUET

Final Report

June, 2021

**Water Resources
Planning Organization**

**Dept. of Water Resources
Engineering, BUET**

Memo No. WRE-129/BRTC/WARPO/2021 (03)   Date: 03.06.2021

To
Mr. Md. Delwar Hossain
Director General
Water Resources Planning Organization
Ministry of Water Resources
WARPO Bhaban 72 Green Road, Dhaka-1215

Subject: Submission of the Final Report

Reference No: WARPO/42.02.0000.004.14.002.19.5 Dated: 24-01-2019

Project: Research on River Bank Erosion Dynamics using Numerical Modeling and Deep Learning Techniques.

Dear Mr. Hossain,

We have the pleasure to submit herewith 15 (Fifteen) copies of the Final Report for the above-mentioned project for your kind perusal. We are pleased with the opportunity to work with WARPO.

Thanking you for the cooperation.

Yours sincerely,

Dr. Anika Yunus
Professor and Head
Dept. of Water Resources Engineering
BUET, Dhaka.

Copy to: Director, BRTC, BUET, Dhaka

Table of Contents

Contents   **Page No**

Appendix A-1: Research Proposal to DWRE, BUET.

Appendix A-2: Water level, Discharge and Cross section IDs on the study area.

Appendix A-3: Terms of References (ToR)

Appendix A-4: Submission letter for the River Bank Erosion Prediction Tool

Appendix A-5: Minutes of the Final Workshop

Appendix A-6: Field Visit imagery (Field visit 01).

Appendix A-7: Field Visit imagery (Field visit 02

List of Figures

Contents   Page No

List of Tables

Contents   Page No

Acronyms and Abbreviation

AE	Auto Encoder	LANDSAT	Land Remote-Sensing Satellite (System)
AI	Artificial Intelligence	Landsat MSS	Landsat Multispectral Scanner
ANN	Artificial Neural Network	LSTM	Long Short-Term Memory
ASCE	American Society Of Civil Engineers	ML	Machine Learning
BI	Braiding Index	MLNN	Multi-Layer Neural Network
BPTT	Back Propagation Through Time	MODIS	Moderate Resolution Imaging Spectroradiometer
BUET	Bangladesh University of Engineering and Technology	MSE	Mean Squared Error
BWDB	Bangladesh Water Development Board	NLL	Negative Log Likelihood
CEGIS	Center for Environmental and Geographic Information Services	NN	Neural Network
CNN	Convolutional Neural Network	NWMP	National Water Management Plan
Convo-LSTM	Convolutional Long Short-Term Memory	NWPo	National Water Policy
DL	Deep Learning	NWRD	National Water Resources Database
DNN	Deep Neural Network	ReLU	Rectified Linear Unit
EGIS	Environmental and Geographic Information System	RNN	Recurrent Neural Network
ENH	Northeastern Hemisphere	RNN	Recurrent Neural Network
FAP	Flood Action Plan	SAD	Sisteme de Alerta de Deforesation
FC-LSTM	Fully Connected Long Short-Term Memory	SGD	Stochastic Gradient Descent
FCN	Fully Connected Network	SPOT5	Satellite Pour l'Observation de la Terre 5
FRERMIP	Flood and Riverbank Erosion Risk Management Investment Program	SRH	Sedimentation and River Hydraulics
GCM	Global Climate Model	TM	Thematic Mapper
GIS	Geographic Information System	TOR	Terms of References
GPU	Graphics Processing Unit	USBR	United States Bureau of Reclamation
GUI	Graphical User Interface	WARPO	Water Resources Planning Organization
HEC-RAS	Hydrologic Engineering Centers River Analysis System	WRE	Water Resources Engineering

Executive Summary

The complex geological formation and hydrodynamics of the rivers of Bangladesh have exposed the communities along the riverbanks to one of the most devastating natural disasters known as bank erosion. The difficulties in predicting river erosion have hindered the effectiveness of various protection measures undertaken to save thousands of people who are displaced every year. Due to the misery caused by riverbank erosion in Bangladesh and the need for a riverbank erosion prediction tool, Water Resources Planning Organization (WARPO) recognized the importance of carrying a comprehensive research to understand the river bank erosion processes and develop a river bank erosion prediction tool. Therefore, an agreement has been signed between WARPO, Ministry of Water Resources, Government of Bangladesh (GoB) and Bureau of Research, Testing and Consultation (BRTC) represented by Dept. of Water Resources Engineering of Bangladesh University of Engineering and Technology (BUET) to conduct a collaborative research on river bank erosion with full GoB financial support. The objective of the study is to understand the hydro-morphological characteristics of a selected reach of the Jamuna river and to develop a bank erosion prediction tool based on numerical modeling and deep learning technique.

Recently published literatures show that Deep Learning (Neural Network) is a promising methodology to tackle many challenges. Access to big data sources in the recent years and huge leap in parallel computation have allowed deep learning to achieve breakthrough results in a vast number of research domains. It has been shown time and time that neural network-based techniques are able to excel in non-linear problem domains where some sort of probabilistic modeling is required. The problem of riverbank erosion prediction is a very non-linear one and a novel technique to try out is deep learning.

The Jamuna, being one of the largest braided rivers of the world, is continuously increasing its width due to erosion of the banks. The study area of this research encompasses a selective reach of approximately 80 km, from downstream of the Bangabandhu Multipurpose Bridge to 15 km downstream of the confluence of the Jamuna and the Ganges. The historical planforms of the Jamuna river during the last 180 years define a sinuous, active migration corridor within the wider floodplain. Recent trend of the bank erosion of this river shows that the banks continued to erode on both east and west side resulting in widening of the river and causing displacement of inhabitants on both banks.

The approach of this research comprises of data collection and analysis, satellite image processing, application of numerical modeling and deep learning. Landsat images of the study area for last thirty-two years, historical water level and discharge at eighteen stations for forty four years, cross sections data at sixty one locations and bathymetric data of the study area for last four years have been collected from WARPO and BWDB. The full batch of Surface Reflectance Landsat images were downloaded using Google's Earth Engine platform to ensure convenience and authenticity. Moreover, pre and post-monsoon bathymetric surveys were carried out at a selected part of the study reach. The quality of the analysis was ensured by effective and thorough data quality checking schemes.

This study comprises of three different analysis and modeling efforts such as a) Hydrological and Morphological Analysis, b) Numerical Modeling and c) Deep Learning. At first, analyses of historical hydrological data, morphological data and satellite images have been done. The hydrological data analyses consist of estimation of maximum, mean and median of historical water level and discharge data. Historical trend of bank erosion of the study area has been delineated from Landsat images to comprehend bankline shifting. Historical bathymetric data has been compared to understand the morphological changes and movement of bar/dunes in the study area. An attempt has been made to correlate historical discharge data, morphological data and bank line shifting from satellite images. These analyses give an insight of the physical processes related to bank erosion for any braided river, in particular the Jamuna river.

From historical hydrologic data analysis, mean annual discharge was found to be around 17000 m^3/s. Maximum and minimum flood discharge was recorded as 102535 m^3/s and 3095 m^3/s respectively. From annual hydrograph at Bahadurabad station it was found that water level varies around 6 m from dry to monsoon season.

Erosion and deposition were calculated for both banks of Jamuna river using 32 years of satellite images to understand the erosion pattern during this period. From 1988 to 2019, total erosion along the Jamuna river left bank was 23800 ha with an average of 770 ha per year. Whereas for the right bank of the river total erosion was 11840 ha and 380 ha per year. It was evident from the data that erosion rate was higher for left bank of the Jamuna river. From the planform analysis it was found that width of the Jamuna river has an increasing trend and it is widening at the left bank side. Since the early 1980s, the Jamuna River in this study area widened from 14.2 km to 15 km in the 2020 and now the average width is 14.69 km.

From hydrological and erosion data a correlation between peak discharge and total erosion was found, with higher discharge erosion will be higher. It was observed that for peak discharge in the year 1996 and 1998, erosion was maximum and erosion was less in case of lower discharge.

Morphological change was observed for four years with available data collected from FRERMIP. The change was also monitored with fine resolution data, specially collected under this project for a specific site. Yearly change in river bathymetry was monitored through both spatial assessment and assessment along thalweg. spatial change was observed through GIS mapping and significant erosion and deposition was observed along the active channels. The analysis with thalweg line also indicates the same. Longitudinal profiles show a high spike of deposition, always followed by a steep crest erosion and a medium crest deposition is followed by medium to low crest erosion. Maximum erosion(-15.07m) occurred along the center profile in 2017-2018 and Minimum erosion (-8.06 m) occurred along the right profile in the year 2016-2017. Maximum deposition was observed as 20.81 m along the left profile in the year 2018-2019.

Combination of morphological change analysis and planform change analysis provided a very thought-provoking finding. When a sand bar is formed in the middle of a channel it diverts the flow towards the riverbank. when these diverted flows hit the riverbank, it exerts impact pressure almost perpendicularly and with higher impact the erosion will be higher. The

magnitude of the impact may vary with the flow angle. This analysis was made at six erosion prone area identified from planform analysis. It was found that due to formation of bar when flows were directly diverted towards the bank significant amount of erosion occurred.

In numerical modeling, bank erosion processes for the study area have been studied using a 2D hydro-morphological model. The main objective was to develop a 2D morphological model for the study area and to predict the morphological changes for a year and compared with the observed data. To do so, first a 1D hydraulic model has been developed for a 150 km reach starting from Bahadurabad to the confluence of Ganges and Jamuna. This 1D model provides the necessary boundary conditions for the 2D model. 2D hydrodynamic model was also calibrated and validated using HecRas model results. 2D hydrodynamic model was developed to understand the flow characteristics of the model domain. Flow velocity, flow direction, and water depth was examined to get a better understanding of the situation. Using well calibrated 2D hydrodynamic model, 2D morphologic model was developed. Morphological model was developed to reproduce the morphological scenario of Jamuna river.

Morphological modeling of such active river like Jamuna was very challenging. Moreover, there was limitation on fine resolution data, computational power etc. The best available bathymetry data have a resolution of 500 m but in Jamuna river within 500 m the river bed may change several times. Again, there is constraints on model capacity, for morphological modeling SRH 2D can handle about thirty thousand to forty thousand. To accommodate this model cell size was coarse. Including all these uncertainties it was very difficult to replicate the real scenario.

Model may predict erosion or deposition correctly but the extent of erosion and deposition was not obtained. This may be due to very coarse resolution data and mesh grid size. Although the model cannot predict the bed form change accurately for this grid size it could give some indication of bank erosion. To assess the probability of bank erosion bed shear stress along the bank was observed. It was found from the simulation that at the places where erosion took place in the year 2019, shear stress is higher and where the bank remained almost at the same position shear stress is relatively lower. In erosion prone areas, erosion took place in 2019 and from model result it can be found that shear stress is relatively higher in those areas. Similarly, in areas, where there was little to no erosion and bed shear stress along the bank are relatively lower.

In the final part of this study, deep learning modeling technique has been applied to predict future banks using historical satellite images. Total thirty-two years of satellite images from 1988 to 2020 have been used in this modeling. Model architecture of neural network consists of six convolution layers, one LSTM layer and two fully connected layers. This trained and validated model has been used to predict river banks for the year of 2018, 2019 and 2020 and the predicted river banks have been compared with the actual river banks respectively.

The banklines predicted by the Deep Learning Technique for different years have been compared with corresponding actual bankline. A number of erosion prone regions have been selected to closely compare the model results. The regions of erosion have been selected based

on visual inspection with a general principle of having erosion of more than 100-150 m as the average error in prediction is around 3 to 4 pixels equivalent to 90 to 120 meters. In 2019-2020, the model can predict 4 erosion areas more or less accurately in the left bank. However, in the right bank the model predicts erosion in 3 locations but cannot predict only at one location. In 2018-2019, the model can predict erosion in all five locations in the left bank and failed to predict the erosion at one location in the right bank. In 2017-2018 the model predicts erosion in 4 locations along left bank but failed to predict in two locations and in the right bank, the model predicts erosion in 3 locations and could not predict at one location. It is to be noted that the bankline prediction by CEGIS model marked in 2018-2019 has also been compared.

A summary of the model performance in predicting number of erosion prone areas is provided. Out of 24 erosion locations during 2017 to 2020, the model could predict erosion in 79% of the locations. Although the model generally underpredicted the magnitude of the erosion, the prediction of location in the erosion prone area is very satisfactory.

After developing the model using deep learning technique, a predictive tool has been developed using python script and PyQt5 library. The software will enable users to easily apply the full deep learning pipeline explained in this research by accessing the underlying Application Programming Interface (API) through an intuitive Graphical User Interface (GUI). This will help people easily get reliable prediction results of future bank erosion events by following some easy to use steps. The software has four different pages for using different features of the deep learning modeling approach. A training workshop has been conducted on the use of the prediction tool to develop the capacity of WARPO in predicting bank erosion and suggesting effective bank protection measures. Furthermore, the prediction tool has been handed over to WARPO after the training session. A national workshop has been arranged on May 19, 2021 to disseminate the outcomes of this research. All the participants, including the chief guest, appreciated the research outcomes and requested to develop prediction tool for other rivers, especially for the part of lower Meghna estuary.

Defining bank lines was found to be a hard problem given the versatile nature of river planform. But identifying prominent features like bars, vegetation, waterbody is an easier task and consensus can be reached. Future work can look into predicting all of these prominent features as a semantic segmentation mask. This is a promising avenue as a lot of recent deep learning works deal with semantic segmentation problems. Prediction tool can be also be developed for other rivers.

In addition to the research carried out by the research team, two workshops (Inception and final), two field visits, three training workshops (on SRH2D, on QGIS and on Prediction Tool) have been conducted as a part of capacity building of WARPO. Four research team members from WARPO were also engaged throughout the project period. Their inputs in this research are highly appreciated. BWDB supported the project by providing various bathymetric data which are also acknowledged. Last but not the least, we appreciate WARPO and Ministry of Water Resources, Government of Bangladesh, for funding this research.

Chapter 1: Introduction

1.1 Background

Riverbank erosion (Figure 1-1 and Figure 1-2) is a major problem in Bangladesh. It is one of the devastating recurrent natural hazards that costs loss of large areas of floodplain and displacement of huge population. The rivers of Bangladesh lie in an active delta which is a part of the Ganges, Brahmaputra, and Meghna basins. These rivers are meandering and braided and become very active during flood season. These rivers bring huge amounts of sediments during high monsoon flow. High flow in the monsoon causes flood as well as bank erosion. The flat delta lands of Bangladesh offer little resistance to the hydraulic forces of the rivers, particularly during the periods of high flow. It is estimated that about 5% of the total floodplain of Bangladesh is directly affected by river erosion (Rahman, 2010). It has been estimated that tens of thousands of people are displaced annually by river erosion in Bangladesh, possibly up to 100,000 (Rahman, 2010; Faruque, 2007).

Bangladesh Government pays attention to prevent bank erosion and ensuring the safety of the people. National Water Policy, 1999 (NWPo, 1999) in its directives *4.2q* gives instruction to undertake survey and investigation of the problem of riverbank erosion, and develop and implement master plans for river training and erosion control works for preservation of scarce land and prevention of landlessness and pauperization. In compliance with the NWPo (1999), National Water Management Plan (NWMP, 1999) presents some programs to take preventive work at selected locations of the major rivers.

Figure 1.1 Bank Erosion in Jamuna River

Water Resources Planning Organization (WARPO) is mandated to give clearance to water resources projects according to Bangladesh Water Act, 2013. However, WARPO have already been providing clearance to projects taken by BWDB on pilot basis since 2007. FRERMIP

(2014-2018) is one the most important projects undertaken by BWDB for the improvement of bank erosion scenario. This is the part of master plan of stabilizing the river Jamuna and the Padma. As per the draft plan, the width of the Jamuna River could be reduced to 7.5 kilometers by 2030 from 11.6 kilometers estimated in 2015, which will help reclaim 87,000 hectares of land (Dhaka tribune, December, 2016) The intensity of bank erosion varies widely from river to river as it depends on several factors like river flow, water level, flow velocity, sediment transportation, bank material, river planform etc.

Figure 1.2 Erosion and Accretion along three major rivers.(Source: CEGIS)

Center for Environmental and Geographic Information Services (CEGIS) has been making yearly prediction of bank erosions and morphological changes of the Ganges and Brahmaputra rivers using time-series satellite images, GIS and RS techniques. However, their prediction is mostly based on empirical equations and analysis of good quality long time series images (CEGIS, 2017). Numerical modeling has been using to predict the time-evolution of the braided pattern in time (Jagers, 2003) and temporal developments of selected bars/islands of the Jamuna River (Shapma, 2018). Recent trends on various literatures shows that Deep Learning (Neural Network) is a promising methodology to tackle many challenging tasks such as object recognition, machine translation, sequence to sequence prediction, weather

forecasting. Hasan (2018) demonstrated that missing portion of LANDSAT images could be reproduced with significant amount of accuracy by two previous years' data. There is immense scope for research by posing river bank erosion as a spatiotemporal sequence prediction problem and use deep learning techniques to predict future scenarios from historical satellite images along with other relevant types of data.

Considering the misery caused by river bank erosion in Bangladesh and the need for a river bank erosion prediction tool WARPO realized the importance of carrying a comprehensive research to develop a river bank erosion prediction tool. As such WARPO requested Dept. of Water Resources Engineering (DWRE) of Bangladesh University of Engineering and Technology (BUET) to conduct a study to understand river bank erosion process and develop a prediction tool (Appendix A-1). DWRE realized the importance of this study and gladly agreed to conduct a study on river bank erosion. Therefore, a collaborative research project has been initiated with the active participation of dept. of DWRE and WARPO with the full financial support from Government of Bangladesh (GoB). An agreement has been signed between WARPO, Ministry of Water Resources, Government of Bangladesh and Bureau of Research, Testing and Consultation (BRTC) represented by the DWRE, BUET to conduct the study.

In this research, a comprehensive study will be carried out to understand river bank erosion processes of rivers of Bangladesh using numerical modeling and deep learning techniques of satellite images. As a pilot basis, the research would concentrate on a selected reach of the Jamuna river. The study area consists of an 80 km reach of the Jamuna river. The upstream boundary is located just downstream of the Bangabandhu bridge and ended approximately 15 km downstream of the confluence of the Jamuna and the Ganges. It is clear that riverbank erosion causes tremendous miseries every year to thousands of people living along the banks of the selected reach. Based the outcome of this study, a bank erosion prediction tool for the study area will be developed. This tool will be an asset for WARPO in predicting future river bank erosion for the selected river.

1.2 Research Objective

The goal of the aforesaid research is to understand river hydrodynamics and morphological processes including river bank erosion and finally to develop a riverbank erosion prediction tool for the selected study area.

The following specific objectives have been set to achieve the goal of this research:

- To collect all necessary secondary data including satellite images, historical hydrological data and bathymetric data from different sources
- To conduct hydrographic survey in a selective region of the study area to obtain high resolution bathymetry data.
- To analyze the historical trend of river bank erosion in the study area using satellite images

- To apply deep learning techniques to predict bank erosion rate for the study area.
- To analyze measured bathymetric data of different years to understand the morphological characteristics of the study area
- To develop a 2D hydrodynamic model to understand the flow hydraulics in the study area
- To develop a 2D morphological model to understand the general morphodynamics and bank erosion processes for the study area.
- To develop a tool to predict riverbank erosion for the selective study area combining deep learning and numerical model results.
- To arrange workshops to disseminate research progress and findings.
- To provide technical support to WARPO professionals on river bank erosion process, modeling and prediction.

1.3 Research Team Composition

As mentioned before this is a collaborative research project with the participation of department of WRE and WARPO. WRE team consists of one Principal Investigator, one Co-Principal Investigator and two Research Assistants. WARPO team consists of four members. Team composition is shown in Table 1-1

Table 1-1 Research Team Composition

Team	Designation	Name
BUET TEAM	Principal Investigator	Prof. Dr. Md. Mostafa Ali
	Co-Principal Investigator	Prof. Dr. Hasan Zobeyer
	Research Assistant	A.S.M Julker Naem
	Research Assistant	Kazi Antor Hasan
WARPO TEAM	Senior Scientific Officer (Navigation)	Kazi Saidur Rahman
	Scientific Officer (Water)	Alamin Kabir
	Scientific Officer (Ground Water)	Jamal Haidar
	Scientific Officer (Soil)	Shuvro Bhoumic

1.4 Organization of the Report

Chapter 1 includes background of the research, objectives and organization of the report. This chapter describes why this research is necessary. The research team composition is also described in this chapter.

Chapter 2 includes literature review which describes the process of braiding and different bank erosion mechanisms. Important factors of bank erosion along with previous works on the research problem are presented here. A brief introduction to the machine learning techniques and previous studies on sequence to sequence modeling are also discussed.

Chapter 3 comprises of the extent of the study area and its hydrological and morphological characteristics followed by methodology of the research and data required along with source in Chapter 4.

Chapter 5 comprises of the 1D and 2D numerical modeling and result analysis. Chapter six includes deep learning modeling approach and result. The Chapter 7 provides a description on the use of the prediction tool developed in this study. Chapter 8 describes the activities related to capacity building of WARPO officials.

Chapter 9 provides concluding remarks on the finding of this study followed by references and Appendices.

Chapter 2: River Bank Erosion: Theory and Literature

2.1 Introduction

The Jamuna is one of the world's largest braided rivers. Braided rivers consist of a network of wide and shallow channels flowing around braid bars or islands. These bars reposition themselves along with the channel bed. Bank erosion phenomena is part of bathymetry change, as the process of bank erosion begins with toe scour. The largest rivers may have bank line shifts of hundreds of meters per year (Baki and Gan, 2012).

Braided rivers in general have been extensively researched in the past concerning various subjects (Bristow and Best, 1993). Research into braided river morphodynamics has been largely focused on scale experiments of gravel-bed rivers. General behavior and planform changes of sand bed braided rivers were studied (Coleman, 1969; Bristow, 1987; Thorne et al., 1993; Sarker et al., 2014) as well as development (Ashworth et al., 2000) and flow patterns around braid-bars (McLellan, et al., 1990) and bankline shifts (Takagi et al., 2007; Baki and Gan, 2012).

2.2 Overview of River Morphology

Erosion and deposition in a braided river cause the river to extend its extent over a large time period. Several factors influence these processes. Eroded material moves downstream and eventually deposited causing the changes in the planform of the river bed. Thus, these processes are to be known to understand the river morphology.

2.2.1 Riverbank erosion and deposition process

Erosion:

Vanoni, 1975 distinguished between geological (or natural) erosion and accelerated (or human-induced) erosion, viewing the latter as a mainly local phenomenon. Valdiya (1998) had shown that geological erosion through mountain ranges, such as the Himalayas, continues to produce immense volumes of sediment. It is often difficult to determine whether an observed erosional process is natural or whether it results wholly or partly from human influences. For example, gullying and landslides that appear natural may have been triggered or aggravated by overgrazing, significant land use modifications such as urbanization, infiltration of irrigation water, or deforestation. However, some sources accelerate the erosion rate. Among which- agricultural activities, forest activities, urbanization, dams and river regulation, warfare and population migrations are significant (Garcia, 2007)

Deposition:

Geologic deposition occurs because of natural processes of tectonic uplift, volcanic eruptions, earthquakes, climate warming, glacial movements, and so on. On the other hand, human-induced deposition resulting from various human activities usually results in relatively rapid

changes in river morphology and sedimentation. Products of erosion may be transported and deposited over a wide range of distances from their source. Where there are long distances to the ultimate sink of the oceans, only a minor fraction of the source load may arrive there. Causes of sediment deposition can be characterized as upland river deposits, intermediate and lowland river deposits, sedimentation due to mining activities, deposits in lakes and reservoirs (Garcia, 2007).

2.2.2 Sediment Transport

There are two common ways of classifying the sediment load. The first divides the sediment load according to the mechanism for transport into bed load and suspended load. The second classifies the load based on particle size into wash load and bed sediment load. The suspended load, as the term denotes, moves in suspension and is that part of the load which is not bed load. Wash load is fine sediment moving in suspension which makes up a very small part, usually a few percent, of the sediment on the bed. Wash load is commonly taken as the silt and clay fraction of the bed sediment, i.e., that fraction with grain sizes finer than 0.062 mm. The bed sediment load consists of particles that are coarser than the wash load.

Bagnold (1956) defined the bed load transport as which is in contact of bed and has negligible gravity effect, whereas the suspended load transport is defined as in which the excess weight of the particles is supported by random successions of upward impulses imported by turbulent eddies. But Einstein (1965) defined bed load transport as the transport of sediment particles in a thin layer about two particle diameters thick just above the bed by sliding, rolling, and making jumps with a longitudinal distance of a few particle diameters. The bed load layer is considered to be a layer in which mixing due to turbulence is so small that it cannot directly influence the sediment particles, and therefore suspension of particles is impossible in the bed load layer. Further, Einstein (1965) assumed that the average distance traveled by any bed load particle (as a series of successive movements) is a constant distance of about 100 particle diameters, independent of the flow condition, transport rate, and bed composition. In Einstein's (1965) view, saltating particles belong to the suspension mode of transport, because the jump heights and lengths of saltating particles are greater than a few grain diameters. On the other hand, Bagnold (1956, 1973) regards saltation as the main mechanism responsible for bed load transport.

Bed Load Transport

Bed load particles roll, slide, or saltate along the bed thus essentially tangential to the bed. In general, q_b is a function of boundary shear stress τ_b and other sediment parameters; that is,

$$q_b = u_b C_b \delta_b \qquad\qquad (2\text{-}1)$$

in which q_b is the volumetric bed load transport rate (m²/s), C_b is the volumetric sediment concentration (i.e. volume of sediment/ volume of water-sediment mixture), u_b is particle velocity (m/s), and δ_b is the thickness of the bed load layer (m).

The bed load transport rate can also be defined as the product of the number of moving particles per unit area, the particle volume and the particle velocity (García 2000),

$$q_b = N_b V_b u_b \tag{2-2}$$

in which N_b is the number of particles per unit bed area(m^{-2}), V_b is the particle volume (m^3), and u_b is the particle velocity (m/s).

Erosion-Deposition in a Bed

The interaction between bed sediment and the water column through erosion and deposition has been developed so that the sediment mass conservation can be formulated.

$$\left(1 - \lambda_p\right)\frac{\partial \eta}{\partial t} = -\frac{\partial q_{bs}}{\partial s} - \frac{\partial q_{bn}}{\partial \eta} - V_s(\overline{C_b} - E_s) \tag{2-3}$$

Where λ_p is the porosity of the bed material, $\overline{C_b}$ is a near-bed value of the volumetric sediment concentration, η is bed elevation with respect to the datum, s denotes the streamwise direction and n denotes the lateral direction in a two-dimensional case; then two components, q$_{Ss}$ and q$_{Sn}$ result, V_s is sediment fall velocity.

The basic form of Eq. (2-3), without the suspended sediment component, was first proposed for the case of a one-dimensional flow interacting with a sediment covered bed by Felix Exner (1925).

Bed Load Transport Formulae

A large number of bed load relations can be expressed in general dimensionless form.

Meyer-Peter and Muller (1948):

$$q^* = 8(\tau^* - \tau_c^*)^{3/2} \tag{2-4}$$

where τ_c^* is 0.047. This formula is empirical in nature; it has been verified with data for uniform coarse sand and gravel. Even though it was developed for alpine streams in Switzerland, it enjoys wide use in coastal sediment transport (Soulsby, 1997).

Einstein (1950):

$$q^* = q^*(\tau^*) \tag{2-5}$$

$$1 - \frac{1}{\sqrt{\pi}}\int_{-\left(\frac{0.413}{\tau^*}\right)-2}^{\left(\frac{0.413}{\tau^*}\right)-2} e^{-t^2}dt = \frac{43.5\, q^*}{1 + 43.5\, q^*} \tag{2-6}$$

This relation constitutes the first attempt to derive a bed load function. Note that this relation contains no critical shear stress. It has been used for uniform sand and gravel. Gomez and Church (1989) recommend its use for cases where the local bed load transport rate needs to be calculated. Yang and Wan (1991) found that it could predict sediment transport rates in large rivers but not in small rivers and flumes.

Egluend Hanson (1967):

Engelund-Hansen's (1967) equation is based on the energy balance method. The equation can be written as:

$$q_t = \frac{0.05u^5}{(s-1)^2 g^{0.5} d_{50} c^3}$$

Where,

        s= Bed slope

        u= Average velocity

        d= Mean particle diameter

Yalin (1963):

$$q^* = 0.635 s (\tau^*)^{\frac{1}{2}} \left[1 - \frac{\ln(1 + a_2 s)}{a_2 s} \right]$$

(2-7)

Where,

$$a_2 = 2.4(1 + R)^{.4}(\tau_c^*)^{1/2}$$ (2-8)

$$s = \frac{\tau^* - \tau_c^*}{\tau_c^*}$$

(2-9)

τ_c^* is evaluated from the Shields curve. Two constants in this formula have been evaluated with the aid of data quoted by Einstein (1950), pertaining to 0.8 mm and 28.6 mm material. Wiberg and Smith (1985, 1989) were able to reproduce Yalin's relation, with their saltation-based bed load transport model.

2.2.3 Bed Forms

The major influence of sediment wave is related to changes in bed configuration following changes in water temperature (Southard 1989). Large bed forms, such as megadunes, can make

navigation difficult by increasing shoaling rates and endangering the stability of pipelines and tunnels (Kennedy and Odgaard 1991; Nemeth et al. 2002).

The ripples, dunes, and antidunes are the classic bed forms of erodible-bed, open-channel flow, which are the product of flow and sediment transport, and profoundly influence flow and sediment transport. In fact, all of the bed load equations are strictly invalid in the presence of bed forms. The adjustment necessary to render them valid (i.e., removal of form drag). Figure 2-1 illustrates the schematics of different bedforms.

Dunes

Dunes are well-developed and tend to have wave heights scaling up to about one-sixth of the depth.

$$\frac{\Delta}{H} \leq \frac{1}{6} \tag{2-10}$$

Where, wave height, Δ that scale with the flow depth H. Dunes migrate downstream. They are approximately triangular in shape and usually possess a slip face, beyond which the flow is separated for a certain length. A dune progresses forward as bed load accretes on the slip face. Generally, very little bed load is able to pass beyond the face without depositing on it, whereas most of the suspended load is not directly affected by it. Dunes are characteristic of subcritical flow.

The celerity of dunes is a small fraction of the mean flow velocity. For the case of large sand bed rivers, Fedele (1995) obtained an empirical relation to estimate the velocity of dunes in the Paraná and Paraguay Rivers in South America. Vionnet et al (1998) have also proposed a methodology to compute sediment transport from dune celeritiy and amplitude based on kinematic-wave theory. More recently, Serra and Vionnet (2006) extended the analysis to account for the transport of smaller dunes superimposed on larger ones.
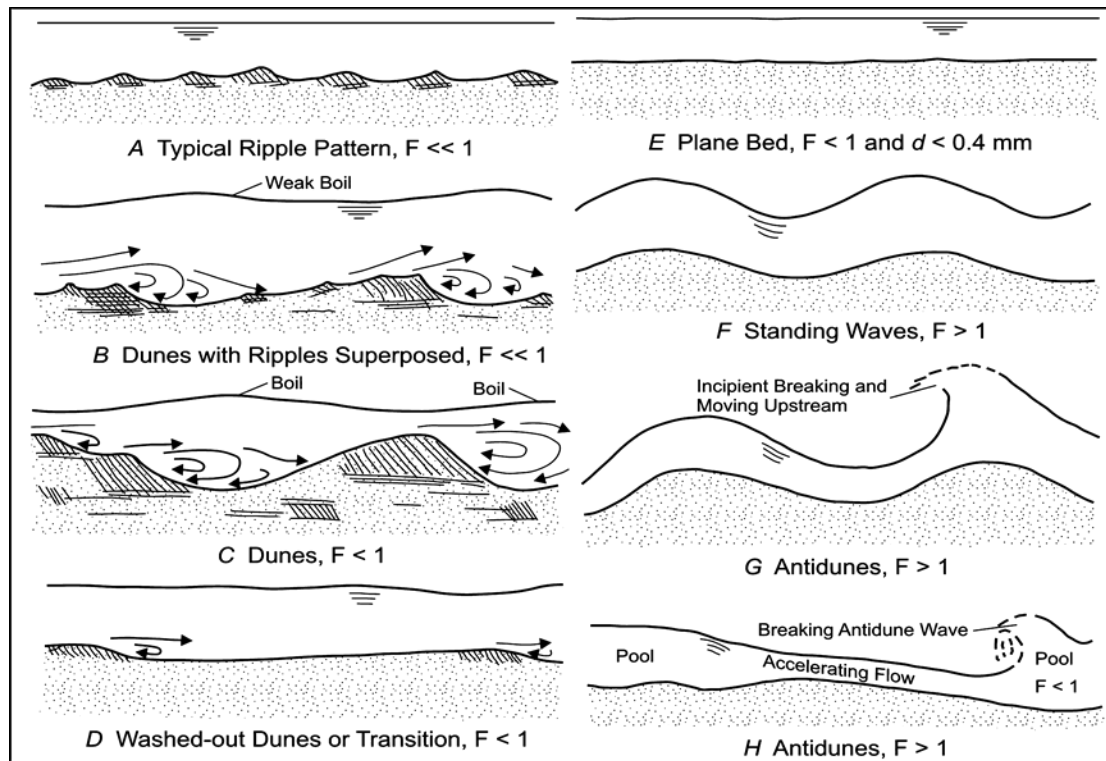
Figure 2.1 Schematic of different bedforms.(F= Froude number; d =sediment size)

(Source: Sedimentation Engineering, ASCE)

Antidunes

Antidunes are distinguished from dunes by the fact that the water surface undulations are nearly in phase with those of the bed. They are associated with supercritical flow. Antidunes may migrate either upstream or downstream. Upstream-migrating antidunes are usually rather symmetrical in shape and lack a slip face. Downstream-migrating antidunes are rather rarer; these have a well-defined slip face and look rather like dunes. The distinguishing feature is the water surface undulations, which are very pronounced in the case of antidunes. The potential-flow criterion dividing upstream-migrating antidunes from downstream-migrating antidunes is (Kennedy, 1963). Values lower than the equation 2-11 are associated with upstreammigrating antidunes.

$$Fr^2 = \frac{1}{k \tanh(k)} \qquad (2\text{-}11)$$

Ripples

Ripples are dune-like features that occur most of the time in the presence of a viscous sublayer. The existence of a viscous sublayer does not imply that the flow is either laminar or turbulent. Rather, when the flow is turbulent, the existence of a well-defined viscous sublayer implies flow in the turbulent smooth regime rather than the turbulent rough regime. Ripples look very much like dunes in that they migrate downstream and have a pronounced slip face. They generally are much more three-dimensional in structure than dunes, however, and have little effect on the water surface.

Alternate Bars

Alternate bars are bed forms most commonly found in straight alluvial channels (Bridge 2003). Their geometry is three-dimensional. Navigation conditions and streambank stability can be affected by alternate bars. When alternate bars are present, pools develop on alternate sides of the channel and the floor meanders from pool to pool. Under these conditions, the flow might start to attack the stream banks, eventually causing bank erosion and leading to the initiation of stream meandering (Blondeaux and Seminara 1985; Rhoads and Welford 1991). The pools formed by alternate bars also provide habitat and play an important role in stream ecology.

Progression of Bed Forms

Various bed forms are associated with various flow regimes. In the case of a sand-bed stream with a characteristic size less than about 0.5 mm, a clear progression is evident as flow velocity increases. The bed is assumed to be initially flat. At very low imposed velocity U, the bed remains flat because no sediment is moved. As the velocity exceeds the critical value, ripples are formed. At higher values, dunes form and coexist with ripples. For even higher velocities, well-developed dunes form in the absence of ripples. At some point, the velocity reaches a value near the short-wave critical value. Near this point, the dunes are often suddenly and dramatically washed out. This results in a flatbed known as an upper-regime (supercritical) flat bed. Further increases in velocity lead to the formation of antidunes, and finally to the chute and pool pattern. The last of these is characterized by a series of hydraulic jumps.

Relationship in bedform of resistance:

For equilibrium flows in wide straight channels, the relation for bed resistance can be expressed

in the form

$$\tau_b = \rho C_f U_2 \qquad\qquad (2\text{-}12)$$

where C_f is bed friction coefficient. If the bed were rigid and the flow rough, C_f would vary only weakly with the flow. As a result, the relation between τ_b and U is approximately parabolic for a flat rough bed. Figure 2-2 illustrates variation of bed shear stress and Weisbach friction factor.
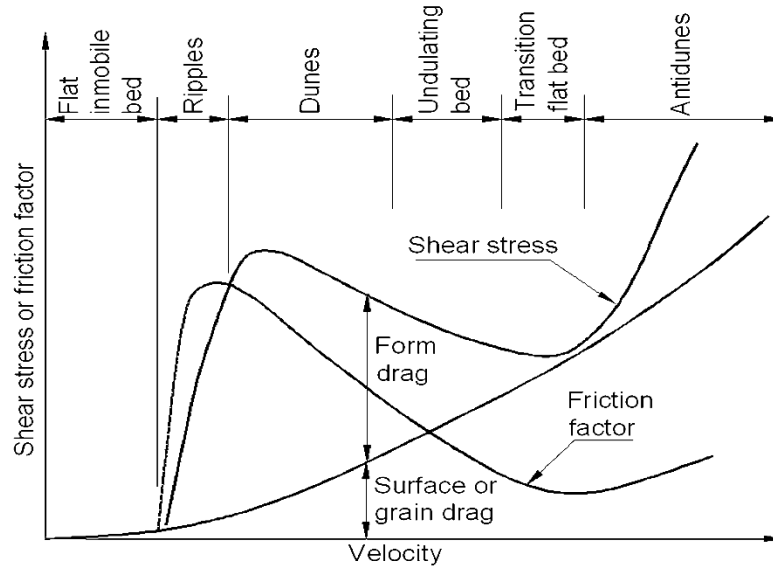
Figure 2.2 Variations of bed shear stress b and Darcy Weisbach friction factor
with mean velocity U in flow over a finesand bed (after Raudkivi, 1990).

2.2.4 Bank erosion and bed scour

The major problem of braided river is bank erosion. The main objective of this research hence is to predict erosion prone area. Stream bank erosion is a natural geomorphic process occurring in all channels. It is one of the important mechanisms by which a channel adjusts its size, shape and slope to convey the discharge and sediment supplied to it from the upstream watershed. Most existing numerical models do not consider bank erosion explicitly and therefore, have limited use for studying the geomorphic response of a channel.

Stream bank erosion is also a dominant source of sediment supply in many river systems, leading to sediment management problems. It contributed about 37% in the River Ouse, Yorkshire, UK (Walling et. al., 1999), 50% in the Midwestern streams, USA (Wilkin and Hebel, 1982), 78% in the Gowrie Creek, Murray Darling Basin, Australia (Howard et. al., 1998), 80% in the loess area of Midwest United States (Simon et. al., 1996), and up to 92% (including channel scour) in Gelbaek stream, Denmark (Kronvang et. al., 1997). An increase in sediment supply due to accelerated bank erosion can be a major cause of non-point source pollution within river systems (Technical Report No. SRH-2010-22).

Bank erosion occurs by a wide variety of processes. Broadly, they can be divided into two groups (Watson and Basher, 2006). Figure 2-3 illustrates the whole divisional classification of bank erosion.

Figure 2.3 Processes of Bank Erosion

In cohesive bank, the main erosion process is undercutting by the flow, which destabilizes the upper part of the bank. Failed material deposits at the toe and is eventually washed away. Banks may collapse due to water saturation, especially after a water level drop in the channel (Jagers, 2003). Uddin and Rahman (2011) found that in a bend in the Jamuna River, near-bank shear stresses were six times higher than the critical stress. All of this leads to rapid erosion.

Subsurface flow is known to play a part in riverbank erosion. It usually follows bank recharge by high flow or rainfall. Due to the presence of a less permeable layer the outflowing water concentrates. If the gradient is sufficient, entrainment of particles and possibly larger scale erosion occurs (Hagerty, 1991). Bank erosion due to seepage is documented by Karmaker and Dutta (2013) in the Brahmaputra River.

In the Jamuna River, eroding banks cause bank erosion of up to 500 m or even 1000 m per year in extreme conditions (Klaassen and Masselink, 1992). The average erosion rates were found to be around 200 m per year by Baki and Gan (2012). Sharper bends were found to cause faster erosion. Influence of vegetation is negligible, as its roots do not penetrate deep enough to have an effect on the undercutting process (Klaassen and Masselink, 1992). Erosion is not limited to extreme events and is common even during the dry season and in smaller channels (Sarker et al., 2014).

Important Factors Associated with Bank Erosion

Knighton (1998) provided a detailed discussion on factors influencing bank erosion processes.

Some important factors are:

i)   Flow Properties: Important Properties are magnitude, frequency and duration of flow discharge, magnitude and distribution of stream velocity and shear stress, and level of turbulence.

ii)   Channel Geometry: Including channel width, depth, slope of channel, and stream curvature (concave, convex, straight).

iii) Bank Geometry: characterized by height, slope, length, profile, and shape. Bank height and slope are critical parameters when assessing stream bank erosion potential, particularly when dealing with cohesive bank material.

iv)   Bank Material: Bank properties include size, gradation, cohesiveness and stratification of bank materials.

v)   Bank soil moisture condition: includes moisture content, seepage, pore water pressure and piping.

vi)   Vegetation: includes type, percentage of cover, age, root depth, and exposed roots.

vii) Storm Frequency: characterized by rainfall intensity and duration, and is related to the pore-water pressure, seepage flow, and piping failure.

2.2.5 2D Hydrodynamics and Morphological Model

Numerical modeling has been using to predict the time-evolution of the braided pattern in time (Jagers, 2003) and temporal developments of selected bars/islands of the Jamuna River (Shapma, 2018). One of the objectives of this study is to apply 2D morphological model to simulate morphological behavior and to understand the morphological processes for the study area. Therefore, 2D hydrodynamic and morphological model will be developed for the study area using a well-known 2D hydraulics model, e.g., SRH-2D. SRH-2D model is a 2D depth averaged hydrodynamic and morphological model developed by United States Bureau of Reclamation (USBR). SRH-2D model is a finite volume-based model and can handle flexible mesh. It can also solve 2D hydraulics and morphological change with any hydraulic structures such as Bridge, Culvert and Levee. 2D model will be developed using recent hydrologic and bathymetric data. Once the model is calibrated, the model will be used to predict future morphological changes.

The following 2D Saint-Venant eq. (2-13 to 2-15) is being solved in numerical modeling using SRH-2D model.

$$\frac{\delta h}{\delta t} + \frac{\delta q_s}{\delta x} + \frac{\delta q_y}{\delta y} = 0$$

(2-13)

$$\frac{\delta q_x}{\delta t} + \frac{\delta u q_x}{\delta x} + \frac{\delta v q_x}{\delta y} + \frac{g}{2}\frac{\delta h^2}{\delta x} = gh(S_{bx} - S_{fx}) + \frac{1}{\rho}\frac{\delta h\tau_{xx}}{\delta x} + \frac{1}{\rho}\frac{\delta h\tau_{xy}}{\delta y}$$

(2-14)

$$\frac{\delta q_y}{\delta t} + \frac{\delta u q_y}{\delta x} + \frac{\delta v q_y}{\delta y} + \frac{g}{2}\frac{\delta h^2}{\delta y} = gh(S_{by} - S_{fy}) + \frac{1}{\rho}\frac{\delta h\tau_{yx}}{\delta x} + \frac{1}{\rho}\frac{\delta h\tau_{yy}}{\delta y}$$

(2-15)

After solving for h (depth), q (discharge) is solved thus having bed elevation (z) and local velocity (v).

2.3 The Machine Learning Perspective

The goal of predicting riverbank line shifting, is to predict the future planform of the reach over a specific period of time. Very few previous studies have examined this crucial and challenging water resources prediction problem from the machine learning perspective. In this project, riverbank line shifting is formulated as a spatiotemporal sequence forecasting problem in which both the input and the predicted output are spatiotemporal sequences. The technical issues of mathematical modeling may be addressed by viewing the problem from this perspective. However, such learning problems, regardless of their exact applications, are nontrivial in the first place, due to the high dimensionality of the spatiotemporal sequences; especially when multi-step predictions have to be made, unless the spatiotemporal structure of the data is captured well by the prediction model. Moreover, building an effective prediction model for the river planform satellite data is even more challenging due to the chaotic nature of braided rivers.

2.3.1 Machine Learning

The science of Machine Learning (ML) involves enabling computers to learn from data, without being explicitly programmed. Data is used to train the system to perform a specific task. The model, which uses some form of mathematical optimization and statistical methods, recognizes the patterns and intricacies within the data. This can be then used to automate tasks or guide decision making, simply based on data and the mathematical model.

Machine learning is being increasingly used in our day-to-day lives. For example, all email service providers today use ML to filter out spam emails. Similarly, the online shopping recommendations provided to us by ecommerce websites is based on ML. The field of machine learning is developing at a fast pace. Researchers have been developing algorithms and new methodologies and also simultaneously applying these techniques to new application areas such as medical diagnosis (Kourou et al., 2015; Foster et al., 2014) and climate change (Lakshmanan et al., 2015)). The evolution of intelligent systems is definitely beneficial because it makes processes more efficient, and at the same time, requiring minimal human intervention.

Machine learning is a field that is focused on the construction of algorithms that make predictions based on data. A machine learning task aims to identify (to learn) a function $f : X \rightarrow Y$ that maps the input domain X (of data) onto output domain Y (of possible predictions) (Bekkerman et al., 2012). Functions f are chosen from different function classes, dependent on the type of learning algorithm that is being used. Mitchell (1997) defines "learning" as follows: "A computer program is said to learn from experience E with respect to some class of tasks T and performance measure P, if its performance at tasks in T, as measured by P, improves with experience E" (Mitchell, T., 1997). The performance measure P tells us quantitatively how well a certain machine learning algorithm is performing. For a classification task, the accuracy

of the system is usually chosen as the performance measure, where accuracy is defined as the proportion for which the system correctly produces the output. Experience E that machine learning algorithms undergo are datasets. These datasets contain a set of examples that are used to train and test these algorithms.

2.3.2 Solving Machine Learning Tasks

A wide variety of tasks exist that could be solved with machine learning. Two popular machine learning tasks are regression analysis and classification. In regression analysis, the relationship amongst variables is approximated, for the successful prediction of a value given some input. This task is solved by outputting a function $f : \mathrm{R}^n \to \mathrm{R}$ that fits the data. Regression analysis can be used for example to forecast future stock prices in the trading world. In classification, the machine is asked to determine the category n that a certain input belongs to. The task can be solved by outputting a function $f : \mathrm{R}^n \to \{1, ..., n\}$. A popular classification problem is object recognition for intelligent systems. Classification can be used for example to classify objects in a warehouse to determine the correct destination of each object, with current state-of-the-art object recognition making use of deep learning algorithms (Krizhevsky et al., 2012).

2.3.3 Deep Learning

Artificial Neural Networks (ANN) are an important class of machine learning models, used for both supervised and unsupervised tasks. The distinction among deep learning, machine learning and artificial intelligence is shown in Figure 2-4. The structure and functioning of ANNs are loosely inspired by biological neural networks. The brain consists of a large number of interconnected neurons, which ANNs try to mimic. ANNs consist of multiple layers of simple processing units known as nodes, which are connected by edges with weights (Gurney, 2014). An analogy between biological and artificial neuron is depicted in Figure 2-5.
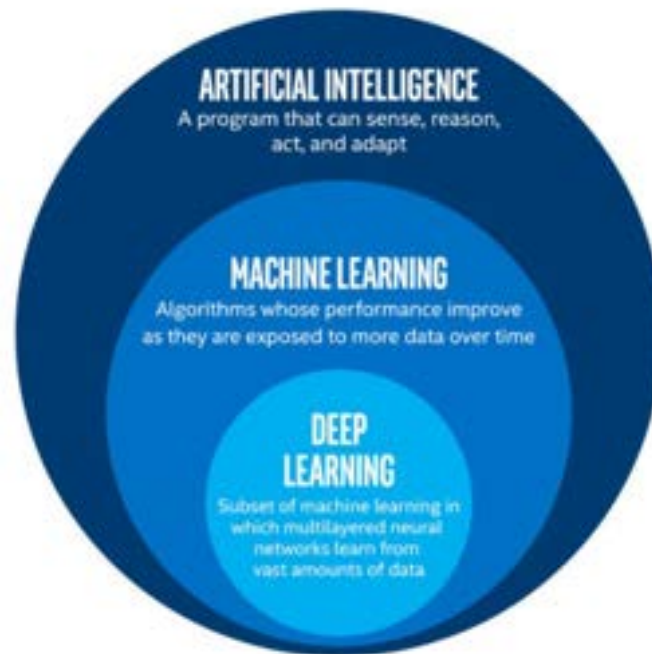
Figure 2.4 Distinction between AI, ML and DL
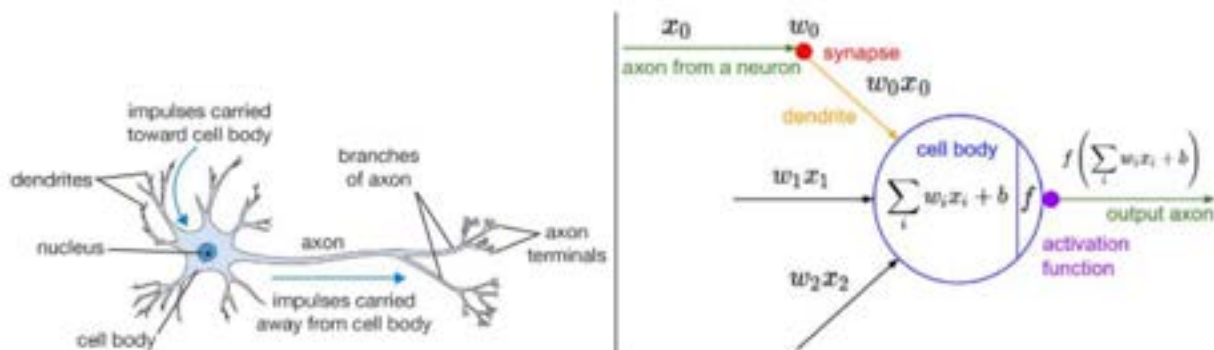
Figure 2.5 Analogy of biological neuron (left) and its mathematical model (right)

Over the last decade, there has been an increasing interest in neural network architectures consisting of many layers. Along with the availability of massive amounts of data and powerful hardware for computation, such model architectures were able to outperform humans in a number of cognitive tasks (Schmidhuber, 2015; Najafabadi et al., 2015). This led to the creation of a sub-field of machine learning known as deep learning (LeCun et al., 2015).

The most basic version of an ANN model is a feed-forward neural network (Figure 2-6). However, there exist other architectures such as Recurrent Neural Network (RNN) (Williams and Zipser, 1989; Elman, 1990) and Convolutional Neural Network (CNN) (LeCun et al.,

1995). RNNs perform particularly well on sequential data such as in natural language processing (where sentences are considered as sequences of words). Hence, the focus of this project will be on RNNs.

2.3.4 Introduction to Neural Networks

In order to understand the computational model of artificial neural networks, one needs to begin from its building block, known as the perceptron (Rosenblatt, 1958). Inspired from the brain's neurons, a perceptron is a simple computational model that takes in one or more inputs and provides a single value as output. This is illustrated in Figure 2-7. Based on this output and a pre-defined threshold, the perceptron acts as a binary classifier, i.e., if the output value is greater than the threshold, the input is assigned to class 1, else it is assigned to class 0.

Let x_1, x_2, x_3 be the inputs to the perceptron model. w_1, w_2, w_3 are the series of model weights corresponding to each input variable. This simple model consists of two operations:

- The first step is to multiply each input with its weight, followed by a summation. To this result, we also add the bias term b so that the model has a flexibility for location shift.
- Next, we assign a class label (either 0 or 1), based on a binary activation function which requires a pre-defined threshold (refer Figure 2-7).
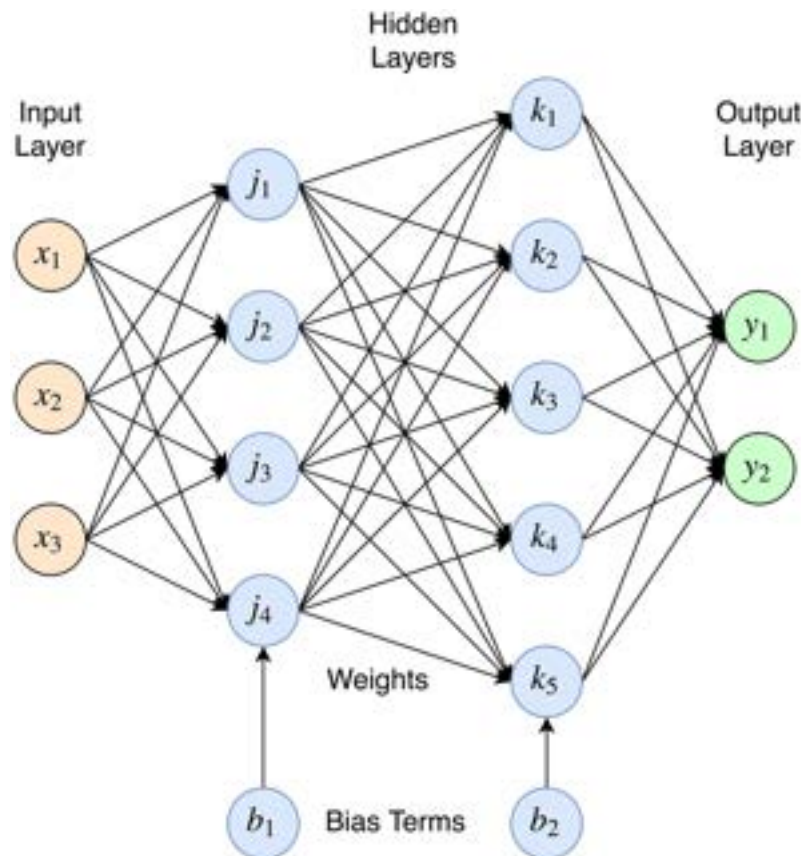
Figure 2.6 Feed Forward Neural Netrork

$$z = b + \sum_{i=1}^{3} w_i x_i$$

$$y = \begin{cases} 1, & \text{if } z > \text{ threshold} \\ 0, & \text{otherwise} \end{cases}$$
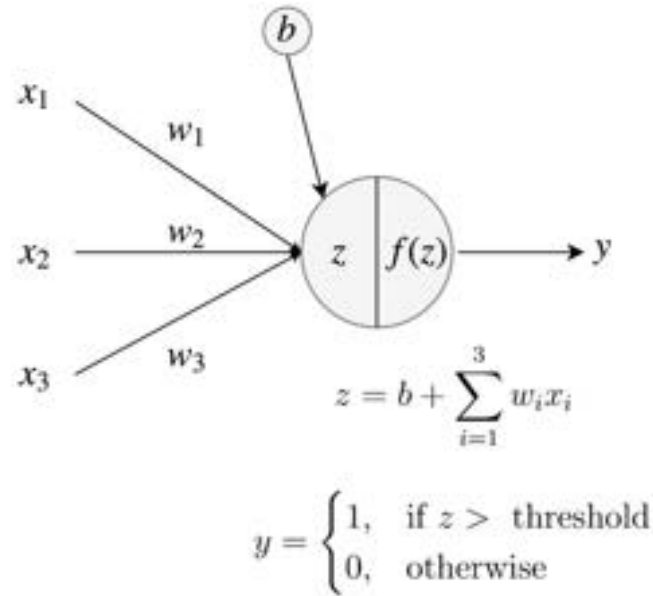
Figure 2.7 Perceptron Model

The result is the predicted value of output y corresponding to the given set of inputs. In order for the predicted output to be close to the desired output (ground truth), we would need to make adjustments to the weights w_1, w_2, w_3 and bias term b.

Typical activation functions include: *logistic sigmoid* (σ), *tanh*, and *rectified linear units (ReLU)*. The functions are defined by equations, 2-13, 2-14, and 2-15 respectively. For regression problems which require predicting continuous values, *linear activation* is used. Linear activation applies the identity function shown in equation 2-16.

$$\sigma(z) = \frac{1}{1 + e^{-z}} \qquad\qquad 2 - 13$$

$$tanh(z) = \frac{e^z - e^{-z}}{e^z + e^{-z}} \qquad\qquad 2 - 14$$

$$ReLU(z) = \max(0, z) \qquad\qquad 2 - 15$$

$$a(z) = z \qquad\qquad 2 - 16$$

2.3.5 Backpropagation

Although artificial neural networks have been around since the 1960s, it was not until the late 1980s that an efficient training procedure for ANNs was discovered. There existed no

structured methodology to adjust the model weights, other than by trial and error. Researchers like Rumelhart et al. (1986) and Werbos (1990) contributed to the development of the method known as backpropagation of errors, which made it possible to estimate the weights in an ANN model. Backpropagation makes use of the chain rule of differentiation, and computes the gradients in an iterative manner.

In order to develop an intuition of backpropagation, it is necessary to understand how an optimization method known as Gradient Descent works. In neural networks, the predicted output is compared to the actual output based on a pre-defined loss function. Common examples of loss functions are mean squared error (MSE) and negative log-likelihood (NLL). The objective is to adjust the model weights in a way that minimizes the loss. It is mathematically guaranteed that moving in the direction of the gradient of the loss function (derivative with respect to the model weights), results in loss minimization.

2.3.6 Gradient Descent

A pass over training data is called an *epoch* and after every epoch the parameters move closer to their optimum values which minimizes the loss function. If the dataset size is large, calculating the loss and gradient over the entire dataset may be too slow and computationally infeasible. Thus, in practice, a variant of gradient descent called *stochastic gradient descent* (*SGD*) is commonly used. In SGD data is divided into subsets called *batches*, and the parameters are updated after calculating the loss function over one batch. Other popular variants are: RMSprop, AdaGrad, Adam (Ruder, 2016). In some of these variants, an additional parameter called *decay* is used to decrease the learning rate gradually as parameters approach the optimum values.

Assume $\mathcal{L}(\omega)$ to be the loss function, with w being the model weights. First, the weights are randomly initialized, followed by an iterative update rule as shown in Equation 2-17,

$$\omega \leftarrow \omega - \eta \,.\, \nabla_w \, \mathcal{L}(\omega) \qquad\qquad 2-17$$

Where, η is a hyperparameter (set by the user) known as the learning rate, which corresponds to the step size towards the local minima in each iteration and ∇ refers to the gradient operator. While a low learning rate results in the training process to progress slowly, a high learning rate may cause the training to diverge from the minima. Because of this trade-off, the learning rate needs to be set carefully. We stop the iteration process either when we reach the pre-defined maximum number of iterations (known as epochs) or when the change in model weights between iterations is smaller than a specified threshold ϵ. Readers are referred to Bishop (2006) for further details on backpropagation and Gradient Descent.

2.3.7 Training Problems and Hyperparameters

An often-encountered problem in training NNs is *overfitting*. Overfitting occurs when the model tries to fit the noise in training data and is often the result of using a more complex model than required. In the presence of overfitting, model performs well on training data but poorly on new data. There are several ways to prevent overfitting. In *early-stopping* a small

subset of training data is used as a validation set. After every epoch the value of the loss function on the training set is compared to the value on the validation set. If the loss on the validation set starts increasing even though the loss on the training set is decreasing, it is an indication of overfitting, and the model training can be stopped. Another method commonly used in deep learning is *dropout*. In dropout, a fixed percentage of NN connections are removed randomly in each training epoch.

It is important to note that network parameters (weights and biases) are learned by the training algorithm. On the other hand, parameters like learning rate, dropout, training batch size, decay, etc. are parameters of the learning algorithm and need to be set to appropriate values by the user. These latter parameters are collectively termed as *hyper-parameters*.

2.3.8 Deep Neural Networks

A vital component of traditional machine learning pipelines is feature engineering (Domingos, 2012) Conventional machine learning algorithms require carefully designed features and do not perform well with raw data. However, feature engineering is not straightforward and requires considerable domain expertise. One of the primary reasons for the success of deep learning models is the ability to automatically learn high level representations relevant for the task at hand. Deep neural networks (DNNs) are NNs with multiple hidden layers stacked together. Each layer is a non-linear module, which receives the output of its previous layer. Progressively more complex/abstract features are learned from bottom to top layer. Thus a DNN is similar to a processing pipeline where each layer does part of the task and hands its output to the next layer.

Deep learning techniques have given state-of-the-art results in a variety of domains from computer vision to language translation (Goodfellow et al., 2016). This success has been facilitated by many different factors: availability of large labeled datasets, advances made in computer engineering, distributed systems, and computational power including GPUs.

2.3.9 Convolutional Neural Networks:

Although multi-layer neural network (MLNN) is able to approximate any function, it is not suitable when dealing with visual information, i.e. images. Firstly, the full-connectivity of the network leads to slow learning as the number of weights rapidly increases with the higher dimensionality of visual input. Secondly, the spatial organization of the visual input is not utilized in MLNN, since every pair of neurons between two layers has their own weight. For example, learning to recognize an object in one location wouldn't transfer to the same object presented in a different location because separate weights would be involved in these calculations. Such drawbacks led to invention of CNN architecture, which exploits the spatial dimension properties of visual input whilst reducing the number of parameters to train.

The design of CNN was inspired by the structure of mammalian visual cortex where visual information received through the eyes is processed by neurons in the brain organized in

hierarchical way. When visual stimuli reach the receptive field of a neuron it may be activated depending on its neuronal tuning. Neurons in the earlier visual areas have simpler tuning and smaller size of receptive field. Therefore, the most primitive visual forms such as corners or edges are recognized in the primary visual cortex areas and more complex forms (feature groups, objects, object descriptions) - in the collateral areas (see Figure 2-8).
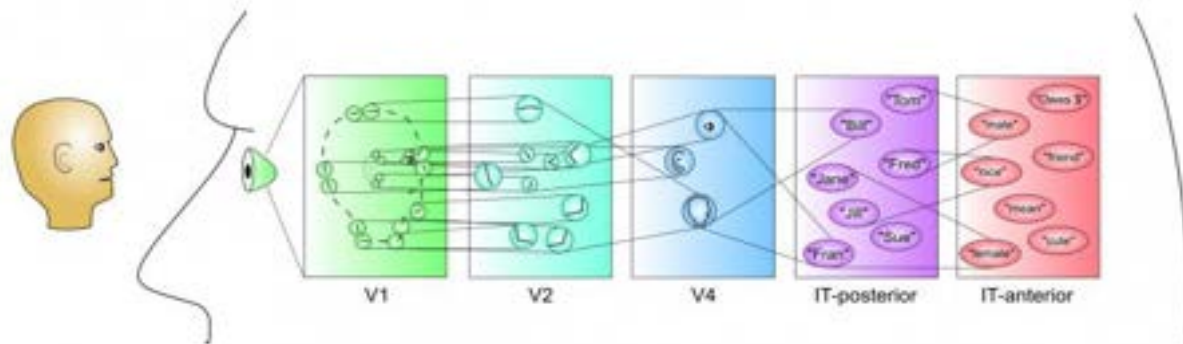
Figure 2.8 Visual information processing in hierarchical way

In Figure 2-8 a schematic of a hierarchical sequence of categorical representations of processing a face input stimulus is detailed. Representations are distributed at each level (multiple neural detectors active). At the lowest level, there are elementary feature detectors (oriented edges). Next, these are combined into junctions of lines, followed by more complex visual features. Individual faces are recognized at the next level (even here multiple face units are active in graded proportion to how similar people look). Finally, at the highest level are important functional "semantic" categories that serve as a good basis for actions that one might take - being able to develop such high level categories is critical for intelligent behavior (O'Reilly et al., 2012).

Convolutional neural networks are currently one of the most prominent algorithms for deep learning with image data. Whereas for traditional machine learning relevant features have to be extracted manually, deep learning uses raw images as input to learn certain features. CNNs consist of an input- and output layer, and several hidden layers between the input and output. Examples of in between layers are convolutional layers, max-pooling layers and fully connected layers.

2.3.10 Recurrent Neural Networks

One of shortcomings of feed forward neural networks such as the one illustrated in Figure 2-6 is that it assumes that all input data are independent of each other. As a result, it fails to capture the notion of sequential order which is present in some types of data. Consider the task of predicting the next character in a word. If an incomplete word such as `neura' is given, one can guess that the next character in the sequence would be `l ' and the word is `neural '. However, if the order of the previous characters was jumbled (such as `renau') and provided independently, it would be very difficult to identify the final character. This is where RNNs are found to be extremely useful. One of the earliest versions of the recurrent neural network was proposed by Elman (1990). The input to an RNN is provided in a sequential manner, and

the network makes use of the inputs in the previous timesteps in order to make a decision at the current timestep.

A recurrent neural network can be depicted as a network with loops (see Figure 2-9), through which information is transferred between timesteps of the network. By unrolling the network, we realize that the information at each timestep passes through multiple copies of the same network (Olah, 2015).
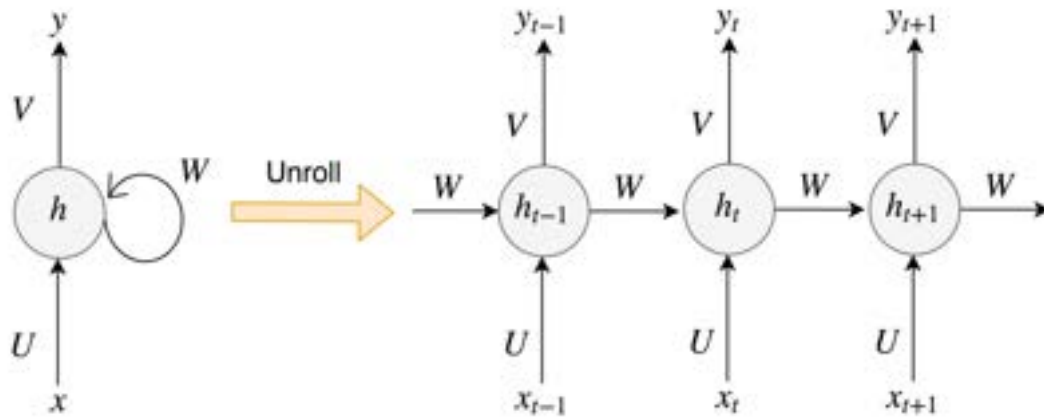
Figure 2.9 Unrolling of a recurrent neural network (RNN)

The notation in Figure 2-9, adapted from (Britz, 2015) is described below:

- x_t corresponds to the input at each timestep t
- y_t refers to the output at each timestep t
- h_t is called the hidden state at each timestep t, and is calculated using the input at the current timestep x_t and the hidden state from the previous timestep h_{t-1}, i.e.,

$$h_t = f(Ux_t + Wh_{t-1}) \qquad\qquad 2-18$$

Where f corresponds to some non-linear activation function such as tanh or ReLU. In RNN literature, h_t is also referred to as the memory because in theory, it is assumed to capture information from all previous timesteps. However, this does not hold true in practice since the RNN memory fails to remember information beyond few previous timesteps.

- U, V and W are weight matrices. From the unrolled RNN figure, one can note that these weights are shared across all timesteps of the RNN. Doing this reduces the model complexity by reducing the number of parameters that need to be optimized. Moreover, we aim to perform the same operation across timesteps, just with different inputs.

Training of RNNs is done via an extension of the backpropagation algorithm, known as backpropagation through time (BPTT). As discussed earlier, RNNs perform well on sequential

data and have been extensively used for tasks such as language modelling (Mikolov et al., 2010), text generation (Graves, 2013) and speech recognition (Graves et al., 2013).

2.3.11 Convolutional LSTM

In order to understand the details of ConvLSTM blocks and how they differ from the traditional LSTM blocks a little bit of theory has been introduced here.

The major drawback of FC-LSTM in handling spatiotemporal data is its usage of full connections in input-to-state and state-to-state transitions in which no spatial information is encoded. To overcome this problem, a distinguishing feature of ConvLSTM design is that all the inputs $X_1, \ldots, X_t$, cell outputs $C_1, \ldots, C_t$, hidden states $H_1, \ldots, H_t$, and gates i_t (input gate), f_t (forget gate), o_t (output gate) of the ConvLSTM are 3D tensors whose last two dimensions are spatial dimensions (rows and columns). To get a better picture of the inputs and states, we may imagine them as vectors standing on a spatial grid. The ConvLSTM determines the future state of a certain cell in the grid by the inputs and past states of its local neighbors.
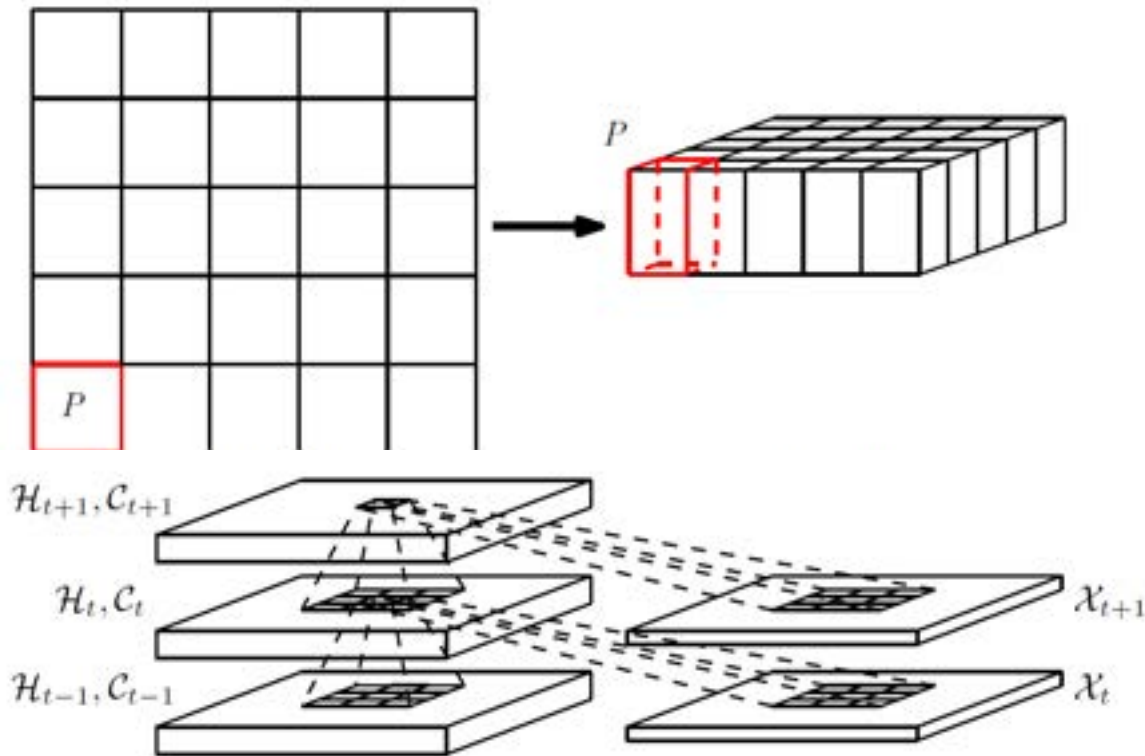
Figure 2.10 Convolutional LSTM operations

This can easily be achieved by using a convolution operator in the state-to-state and input-to-state transitions (see Fig. 2-10). The key equations of ConvLSTM are shown below, where '*' denotes the convolution operator and '$\odot$', denotes the Hadamard product:

$$i_t = \sigma(W_{xi} * X_t + W_{hi} * H_{t-1} + W_{ci} \odot C_{t-1} + b_i) \qquad 4.5$$

$$f_t = \sigma(W_{xf} * X_t + W_{hf} * H_{t-1} + W_{cf} \odot C_{t-1} + b_f) \qquad 4.6$$

$$C_t = f_t \odot C_{t-1} + i_t \odot tanh(W_{xc} * X_t + W_{hc} * H_{t-1} + b_c) \qquad 4.7$$

$$o_t = \sigma(W_{xo} * X_t + W_{ho} * H_{t-1} + W_{co} \odot C_t + b_o) \qquad 4.8$$

$$H_t = o_t \odot tanh(C_t) \qquad 4.9$$

If we view the states as the hidden representations of moving objects, a ConvLSTM with a larger transitional kernel should be able to capture faster motions while one with a smaller kernel can capture slower motions.

To ensure that the states have the same number of rows and same number of columns as the inputs, padding is needed before applying the convolution operation. Here, padding of the hidden states on the boundary points can be viewed as using the state of the outside world for calculation. Usually, before the first input comes, all the states of the LSTM were initialized to zero which corresponds to "total ignorance" of the future. Similarly, if zero-padding (which is used in this paper) is performed on the hidden states, actually the state of the outside world is being set to zero and no prior knowledge about the outside is being assumed. By padding on the states, the boundary points can be treated differently, which is helpful in many cases.

2.3.12 Advantages and Challenges

The main issue of NN implementation is deriving the correct hidden layer size. When the amount of neurons is not determined properly, the derived system does not generalize well to unseen instances. On the other hand, when too much nodes are used, overfitting may occur and the desired optimum may not be found at all. Deriving the right quantity of neurons is discussed in a study by Kon et al., 2000. The main advantage of using artificial neural networks is its capability to process data with high dimensional features such as images. Drawbacks of artificial neural networks are high computing costs that consume large amounts of processing power and physical memory usage, and difficult comprehensibility for average machine learning users (Kotsiantis et al., 2007) (Baharudin et al., 2010).

2.4 Previous Studies on River Bank Erosion

To properly understand the bank erosion process and bed form of this large braided Jamuna river and develop a proper methodology to apprehend the situation of the study are and its physical process different relevant reports were collected from various sources and reviewed. A brief summary of some relevant reports and papers are described below.

2.4.1 Studies using Image Analysis

Studies on the river morphology of major rivers using remotely sensed images are such as that of Kummu et al. (2008) for the Mekong River using SPOT5 images, the accretion/erosion of the Yellow River by Chu et al. (2006) using Landsat images, and the estimation of suspended sediment of the Lower Yangtze River by Wang and Lu (2010) using Terra MODIS. Since the 1960s, many studies have already been carried out, particularly with regard to morphological processes in the Jamuna River. By comparing Bangladesh survey maps and aerial photographs from the 1950s with a 1989 SPOT image, Thorne et al. (1993) detected the riverbank migration of the Jamuna River. Similarly, by comparing Landsat-MSS for 1973-1987 with Landsat-TM images for 1990-1992, ISPAN (1993) estimated the short-term bank migration of the Jamuna River. ISPAN (1993) and Thorne et al. (1993) found that the right bank of Jamuna was more prone to erosion than the left bank where both erosion and accretion together produced relatively low net movements. In the early 21st century, using satellite images, EGIS (1999, 2002), and Khan and Islam (2003) studied the geomorphological characteristics of Brahmaputra-Jamuna. Sarker and Thorne (2006) examined the morphological response of major river systems of Bangladesh due to the Assam earthquake. Sarker et al. (2003) investigated the dynamics and chars of major river systems of Bangladesh and their socio-economic aspects.

Takagi et al. (2007) analyzed the spatial and temporal changes in the channels of Brahmaputra. Their results suggested that Jamuna River widened at a relatively high rate of about 150 m/y during 1970-1980 and then decreased to about 50 m/y during 1980-1990. Even though river bank erosion is one of the foremost natural disasters responsible for poverty in Bangladesh because of the enormous destruction of resources and displacement of large numbers of the population (Khan and Islam, 2003).

Given the widespread and persistent bank erosion that causes serious problems along the Jamuna River of vital importance to Bangladesh Baki and Gan (2012) focused on Landsat MSS and TM images spanned over 30 years (1973-2003). Khan et.al. (2014) studied on river bank erosion of Jamuna River by using GIS and Remote Sensing Technology. Hossain et al. (2013) assessed morphological changes of Ganges River. Afrose et.al (2012) analyzed morphological changes of Teesta River.

Sarkar et al. (2014) has used all the sources to chronicle the morphological evolution of the Jamuna River since the avulsion that created it about 200 years ago. It established temporal trends and spatial patterns in the changes that have characterized process–response mechanisms in this fluvial system since then. Process–response mechanisms and their relation to various drivers of morphological change in the Brahmaputra–Jamuna River have been recognized. Finally, the analyses developed were combined with existing, conceptual and empirical process–response models for the Jamuna to predict possible future morphological adjustments.

2.4.2 Studies using Computational Model

Many studies have been conducted to understand and predict the river morphology including bank erosion process using computational model.

Several studies consider bed deformation and bankline shifting. Notably, Kovacs and Parker (1994), Nagata et al. (1996), Shimizu et al. (1996), and Duan et al. (1997) developed numerical models to analyze temporal changes in channel forms due to bank erosion. The model proposed by Kovacs and Parker, however, assumes constant hydraulic and geometric conditions in the streamwise direction. All the models have been applied only to few cases of laboratory channel processes. Darby and Thorne (1996) and Darby et al. (1996) developed a numerical model of bank erosion that introduces rotational slip and planar failure of the bank, and applied the model to the morphological behavior of a natural river. However, the 2D plan form variation caused by bank erosion cannot be predicted, which is an important factor in anticipating disasters consequent to riverbank shifting. Nagata et al. (2000) developed a numerical model that calculates 2D bed deformation and plan form variations. The model has been applied successfully to examine the morphological behavior of laboratory channels with meandering and straight plan forms. Using the model, the development of meandering is explained in terms of the relation between sediment transport and the flow field near the bank.

An increased awareness that braided river dynamics which cannot be described by the development of the channel structure independently has emerged (Ashmore, 2000; Murray and Paola, 1997; Furbish, 2003). However, progress in developing physical and computational models as a base to study the dynamic behaviour of braided rivers, as well as the coupled behaviour between flow and topographic characteristics, also raises the demand for appropriate model evaluation tools that capture these multiple aspects of braided river morpho-dynamics. Present quantitative methods for model evaluation concentrate mainly on static flow or planform properties, but the evaluation of topography and dynamics is, at present, primarily restricted to qualitative assessment (Sapozhnikov et al., 1998; Murray and Paola, 1997, 1998; Paola, 2000; Thomas and Nicholas, 2002; Jagers, 2003). Essentially the problem is to find quantitative criteria that characterize braided rivers and allow modelers to assess the extent to which model output reproduces the morphology, dynamics and response to external forcing, of 'real' braiding.

Nicholas et al. (2013) attempted the numerical simulation of bar and island morphodynamics in anabranching rivers. Their study can be considered as a first attempt to assess physics-based morphodynamic modeling of large rivers over centennial time scales is feasible or not, and whether it can contribute to the understanding of bar and island morphodynamics. They use 2D HSTAR model to simulate the river. They concluded that the model results were sensitive to the parameterization of the processes and to the representation of bed roughness.

Schuurman et al. (2013) tried to determine the capability of a widely used physics-based model to produce key characteristics of braided sand-bed rivers such as bar and channel dimensions, braiding intensity and shape of bars, and the channel network. They used Delft 3D software to simulate the river and concluded that the morphological model results are very sensitive to the

constitutive relation for bed slope effects and also to the type and parameter values of the constitutive relations for flow resistance and sediment transport. Also, multiple mechanisms for bifurcation initiation, bifurcation closure, bar migration, and bar growth occurring in the model are comparable to observations in nature and flume experiments.

Shampa and Ali (2015) focusing on bar dynamics of a sand-bed braided river Jamuna used 2D depth average Delft 3D model. Special emphasis was given on braided bar. Khan and Ali, (2017) focused on hydraulic erosion of river bank is one of the key factors controlling the bank erosion rates. In their study hydraulic bank erosion rate has been quantified with the help of analytical formulae and 2-dimensional numerical model. A 2-dimensional morphological model was developed for the selected reach of Jamuna River using the modeling platform MIKE 21C.

2.4.3 Studies on Laboratory Experiments

Several investigators have done noteworthy work on dune geometry and its resistance to flow by conducting laboratory experiment. Early important works on dune geometry were done by Yalin (1964), Ranja Raju and Soni (1976) and Allen (1998) who developed relations for dune height as a function of bed shear stress and other variables according to experimental and field data. Van Rijn (1984) analyzed data from several numbers of flumes and some field data and developed a relation for relative dune height and length as a function of flow depth, particle diameter and a transport stage parameter (function of grain and critical shear stress).

Flume studies of confluence scour (Ashmore and Parker, 1983), sediment transport rates (Ashmore, 1988; Hoey and Sutherland, 1991; Warburton and Davies, 1994) and sediment sorting (Ashworth et al., 1992) in braided rivers and flume studies of depositional structures by braided rivers (Ashworth et al., 1994) have contributed significantly on braiding process.

Ashmore (1991) describes eleven flume experiments with varying slopes and discharges in which the processes leading to braiding were studied. The streams were generic models of gravel-bed braided streams. Each of the experiments started from a straight trapezoidal channel.

Observations in physical models of braided channels (Ashmore, 1991a, 2001; Bertoldi et al., 2006) suggest that at any given time, only a subset of the total channels are actually transporting bed material and actively forming the braided pattern and river morphology, i.e., BI_A is always less than BI_T and the remaining channels convey water and wash load, but no bed load. The implication is that the braided channel network observed at a given time forms progressively over time by shifting of a few active channels rather than by simultaneous development of all channels.

2.4.4 Specific Studies on the morphodynamics of the Jamuna River

Several studies have been conducted to understand the morphodynamic of the rive Jamuna and predict bank erosion. Some of these are briefly described in the following section.

Akhtar et al. (2011):

The work explored relations between stream power, braiding intensities and bank erosion in certain stretches of the Brahmaputra River. Objective was to enable quantitative assessment of spatio-temporal behavior of channel braiding process of the Brahmaputra River by using the Plan Form Index and corresponding estimation of stream power to establish a behavioral pattern of variability of potential energy expenditure. The braiding index was compared for discrete years to understand the morphological behavior. Subsequently, a real time estimation of stream power for certain stretches of Brahmaputra River was done in order to analyze its variability in braiding intensity and bank erosion. The dynamic behavior of the channel pattern of the Brahmaputra River System in Assam valley of India was presented for over a time span of 18 years. The procedure addressed the selection of input parameters from digital satellite images, comprising scenes for the years 1990, 1997 and 2007 with specific dates, from Dhubri near Indo-Bangladesh Border to Upper Assam. Deployment of GIS technique had been made to extract the required parameters to derive Plan Form Indices for the entire study reach. Stream power estimation was done for corresponding latest floods and for corresponding dates of image scenes. The study indicated that due to consistent aggradation of riverbed inducing temporal declination of stream power, there was an occurrence of wide spread braiding. This in turn incurs substantial yearly land loss due to bank erosion, caused by flow concentrations due to temporal evolution of multiple channels in the Brahmaputra River.

The study identified three to four major geological channel control points present along the Brahmaputra River in Assam flood plains. These control points were located in the vicinity of Jogighopa near Goalpara, Pandu near Guwahati, Tezpur and Bessemora in Majuli. These channel control points usually have well defined and stable hydrographical profiles. The variability of stream power with bank erosion and braiding processes was investigated and a distinct behavioural pattern between these processes was observed. For example, with a low stream power, braiding appears to intensify which in turn may indicate a higher possibility of bank erosion.

Baki and Gan (2012):

In this study, using thirteen selected images of Landsat MSS and TM acquired from 1973 to 2003, the riverbank migration patterns and island dynamics of Jamuna river resulted from accretion/erosion processes for 30 years were investigated. For short-term analysis, the migration rate from one Landsat image to the next is estimated. For long-term analysis, the migration rates are based on the difference between the 1973 (Figure 2-11) , and subsequent images. For the short-term (long-term) analysis, the average erosion and accretion rates are

227 and 271 m/y (90 and 104 m/y) on the left bank, and 187 and 148 m/y (75 and 50 m/y) on the right bank of Jamuna, respectively.
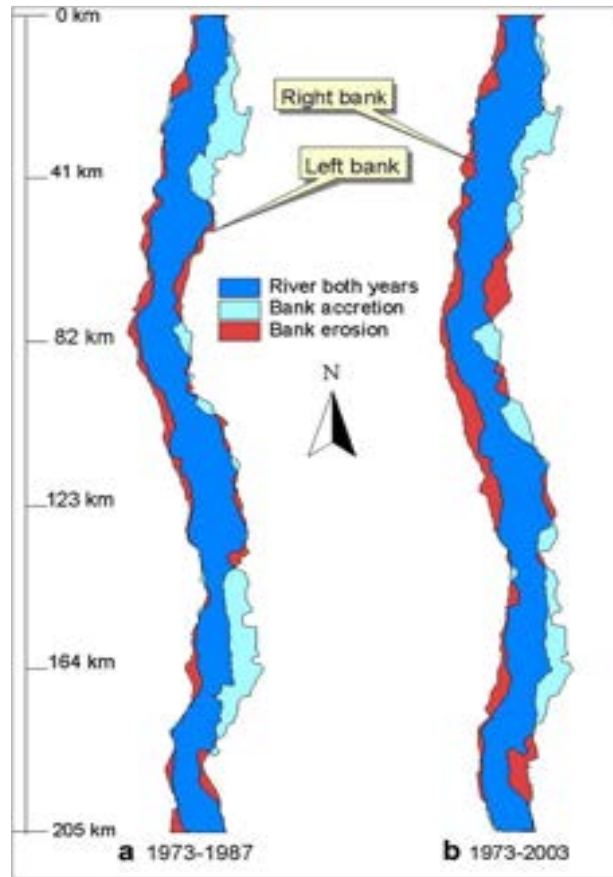
Figure 2.11 Low-flow bank erosion and accretion of the Jamuna river, (a) between 1987 and 1973, and (b) between 2003 and 1973.(Baki and Gan,2012)

Because of human interventions and the averaging effect of erosion and accretion, the long-term migration rate was lower than that of the short-term migration rate on both banks. The short-term rate of accretion (erosion) on the left (right) bank follows the general pattern of river bank migration, while the accretion (erosion) of the right (left) bank does not follow such a pattern. On the other hand, the long-term erosion and accretion processes for both banks partly follow the general pattern of river bank migrations. From one flood to another, large islands tend to be more stable with little changes, but smaller islands underwent more changes.

Sarker et al. (2014):

This paper has drawn on all the image sources to chronicle the morphological evolution of the Jamuna River since the avulsion that created it about 200 years ago. It established temporal trends and spatial patterns in the changes that have characterized process–response mechanisms in this fluvial system since then. The historical migration of the river westward has produced significant contrasts between left and right (west) bank material properties; elucidate the relationships between discharge, fluvial processes, anabranch instability and

floodplain erosion rates, and; identify causal links between drivers and morphological responses at a variety of time and space scales. Process–response mechanisms and their relation to various drivers of morphological change in the Brahmaputra–Jamuna River have been recognized and fluvial processes in this large, braided river assessed using available temporal, spatial and hydro-morphological data. Different process–response models and relations have been developed using the available data, information and knowledge, while recognizing its limitations.

Finally, the analyses developed were combined with existing, conceptual and empirical process–response models for the Jamuna to predict possible future morphological adjustments in ways helpful in identifying appropriate strategies for climate change adaptation in Bangladesh. The enhanced knowledge gained from these historical and contemporary investigations may also be useful in assessing the impacts of natural and anthropogenic drivers on other large, braided rivers.

Shampa (2018):

In this research, some prevailing physical processes which may affect the growth of bar after its emergence have been examined. An attempt to identify the relationships between the bars and their adjacent channels has been made. For this, a two-dimensional-depth-averaged morphodynamic model, Delft3D was used to study the interaction between the braided bar and adjacent channel during a flood in a compound bar dominated area at a large sand-bed braided River-Brahmaputra–Jamuna. River has been analyzed using satellite imagery and numerical modeling. the dry season satellite image of the years 2011 and 2012 have been analyzed to identify the major morphological process occurred. Then, a 2D numerical model was developed using the hydrodynamic boundary condition of the year 2011 for the lower reach of the river. The numerical simulation was quite successful to capture the effect of one monsoon/wet season on the main anabranching system of the braided river but in case of chute channel prediction, a further modification was needed. peak discharge time remains active up to the next monsoon season. During the monsoon period, the general tendency of sedimentation pattern in the channel is 'erosion' (average 2.58 m) and in the bar is 'deposition' (average 2.0 m). the percentage of flow sharing decreased with the increased flow angle. It can be explained by the lab experiments done by Federici and Paola (2003).

Khan and Ali (2016):

In this study hydraulic bank erosion rate has been quantified with the help of analytical formulae and 2-dimensional numerical model. A 2-dimensional morphological model was developed for the selected reach of Jamuna River using the modeling platform MIKE 21C. The erosion rates were used to calculate bank shear stress. Since primary discharge data was not available at different reaches model simulated discharge for different hydrologic events were utilized to correlate it with bank shear stress. The erosion rates thus obtained was compared to that revealed by satellite imagery. Utilizing the outcomes of scenario simulations, a relationship between τa and discharge was established for five erosion prone reaches. The

relationship thus obtained was used to calculate the bank erosion rate from the discharge after the passage of hydrological event 2013. The 2-D model setup includes the generation of computational grids, the preparation of the bathymetry, boundary conditions and selection of calibration parameters.

CEGIS (2017):

Since 2004, predictions for morphological changes have been conducted for the Jamuna river followed by the Ganges and the Padma river. Evaluation of such predictions have shown a good match with the occurrences.

Predictions have been made for the locations having less erodible bank materials. Since it was difficult to estimate small amount of erosion (1 to 50 m) with reliable accuracy using satellite image of 15m ×15m resolution. If the predicted erosion is less than 100m, it was not incorporated in the report. No predictions had been made for the areas where there are bank protection structures along the riverbank.

In 2016, the land eroded along the Jamuna was 1468 ha. The Brahmaputra flood embankment is one of the important features that provides protection against floods along the right bank of the Jamuna river. Jamuna right and left banks were predicted to be eroded in 611 ha. and 1289 ha. respectively for 50 % probability. The actual erosion for those banks were 529ha. and 1422 ha. respectively, which was a pretty close prediction.

Erosion prediction had been done for both banks of Jamuna river for 2017. There were 20 vulnerable locations (10 along the left bank and 10 along the right bank), the lateral extension was more than 100m. Among these, four are in Kurigram, four in Gaibandha, one in kurigram and Gaibandha district, two in Bogra, five in Sirajganj, one in Jamalpur, two in Tangail and one in Pabna and Sirajganj district. Apart from these, Predictions of erosion along the river Ganges and the Padma had also been made in this report.

2.4.5 Studies using Deep Learning

A prediction task of future riverbank conditions is a joint task comprising two separate meteorological processes: (1) understanding visual clues for riverbank transition from spatiotemporal riverbank observations, and (2) image restoration from low-dimensional encoded information into high-dimensional visual situations through time.

Jagers (2003), in his Ph.D. thesis modeled planform changes of braided rivers. He carried out his study with Jamuna River in Bangladesh. A multi-layer perceptron network was trained to predict bank erosion based on a limited amount of geometrical information: the location (distance and direction) relative to the nearest channel, the local width of the nearest channel, and the fraction of water in the neighborhood. Based on these data the neural network was able to learn a number of simple rules, such as: erosion is more likely along wide channels. Furthermore, the output of an appropriately trained network could be used as an indication of the probability that erosion would occur. One of the major disadvantages of that approach was

that the neural network was a black box approach: the empirical knowledge represented by the network could not be extended easily.

Recently, several studies focused on weather events prediction using either observation or simulation data. Shi et al., 2015 and Kim et al., 2017 predicted future precipitation from historical multichannel radar reflectivity images with a convolutional long short-term memory (ConvLSTM) network (Hochreiter et al., 1997) based on recurrent neural network (RNN) (Elman, 1993) and convolutional neural networks (CNNs). In Shi et al., 2015 and Kim et al,. 2017, they found that by extending the fully connected LSTM (FC-LSTM) to have convolutional structures in both the input-to-state and state-to-state transitions, the convolutional LSTM (ConvLSTM) network captured spatiotemporal correlations better and consistently outperformed FC-LSTM and the state-of-the art operational ROVER algorithm for precipitation nowcasting.

Racah et al., 2016 suggested a 3D convolutional autoencoder (AE) model for extreme weather events detection using 27-years CAM-5 simulation model results. They presented a multichannel spatiotemporal CNN architecture for semi-supervised bounding box prediction and exploratory data analysis. They demonstrated that their approach was able to leverage temporal information and unlabeled data to improve the localization of extreme weather events. Hong et al., 2017 surveyed multiple CNNs for predicting the coordinates of a typhoon eye from a single satellite image. They proposed the use of multi-layer neural networks for understanding complex atmospheric dynamics based on multichannel satellite images. The capability of their model was evaluated by using a linear regression task for single typhoon coordinates prediction. A specific combination of models and different activation policies enabled them to obtain an interesting prediction result in the northeastern hemisphere (ENH). Kim et al. suggested a tropical cyclone detection system based on GCM reanalysis data using 5-layer CNNs. These works depend on historical visual datasets for predicting weather events.

However, it is not confirmed if unseen weather events can be predicted for specific occasions without observation data such as an observation failure and future events prediction. For the issue of missing/lost data, several studies on deep neural memory networks have been conducted for predicting undiscovered data.Based on the LSTM-RNN, Srivastava et al., 2015 surveyed an unsupervised video representation on a fully-connected LSTM (fcLSTM) network with flatten data. They explored different design choices such as whether the decoder LSTMs should condition on the generated output. They analyzed the outputs of the model qualitatively to see how well the model could extrapolate the learned video representation into the future and into the past. They tried to visualize and interpret the learned features. They stress tested the model by running it on longer time scales and on out-of-domain data. They showed that the representations helped improve classification accuracy, especially when there were only a few training examples.

Accordingly, Patraucean et al., 2015 used intermediate differentiable memory on a temporal video auto-encoder network, and trained extensive optical flow transition differences through time between encoding and decoding steps. By minimizing the reconstruction error between

the predicted next frame and the corresponding ground truth next frame, they trained the whole system to extract features useful for motion estimation without any supervision effort. They presented one direct application of the proposed framework in weakly-supervised semantic segmentation of videos through label propagation using optical flow.

Chen et al., 2016 considered a 3D biomedical image as the spatial data continuum and adopted a bi-directional LSTM structure for understanding 3D contexts beyond correlated 2D slices. They proposed a DL framework for 3D image segmentation, based on a combination of a fully convolutional network (FCN) and a recurrent neural network (RNN), which were responsible for exploiting the intra-slice and inter-slice contexts, respectively.

With the advantages of a memory network, several research studies also discovered the effectiveness of structural separation into discrete encoder and decoder units for both sequenced input and output. Cho et al., 2014suggested an RNN encoder–decoder architecture associated with two separated RNNs as an encoder and divaricated decoder parts. The encoder and decoder of the proposed model were jointly trained to maximize the conditional probability of a target sequence given a source sequence.

Accordingly, Sutskever et al., 2014 employed the structure of Cho et al., 2014 and an adopting LSTM cell on the overall topology, entitled sequence-to-sequence (Seq2Seq). Next, Chorowski et al., 2015 introduced an external memory in Seq2Seq called attention memory, as well as which is similar to a differentiable memory, which was used in a convolutional attention-based Seq2Seq 2017. For image restoration issues, Mao et al., 2016 introduced the residual connectivity of the results of convolutional processes into the deconvolutional step for maximizing plausible image reconstruction. Enriched with abundant visual clues from deep convolutional filters, symmetric skip connections (SkipConx) helped achieve high performance as a denoising application, and as a conventional image autoencoder.

In conclusion, few surveys have been conducted on image reconstruction for remote sensing imagery, particularly on a satellite image dataset. Therefore, the initial structure of learning changes through time, with minimal available parameters, was studied. In other words, it was studied how changes in satellite images can be represented as fundamental structures of a memory network.

In their work, Hong et al. studied how a Seq2Seq-based convolutional autoencoder can predict unseen weather situations by referencing historical weather observation datasets. Further, they found that adding symmetric skip connection from the convolutional encoder to the deconvolutional decoder in the Seq2Seq autoencoder provided more reliable image prediction compared to bare LSTM or primitive convolutional LSTM connectivity.

In fields close to water such as remote sensing, DL is growing to be the preferred method of choice, proving it a crucial tool in discovering information from raw images (L. Zhang et al., 2016). Since CNNs excel in extracting information from geometric shapes, textures, and spatial patterns, they easily outperform earlier methods that only utilize spectral signatures or handcrafted features (Makantasis et al., 2015). Main RS applications (X. X. Zhu et al., 2017)

include using CNN to classify or segment images (assigning classes to each pixel on an image for what they are, e.g., land use classes, crops types) (Geng et al., 2015), object recognition (finding targets from a series of images) (Wagner, 2016), object localization (Long et al., 2017), and terrain attribute extraction, e.g., sea ice concentration (L. Wang et al., 2016). Remote sensing applications often started with standard CNN and RNN designs, and then made incremental modifications for efficiency and accuracy gains (Long et al., 2017; Mou et al., 2017; X. X. Zhu et al., 2017). In global change analysis, DL models show advantages in estimating crop yield (Kuwata & Shibasaki, 2015; You et al., 2017). Pryzant et al. (2017) forgo the conventional spectral features method in favor of a combined CNN-LSTM model to estimate outbreaks of wheat fungus in Ethiopia. Their LSTM is stacked on CNN-extracted feature representations to incorporate both spatial structural and temporal change. In addition, CNN is used for overall interpretation of images such as scene classification (for an image, recognize a theme from a list of possible themes) (Marmanis et al., 2016; Nogueira et al., 2017), change detection (Puzhao Zhang et al., 2016), and object detection, e.g., vehicles (X. Chen et al., 2014). Such high-level tasks were difficult to achieve using earlier machine learning techniques.

In disaster detection and categorization studies, researchers have started to employ DL to detect wildfires (Lee et al., 2017; Sharma et al., 2017; Q. Zhang et al., 2016) and landslides from remote sensing images (Ying Liu & Wu, 2016). Liu and Wu (2016) applied preprocessing steps including discrete wavelet transformation and noise corruption and trained an SDAE to identify landslides on the transformed image. They argued that the transformation is necessary because the resolution of remote sensing images is too low. However, they did not directly show results to support the claim.

Furthermore, the remote-sensing community has exploited transfer learning and data augmentation and has adapted available architectures to suit their data quantity. For example, publicly available trained networks such as GoogLeNet (Szegedy et al., 2015) can be transferred for scene classification for satellite images (Hu et al., 2015; Marmanis et al., 2016; Nogueira et al., 2017). Transfer learning works because the hidden layers that have been trained to distill shape information are also effective even when ported to remotely sensed scenes. Transfer learning also means that certain expertise obtained from training on existing datasets can be modularized, packaged, and assembled. Data augmentation (Ding et al., 2016; Morgan, 2015) means increasing the training data by 22 making perturbations to data that should not have mattered, such as rotation, translation, interpolation, elastic distortions, and affine transformations, etc.

In climate science, the number of applications of deep learning in climate modeling starts to rise quickly, with applications focusing on (1) identification of extreme climate events and (2) addressing the resolution challenge. In a study carried out at the Lawrence Berkeley National Lab, Liu et al. (2016) trained a CNN with two convolutional layers to detect extreme events using thousands of images of tropical cyclones, weather fronts, and atmospheric rivers. This new system achieves 89%-99% accuracy in detecting extreme events and is useful for benchmarking climate models. A significant amount of attention has been paid to using deep learning for precipitation forecasting, (e.g., Hernández et al., 2016; Shi et al., 2017; Pengcheng Zhang et al., 2017).

The model resolution has been a central challenge for climate modeling. For dynamic modeling, researchers trained dynamic convolutional layers, i.e., filters with weights that are dynamically updated using inputs during forward runs, in short-range weather predictions (Klein et al., 2015). Vandal et al. (2017) proposed a generalized stacked superresolution CNN framework for statistical downscaling of climate variables. Superresolution means a network produces an output image with a higher resolution than the input. They argued that a single trained model can downscale spatial heterogeneous regions, and the DL method showed advantages over others. In a recent self-archived paper, authors have employed an MLP to learn fine-resolution dynamics such as convective heating, moistening and cloud-radiative transfer feedbacks from high-resolution simulations, to replace existing multiple parameterization schemes (Gentine et al., 2018). Moreover, the climate modeling community is putting together large datasets to enable big data deep learning on large scales (Racah et al., 2017).

In an interesting application, authors have employed GAN to model urban expansion, which is relevant to water consumption (Albert et al., 2018). Trained on images of 30,000 cities, GAN was able to reproduce realistic concentrations and spreads of urban masses in the absence of externally-imposed constraints, e.g., rules that say cities cannot be built on water. GAN learned these rules by itself.

Chapter 3: Approach and Methodology

3.1 Introduction

To understand the overall hydraulics and morphology of the Jamuna river a two-dimensional numerical model and deep learning approach were adapted. For numerical modeling SRH-2D model was used which was already mentioned in the previous chapter. For these, significant amount of data will be collected.

3.2 Data Collection

Two types of data were collected through this research. Secondary data were collected from different sources including (WARPO, BWDB, USGS). Bangladesh Water Development Board (BWDB) has water level, discharge and several cross-section measuring stations on different rivers. Historical LANDSAT imagery was collected from USGS website and Google earth engine.

3.2.1 Satellite Images

LANDSAT images were necessary to analyze the shift of the main river course with respect of time. Erosion and Depositional area will be identified primarily based on this image analysis. For this purpose, initially LANDSAT-1 to LANDSAT-7 imagery for the years 1970 to present has been collected for free of cost from United States Geological Survey (USGS) and Google Earth Engine website. These images are of 30×30 m resolution. These images were used to identify the movement of the banklines and the sandbar over the years. The most important part of the images was that they were used in the deep learning techniques.

3.2.2 Water Level Discharge and Cross-section Data

Water level, discharge and cross-section measuring stations are used to collect respective data. The following figure 4.1 illustrates the stations on the study area. Water level data for the station have already been collected. Cross section data have been collected. These data will be used to calibrate and validate the 2D hydrodynamic and morphological model. Figure 3-1 shows the water level and discharge station and figure 3-2 shows the cross section measuring station for 1D model development and analysis. A list of water level, discharge and cross-section measuring stations are presented in Appendix A-2.
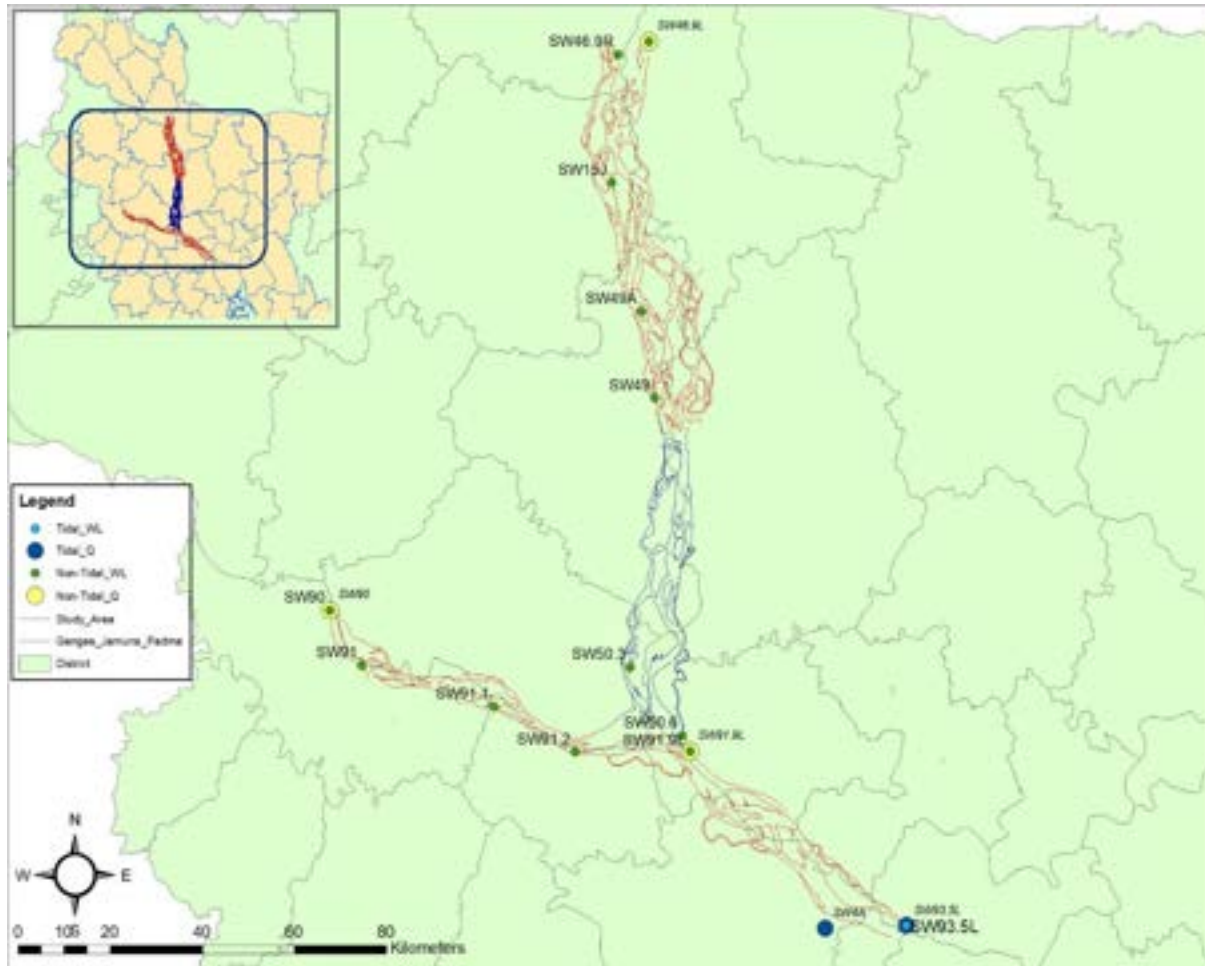
Figure 3.1 Water Level and Discharge Measuring Station and their IDs

3.2.3 Bathymetric Data

One of the most important part of this study was to observe the change pattern of the bathymetry. Therefore, the bathymetric data of the Jamuna river was collected in FRERMIP project on the year 2016, 2017, 2018 and 2019. These data were used in building up the numerical model. This data was of finer resolution which were able to capture the submarine fan and their movement over these years.

The following Figure 3-3 represents the raw bathymetry data of selected reach of the river in 2017. The bathymetry of 2016 to 2019 have also been collected. The analysis of these data were helpful in understanding the morphological change of Jamuna river.
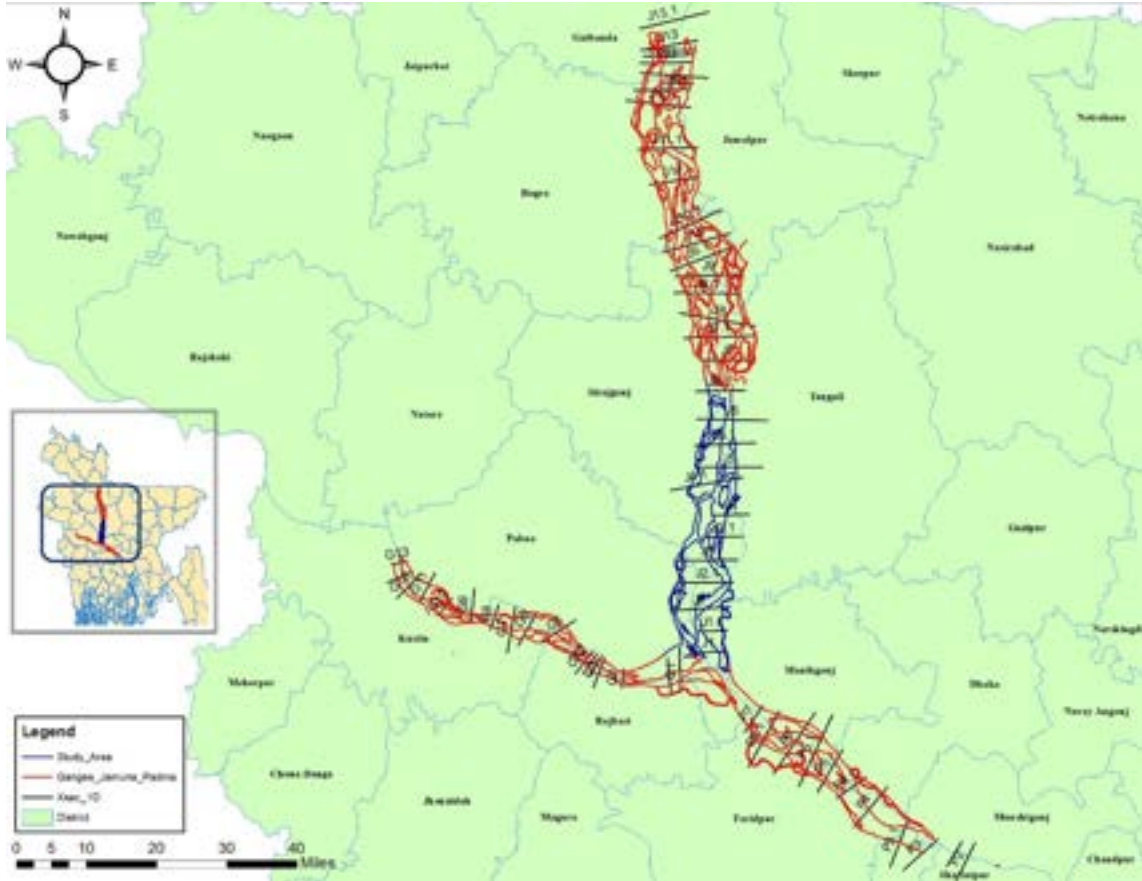
Figure 3.2 Cross section Measuring Station and their IDs

3.2.4 Primary Data

Hydrographic survey was conducted in a selected region to obtain high resolution bathymetry data in the pre and post-monsoon of 2019. A reputed survey company was employed in this regard. Primarily, from the field visit made, location for primary data collection is shown in Figure 3-4. The survey area is approximately 3 km wide and 6 km long.

3.3 Hydrological and morphological data analysis

Historical hydrological data (i.e., water level, discharges) has been analyzed to understand the variation of these data. Maximum, minimum or median water level, discharge was derived from those collected data for different time period. Correlation of these hydrological data with the bed level changes and the bank changes for different periods has been looked at. Before proceeding to analyze the water level, discharge, cross-section and bathymetric data, quality check of the collected data was done.

Figure 3.3 Bathymetric Data of the Jamuna river (2017)
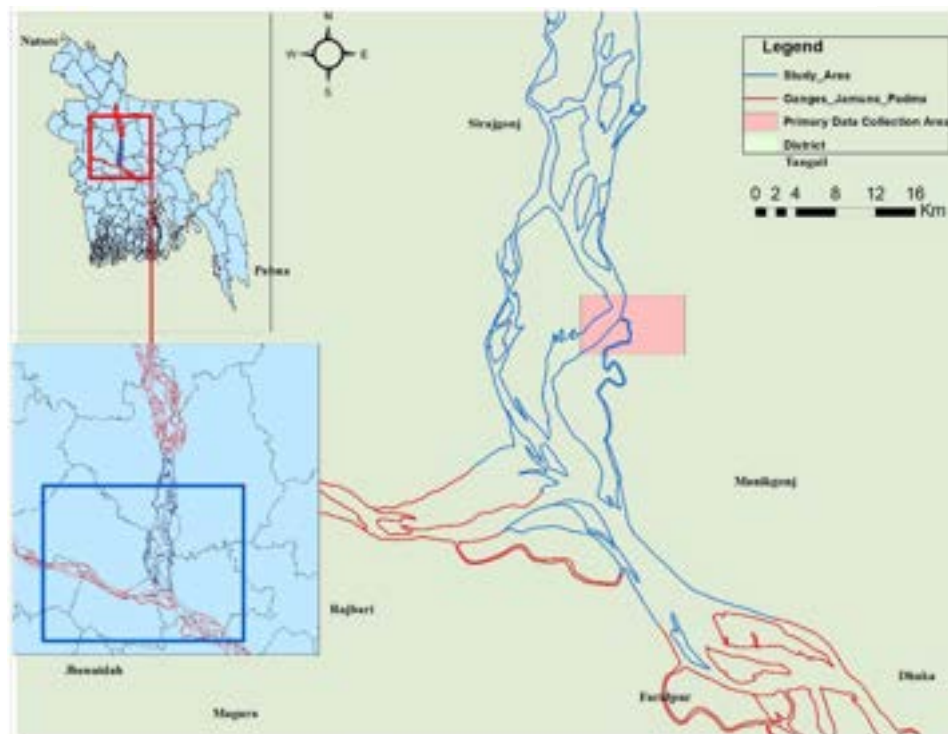
Figure 3.4 Selected area of Primary Data Collection

Changes at different cross-sections and longitudinal profiles have been studied using the bathymetric data from FRERMIP project. In addition, changes in bathymetry of the primary data, which are high resolution data, has been done to understand the morphological changes. This analysis was made to understand the general river dynamics of the study area. Correlation of these changes with hydrologic data or planform changes has been made to understand the morphological behavior of the study area.

River bank lines have been delineated using the historical LANDSAT satellite images with the help of GIS software, QGIS. All banklines have been superimposed to understand the changes of banks and to identify erosion prone area. Correlation of these changes with hydrologic data and bathymetric changes has been made to understand the morphological behavior of the study area.

Results of hydrological and morphological analysis are given in Chapter 4.

3.4 Development of 2D Hydrodynamic and Morphological Model

For developing 2D hydrodynamic and morphological model a depth average SRH-2D model were used. The extent of this model started from just downstream of the Bangbandhu Multipurpose Bridge to 15 km upstream of the confluence of the river Jamuna and Ganges. The bathymetric data collected from FRERMIP project of the year 2018 and 2019 were used in developing this model. To get boundary conditions for 2D model, a 1D hydrodynamic model also has been developed stretching from Bahadurabad station to the confluence of the Ganges and Jamuna.

After simulating the hydrodynamic part, it was calibrated using the historical water level data. Then the morphological model was developed and calibrated and validated using the historical cross section data. 2D model will give an insight of the capabilities of numerical models to predict morphological process in braided river. Process of model development and Results of Mathematical modeling are presented in Chapter 5.

3.5 Deep Learning Model

In the preliminary investigation into machine learning approach to solve river bank erosion prediction problem, it was found that some specific neural network configuration will yield the desirable learning and corresponding results. The past works, mentioned in section 2.4.5 on sequence to sequence learning architectures, were used as inspiration to build the layers and fine tune the neural network. For deep learning approach, methodology starts with all the relevant data source identification and collection required to complete the study.

3.5.1 Data Source

The preferred way to download satellite images was chosen to be through the use of Google Earth Engine, as it had the ability for batch downloading and desired modifications with region selection capabilities. An account was requested for sign up from the https://earthengine.google.com/ site. It took about 3-4 days to get the access to the services

required for downloading images. A brief introduction to google earth engine is presented below.

Google earth engine

Google Earth Engine is a cloud computing platform for processing satellite imagery and other geospatial and observation data. It provides access to a large database of satellite imagery and the computational power needed to analyze those images. Google Earth Engine allows observation of dynamic changes in agriculture, natural resources, and climate using geospatial data from the Landsat satellite program, which passes over the same places on the Earth every sixteen days. Google Earth Engine has become a platform that makes Landsat and Sentinel-2 data easily accessible to researchers in collaboration with the Google Cloud Storage. The Google Earth Engine provides a data catalog along with computers for analysis; this allows scientists to collaborate using data, algorithms, and visualizations. The platform uses Python and Javascript application programming interfaces for making requests to the servers.

Initial applications of the engine have included mapping the forests of Mexico, identifying water in the Congo basin, and detecting deforestation in the Amazon rainforest. Using the Google Earth Engine to track global forest loss or gain, the University of Maryland reported an overall loss in global forest cover. The Carnegie Institute for Science's CLASlite system and Imazon's Sisteme de Alerta de Deforesation (SAD) are two institutions that partnered with Google in the development of Google Earth Engine. Both organizations use the program to build maps of forests that measure environmental disturbances. Additionally, Google Earth Engine has been expanded to further applications. These range from: Tiger Habitat Monitoring, Malaria Risk Mapping and Global Surface Water. These previous studies confirm Google Earth Engine as an authentic and contemporary source for satellite images. After downloading satellite images, the image properties and metadata were observed for future referencing.

Image Properties

Our initial investigation into image properties tells us that each image is composed of a total of $1500 \times 2500 = 3750000$ pixels. Each of these pixels represents a value between 0 and 255.

The image properties in *.tiff* format were:

- Dimensions: 1500×2500
- Width: 1500 pixels
- Height: 2500 pixels
- Horizontal resolution: 96 dpi
- Vertical resolution: 96 dpi
- Compression: LZW

A total of 267 images from Landsat 5 (8 days' interval), 225 images from Landsat 5 (32 days' interval), 295 images from Landsat 7 (8 days' interval), 182 images from Landsat 7 (32 days' interval), 64 images from Landsat 8 (8 days' interval), 49 images from Landsat 8 (32 days' interval) will be downloaded. So, a total of 1082 images will be download.

3.5.2 Data Preprocessing

After data collection follows data preprocessing. It involves all the necessary transformations which is required for converting raw data into model ready format so that we can start training the model. We will be looking into the satellite images from various point of preprocessing. In each stage all the metadata regarding the transformations as well as image properties before and after will be kept for future referencing and paper publishing. The tools used for data preprocessing will be discussed first.

Tensorflow Deep Learning Framework

TensorFlow is an open-source software library for dataflow programming across a range of tasks. It is a symbolic math library, and is also used for machine learning applications such as neural networks. It is used for both research and production at Google, often replacing its closed-source predecessor, DistBelief. TensorFlow was developed by the Google Brain team for internal Google use. It was released under the Apache 2.0 open source license on November 9, 2015.

Python Programming Language

Python is an interpreted high-level programming language for general-purpose programming. Created by Guido van Rossum and first released in 1991, Python has a design philosophy that emphasizes code readability, notably using significant whitespace. It provides constructs that enable clear programming on both small and large scales. Python features a dynamic type system and automatic memory management. It supports multiple programming paradigms, including object-oriented, imperative, functional and procedural, and has a large and comprehensive standard library. Python interpreters are available for many operating systems. CPython, the reference implementation of Python, is open source software and has a community-based development model, as do nearly all of Python's other implementations. Python and CPython are managed by the non-profit Python Software Foundation.

Numpy Library

NumPy is a library for the Python programming language, adding support for large, multi-dimensional arrays and matrices, along with a large collection of high-level mathematical functions to operate on these arrays. The ancestor of NumPy, Numeric, was originally created by Jim Hugunin with contributions from several other developers. In 2005, Travis Oliphant created NumPy by incorporating features of the competing Numarray into Numeric, with extensive modifications. NumPy is open-source software and has many contributors.

Opencv Library

OpenCV (Open Source Computer Vision) is a library of programming functions mainly aimed at real-time computer vision. Originally developed by Intel, it was later supported by Willow Garage then Itseez (which was later acquired by Intel). The library is cross-platform and free for use under the open-source BSD license. OpenCV supports the deep learning frameworks TensorFlow, Torch/PyTorch and Caffe.

The stages of data preprocessing that we have decided upon from initial investigation is discussed in the following sections.

Data Categorization

Data preprocessing starts with proper categorization of all the raw data. Due to an instrument failure of Landsat 7 satellite, some invalid black pixel regions were generated in the satellite images. The corrupted regions are called SLC-off data gaps and we will be addressing this problem. The necessary SLC-off data gaps will be inapainted first and then will be used in the training data for bank erosion prediction model. All of the original images (1082 images) will be filtered and surveyed manually in order to get a reasonable dataset in which there will at least be one image representing every month beginning from 17-11-1987 to 04-07-2017. Because of excessive cloud covering during June, July, August and September it will most likely not be possible to ensure one image per month policy. The prepared final dataset of images will be batch converted to JPEG 12 quality images using Adobe Photoshop. The resolution and noise level of the converted images will be manually checked in order to ensure the quality. Any other JPEG quality format is likely to cause unwanted transformation of the images and introduce unnecessary noise.

There will be about 456 images (.jpg format) in the final filtered dataset after categorization and conversion. There will be about 298 completely valid images (images with no invalid or overlapping regions). Initial analysis showed there were 98 SLC-off images among the 456 images. A total of about 456 images dataset, along with the final inpainted images, will be used for the bank erosion prediction task.
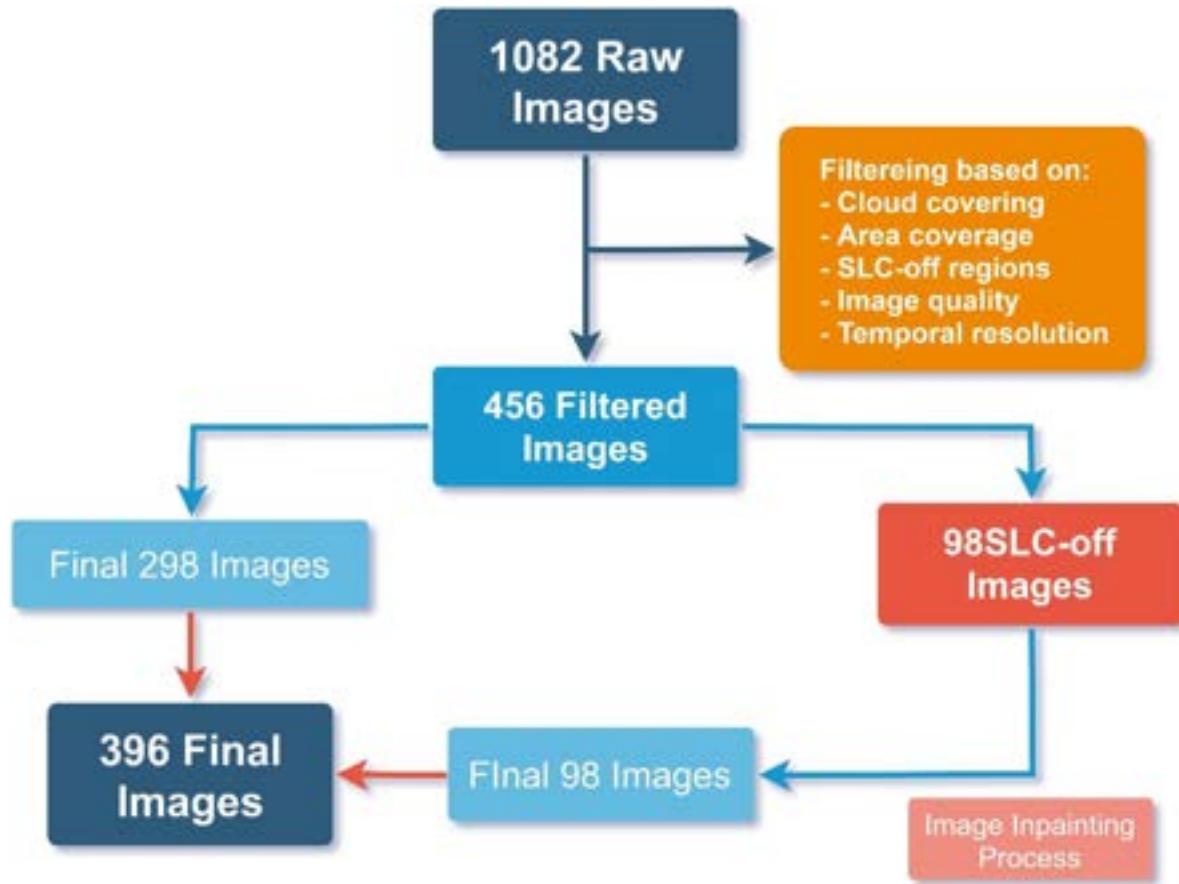
Figure 3.5 Data categorization flow chart

Image cropping

Most space of the full resolution images contain unnecessary information for our bank erosion prediction task. There are a lot of land away from the riverbank lines, which do not provide information necessary for bank erosion prediction task. Also, the full resolution images cannot be used for training purposes for several reasons. Firstly, the required neural network for full resolution images will need to be very complex with a lot of learnable parameters. Secondly, the huge network will not fit into the available GPU bandwidth. Thirdly, there will only be 298 images for training purposes and it is known that neural networks work best when there are a lot of training data. So, taking all of these into account it was decided that the images will be cropped into 256×256 resolution smaller segments and they will be used for training the models.

Handle Missing Values

In order to fill the missing values for the case of the full resolution images, the average will be taken. For the missing months, the average pixel value of the closest months, which will have all valid pixels, will be taken. If it was not possible to get the average from the closest images, then the closest image will be used for that month. In this manner the whole images will be generated and filled in for the missing months.

We also noticed cases of missing segments. This meant that there were images that had black invalid pixel regions and also, there were clouded portions of images that had to be fixed. In order to deal with these two problems, first the full resolution images will be cropped according to previously described manner in order to get rectangles. This way each of the six months will have folders for the corresponding segments/reaches.

Our findings also indicate that unique modification to the LSTM cell of the neural networks, will allow us to handle missing values without manual effort or taking the average as discussed above. We should be able to incorporate time stamp information into each image so that the network knows to which time any particular image belongs to. This incorporation scheme will be one of our main focuses in modifying the deep learning model to our specific use case and will be experimented with for the best accuracy.

After, cropping and handling all the missing values, the cropped images will be ready to be fed as input for the neural network. The complete data preprocessing steps are depicted in Figure 3-5.

3.5.3 Model Architecture

In this section, the architecture for predicting next year bank erosion conditions using historical observation datasets will be discussed. A basic Seq2Seq architecture that consists of two RNNs using an encoder-decoder framework will be used. Both the encoder and the decoder will use a five-layer convolution operation to extract rich features or restore encoded information for deconvolution operations. As convolutional filter weights of the encoder and the decoder can be repeatedly utilized, the encoder and the decoder must be able to save and restore their parameters within a scope of Seq2Seq memory networks because the model will not be restricted to a specific number of input and output sequences. The suggested model will therefore be used for flexible input/output configurations. However, a fixed time gap between each data instance (e.g., 1-year or 1-month gap per input) is suggested to achieve better prediction results.

To achieve better feature extraction from the spatial data space, convolutional LSTM cells will be introduced into both the encoder and the decoder. Further, an auxiliary link in the image regeneration step will be implemented—a symmetric skip connection from the convolutional encoder into the deconvolutional decoder—for better image restoration.

The neural network will be designed as a UNet-like architecture with ConvLSTM blocks in the middle of the network. The input images will be of 256×256 resolution. ReLU will be used

in the encoding stage and LeakyReLU with alpha = 0.2 will be used between all decoding layers except for the last decoding layer. For the last decoding layer sigmoid activation will be used. No batch normalization layers will be used. The encoder will comprise of five convolutional layers with all layers having stride=2. The kernel sizes will be 3, 3, 3, 3 and 3. The channel sizes will be 4, 8, 16, 32, 64 and 80. The decoder will include five deconvolutional layer. The output channel for convolutional layers in the decoder will be 64, 32, 16, 8 and 1. The skip links will feed the decoder stage and concatenate the feature maps channel-wise before being considered as input to the next convolution layer.
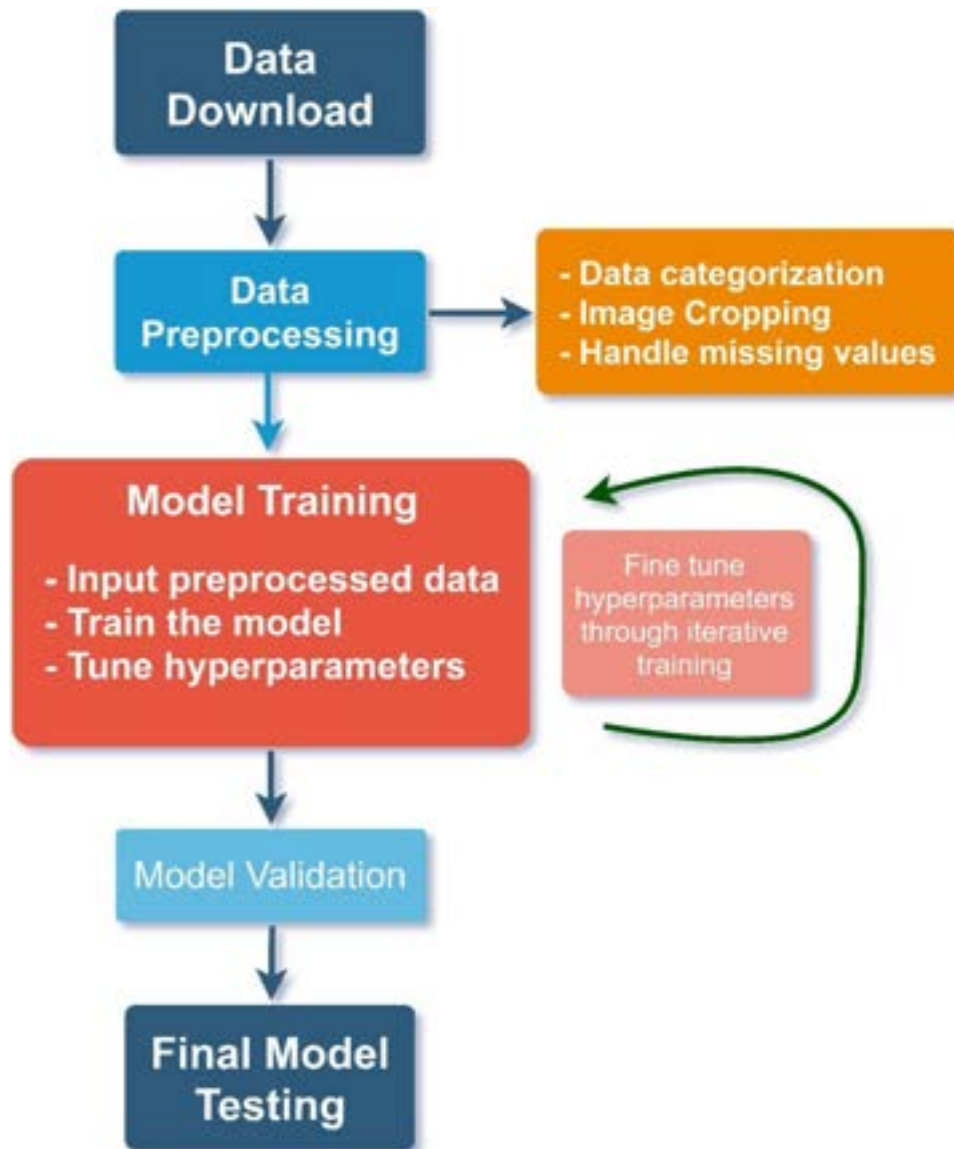

Figure 3.6 Methodology of Deep Learning Technique

We will perform model training from three different perspectives. Firstly, only the satellite images will be used to make the predictions of future river bank conditions. Then other data such as water level, discharge and cross-section data will be incorporated so that the model can further integrate the new data to better it's prediction. Thirdly, the input data per instance of training will be experimented with. This means we will first set one year input data to get output of one year into the future, then further experiment with 12 months' images as input and predict one or two years into the future. All of these different configurations will allow us to base our final result on the best possible output. This will ensure proper investigation into the research problem. The steps of deep learning methodology is depicted in Figure 3-6.

3.6 Development of River Bank Erosion Prediction Tool

A river bank erosion prediction tool will be developed using the results from deep learning algorithm and numerical model. This tool will have the neural network graph along with the necessary weights in the backend of the software and in the frontend there will be an intuitively understood GUI for the customers to interact with the model.
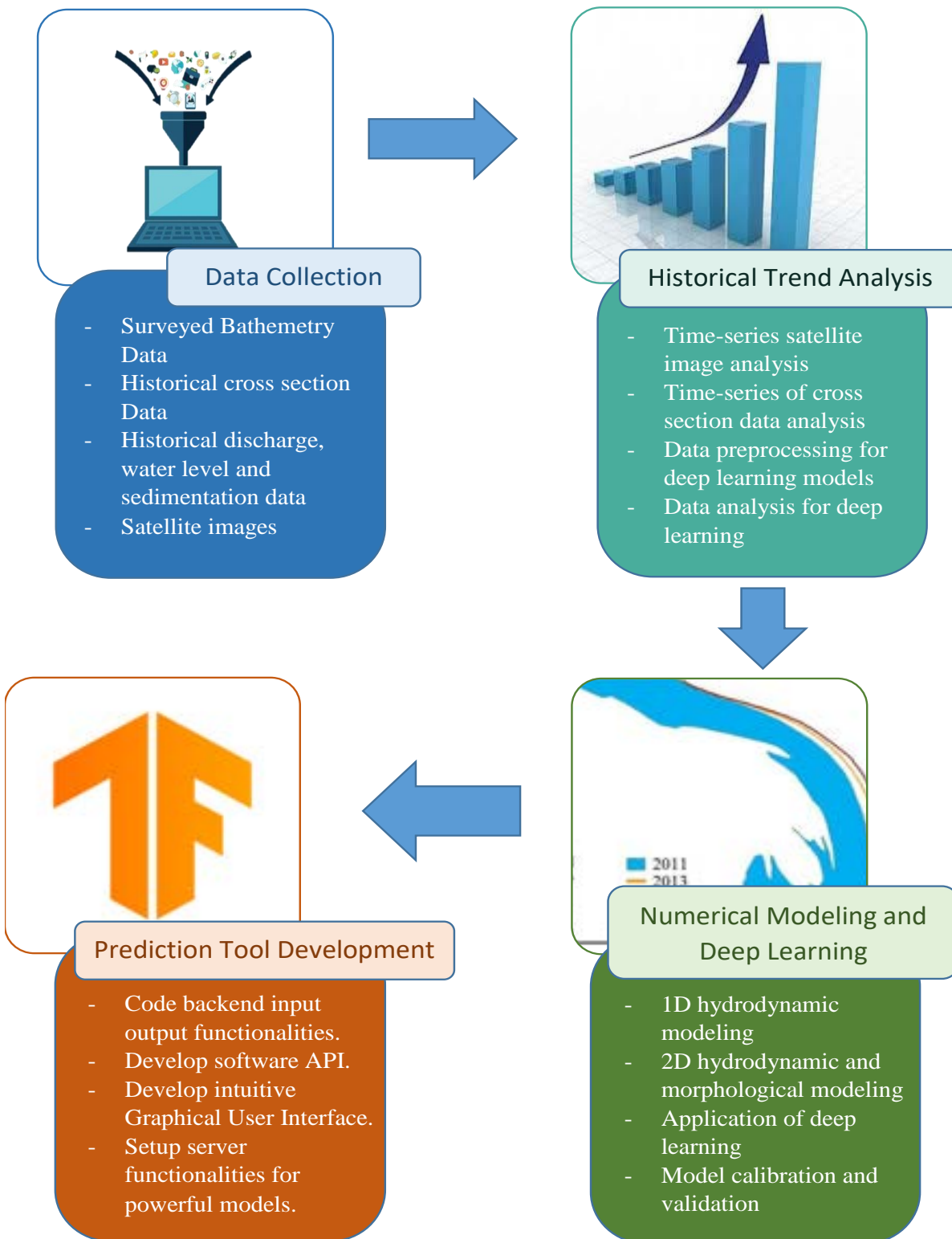
Some of the functionalities of the software will include the rapid input capabilities where the users will be able to input recent satellite images or call satellite images using the backend Planet API. This feature will allow the users to view future bank erosion changes in RGB high resolution image format. Another feature will allow the users to input the data from other sources so that the prediction could be improved. There will be options to tune the hyper parameters of the neural network so that calibration can be performed based on recent ground truth data if required. There will also be an option to further train the model based on the new data. This training feature will have to be carried out using a GPU. The neural network models do not support CPU based computations. The training will allow the model to adjust its prediction based on recent data. The ability to use other machine learning models will also be incorporated for analysis. The ability to generate graphs based on the output will also help users better understand the future scenario of bank erosion.

3.7 Summary of methodology:

The research methodology has begun with collection of data from all the secondary sources. First of all, quality of check of the collected data will be done to ensure no incorrect data is used in this study. After ensuring the quality of the data, those data will be analyzed carefully to interpret the hydrology and eventually the morphology of the study area. The study area consisting of 60 km reach of the Jamuna river will be extended to Bahadurabad, Hardinge Bridge and Mawa in Jamuna, Ganges, Padma reach respectively to develop a preliminary 1D hydrodynamic model using HEC-RAS. The result of this model will be used as boundary condition in the 2D Hydromorphological using SRH-2D. The LANDSAT images will be used to determine erosion and deposition over the year and most importantly these images will be used as input in the deep learning model. Images of previous years or months will be given as input for each instance of sample and an output image one year into the future of the same reach will be generated by the model. This predicted new image will show the new banklines,

which will help to identify areas of interest where erosion might occur next year. To improve image prediction accuracy of the model, several hydrodynamic parameters will also be included as input for the neural network. For this, flow information will be included into the deep learning model and later on, local hydrodynamic information such as local velocity will also be incorporated. These three scenarios will then be analyzed to reach the highest possible accuracy given the data.

The following flow diagram represents the full methodology in a nutshell.

Data Collection

- Surveyed Bathemetry Data
- Historical cross section Data
- Historical discharge, water level and sedimentation data
- Satellite images

Historical Trend Analysis

- Time-series satellite image analysis
- Time-series of cross section data analysis
- Data preprocessing for deep learning models
- Data analysis for deep learning

Prediction Tool Development

- Code backend input output functionalities.
- Develop software API.
- Develop intuitive Graphical User Interface.
- Setup server functionalities for powerful models.

Numerical Modeling and Deep Learning

- 1D hydrodynamic modeling
- 2D hydrodynamic and morphological modeling
- Application of deep learning
- Model calibration and validation

Chapter 4: Hydrological and Morphological Analysis

4.1 Introduction

The Jamuna being one of the largest braided river of the world it continuously increasing its width thus erosion on the bank. The study area of this research starts from the downstream of the Bangabandhu Multipurpose Bridge to 15 km downstream of the confluence of the river Jamuna and Ganges (Figure 4-1). To simulate the bank erosion in this area numerical and deep learning model will be developed, thus a general river bank erosion prediction tool will be developed.

The upstream point is located on the Belkuchi Upazila of Sirajganj district on the right bank and Gopalpur Upazila, Tangail District on the left bank. The downstream point is situated in Harirampur, Manikganj.
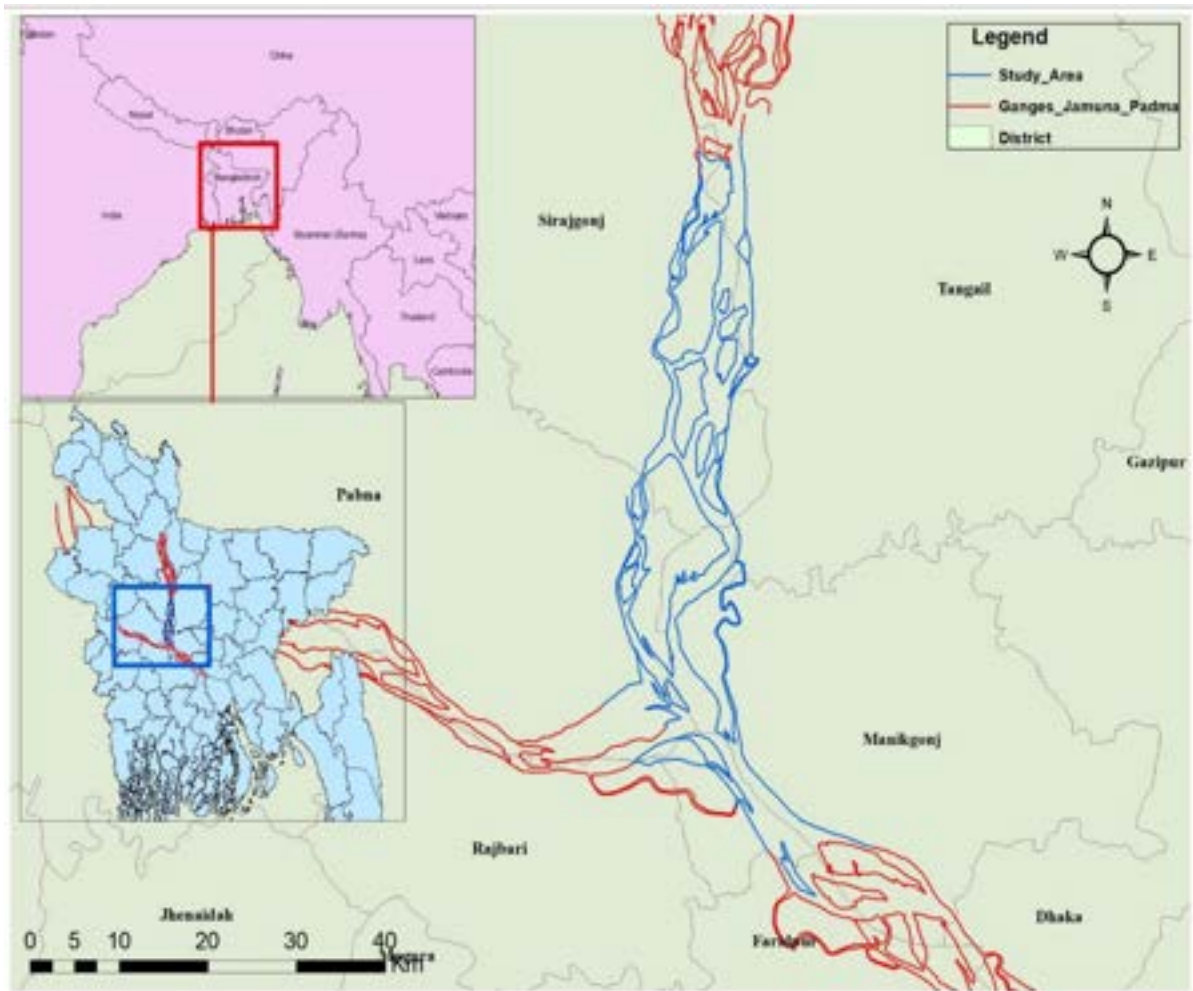

Figure 4.1 Study Area

4.2 Data collection

Both Secondary and primary data were collected through this research (e.g discharge, water level, bathymetry, cross section and satellite images). Secondary data were collected from different sources including (BWDB, WARPO, USGS). Bangladesh Water Development Board (BWDB) has water level, discharge and several cross-section measuring stations on different rivers. Historical LANDSAT imagery was collected from USGS website and Google Earth Engine. Primary data were collected through field survey at the selected region shown in (Figure 3-4).

Table 4-1 List of collected secondary and primary data for this study

Type of data	Data	Source	Station/Region	Time period
Secondary	Water level	BWDB/WARPO	Selected station	1976-2012
	Discharge	BWDB/WARPO	Selected station	1976-2012
	Cross section	BWDB/WARPO	Selected station	1972-2017
	Bathymetry	FRERMIP	Study area	2016-2018
	Satellite image (30x30m)	USGS/Google earth engine	Study area	1988-2019
Primary	Bathymetry	Field Survey	Survey region	2019

4.3 Hydrological characteristics of the study area

At Bahadurabad, the mean annual discharge is 20200 m3/s varying from a minimum dry season flow 2860 m3/s to 100 000 m3/s in the disastrous 1988 flood (EGIS, 1997; Best, 2007), and a record 102,500 m3/s in the 1998 flood (Chowdhury, 2000). The annual hydrograph shows a yearly change in water stage of approximately 6 m (FAP24, 1996a; Best, 2007). Flow velocities within the main channels are of concern in design considerations and depth-averaged velocities may reach over 3.5 m/s (FAP24, 1996c; Best, 2007). The average monthly discharge is highest in July and lowest in February. From November to April, discharge is relatively low ranging from 5000 to 6000 m3/s. Rapid increase in discharge are noticed during a flood, with the maximum increase of about 17,000 m3/s in 24 hours (June 7–8, 1990) and 24,000 m3/s in 48 hours (June 7–9, 1990) (Sarma, 2005).

From this study analysis, mean annual discharge was found to be around 17000 m^3/s. Maximum and minimum flood discharge was recorded as 102535 m^3/s and 3095 m^3/s respectively.

Table 4-2 Hydrologic summary of Bahadurabad and Mathura station

Sl no	Station Name	Station Id	Type of data	Max	Min	Average	St.dev
1	Bahadurabad	SW46.6L	Discharge (cumec)	102535	3095	17044	15936
			Water level (mPWD)	20.28	12.62	15.47	2.01
2	Mathura	SW50.3	Water level (mPWD)	11.90	2.55	6.03	2.50

4.4 Hydrologic data Analysis.

Hydrological analysis was required to find out the hydrological characteristics (i.e. peak discharge, high water level, low water level, time to peak etc.) of the study area. For the study area, its upstream and downstream stations were selected as SW46.9L (Bahadurabad transit) and SW50.3 Mathura respectively. Both discharge and water level were analyzed for the upstream (Bahadurabad) station and only water levels were plotted and analyzed for the downstream (Mathura) station in the following sections. Maximum, minimum, and average water level discharge were also derived from those collected data.

Water levels

The plotted water level hydrograph at Bahadurabad station and Mathura station are shown in Figure 4-2 and in Figure 4-4. Figure 4-2 shows historical water level at Bahadurabad station, historical maximum water level at this station was around 20.2 m and minimum were around 11 m. Figure 4-3 and 4-5 shows average stage hydrograph for Bahadurabad and Mathura station.
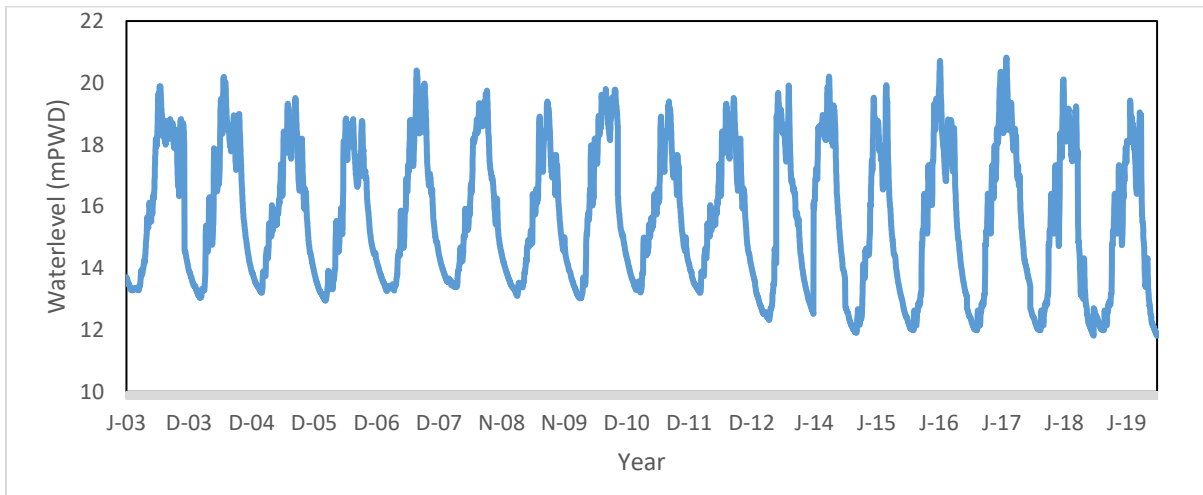

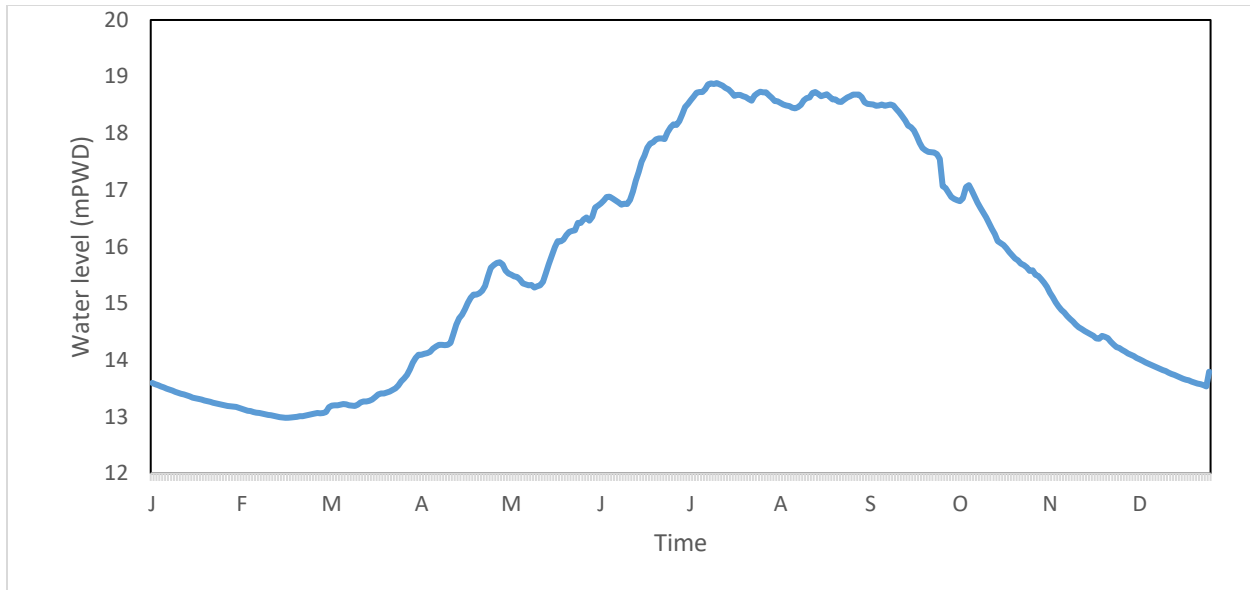Figure 4.2 Historical Waterlevel at Bahadurabad station

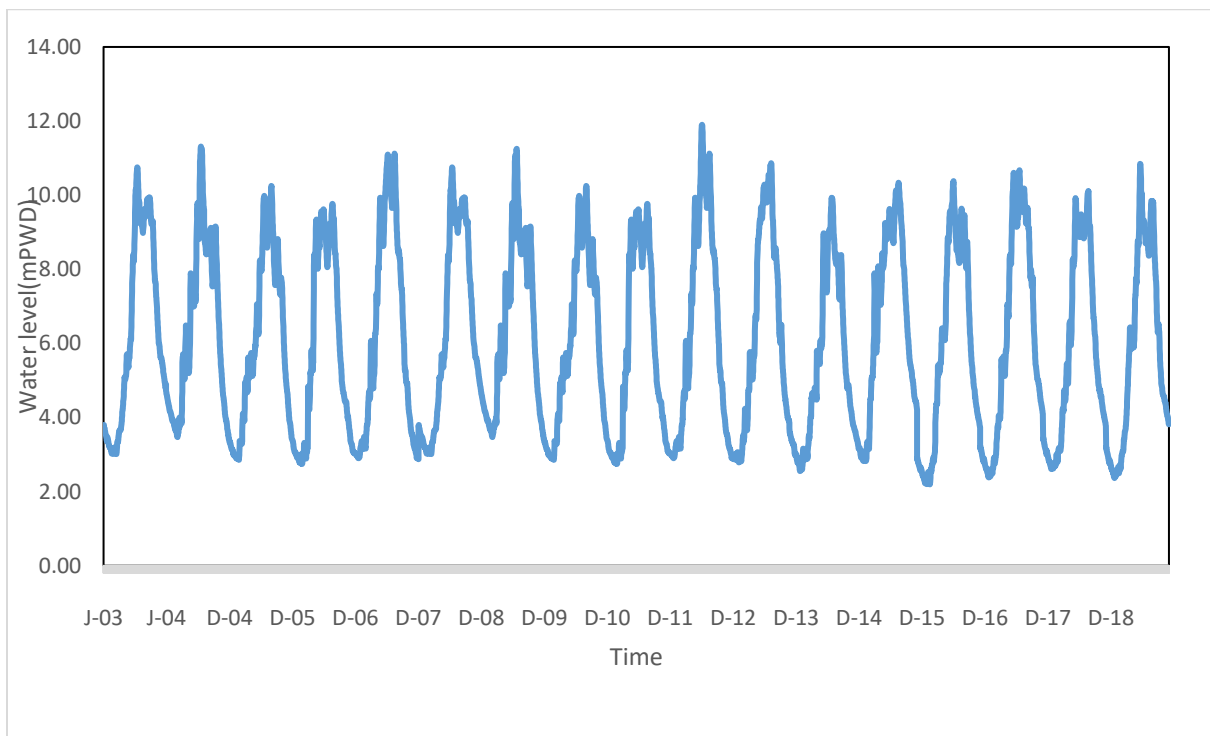Figure 4.3 Average stage hydrograph at Bahadurabad station

Figure 4.4 Histoprical water level hydrograph at Mathura station of Jamuna river
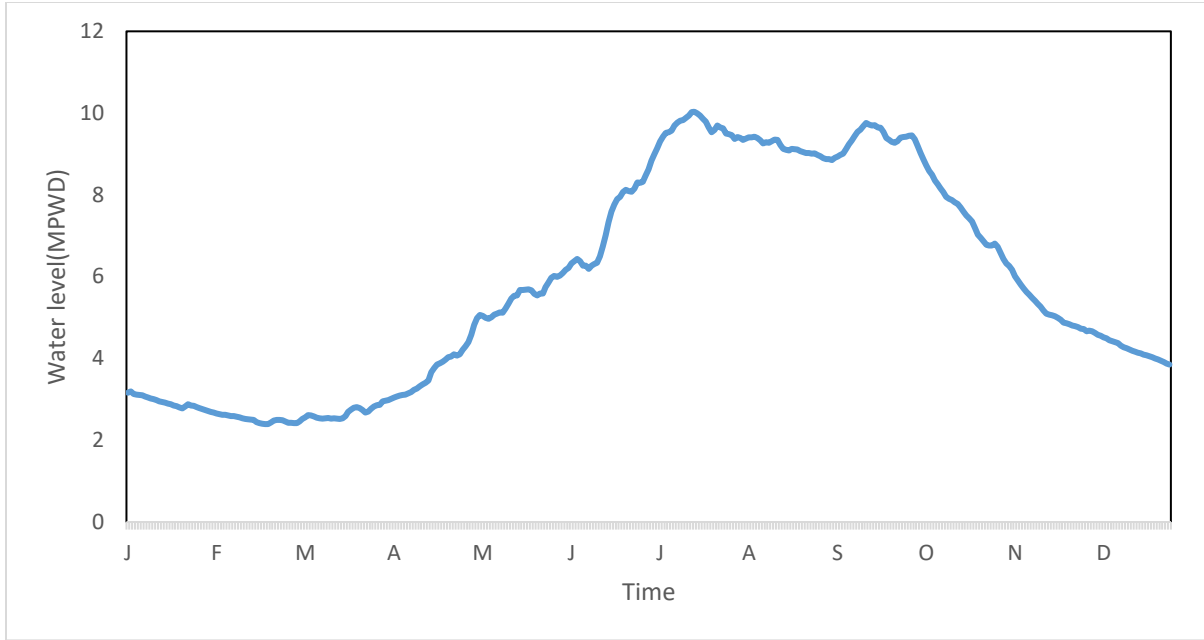
Figure 4.5 Stage hydrograph at Mathura station of Jamuna river

Discharge

Historical measured discharge data of Jamuna River at Bahadurabad station that were collected from BWDB and WARPO were analyzed and plotted in Figure 4-6. From this figure, the maximum (102535 cumec) and minimum discharges (39100 cumec) was detected for the years 1998 and 1994 respectively. From historical data it was observed that the Jamuna began rising in May-June and increased its flow gradually until the peak in July-August. Figure 4-7 shows average discharge hydrograph at Bahadurabad station.
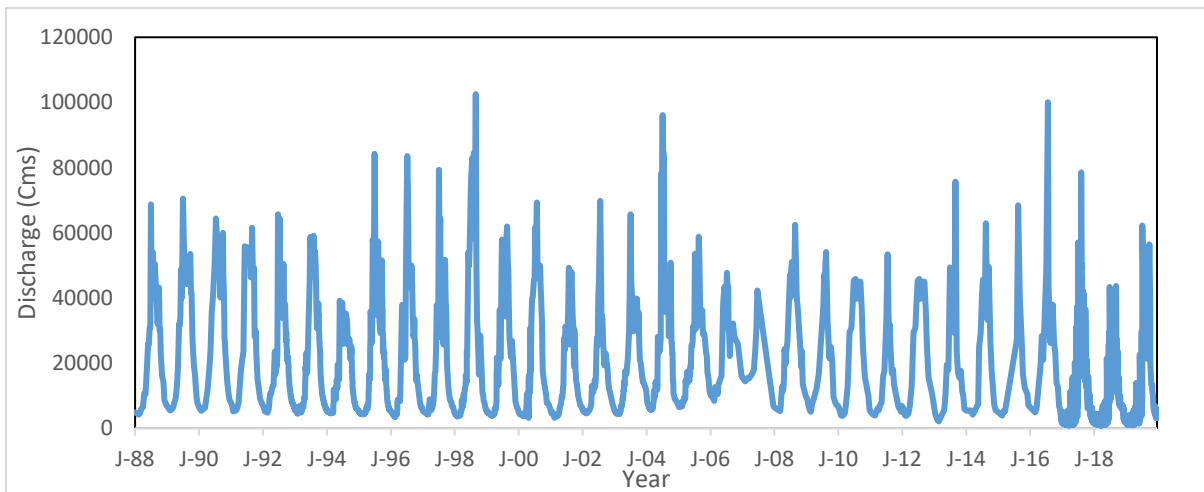

Figure 4.6 Historical Flood hydrograph at Bahadurabad station of Jamuna river
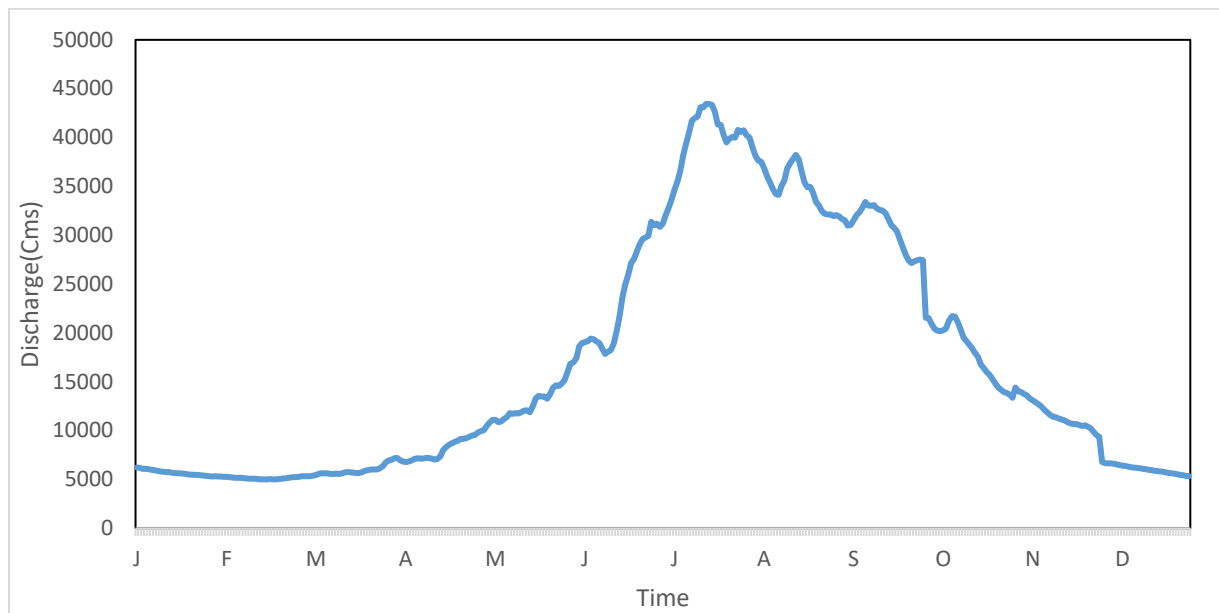
Figure 4.7 Average flood hydrograph at Bahadurabad station of Jamuna river

4.5 Morphological Characteristics of the study area

4.5.1 Dune Shape

Dunes cover 40–95% of the bed of the Jamuna River at all times (Jagers, 2003). Their height averages about 1 m and the average wavelength is about 37 m, the mean lee side angle is 9 degrees. The mean lee side angle is much smaller than the characteristic angle for general dunes which is in the order of 30–45 degrees. Dune migration rates between 1 and 17 m/h have been observed in the Jamuna River (Jagers, 2003). Within the category of dunes, sometimes, three further subgroups are distinguished, being -from small to large –mega ripples, (normal) dunes, and mega dunes or sand waves.

4.5.2 Material consisting the bank and bed

Though most of the flood plain sediments along the Jamuna River have been deposited by other rivers (before the major diversion early in the 19th century), their composition is similar to the sediment transported by the Jamuna River today. It mainly consists of fine sands and a generally small percentage of silt/clay which is characteristic for the very young and unweathered sedimentary rocks that make up the drainage basin of the Brahmaputra River. For this study sediment data was not collected and material size distribution was used as FAP24,1996)

Table 4-3 Grain size (mm) of bed material collected in 1993-1994 (FAP 24, 1996)

River	Gauging Station	D_{16}	D_{35}	D_{50}	D_{84}	D_{90}

Jamuna	Bahadurabad	0.13	0.16	0.22	0.29	0.34
Ganges	Hardinge Bridge	0.10	0.12	0.15	0.18	0.21
Padma	Baruria	0.10	0.12	0.14	0.18	0.22

The banks are in general made of 85% sand and 15% silt (diameter less than 0.063 mm) except for localized deposits that contain up to 55% silt and 35% clay. The sand fraction consists of 44% quartz, 18% rock fragments, 18% mica, 12% heavy minerals, and 8% feldspar (FAP, 1996). The bed material fines in downstream direction from 0.25 mm near the Indian border to 0.16 mm at the confluence with the Ganges River which transports a slightly finer load. The major part of the downstream fining is probably the result of abrasion of the relatively soft mica particles of which a large amount originates from the Teesta River (FAP24, 1996)

4.6 Planform Analysis

Planform Analysis along the Jamuna riverbank was performed by using the multispectral satellite images (LANDSAT) of dry season in ArcGIS using manual demarcation method. To calculate erosion and deposition, first of all 32 years of Jamuna riverbank line was digitized. Then bank line of every two consecutive years were compared (i.e. bank line of the year 1988 and 1989). Here, the bank line of earlier year was considered as a base line. And deviation of the later one would define whether it was erosion or deposition. In a scenario, where the line of the later year deviated outward from the main channel with respect to the base line it was considered as an erosion phenomenon. On the other hand, where the later year's line deviated to the main channel with respect to the base line it was considered as deposition.
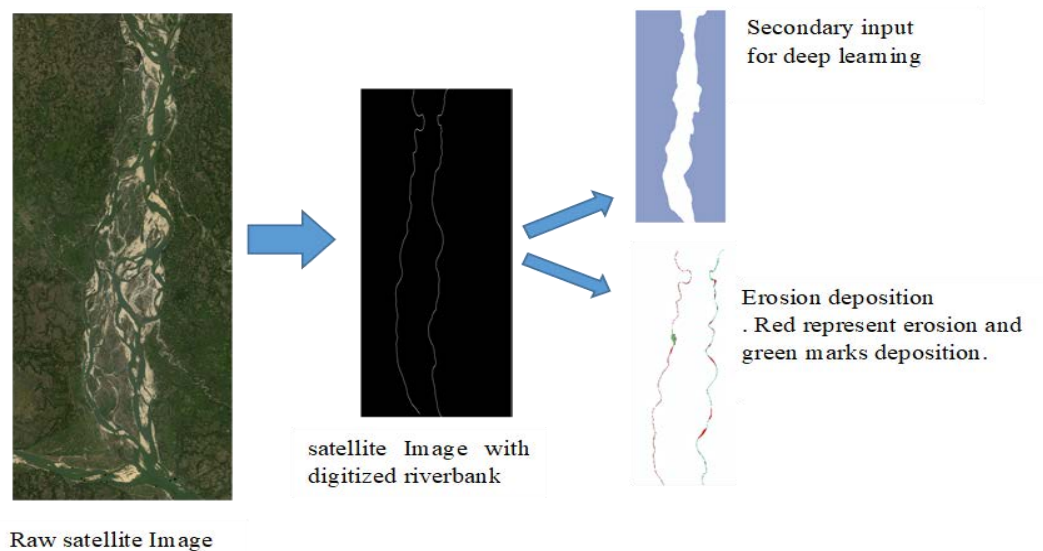

Figure 4.8 Planform Analysis process

4.6.1 Definition of River bank

Geo-referenced images have been used to delineate the banklines of the river. Banklines are generally well defined in meandering rivers, but the task is not straightforward with regard to very dynamic braided rivers. In delineating banklines for large rivers using satellite images, CEGIS followed the criteria developed by EGIS (1997) while carrying out a study on the morpho-dynamics of the Brahmaputra-Jamuna River. In brief, the criteria for bank line delineation are: the bank line should separate the floodplain from the riverbed; all sand bodies except crevasse splays (coarse sediments that are spread over floodplains during floods by overtopping the banks) should be considered as part of the riverbed; vegetated char land, bounded by flanking channels and the width of which is more than 100 m, should be considered as part of the riverbed as well. In this study the same procedure was followed to delineate Jamuna river bank lines.

4.6.2 Limitation Defining River Bank

Braided river systems exhibit strong unsteadiness in flow field and sediment transport. An equilibrium configuration of the system does not seem to exist, rather a recursive process of formation and obliteration of bed forms and planimetric structures is always observed. Braided systems are subjected by strong n on-linearity. The interactions between free responses of the system (due to an inherent instability of free surface turbulent flow over an erodible bed) and forced responses (induced by physical constraints, such as curvature, width variations, confluences) crucially affect the topographic behavior of the network.
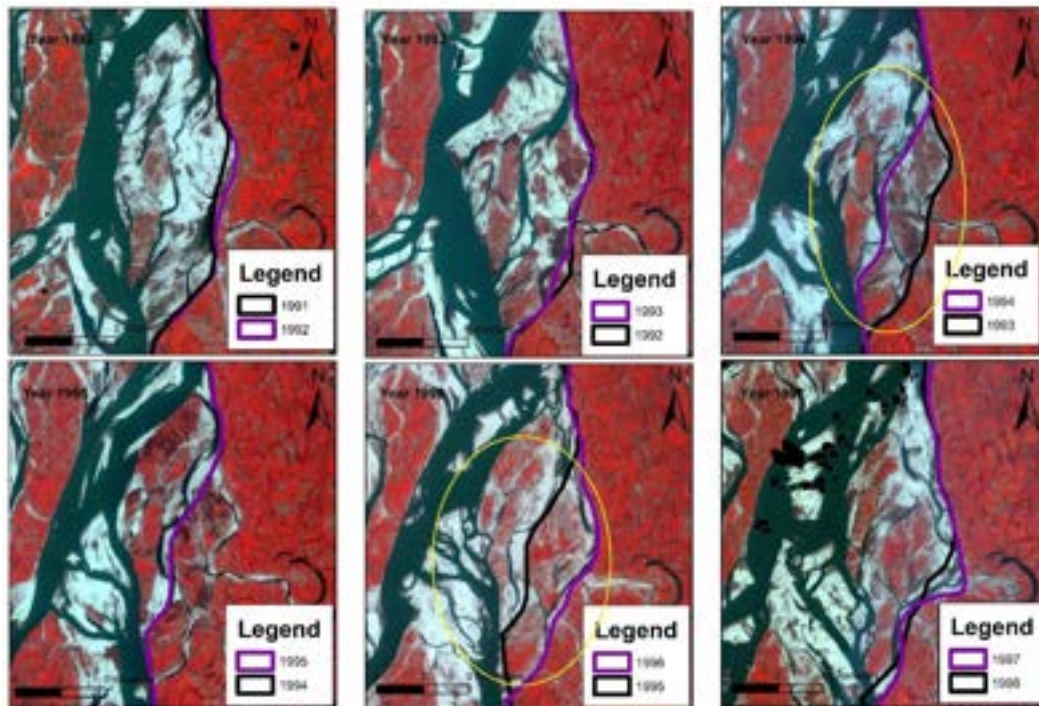

Figure 4.9 Channel migration in braided river-Jamuna

It was very challenging to identify river bank at some point of the reach. For an example in the left bank near Dhaleshwari river offtake exists two or more minor channels. These channels vary in size and changes their path very frequently. Moreover, in the year 1994 and 1995 the secondary channel changes its course as well as shifts the river bank line (marked in yellow circle).As one very important objective of this study is to predict erosion of river bank it was very important to identify single bank line. In this case if the left most, channel was identified as river bank in deep learning technique it would give a false indication of river bank line to the Ai model.
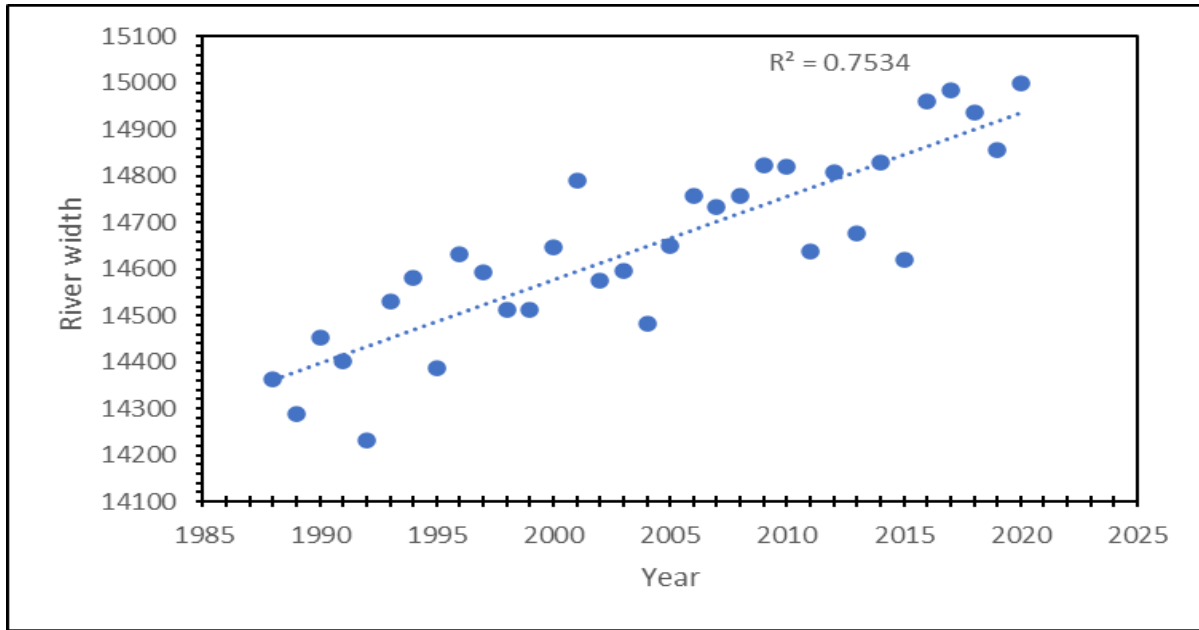

Figure 4.10 Average width of Jamuna river.

4.6.3 Changes in river spatial characteristics

The change in average river width over time is shown in Figure 4-10, Though there is a minor variation in water level and moderately high variation in discharge for different stations of the river, the river exhibits a growing trend in its width. Since the early 1980s, the Jamuna River in this study area widened from 14.2 km to 15 km in the 2020 and now the average width is 14.69 km. Figure 4-10 shows westward migration and width change of Jamuna river with at various time line.

4.6.4 Erosion Deposition

Erosion deposition was calculated for each year but for better visual interpretation Figure 4-11 and Figure 4-12 shows erosion deposition in five years interval. From 1988 to 2019, total erosion along the Jamuna river left bank was 23800 ha with an average of 770 ha per year.

Whereas for the right bank of the river total erosion was 11840 ha and 380 ha per year. It was evident from the data that erosion rate was higher for left bank of the Jamuna river (Figure 4-13). Deposition during this period for left bank and right bank were 12920 ha and 7990 ha respectively. Maximum erosion of about 2550 ha had occurred in the year 1995-1996 and maximum deposition of about 1720 ha had occurred in the year 1988-1989.Figure 4-14 show total erosion and deposition of different year along Jamuna riverbank.
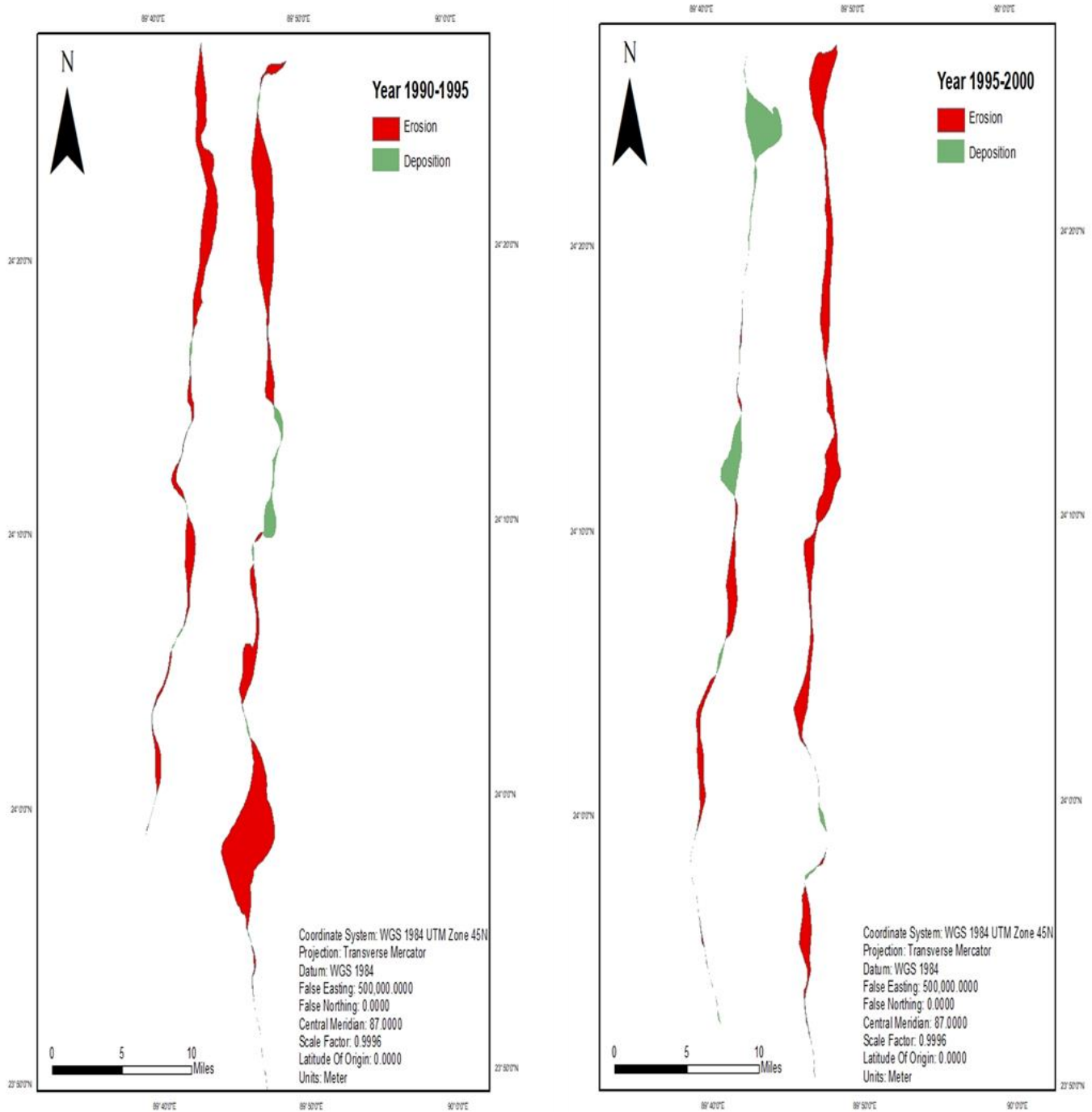
Figure 4.11Jamuna river erosion deposition during 1990-1995(Left) and 1995-2000(Right)
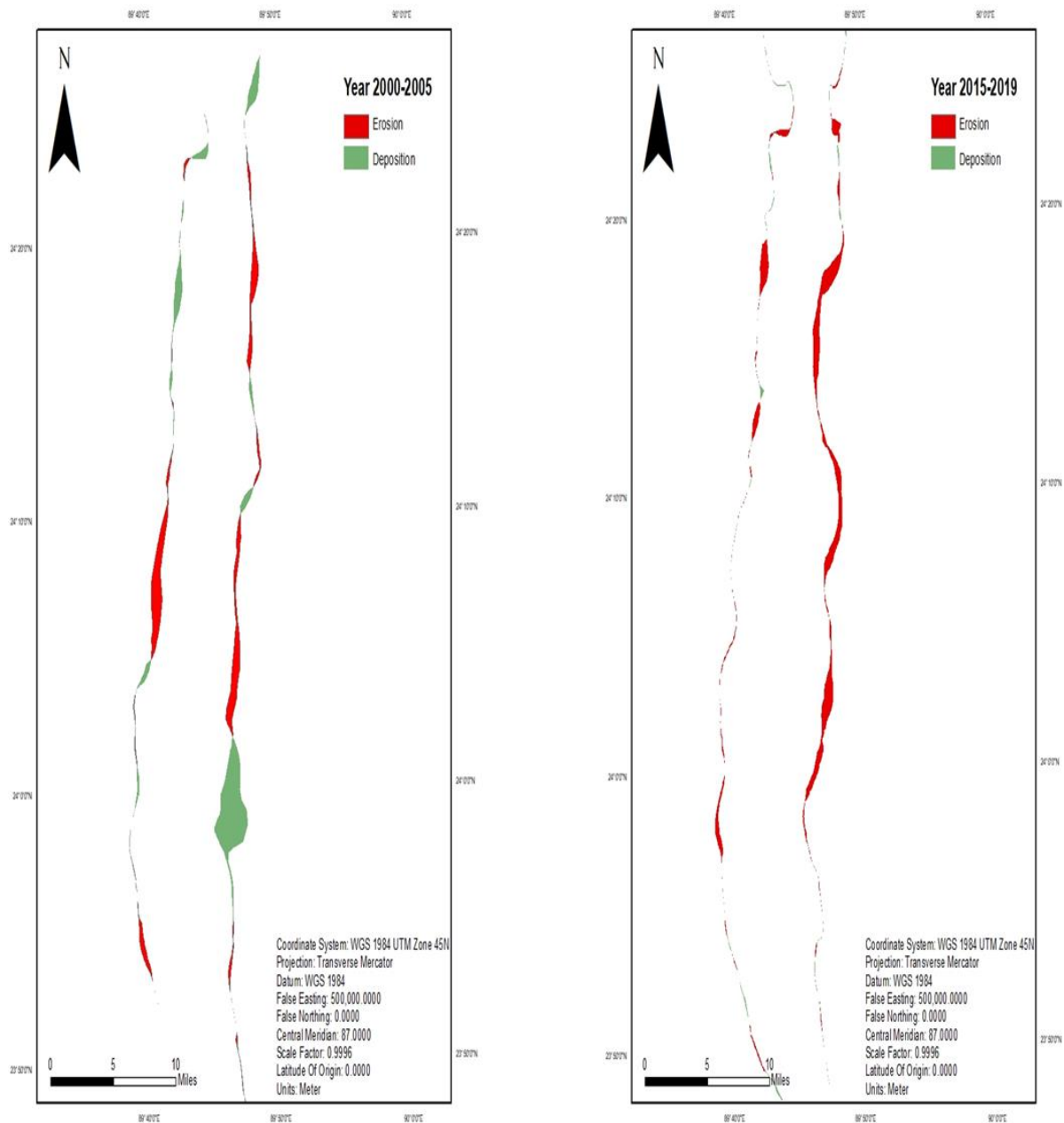
Figure 4.12 Jamuna river erosion deposition during 2000-2005(Left) and 2015-2019(Right)
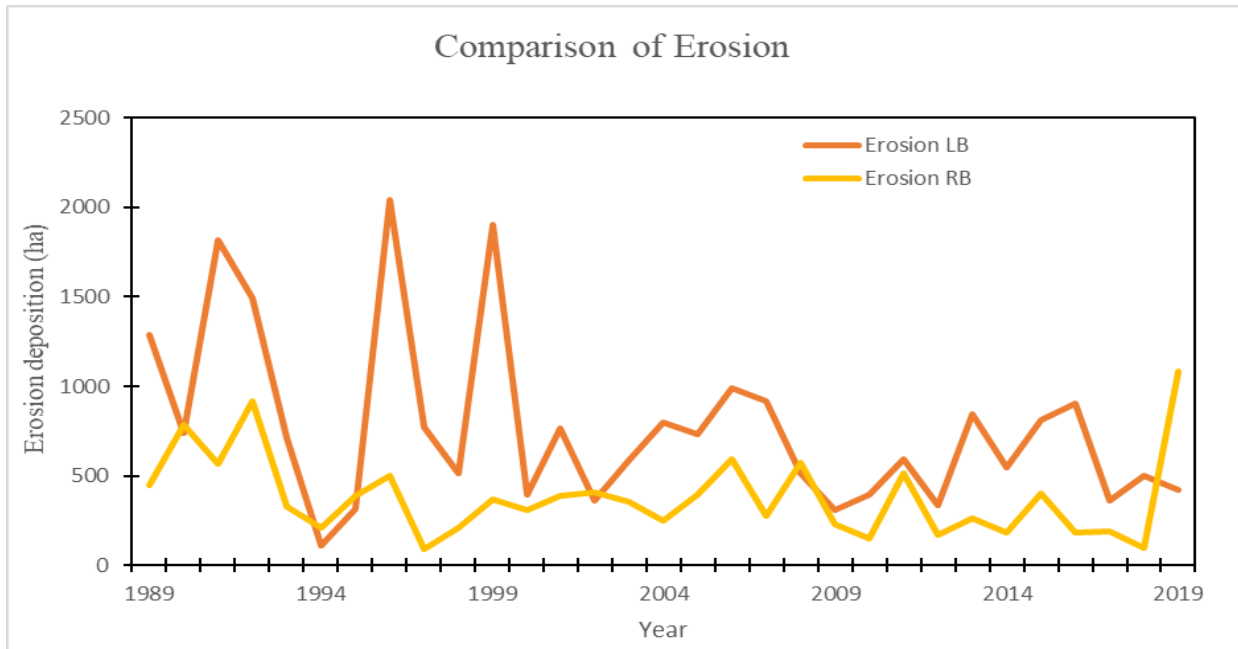
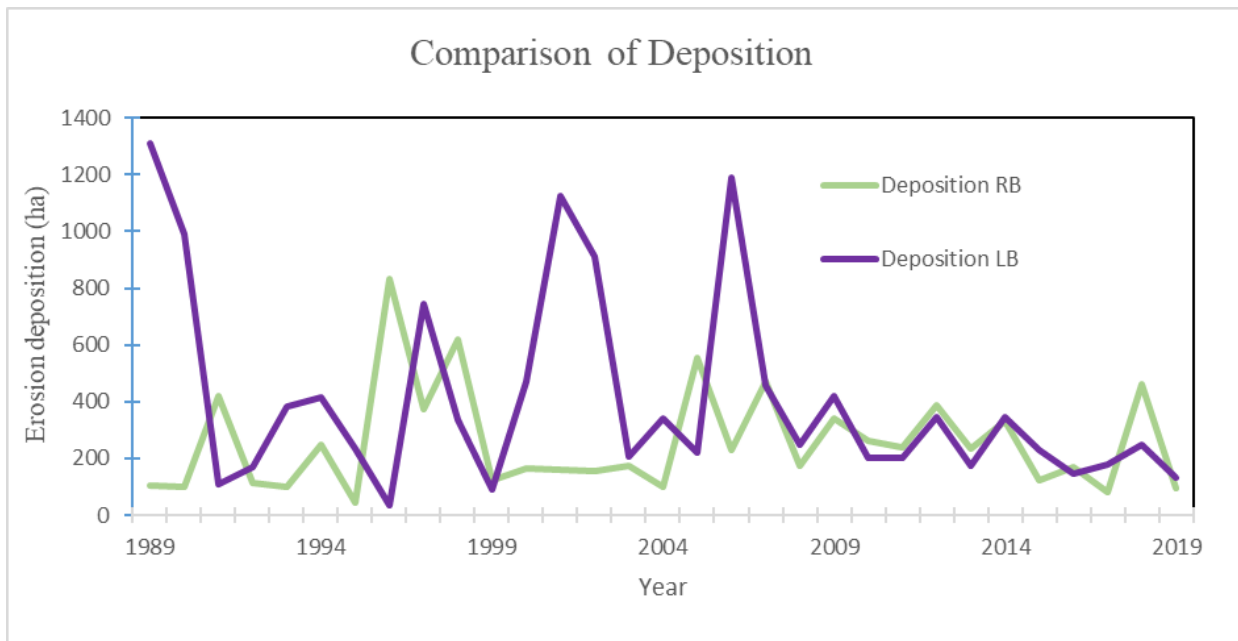Figure 4.13 Comparison of erosion between right bank and left bank of Jamuna river

Figure 4.14 Comparison of deposition between right bank and left bank of Jamuna river

4.6.5 Relation between Erosion and Flood

An attempt was made find out the relationship between peak discharge and riverbank erosion. Simple mathematical relationship has been established by plotting annual peak discharge (in

X-axis) and erosion (in Y-axis) in a graph. Future prediction of erosion has been carried out through calculation using relationship formulas for each of the rivers. It has been found that rate of riverbank erosion varies in decade-scale along the Jamuna. Sometimes variation may be naturally induced and/or sometimes it is induced by anthropogenic activities (such as installation of bank protection structures). It was observed from the figure that for peak discharge in the year 1996 and 1998, erosion was maximum (Figure 4-15). Figure 4-16 and Figure 4-17 show correlation between discharge, maximum water level and erosion.
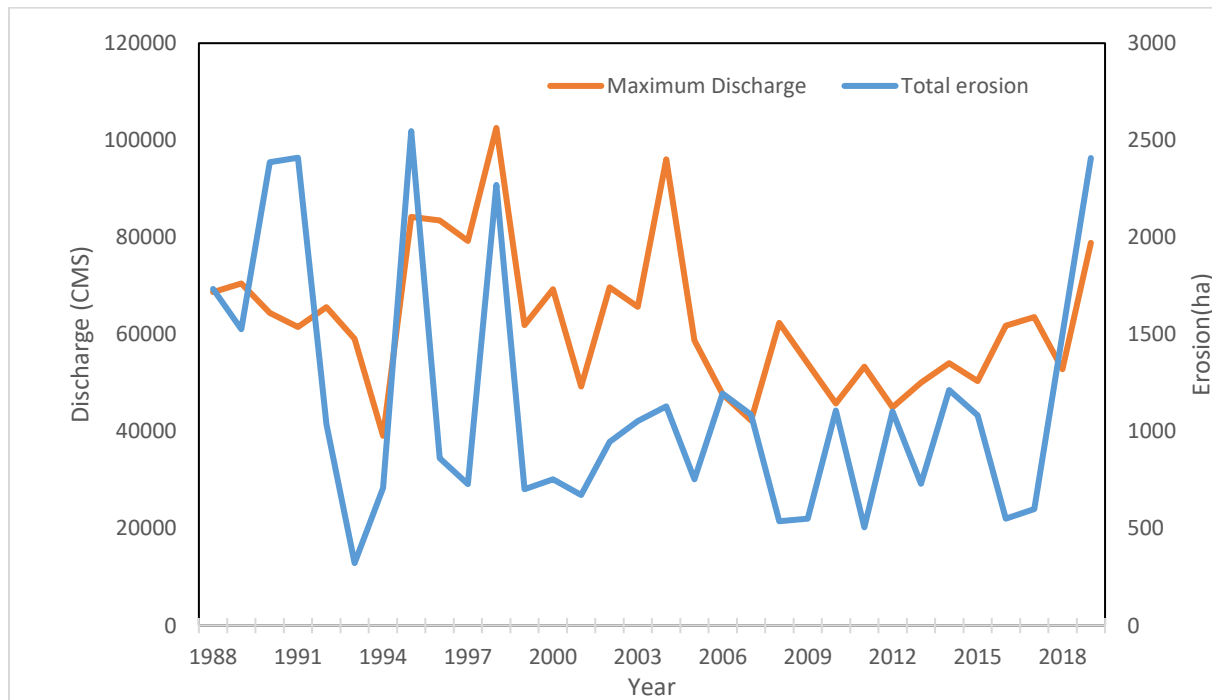

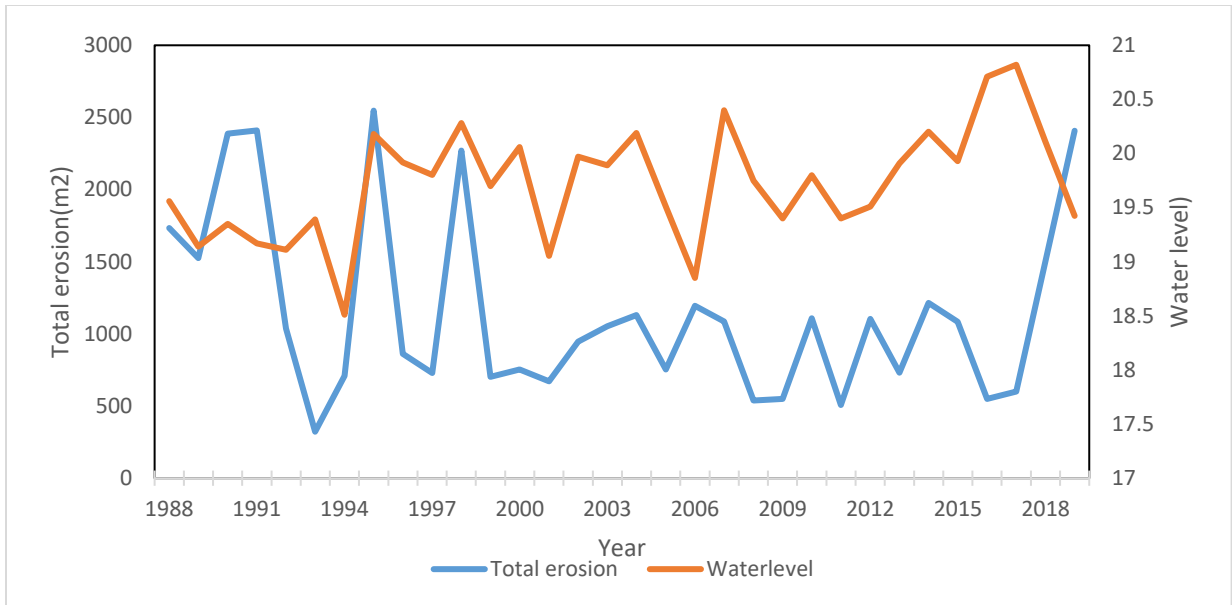Figure 4.15 Relation between discharge and erosion in Jamuna river

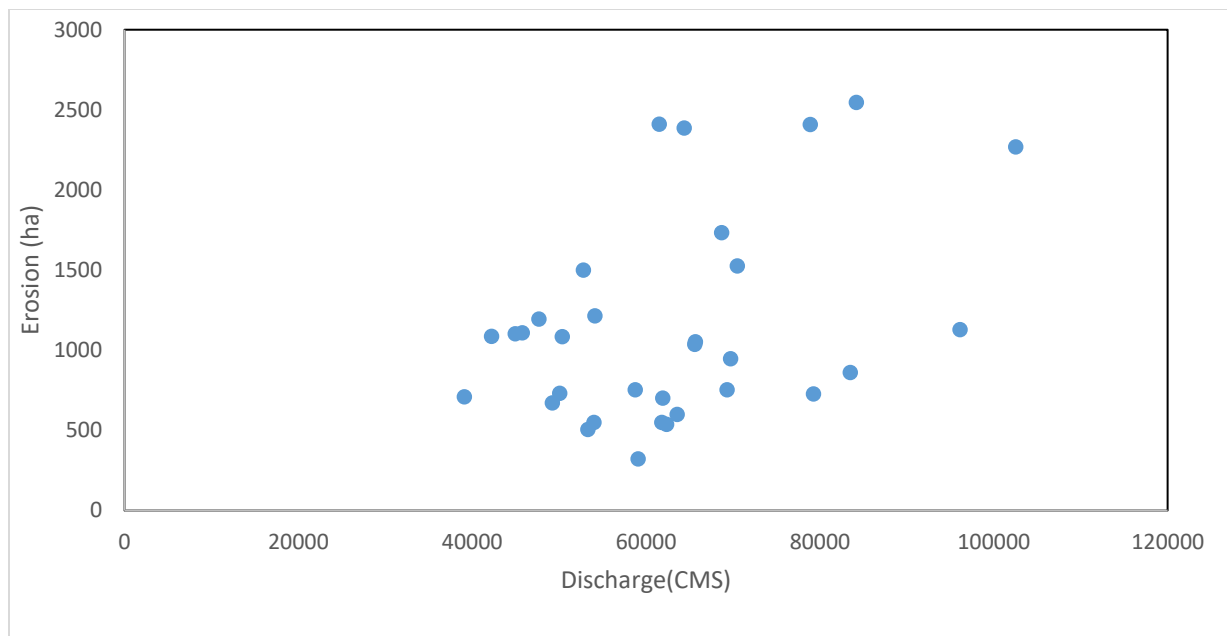Figure 4.16 Relation between water level and erosion in Jamuna river

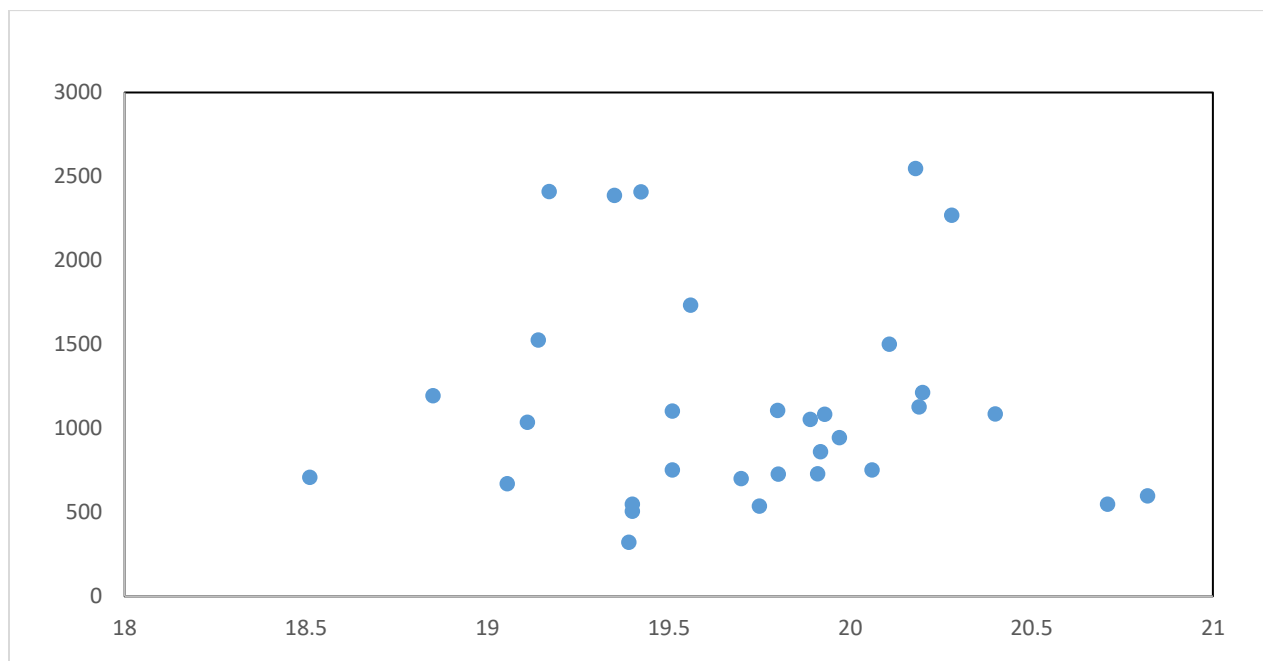Figure 4.17 Corelation between Erosion and Discharge

Figure 4.18 Corelation between Erosion and Water level

4.7 Morphological Change Analysis

The historical migration of the river has produced significant differences between left and right bank material properties; to explain the relationships between discharge, fluvial processes, anabranch instability and floodplain erosion rates, and; identify causal associations between drivers and morphological responses at a variety of time and space scales bed form change was observed throughout 2016 to 2019. It was helpful to recognize Process–response mechanisms and their relation to various drivers of morphological change in the Brahmaputra–Jamuna River.

4.7.1 Data set

Bathymetry analysis was made to reveal the nature of bed material movement. The thalweg line of the main river shows the main course of flow. Changes of course of the thalweg line and its elevation provide information of the main river course over the year of 2016, 2017,2018 and 2019. Analysis was made with 2016, 2017,2018 and 2019 bathymetry data collected from FRERMIP.Data set from 2018 and 2019 are of 500 m resolution whereas resolution varies to 1 to 3 km for the year 2016 and 2017 Figure 4-19 show the scatter data set along with interpolated riverbed for each of the year. From these data the shifting of the thalweg line as well as the riverbed change was observed.
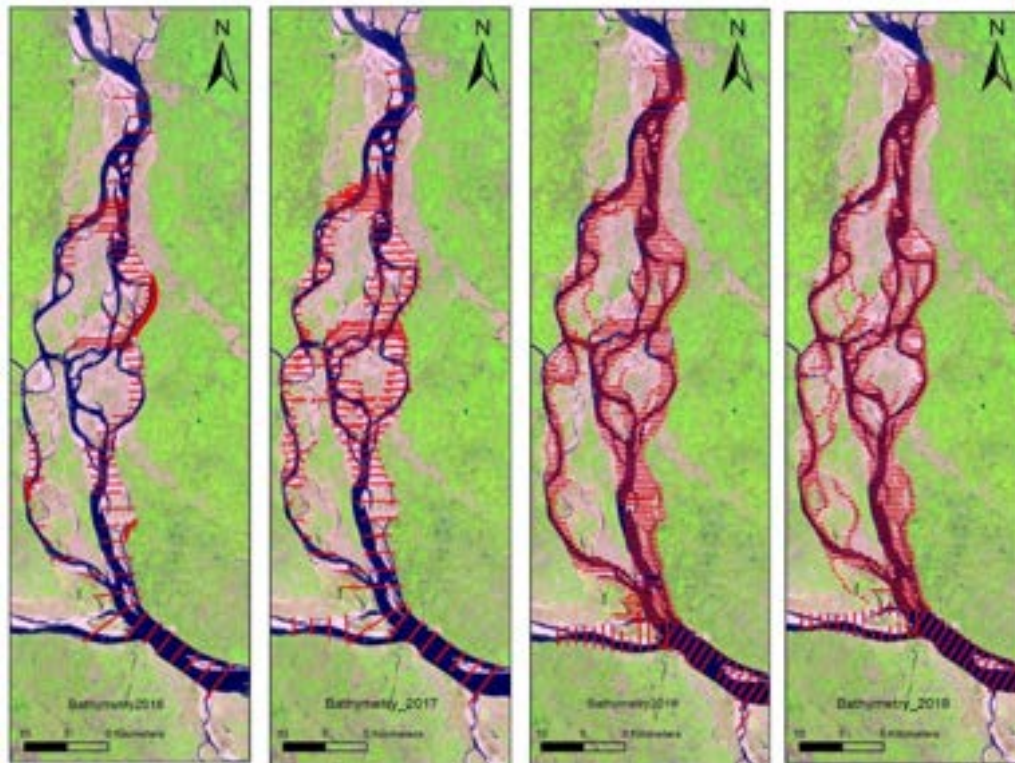
Figure 4.19 Scatter bathymetry Data Set.

4.7.2 Comparison between bed levels

The data was measured with respect to P WD datum. Bathymetry data was collected during the monsoon-post monsoon period of the year 2016,2017,2018 and 2019. Figure 4-20 to 4-22 show interpolated bathymetry and corresponding year erosion deposition. In the figure4-20 dark blue potion at right bank of the year 2016 signifies data scarcity, it can also be seen from the erosion deposition on map.

Figure 4.20 Comparison of river bed level 2016-2017

Figure 4.21 Comparison of River bed level 2017-2018
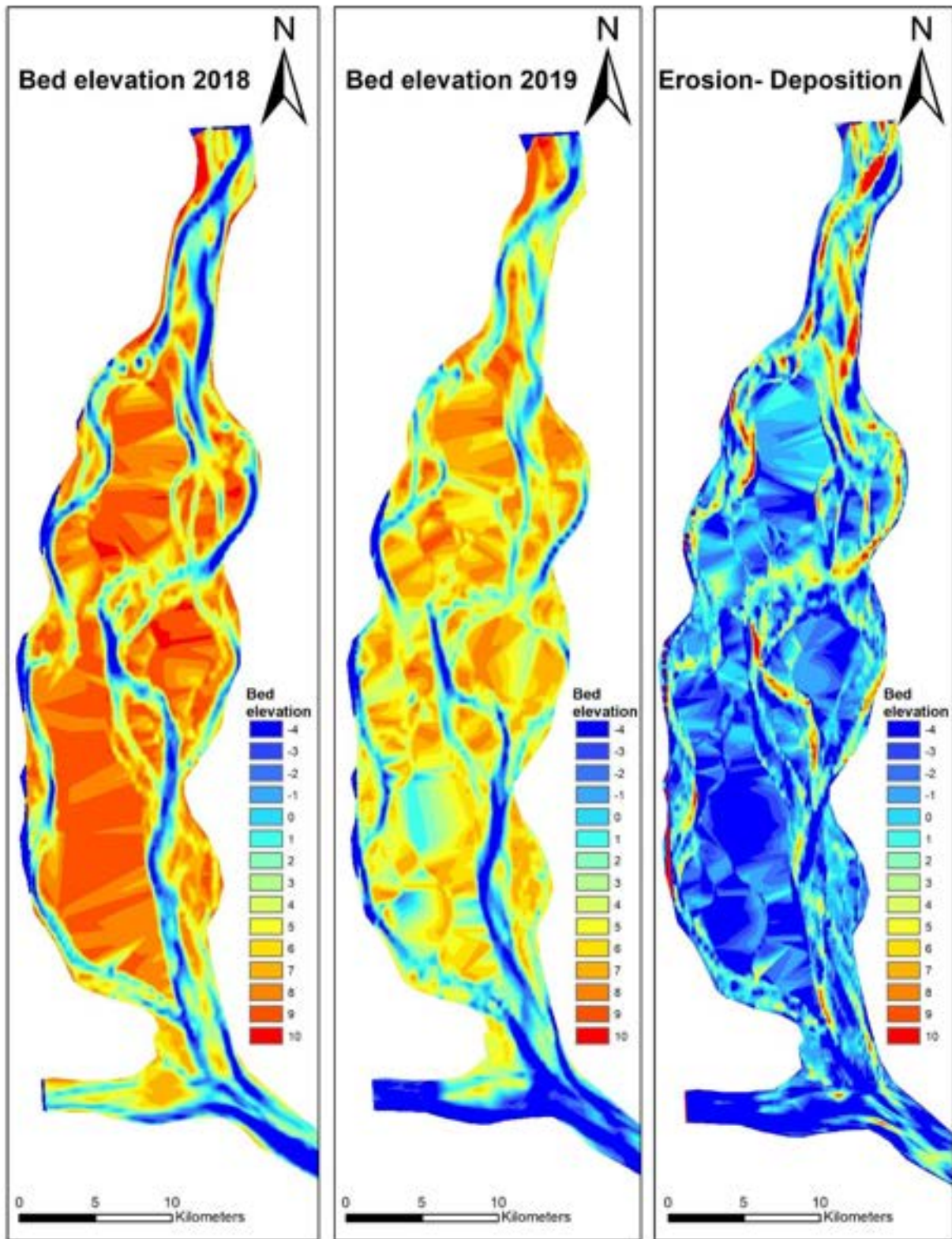
Figure 4.22 Comparison river bed level 2018-2019

4.7.3 Bedform changes along longitudinal profile.

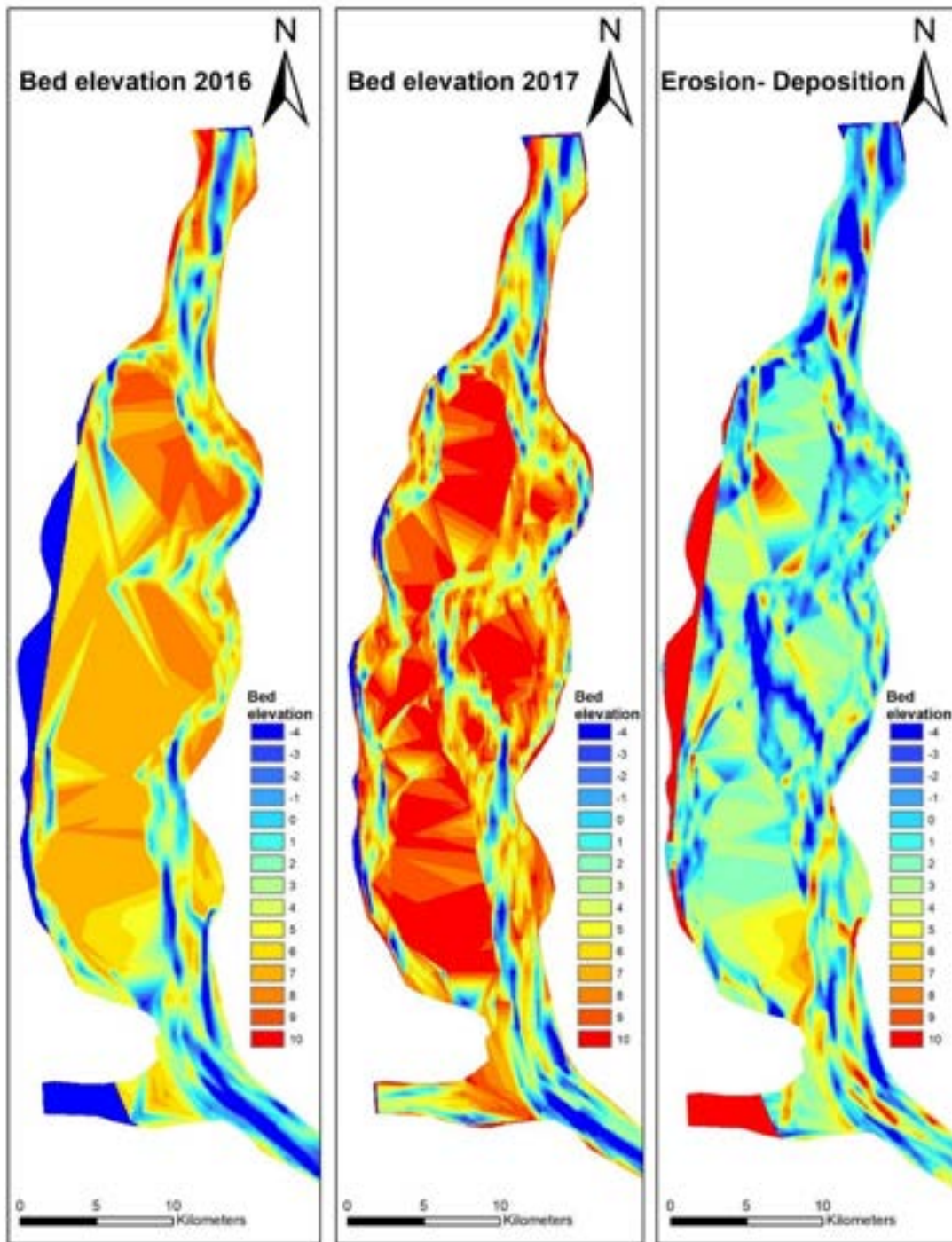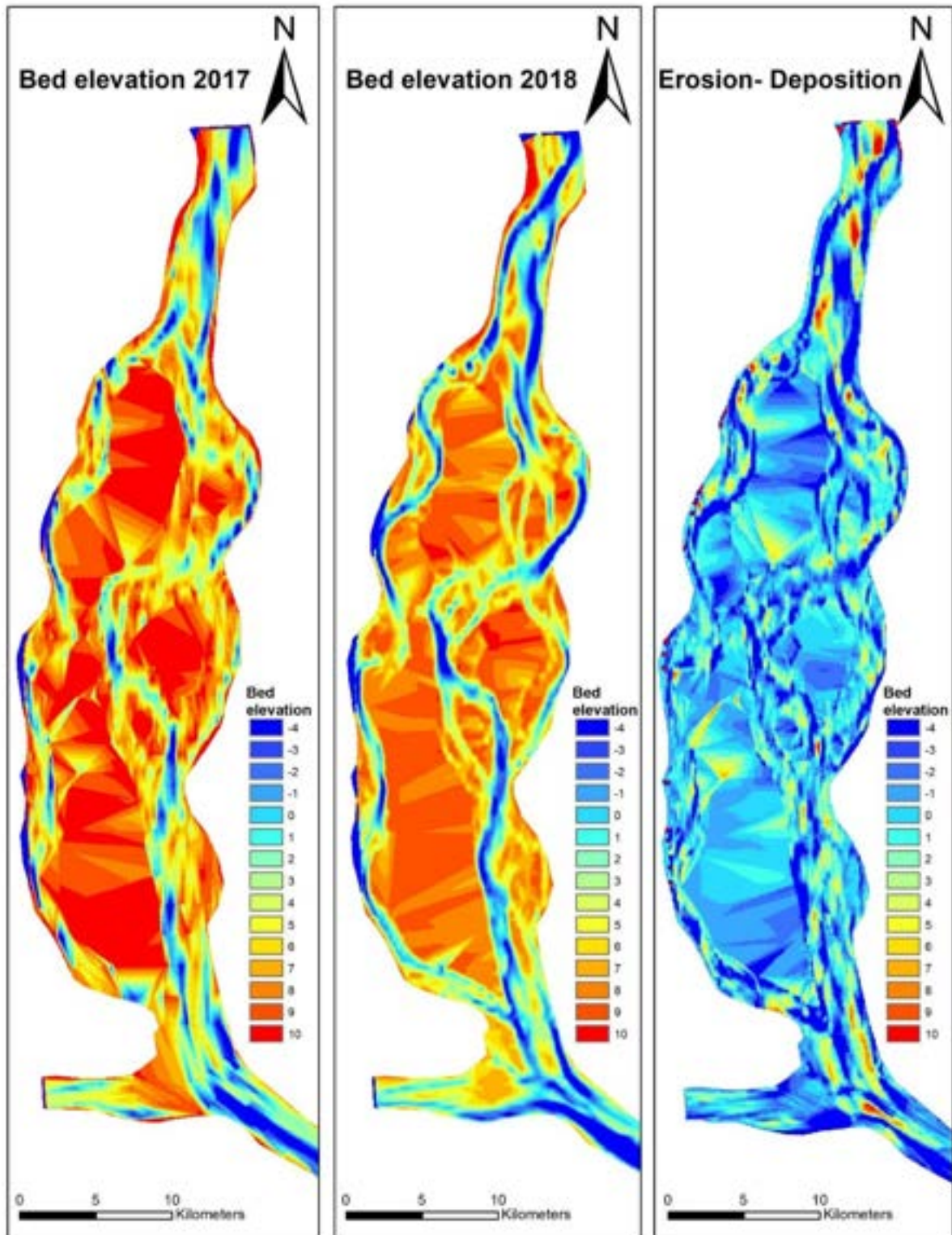To assess bedform changes along the length of the river reach 3 long profile was chosen. In figure the line in the middle represents thalweg line at 2018 and the lines on the left is the thalweg of secondary channel along the right bank and right profile is a thalweg line along the secondary channel on the left bank.
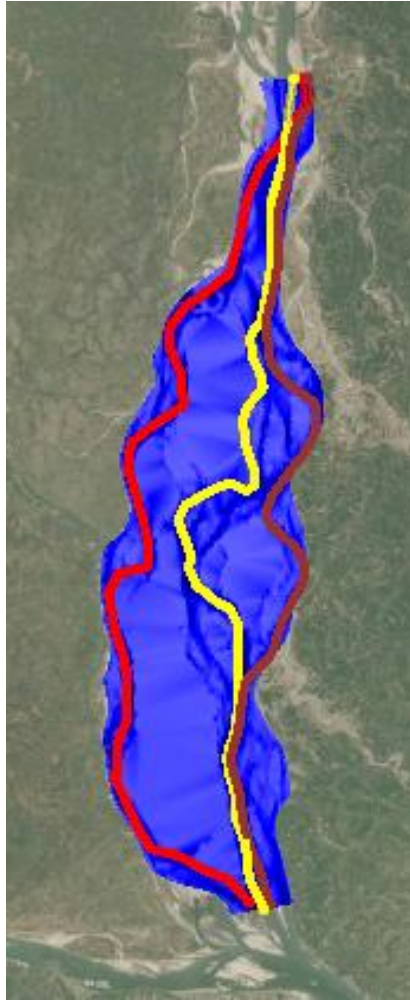
Figure 4.23 Selected longitudinal profiles

Spatial and temporal change of the bathymetry were derived from the collected data. The collected bathymetric data of the year 2016, 2017 and 2018 from the FRERMIP project were used in analyzing the bathymetric information. Primarily Bathymetry of Jamuna river for 2016, 2017,2018 and 2019 was compared with in their common. Figure shows 4-24 to 4 -29 shows bedform and their changes along the long profiles. Here the center profile is marked in yellow and left and right profiles are symbolized by red and brown respectively.
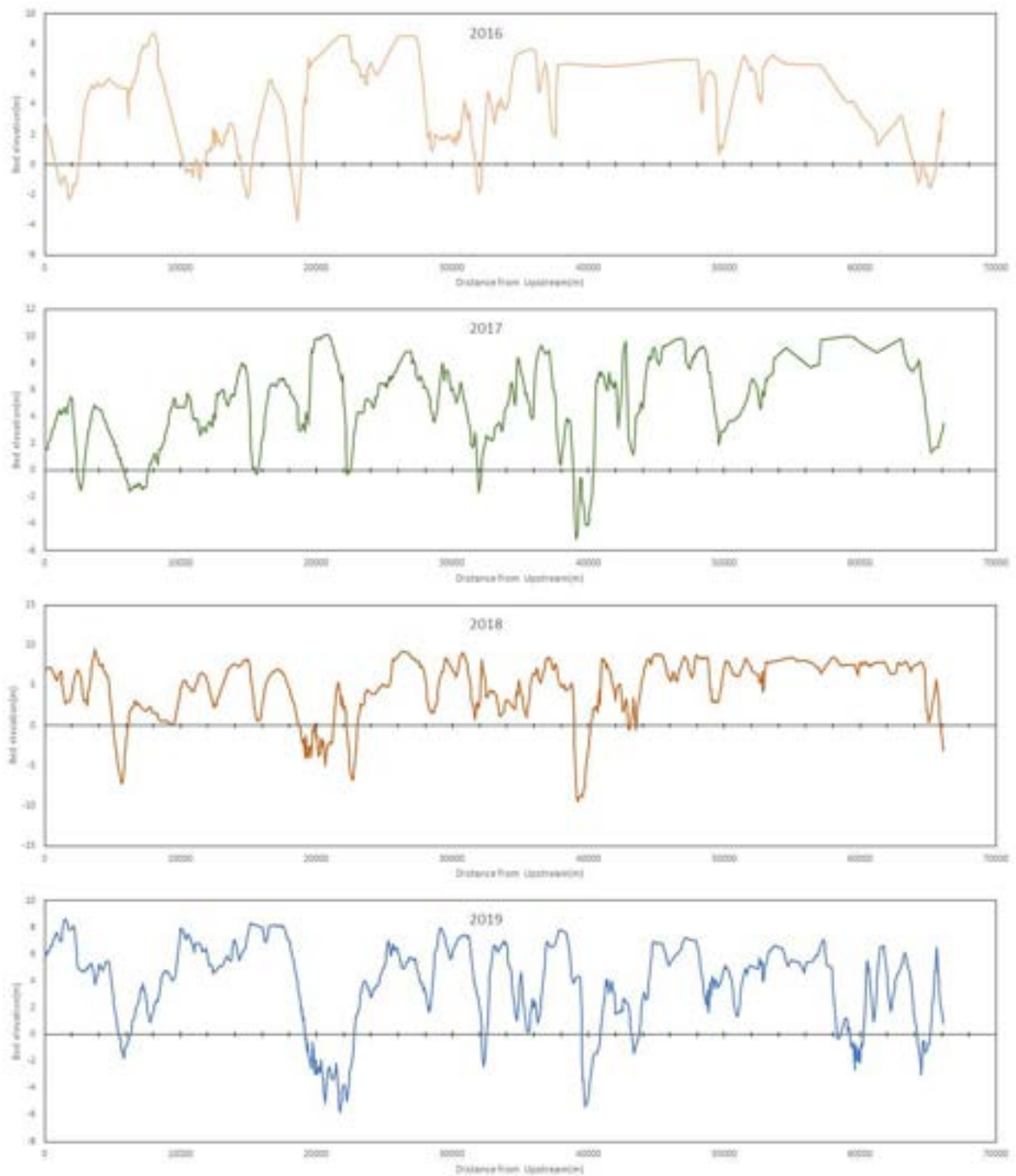
Figure 4.24 Longitudinal profile along center profile.
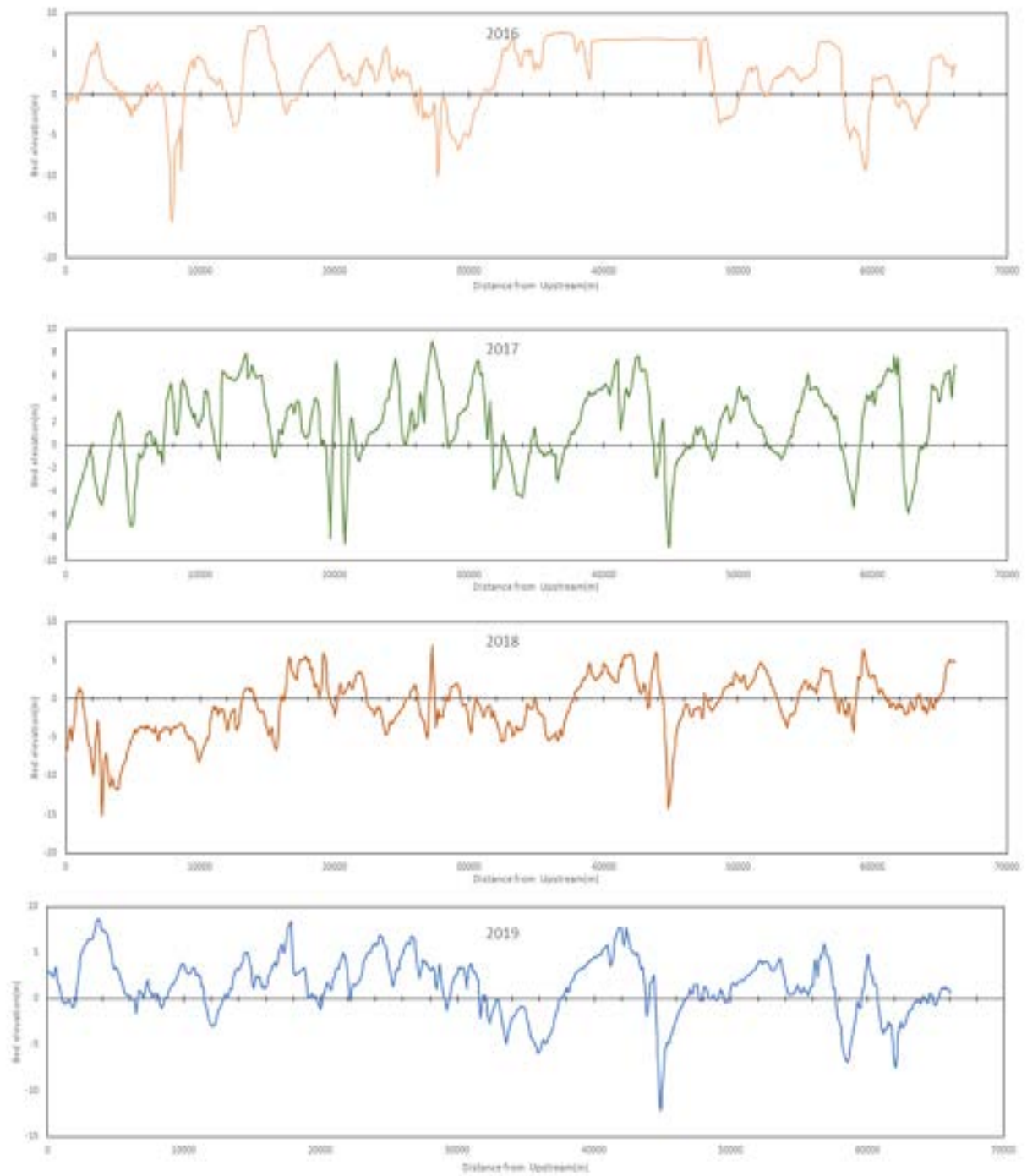
Figure 4.25 Longitudinal profile along left profile.

Figure 4.26 Longitudinal profile along right profile.
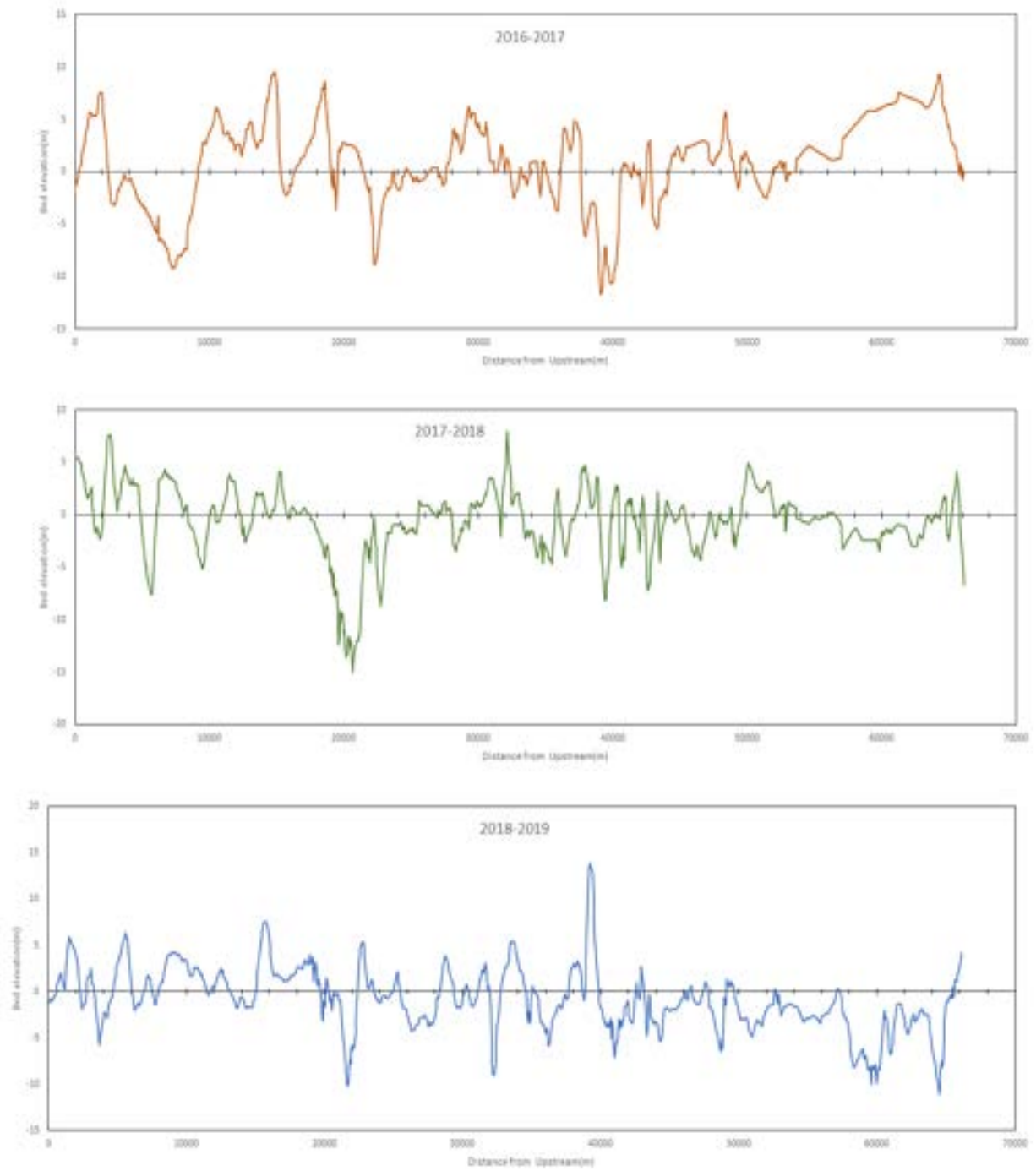
Figure 4.27 Erosion deposition along center long profile
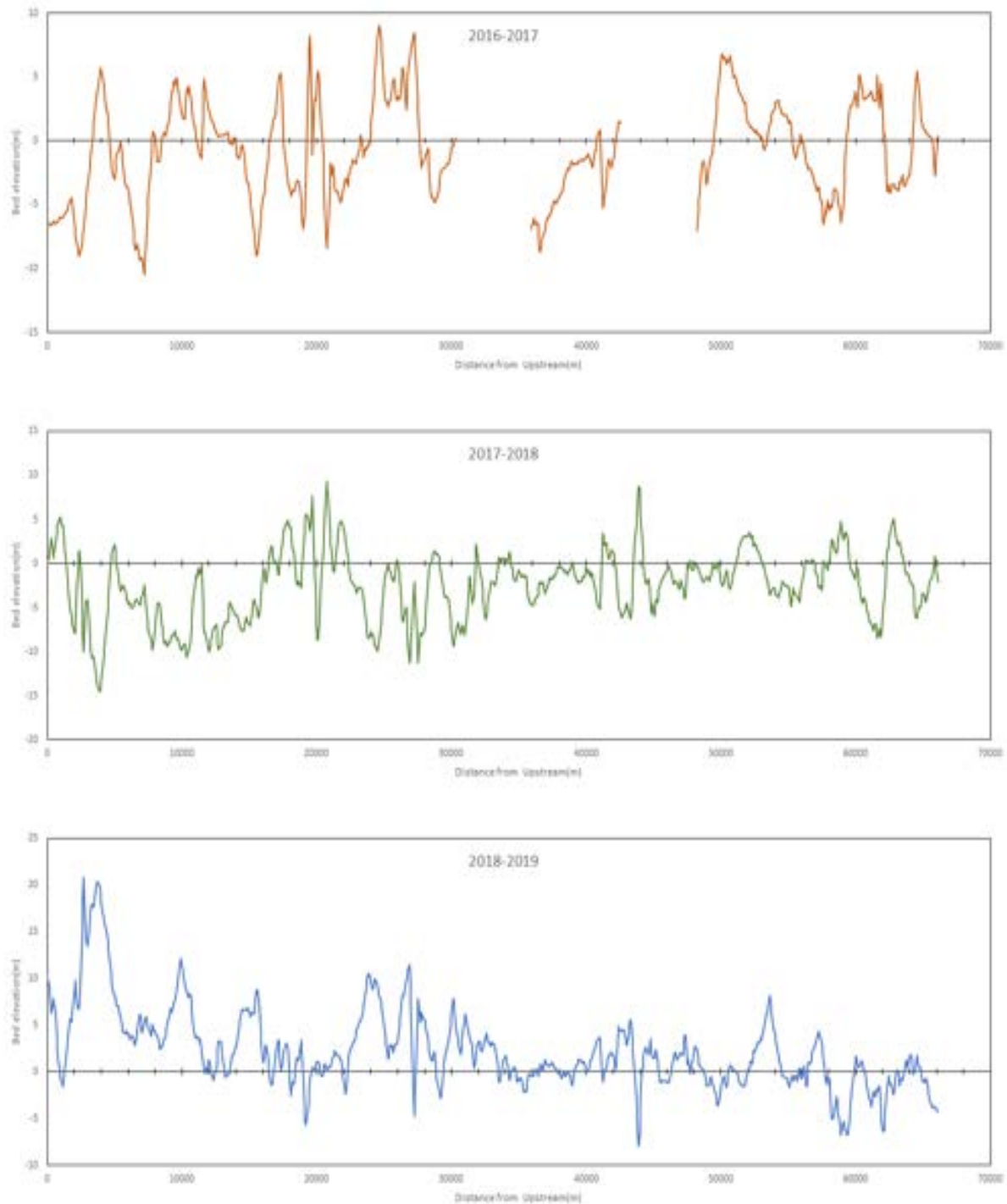
Figure 4.28 Erosion deposition along left long profile
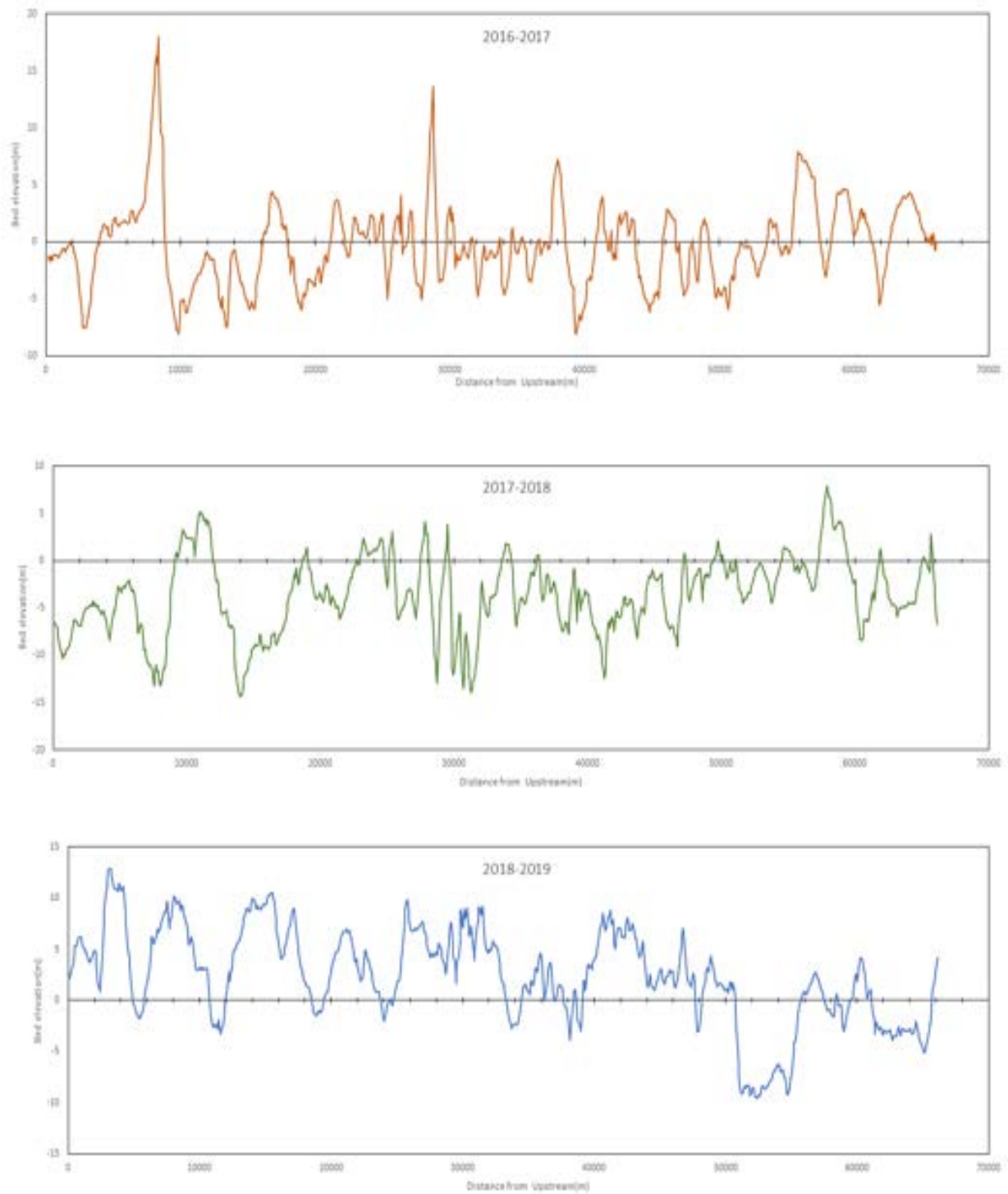
Figure 4.29 Erosion deposition along right long profile

Longitudinal profiles (from figure 4-27 to 4-29) show a high spike of deposition is always followed by a steep crest erosion and a medium crest deposition is followed medium to low crest erosion. In Figure (4-27 to 4-29) negative value signifies bed scour and positive value defines deposition. At point around 800 m from upstream channel be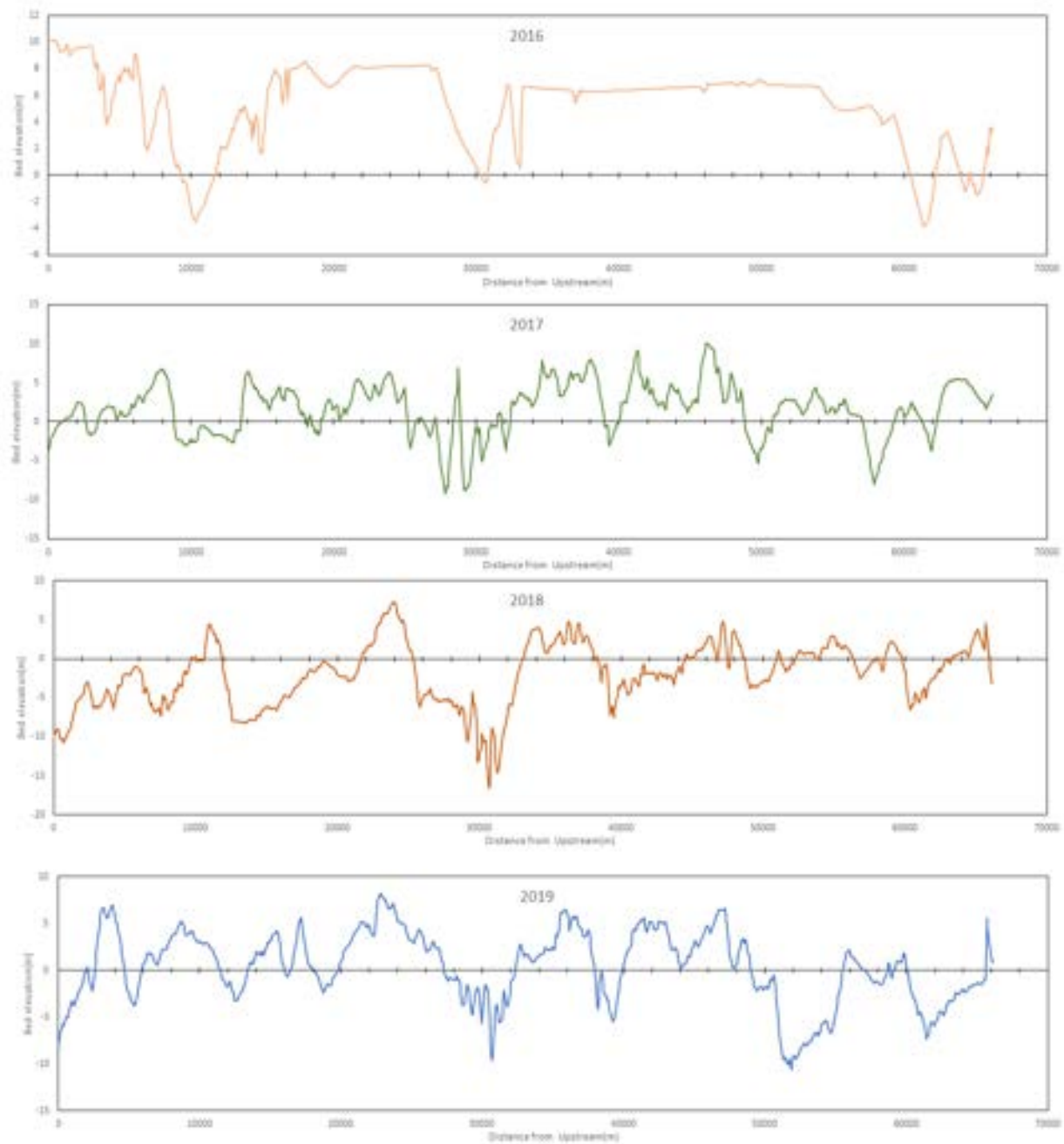d elevation was around -5m in 2016, in 2017 it gets eroded to -10m, after further erosion in 2018 it become -15m but in the year 2019 a huge deposition took place creating a dune, which was followed by an erosion. Maximum erosion(-15.07m) occurred along the center profile in 2017-2018 and Minimum erosion (-8.06 m) occurred along the right profile in the year 2016-2017. Maximum deposition was observed as 20.81 m along the left profile in the year 2018-2019. Table 4-4 below shows variation of bed levels along three profiles

Table 4-4 variation of bed levels along three profiles

Profile	Year	Maximum Erosion (m)	Maximum Deposition(m)	Average change (m)	St.Dev
Center profile	2016-2017	-11.75	9.53	0.53	2.97
	2017-2018	-15.07	8.03	-0.35	2.39
	2018-2019	-11.06	13.82	-0.46	2.53
Left profile	2016-2017	-10.51	9.31	0.20	3.59
	2017-2018	-14.51	9.29	-2.34	3.45
	2018-2019	-8.72	20.81	1.00	3.91
Right profile	2016-2017	-8.06	17.97	-0.19	2.68
	2017-2018	-14.34	7.88	-2.01	3.51
	2018-2019	-9.55	12.86	2.38	4.63

4.7.4 Bedform changes along Cross-sectional profile.

Similar to long profile assessment Cross sectional bedform changes were also analyzed. Total 6 cross sections were taken in this study. Cross section 01,03,04, and 05 are at very erosion prone site at left bank, whereas erosion occur at the right bank in cross section 02 and 6. Figure below shows the 6 cross sections, Cross section 01 at the top to the cross section 06 at the bottom. Figure 27-32 variation of cross section with different year.
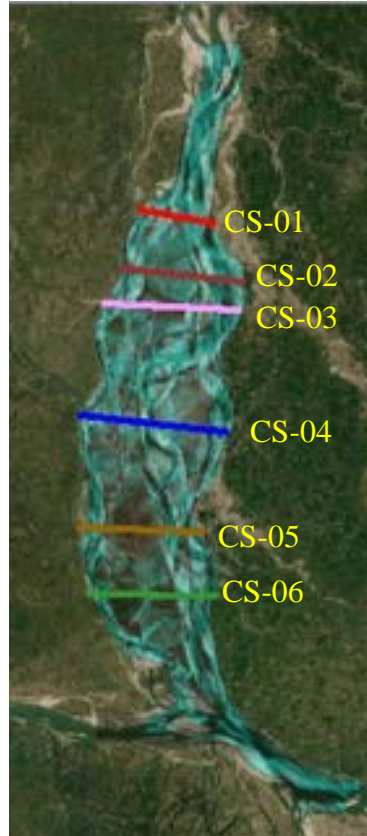
Figure 4.30 Cross sections in the study area.

At Cross section 01(Figure 4-32) in the left bank deposition occur in the year 2017 followed by a erosion of around 2 m in 2018.After that in 2019 a huge erosion took place at this point as the level drop to around 4.5m from 8m.Similar pattern can be found in cross section 03,04,05.On the otherhand a cross section 02(Figure 4-33) continous erosion was observed throughout these four years.Figure 4-34 to 4-36 shows different cross section profiles.
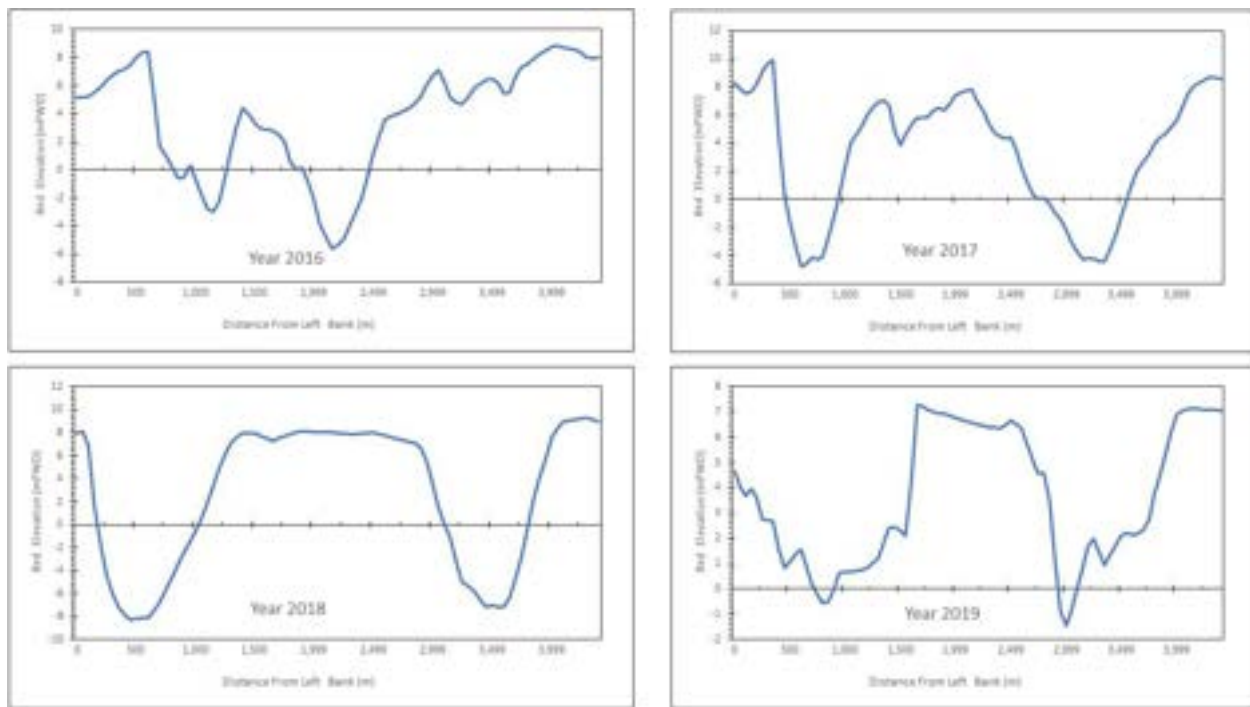
Figure 4.31 Cross section 01
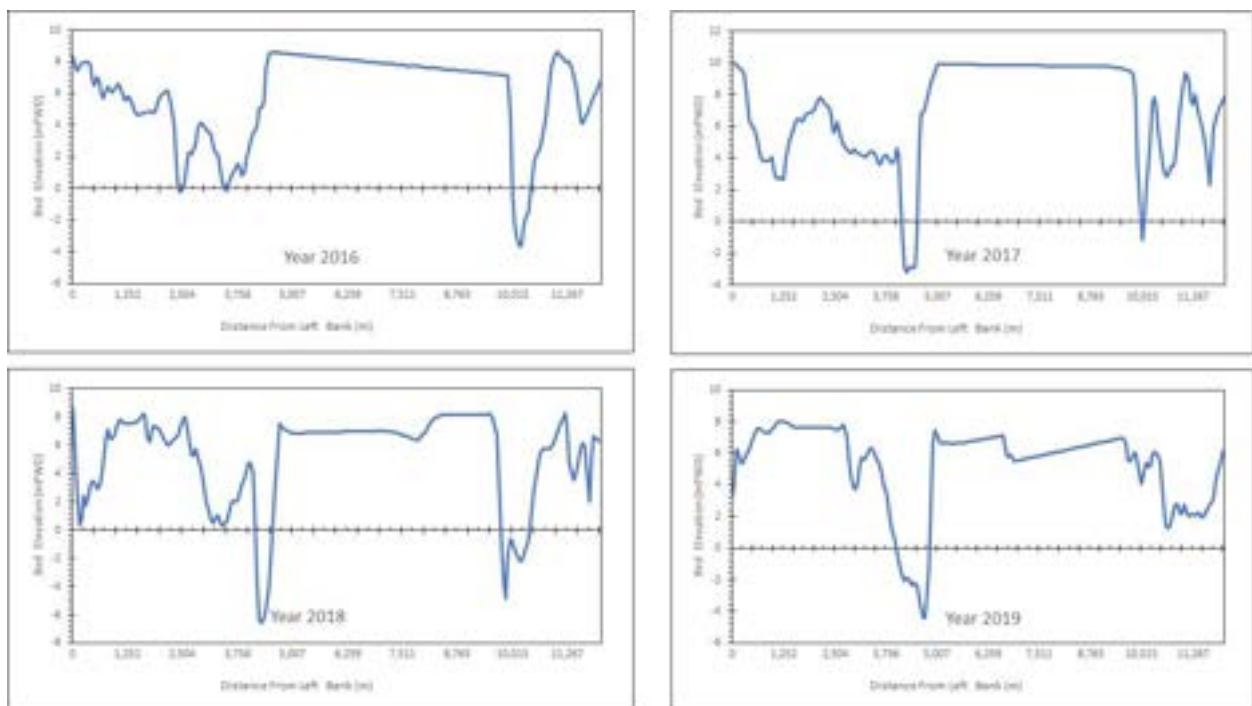
Figure 4.32 Cross section 02
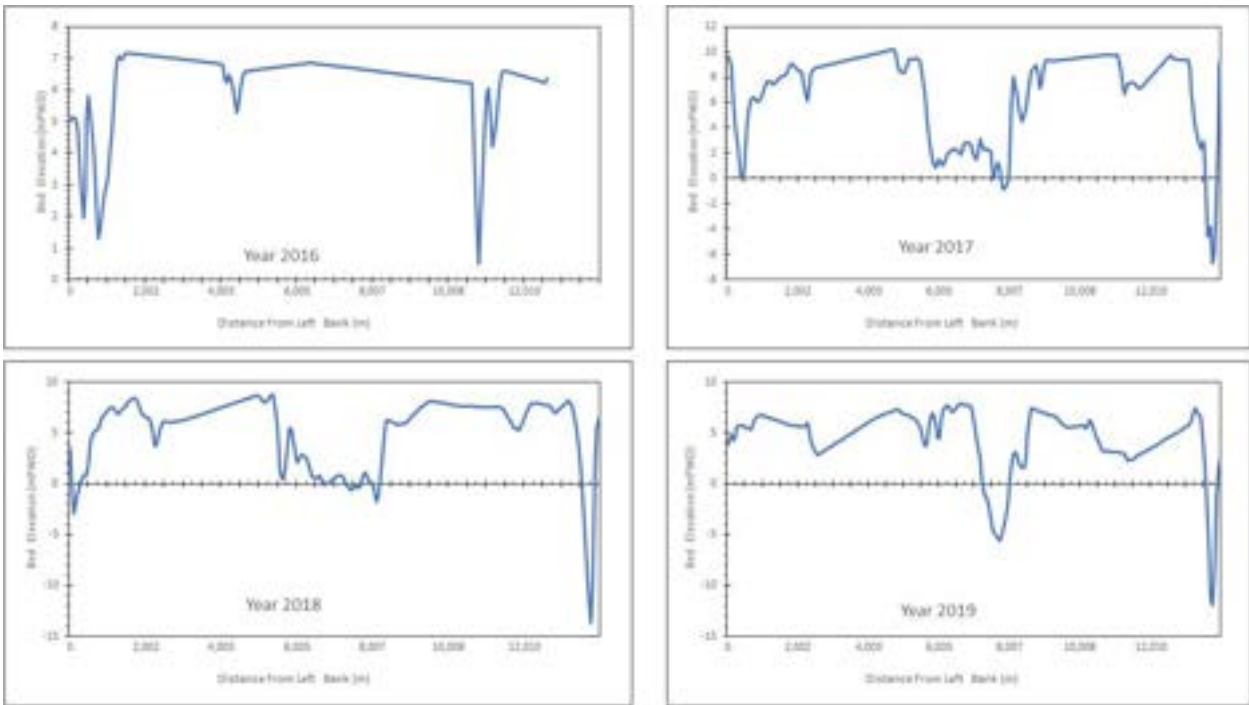
Figure 4.33 Cross section 03
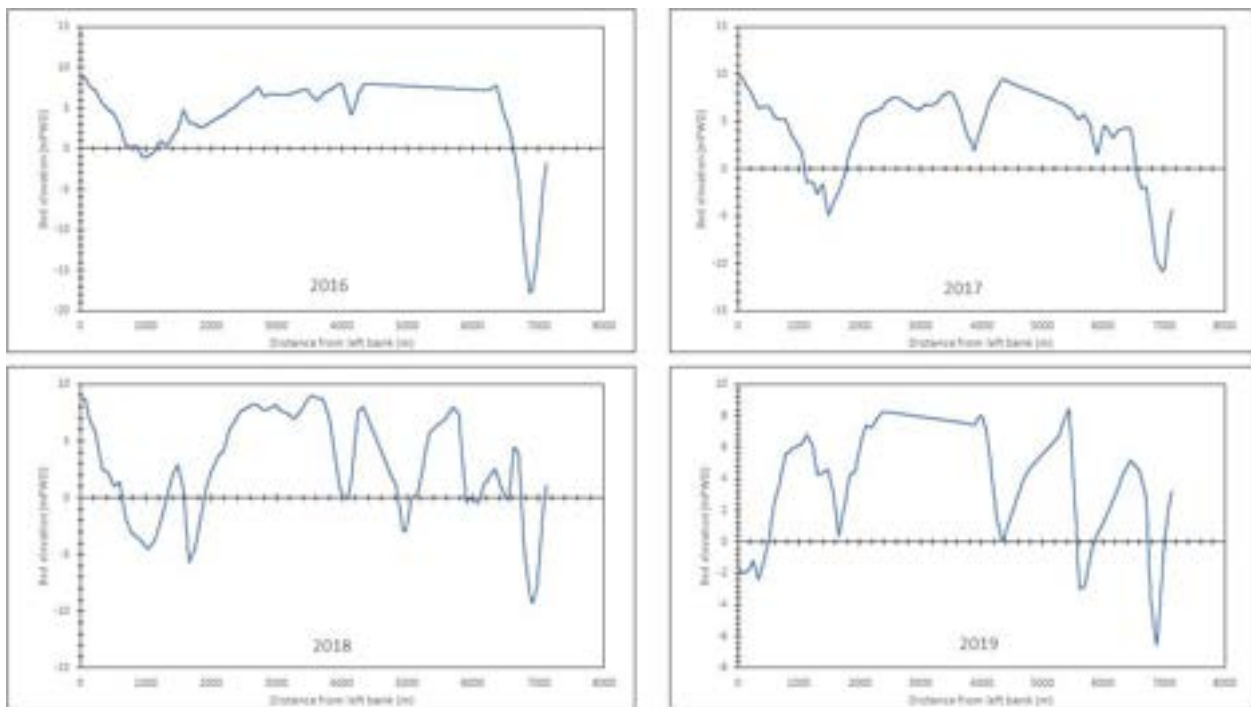
Figure 4.34 cross section 04
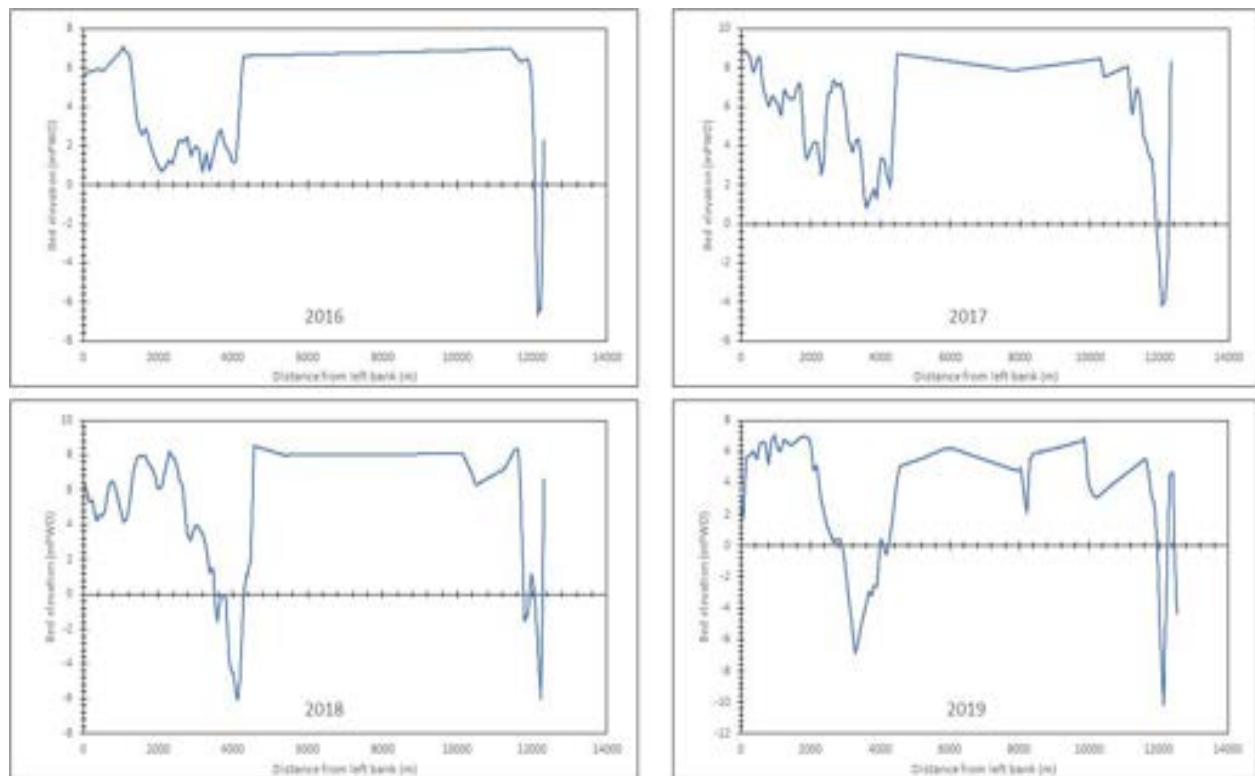
Figure 4.35 Cross section 05
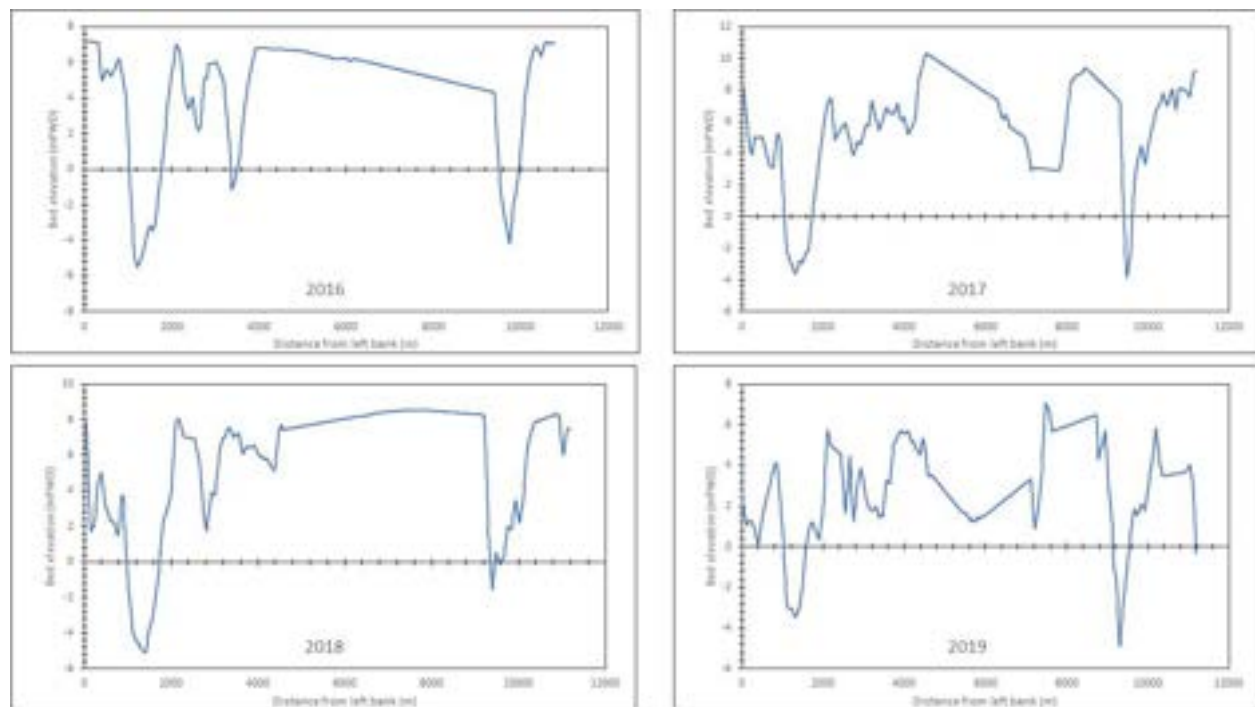
Figure 4.36 Cross section 06

4.7.5 Erosion prone area analysis

From Planform analysis it was evident that there are some erosion prone areas along the Jamuna river bank. These areas are subjected to continuous erosion. In this study an attempt was made to investigate the cause of these severe erosion . Total 6 critical area were identified (Figure 4-37) and investigated. It was found that due to formation of bar when flows were directly diverted towards the bank significant amount of erosion occurred. In these cases, direct shear stress, impact force become very high that the soil cannot withstand the flow. Figure 4-38 to 4-48 shows different erosion prone area.
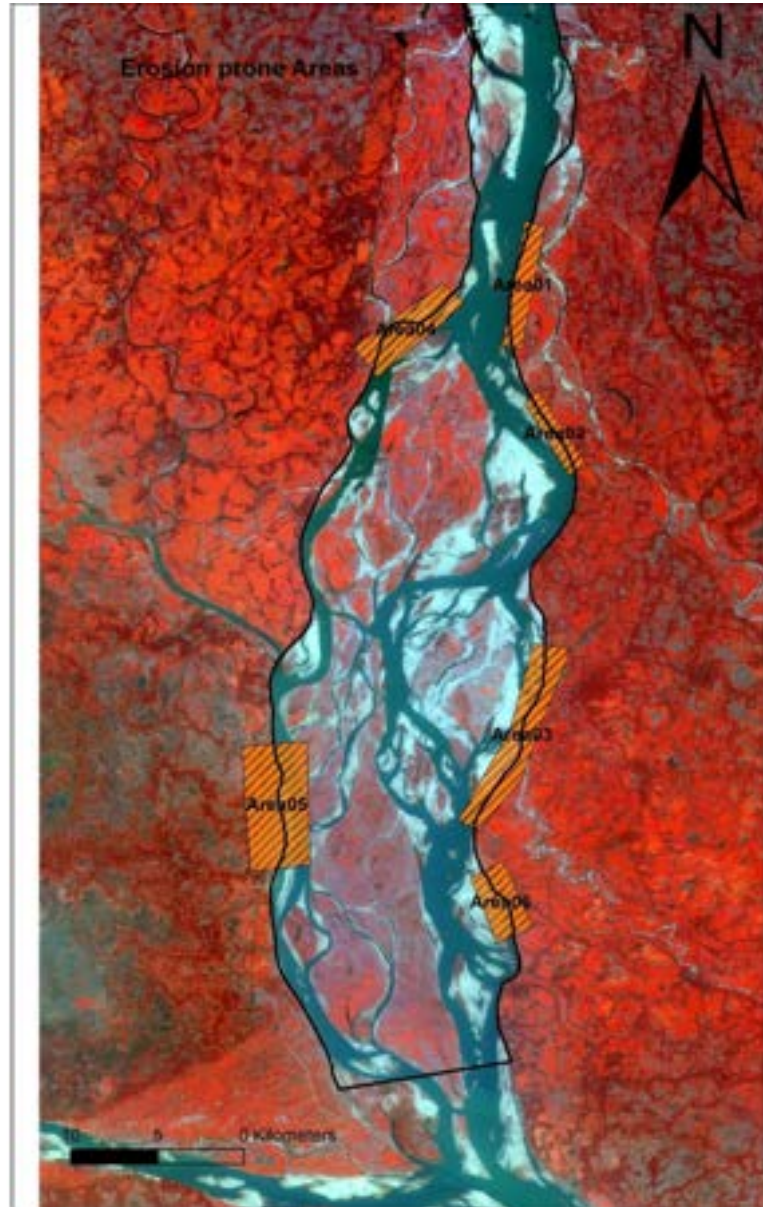
Figure 4.37 Erosion Prone Areas
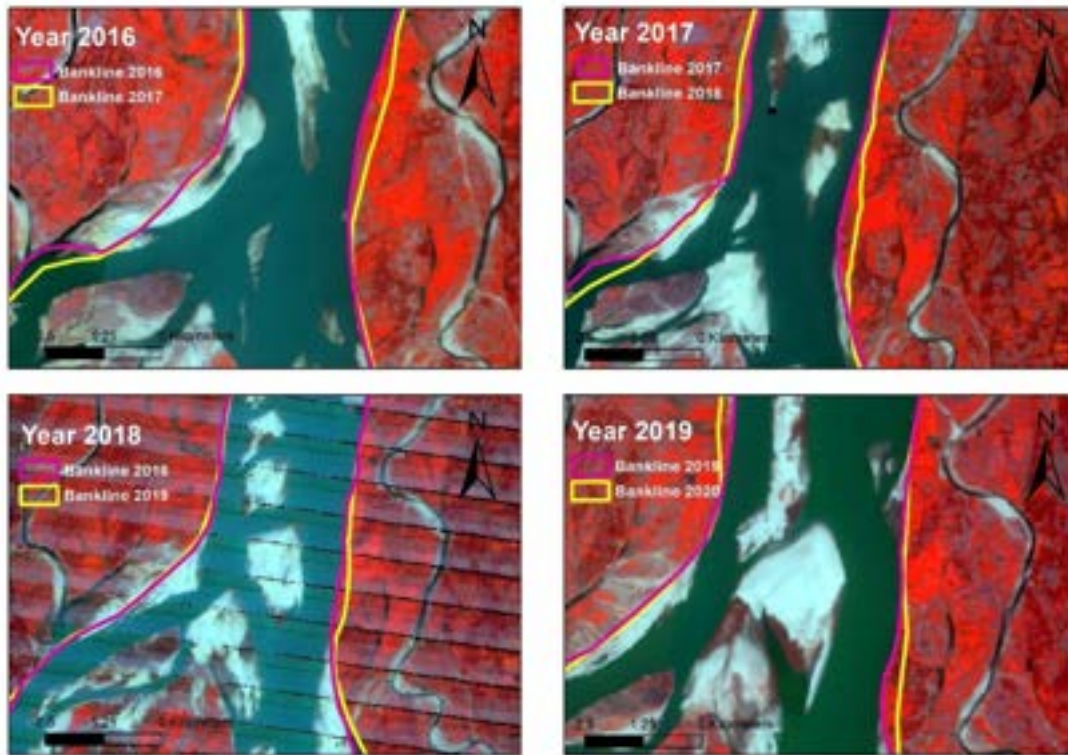
Figure 4.38 Planform Change in Area 01
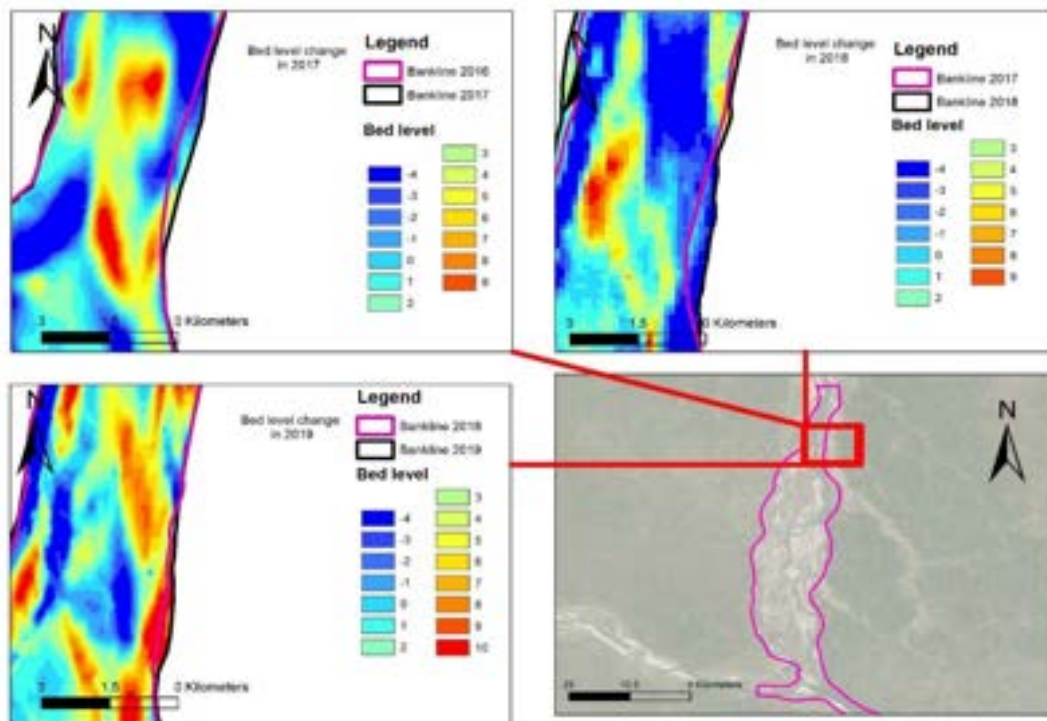
Figure 4.39 Bed level Change in area 01
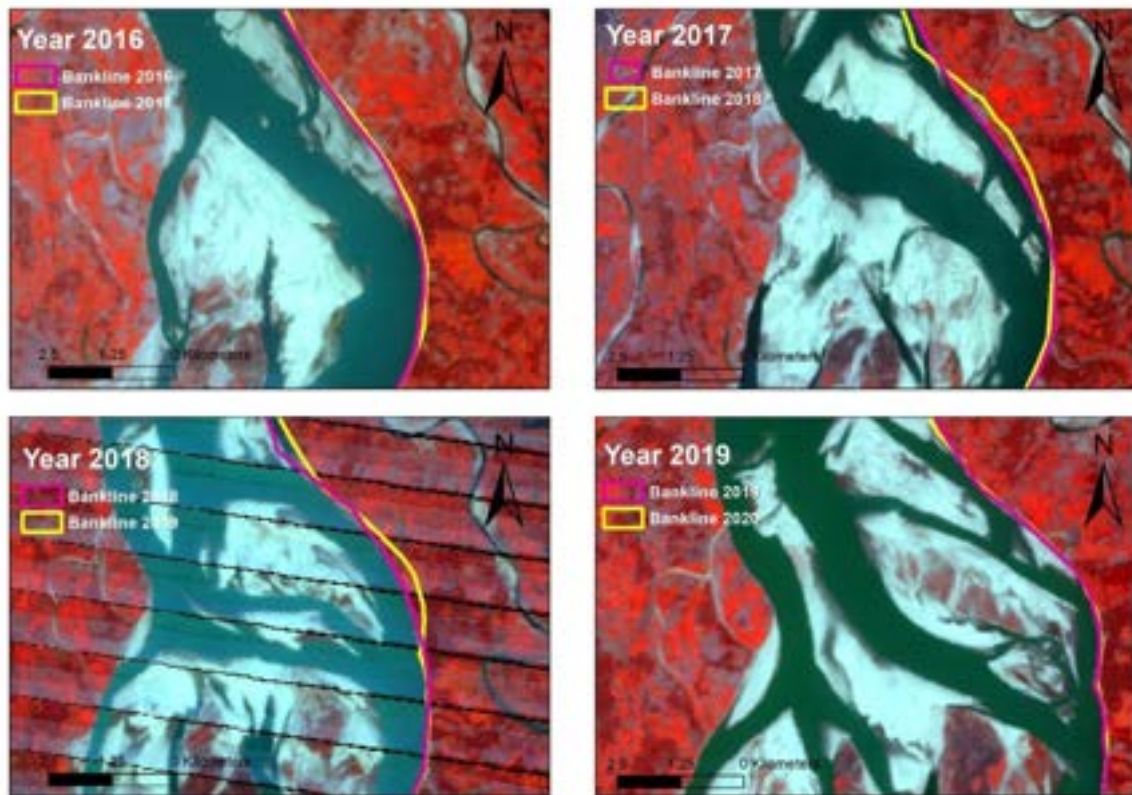
Figure 4.41 Planform Change in area 02
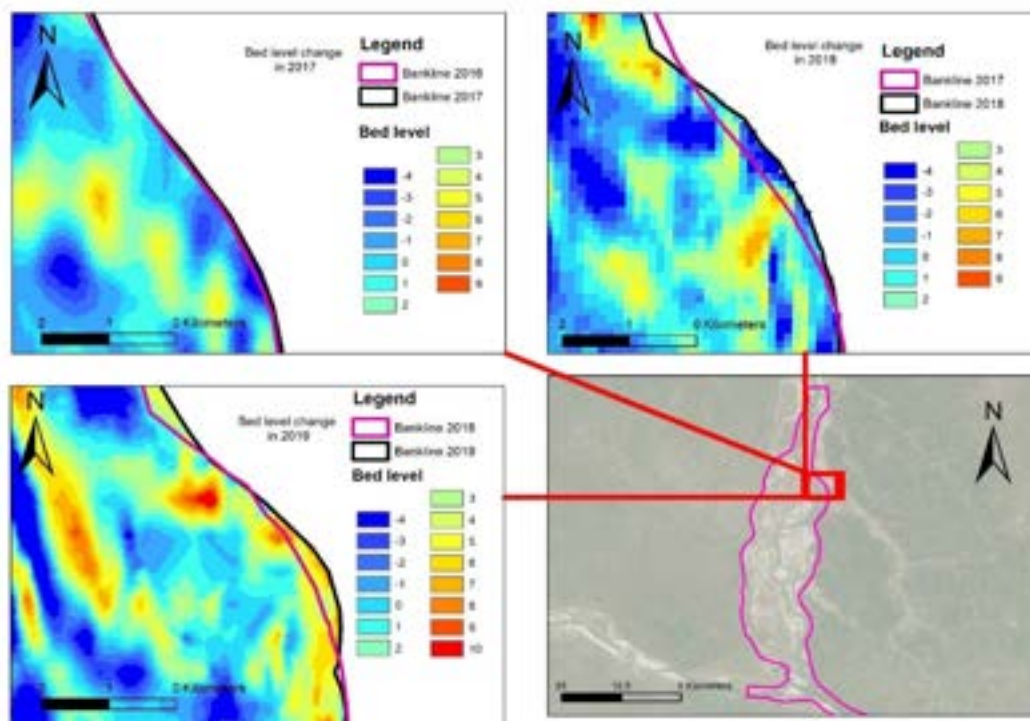
Figure 4.40 Bed level Change in area 02
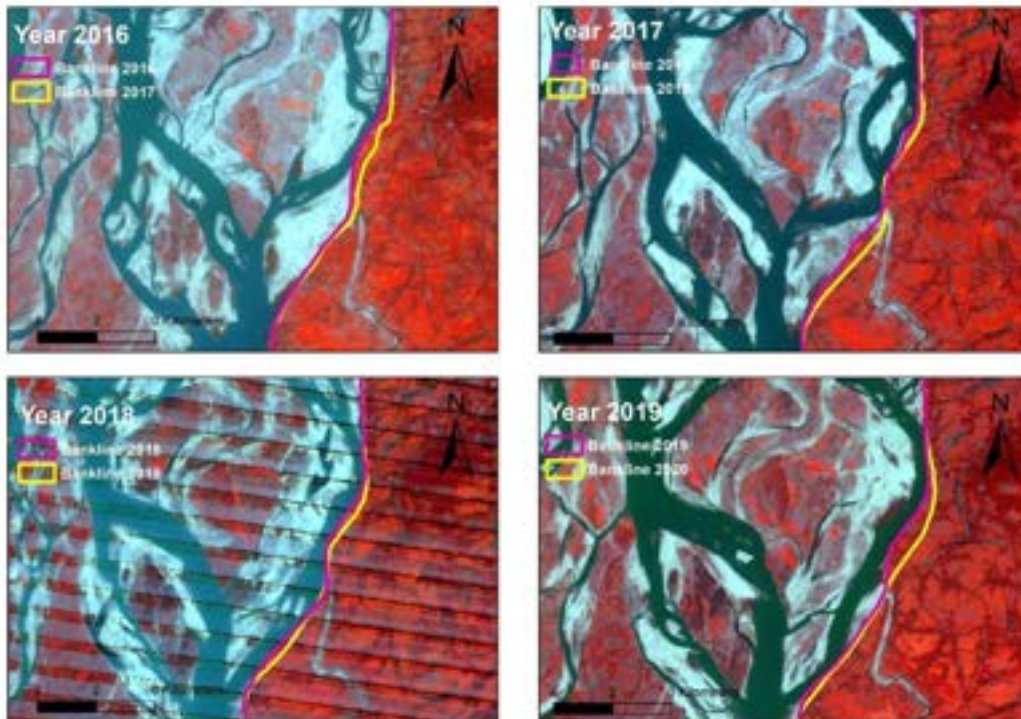
Figure 4.42 Planform Change in area 03
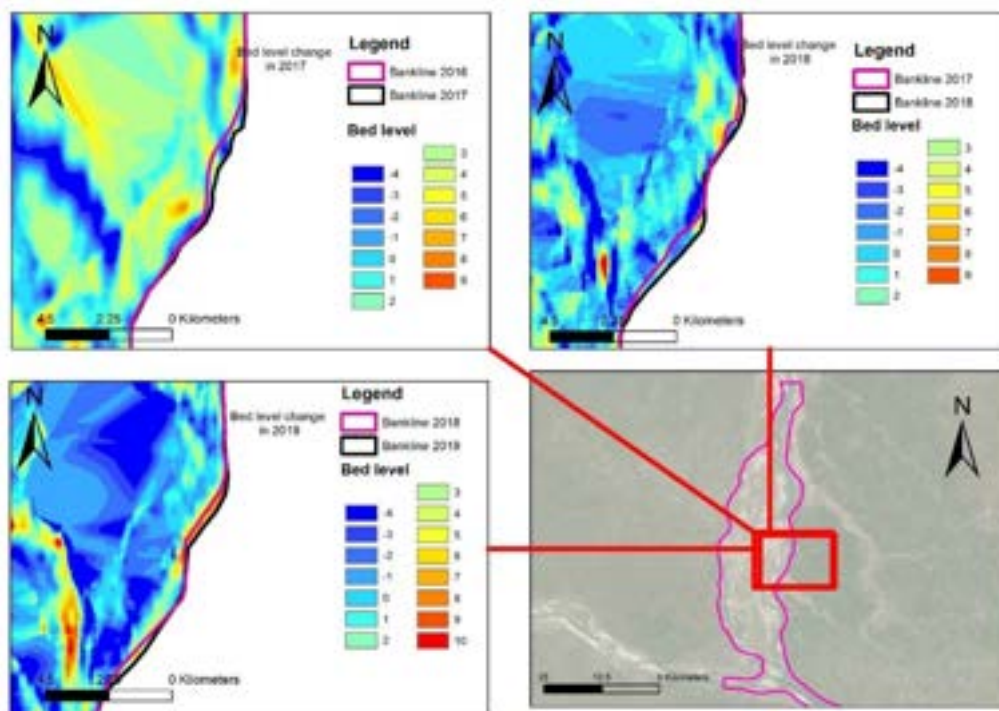
Figure 4.43Bed level Change in area 03
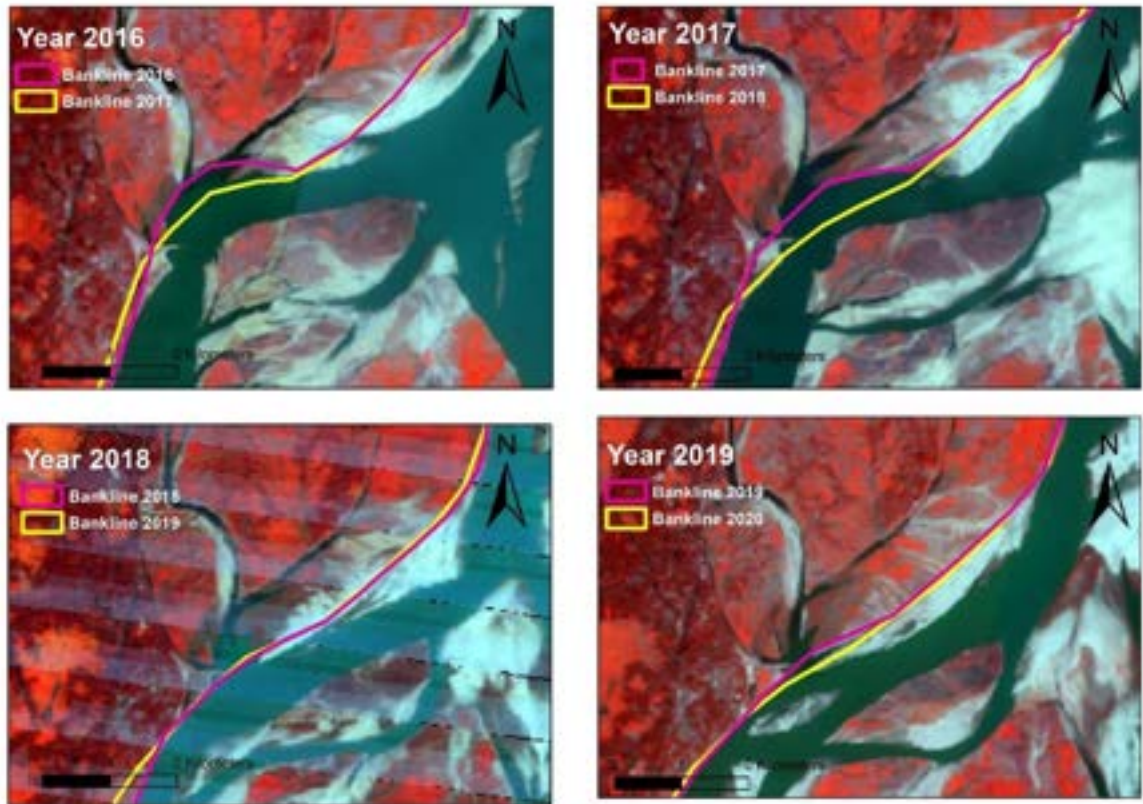
Figure 4.44 Bed level Change in area 04
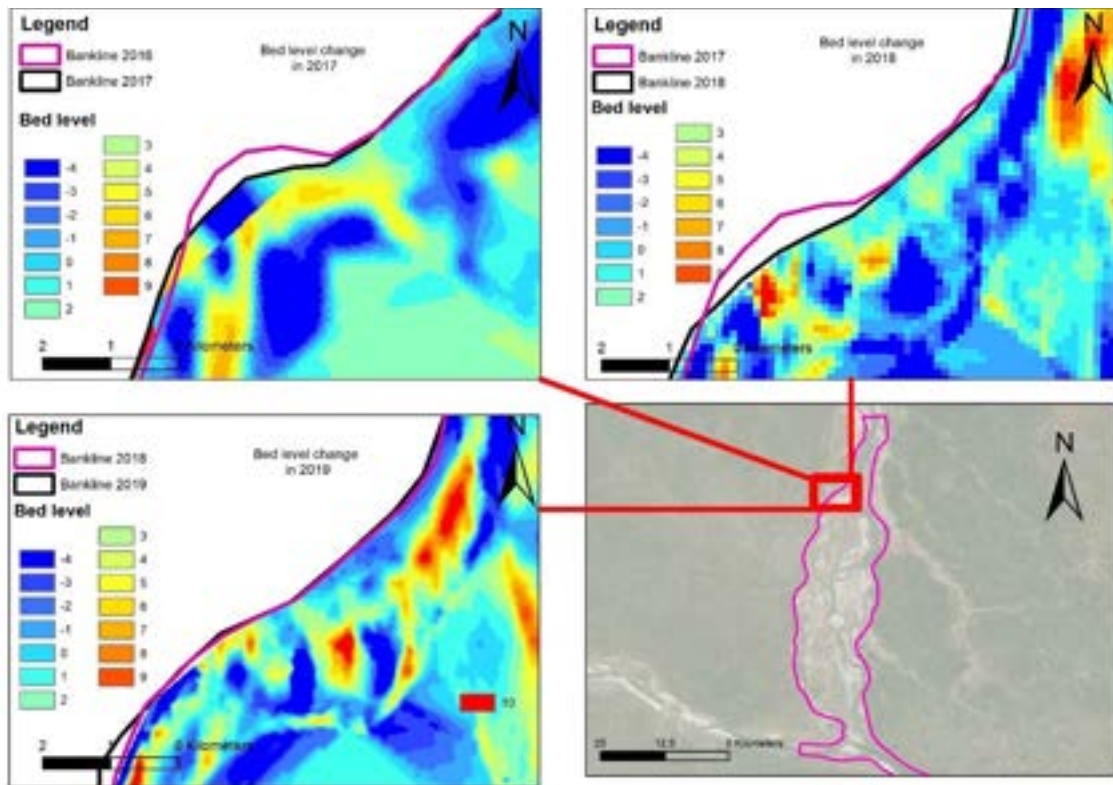
Figure 4.45 Planform Change in area 04
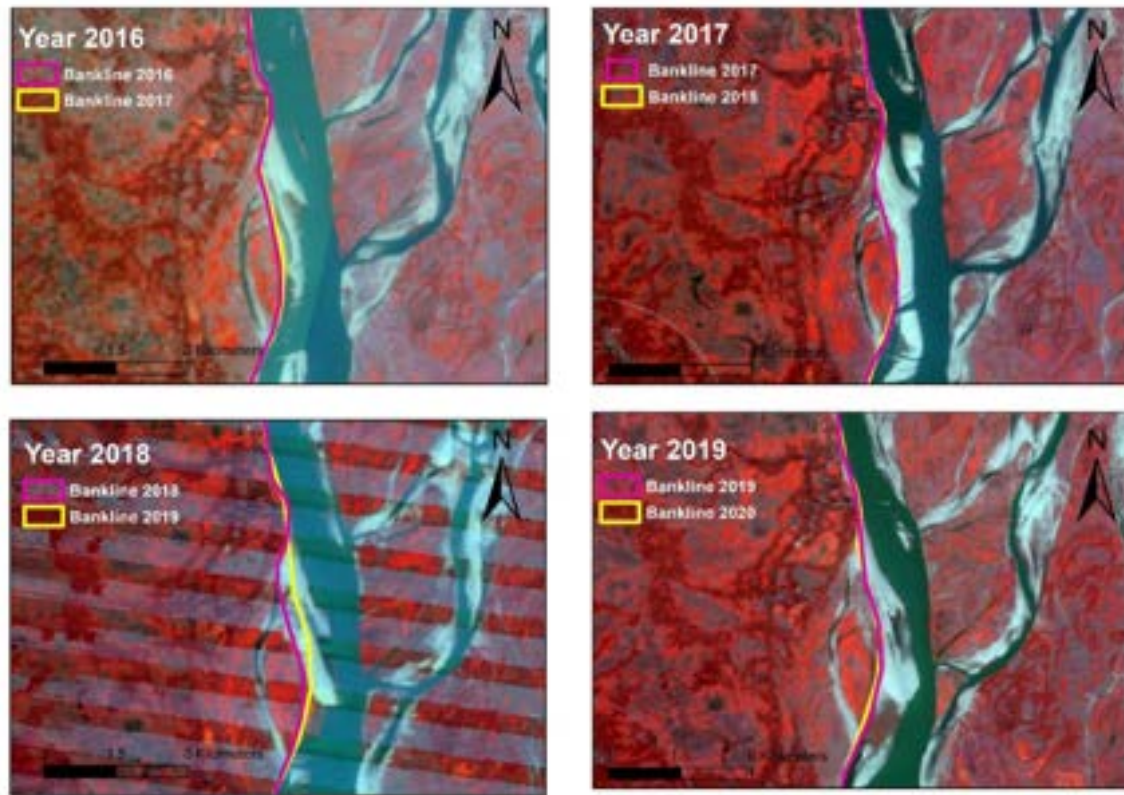
Figure 4.47 Planform Change in area 05
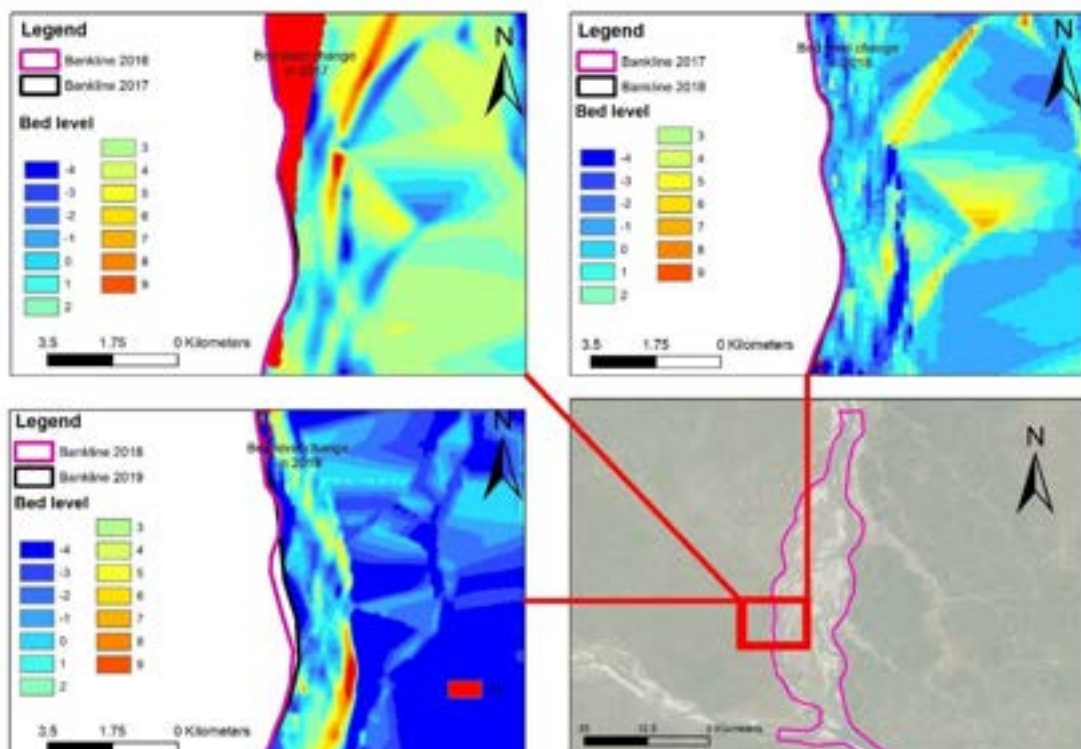
Figure 4.46 Bed level Change in area 05
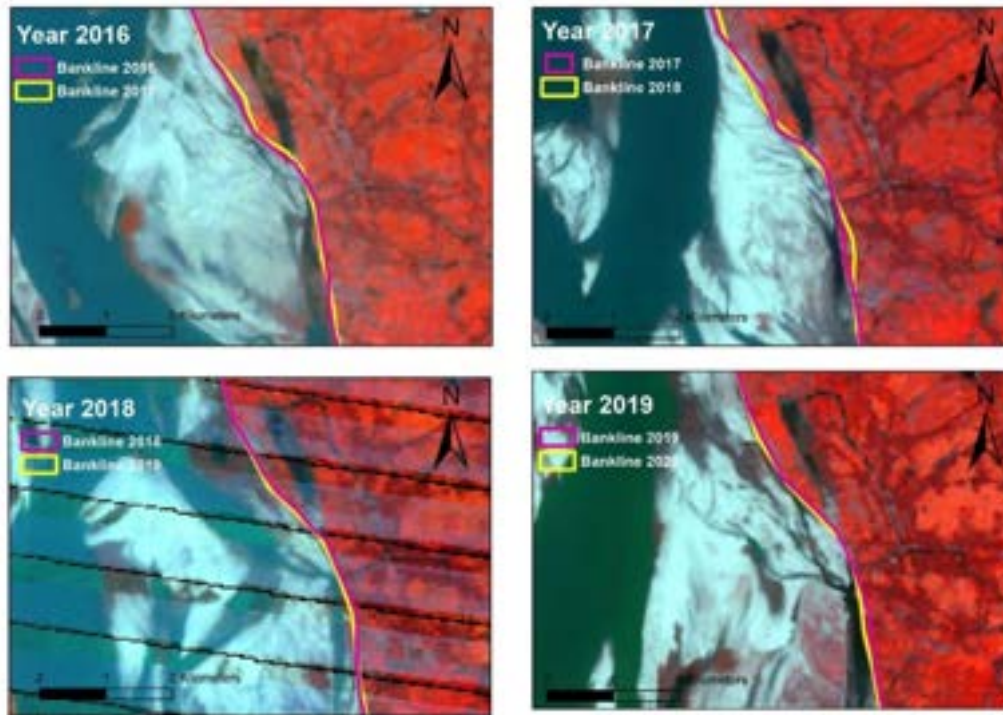
Figure 4.48 Plan form Change in area 06
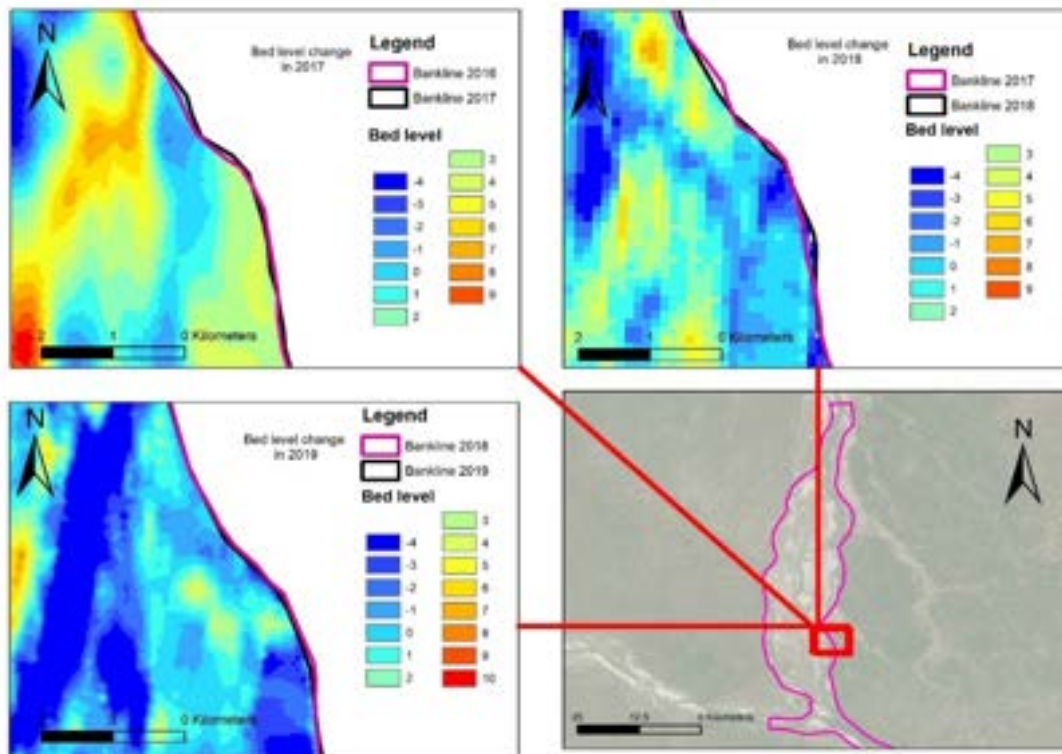
Figure 4.49 Bed level changes in area 06

4.8 Analysis with fine resolution bathymetry data

Bathymetry analysis was also made for the fine resolution survey data collected from field survey in the selected survey area (Figure 3-4) to better understand the riverbed formation. Figure 4-50 shows the scatter dataset of pre- and post-monsoon 2019. Figure 4-51 shows the bed level elevation in pre monsoon and post monsoon and erosion deposition. Three longitudinal profiles were analyzed to understand tbed form change along the reach.From analysis it was evedent that the the post monsoon thalweg line shifted towards right bank with respect to pre monsoon thalweg in the upstream of the cross section and towards left bank in the downstream of the cross section. Cross section profile in Figure 4-55 also indicates the same.
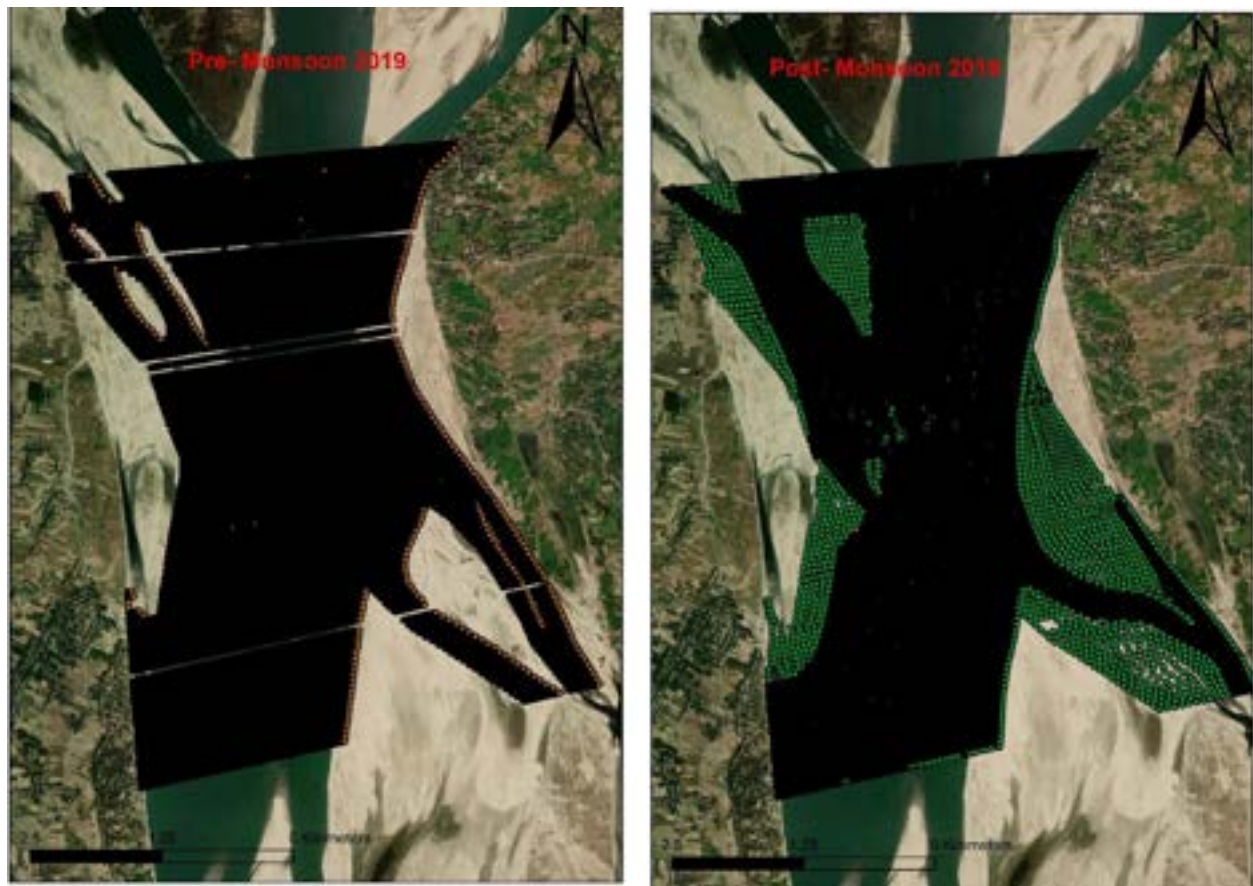
Figure 4.50 High resolution primary dataset
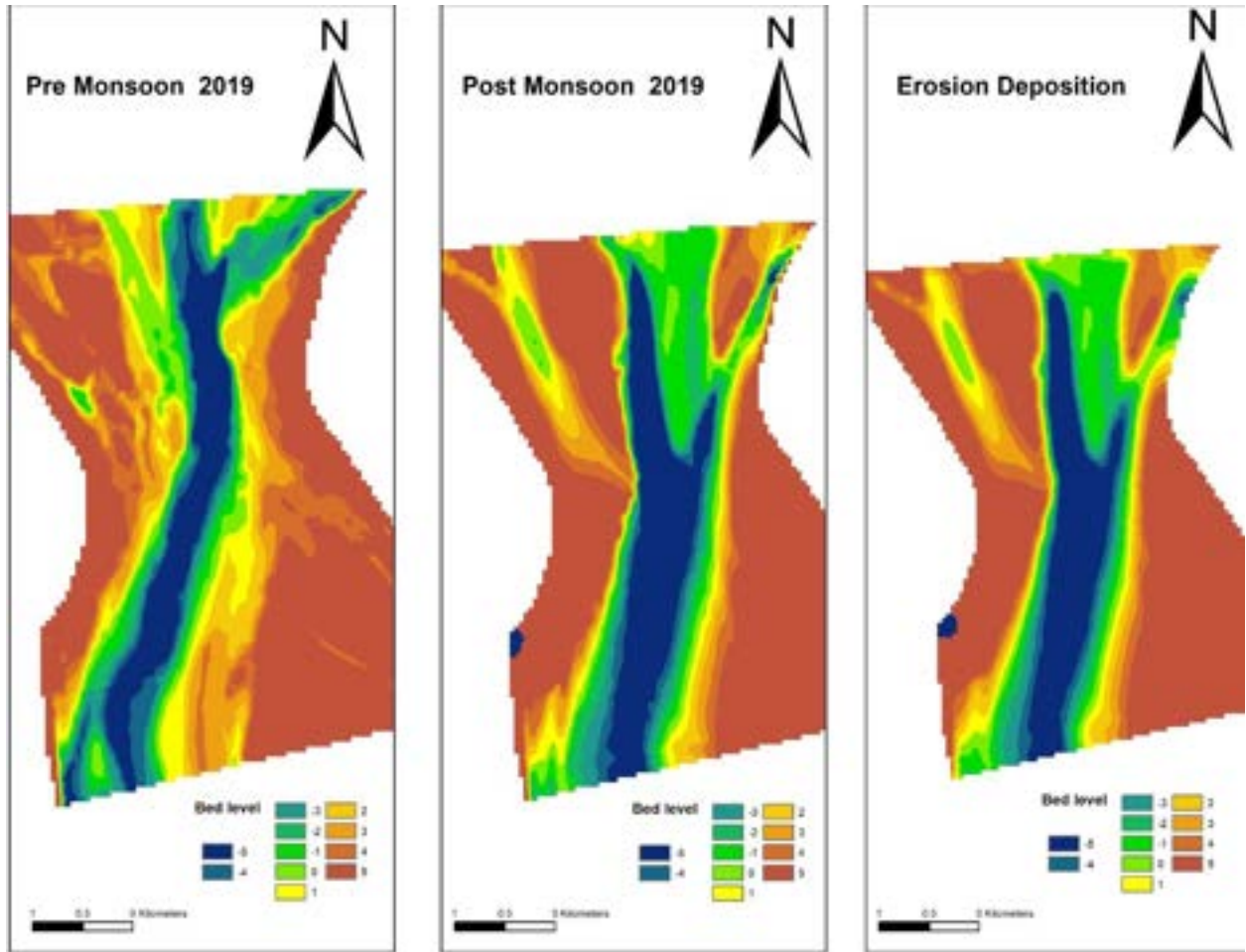
Figure 4.51 Comparison of bathymetry for primary data set

Longitudinal and cross-sectional profile were also scrutinized for these data set. It was found that in pre-monsoon bed profile changes rapidly from around -4 m to -11 m and create a depression. This depression was followed by deposition. In the post monsoon the bed profile follows almost similar pattern but the depression shifted around 2000 m towards downstream Figure (4-53). The left portion from the centerline experienced erosion whereas there was deposition in the right portion.

Six cross sections were evaluated (4-54 to 4-55). From the cross section change in thalweg was observed. From cross section 01 to cross section 03 pre-monsoon thalweg line was on the left of the post monsoon line as the channel propagated to cross-section 04-06 the post monsoon thalweg line shift towards left bank.
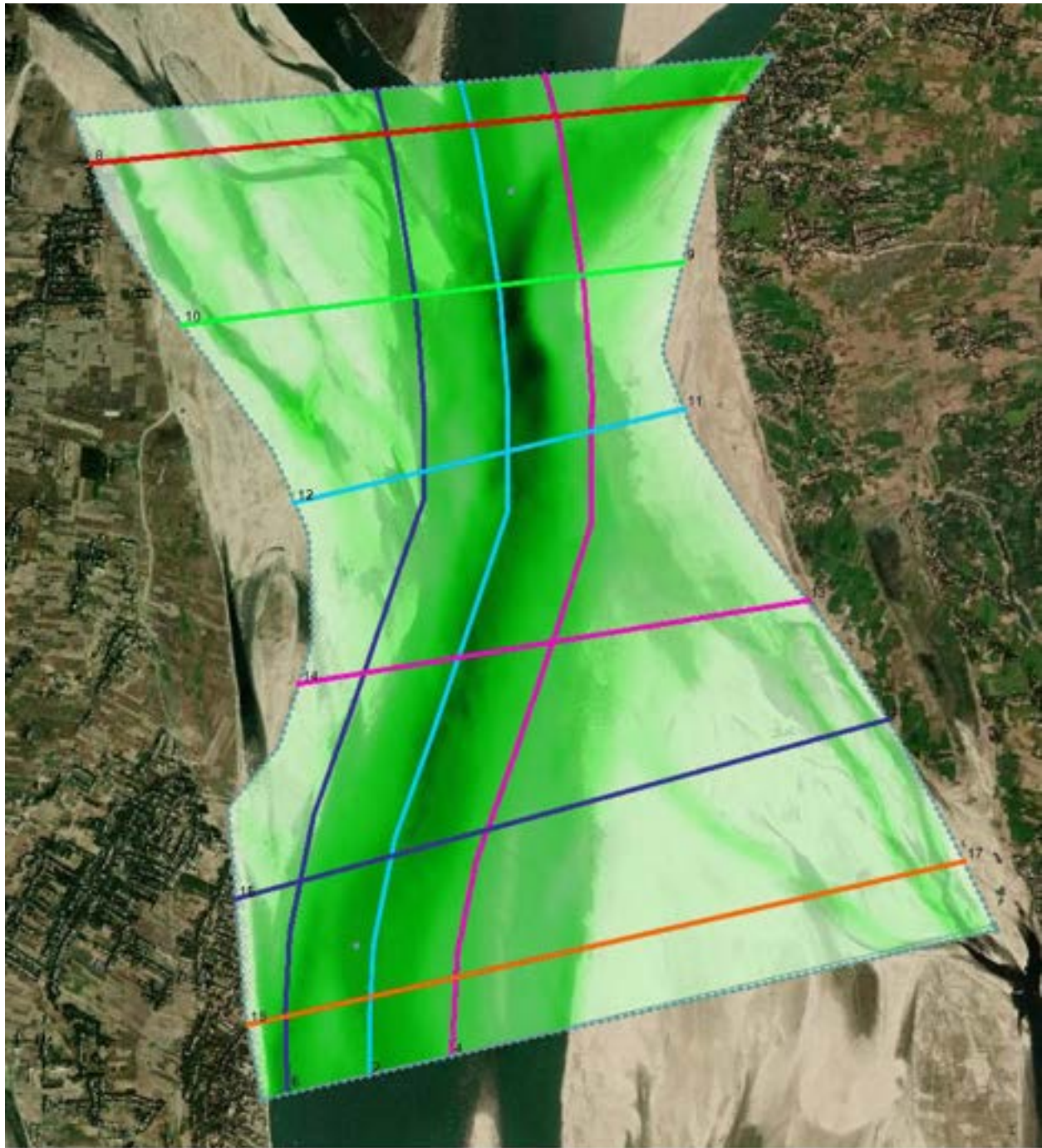
Figure 4.52 Longitudinal and cross-sectional profiles in primary data set.
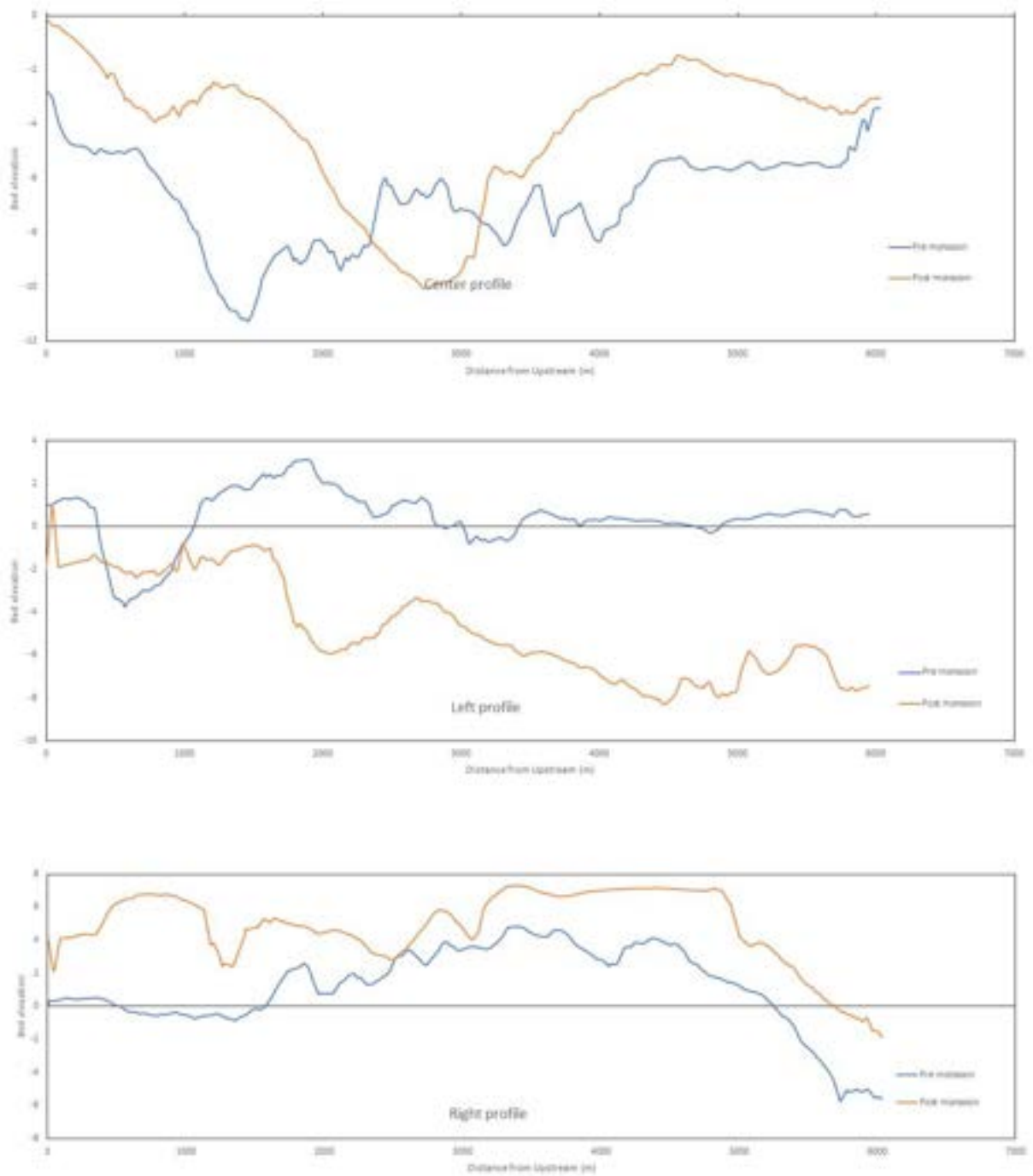
Figure 4.53 Longitudinal profile in the primary data set.
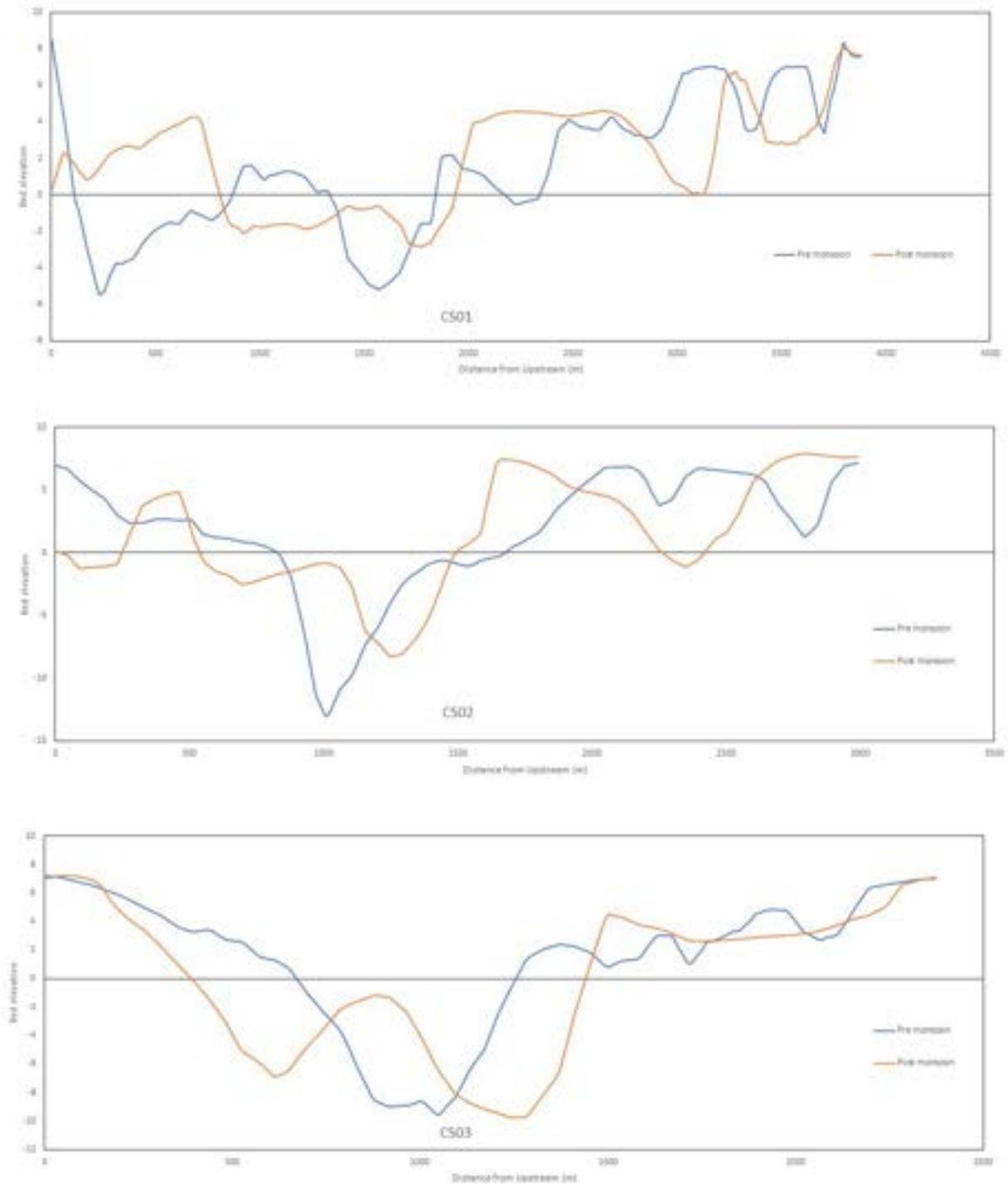
Figure 4.54 Cross sections primary data set.
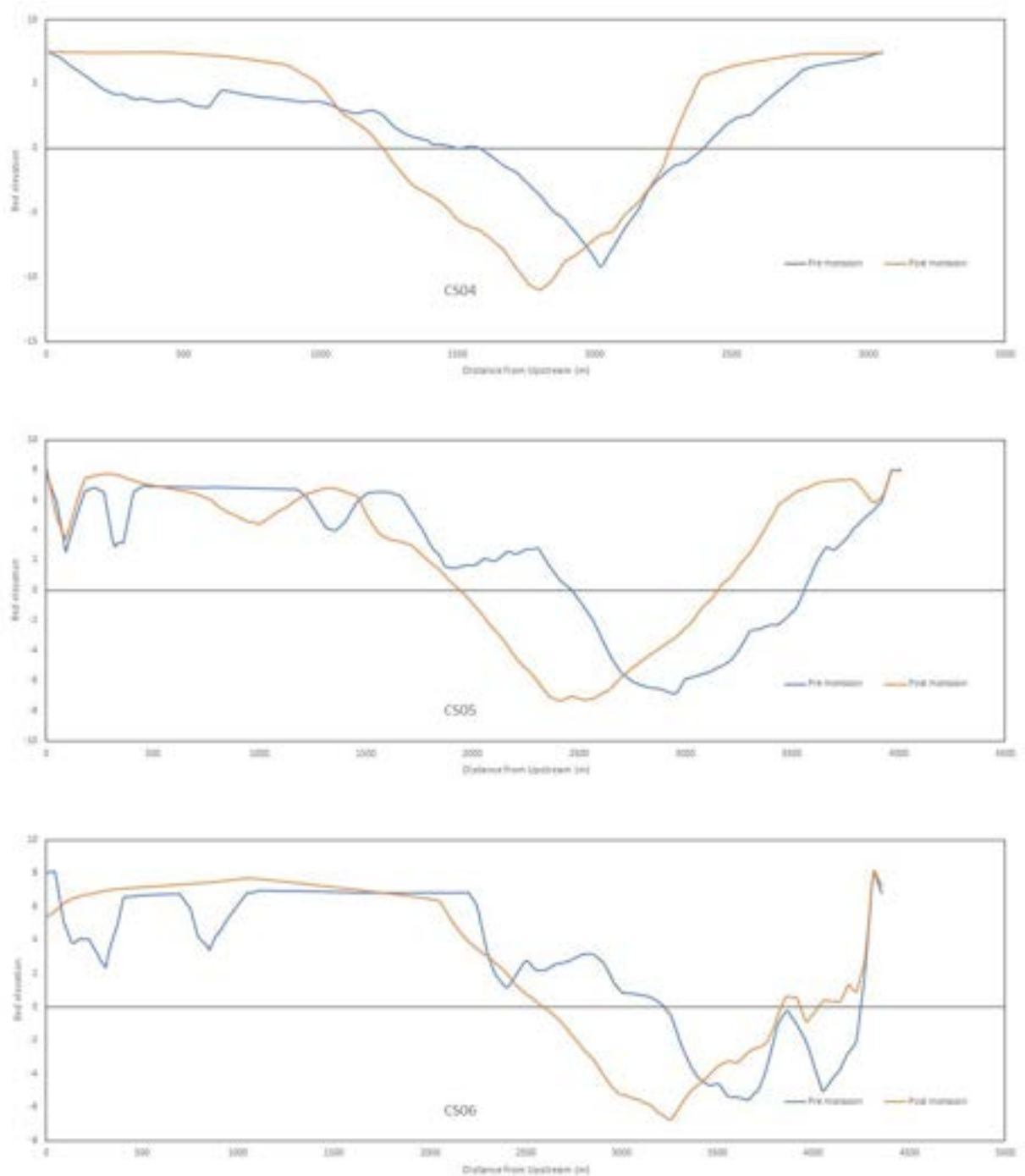
Figure 4.55 Cross sections in primary data set

4.9 Conclusion

In this chapter hydrological and morphological characteristics of Jamuna river was analyzed and an attempt was made to find a relation with bank erosion. In this process hydrological characteristics (Discharge and Water level) of Bahadurabad and Mathura was assessed. In association with that Planform change analysis with 32 years of satellite image, average width change analysis and bedform change analysis with four years of bathymetry data was made. For better understanding of the morphological behavior a fine resolution bathymetry data was also collected under this project.

From historical hydrologic data it was observed that the water level Jamuna river began rising in May-June and increased its flow gradually until the peak in July-August. The average monthly discharge is highest in July and lowest in February. From November to April, discharge is relatively low (Figure 4-7). From this study analysis, mean annual discharge was found to be around 17000 m^3/s. Maximum and minimum flood discharge was recorded as 102535 m^3/s and 3095 m^3/s respectively. From annual hydrograph at Bahadurabad station it was found that water level varies around 6 m from dry to monsoon season (Figure 4-3).

Erosion and deposition were calculated for both banks of Jamuna river using 32 years of satellite images to understand the erosion pattern during this period. From 1988 to 2019, total erosion along the Jamuna river left bank was 23800 ha with an average of 770 ha per year. Whereas for the right bank of the river total erosion was 11840 ha and 380 ha per year. It was evident from the data that erosion rate was higher for left bank of the Jamuna river (Figure 4-13). From the planform analysis it was found that width of the Jamuna river has an increasing trend and it is widening at the left bank side. Since the early 1980s, the Jamuna River in this study area widened from 14.2 km to 15 km in the 2020 and now the average width is 14.69 km (Figure 4-10).

From these hydrological and erosion data a correlation between peak discharge and total erosion was found, with higher discharge erosion will be higher. It was observed from the figure that for peak discharge in the year 1996 and 1998, erosion was maximum and erosion was less in case of lower discharge (Figure 4-15).

Morphological change was observed for four years with available data collected from FRERMIP. The change was also monitored with fine resolution data, specially collected under this project for a specific site. Yearly change in river bathymetry was monitored through both spatial assessment and assessment along thalweg. spatial change was observed through GIS mapping and significant erosion and deposition was observed along the active channels. The analysis with thalweg line also indicates the same. Longitudinal profiles (from figure 4-27 to 4-29) show a high spike of deposition, always followed by a steep crest erosion and a medium crest deposition is followed by medium to low crest erosion. Maximum erosion(-15.07m) occurred along the center profile in 2017-2018 and Minimum erosion (-8.06 m) occurred along the right profile in the year 2016-2017. Maximum deposition was observed as 20.81 m along

the left profile in the year 2018-2019. Table 4-4 below shows variation of bed levels along the profiles.

Combination of morphological change analysis and planform change analysis provided a very thought-provoking finding. When a sand bar is formed in the middle of a channel it diverts the flow towards the riverbank. when these diverted flows hit the riverbank, it exerts impact pressure almost perpendicularly and with higher impact the erosion will be higher. The magnitude of the impact may vary with the flow angle. This analysis was made at six erosion prone area identified from planform analysis. It was found that due to formation of bar when flows were directly diverted towards the bank significant amount of erosion occurred.

Chapter 5: Mathematical Modeling and Results

5.1 1D Hydrodynamic modeling

5.1.1 Introduction

Hydrologic Engineering Center's (CEIWR-HEC) River Analysis System (HEC-RAS) is an integrated software system, designed for interactive use in a multitasking environment and used to perform one-dimensional water surface calculations. This software permits the user to perform one-dimensional steady flow, one and two-dimensional unsteady flow calculations, sediment transport/mobile bed computations, and water temperature/water quality modeling .Four files are compulsory to run a HEC-RAS project.

5.1.2 Purpose of 1D Hydrodynamic modeling

There is no discharge and water level measuring station in study area which can be used as boundary condition in the 2D model. Therefore, 1D hydrodynamic model was developed to find discharge and water level just to the upstream and downstream of the study area respectively. For this the study area for 1D hydrodynamic model was extended to Bahadurabad in the Jamuna reach, to Mathura just upstream of the confluence of the river Jamuna and Ganges. For this a 1D HEC-RAS model will be used. Using this 1D model discharge at the downstream of the Bangabandhu Multipurpose Bridge and water level at the confluence of the Jamuna and Ganges river will be derived. This data was used in developing 2D Hydrodynamic and morphological model as well as to calibrate and validate them.

5.1.3 1D Hydrodynamic model study area

The study reach is selected within the district of Gaibandha, Jamalpur, Bogra, Sirajganj and Tangail, Pabna, and Manikganj and covers about 150 km reach of the Jamuna River (90km upstream and 60km downstream of The Bangabandhu Multi-purpose Bridge). Bahadurabad Transit (SW46.9L) is situated at the upstream of the study reach where as Kazipur (SW49A) and Sirajganj (SW49) is situated at the right bank of the reach and Mathura (SW50.3) is situated at the downstream end of the study reach. The location of the study area is shown in Figure 5-1. To avoid complexities inflow and outflow from the intakes and off takes are neglected.
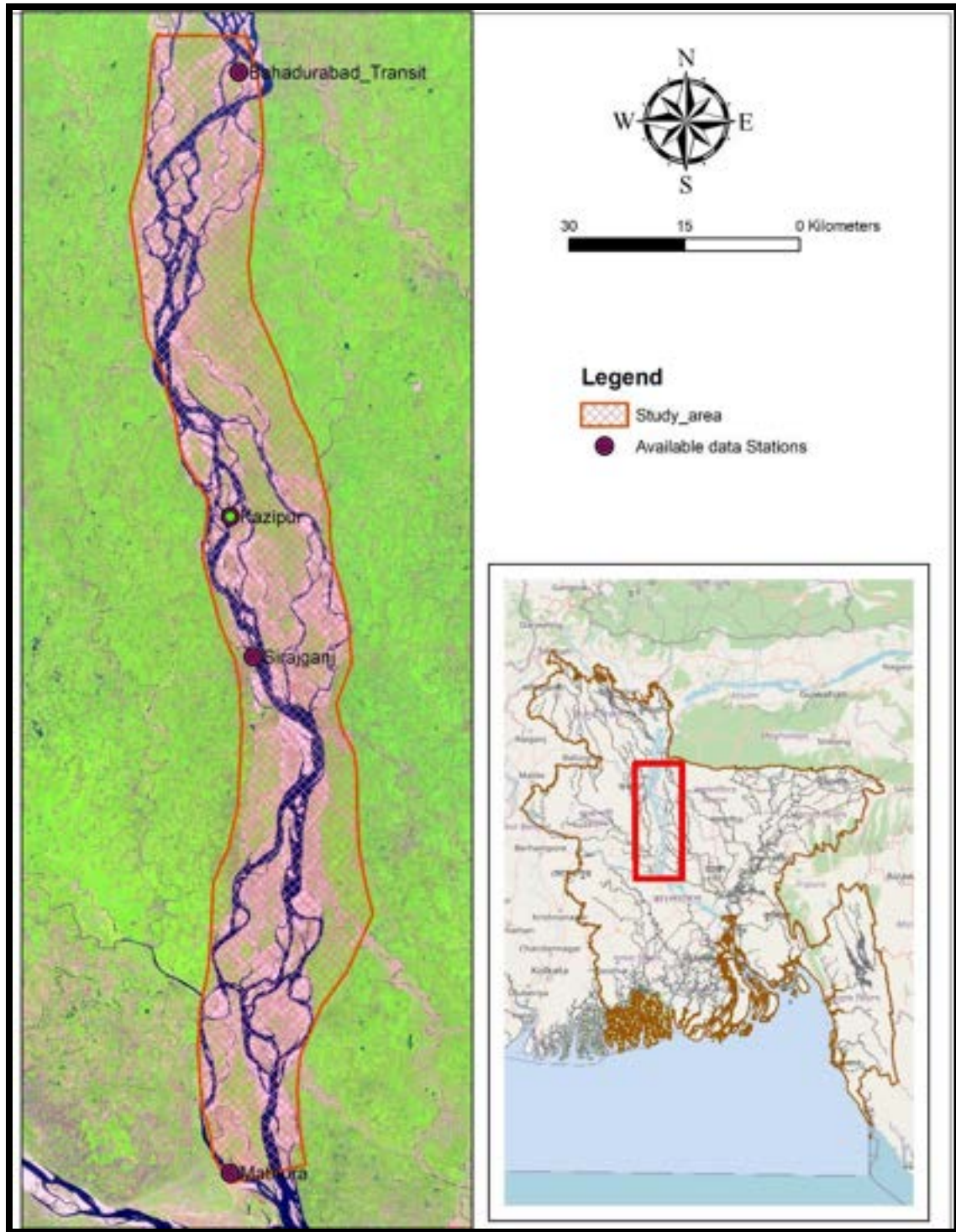
Figure 5.1 Hydrodynamic model study Area.

5.1.4 1D Model data

Cross section data

Jamuna river Cross section data were collected from BWDB. The model was developed with 2016 cross section data. Total 24 cross sections were used to develop Hecras 1D model to generate inflow for 2D model. These cross sections were digitized from a morphological map (By BWDB). Figure 5-2 shows the cross sections used in this study and 5-3 shows a typical cross section of Jamuna river.
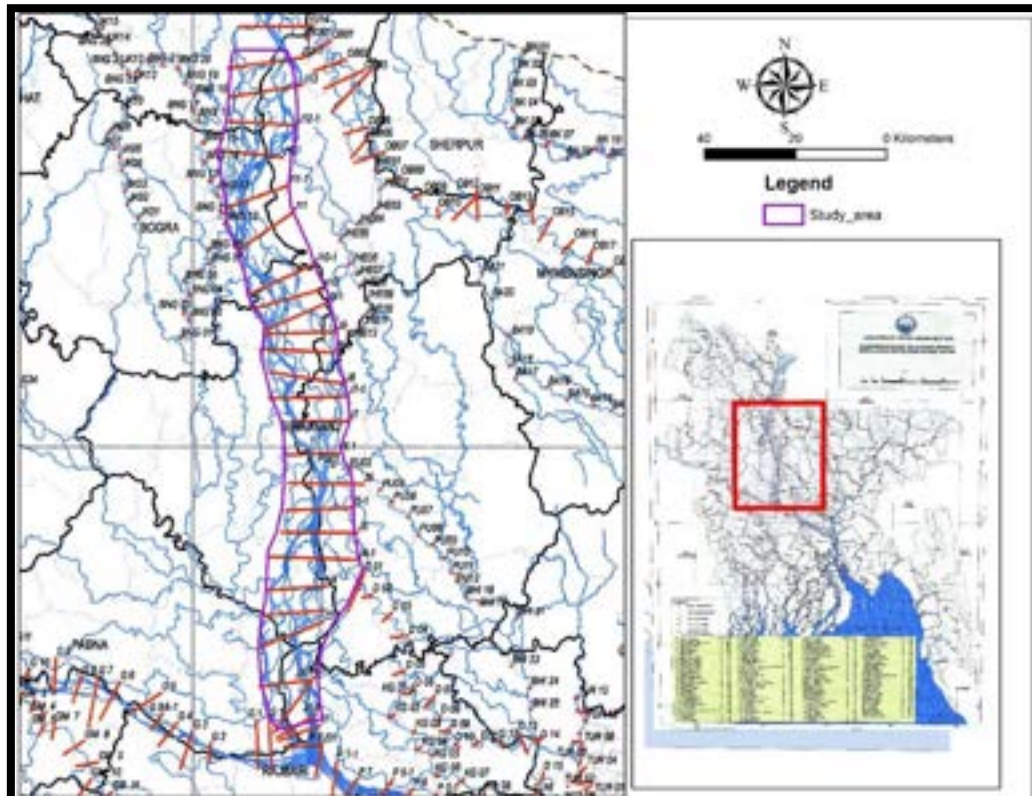
Figure 5.2 Cross section Location
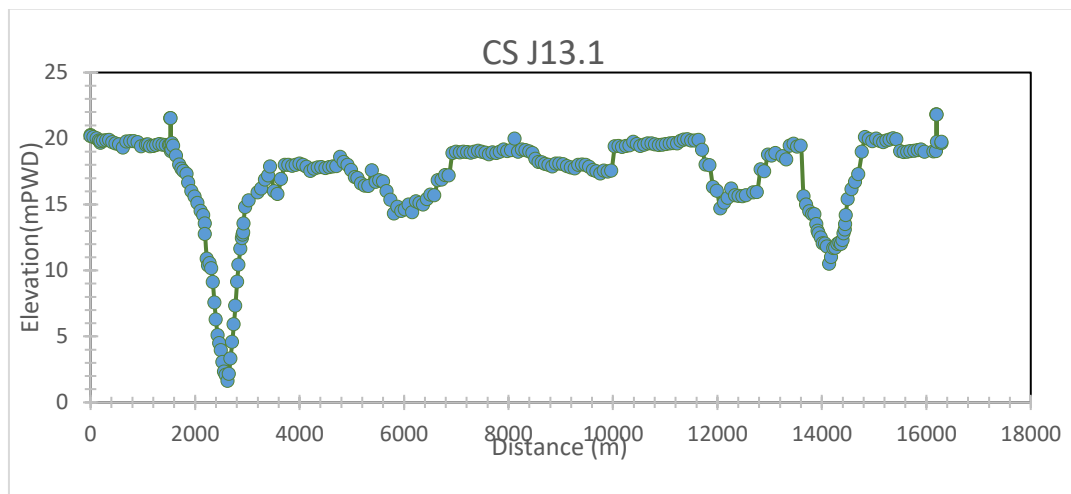
Figure 5.3 A Cross Section Used in Hecras

Boundary condition

Boundaries are important as they define the input conditions to the Modelling process within the model boundary. For the FLOW, two boundaries have been defined. It consists of two open boundaries (Upstream and Downstream boundaries). Normally total discharge is assigned at the upstream inflow boundary and water level at downstream boundary. The model of the Jamuna River had a total discharge boundary at the upstream Bahadurabad and a water level boundary at downstream at Mathura. AS cross section data were available for the year 2016, discharge and water level data of the same year was used. Figure 5-4 show inflow discharge and water level at downstream boundary.
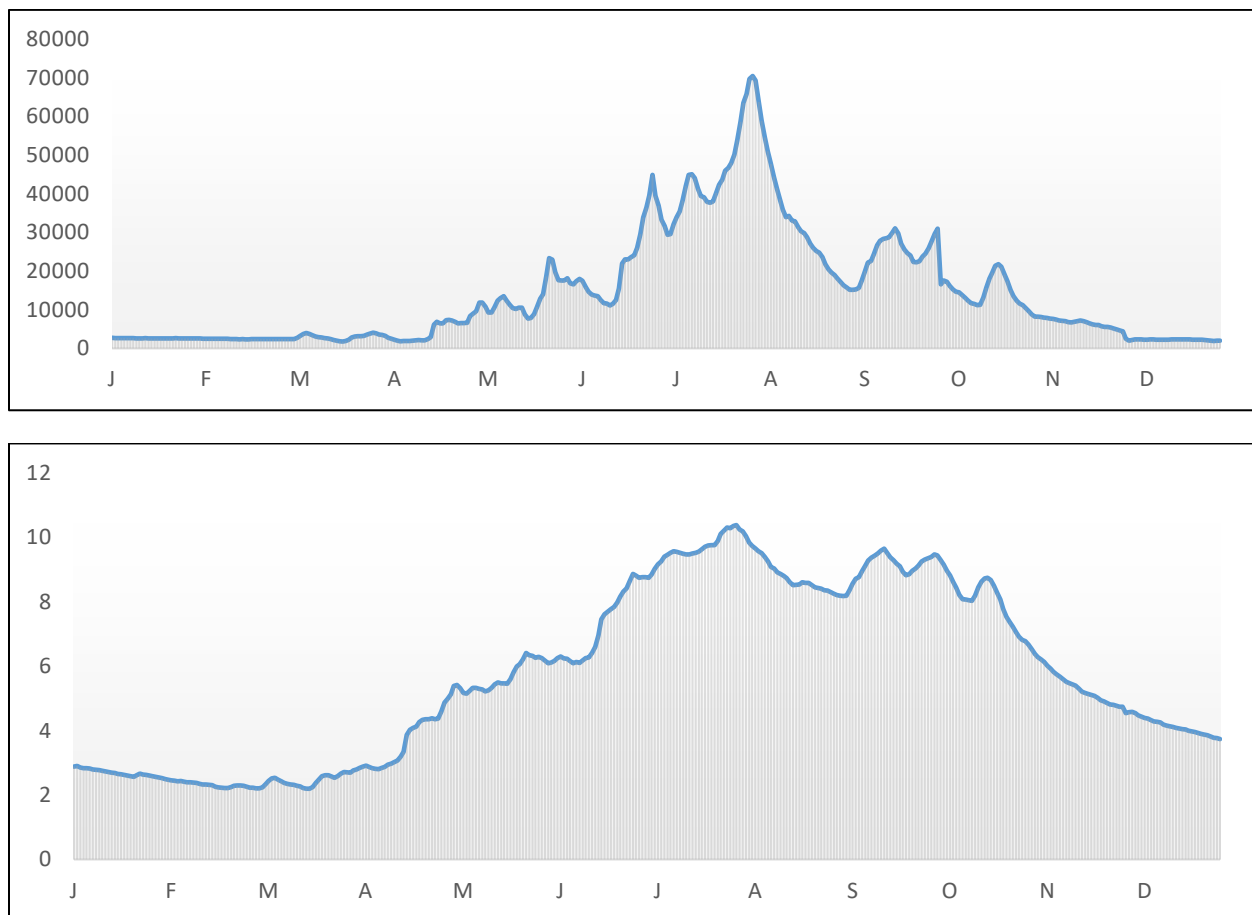
Figure 5.4 Hecras Boundary Condition

5.1.5 Calibration and Validation

During model development, many uncertainties exists related to input as model geometry, boundary conditions, roughness, eddy viscosity etc. which can have momentous impact on

model solutions. Once geometry and boundary conditions have been obtained with reasonable accuracy from the field, it is common practice to set them out of preview of the calibration process. Validation is a multi-step process of model adjustments and comparisons, leavened with careful consideration of both the model and the data. During validation, a new set of observed data have been incorporated to justify whether the calibrated parameters produces satisfactory result for a new condition

For hydrodynamic calibration, roughness is the parameter to play with to obtain an adequate match with the observed field conditions. For the present study, the water levels at Kazipur station were compared with the simulated water levels of the model for the same location. The roughness parameter (Manning's n) was adjusted to get the best result.
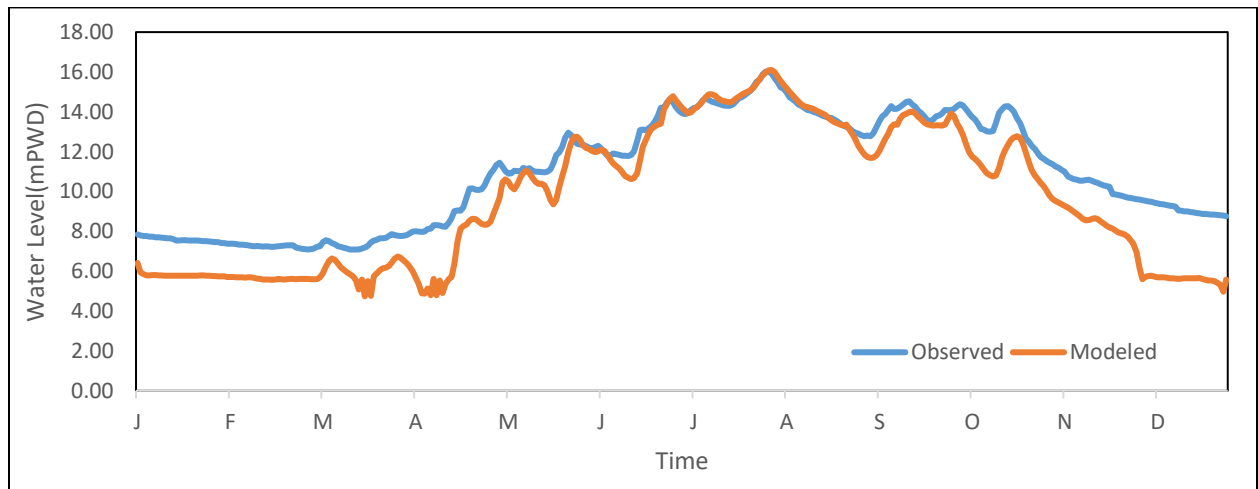
Figure 5.5 Calibration at kazipur Station

The computed water surface elevations by the model were validated with observed water surface elevations at Sirajganj station for the months of 1 January 2016 to 31 December 2016. Good agreement between the observed and simulated water levels indicates satisfactory performance of the model. During the calibration and validation process, the model showed good agreement with observed data for wet periods. Therefore, the model was capable to simulate different conditions and scenarios used in the present study.
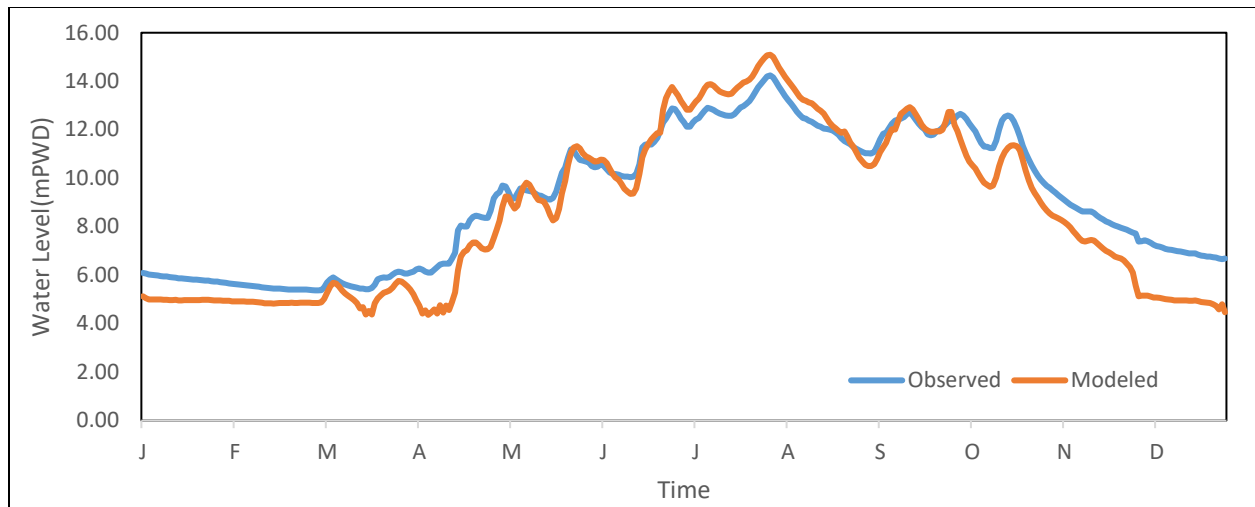
Figure 5.6 Validation at Sirajganj Station.

5.2 2D-Hydrodynamic Modeling

5.2.1 Introduction

A 2D hydrodynamic model was setup using the depth average SRH-2D model. The extent of this model started from just downstream of the Bangabandhu Multipurpose Bridge to 15 km upstream of the confluence of the river Jamuna and Ganges. The bathymetric data collected from FRERMIP project of the year 2018 were used in developing this model. Required water level and discharge data from collected station were used as boundary condition. For modeling paving type mesh was applied and grid size was 175m to keep number of elements with in the calculation limit of SRH 2D. Hydrodynamic model was simulated for 12 months with 30 sec time intervals. The model results were useful to understand the hydrodynamic characteristics of Jamuna river although due to lack of fine resolution data and computational capacity it wasn't possible to replicate the actual scenario.

5.2.2 Modeling approach

Data Collected from FRERMIP was used as elevation data, Following the scatter data internal channel and island were delineated. Boundary Coverage was added both in upstream and downstream. Material coverage was added to define roughness and monitor points to observe simulation status. After defining Model controls model was prepared to simulate. To calibrate validate the model Manning's roughness was used. Following figure shows the modeling approach of SRH 2D.Figure 5-7 shows SRH 2D modeling approach.
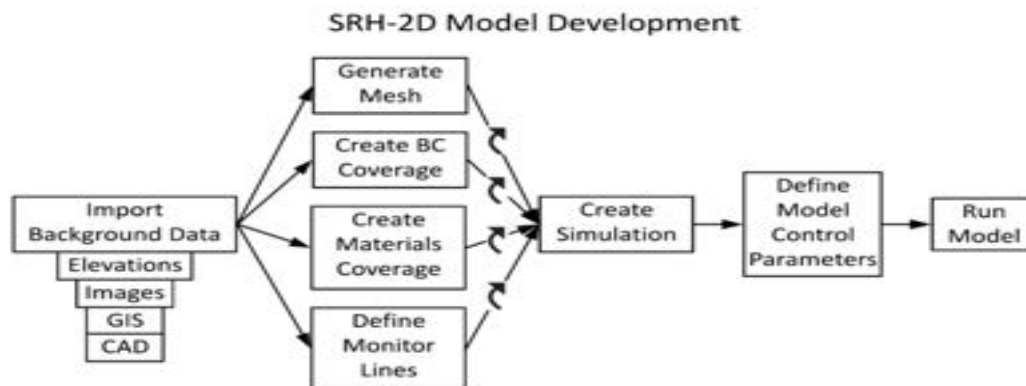
Figure 5.7 SRH 2D Modeling approach

5.2.3Delineation of Model Boundary and parameter.

Model boundary was delineated in SMS Using satellite image of 2018 as bathymetry 2018 was used to define bed level. To keep number of elements within calculation limit of SRH 2D 175m spacing was used to redistribute vertices. Then a 2D mesh was created. all mesh parameter is given below. (Table 5-1)

Table 5-1 Mesh information of SRH 2D model.

Mesh module Information	
Element type	Linear
Number of triangular elements	34288
Number of quadrilateral elements	0
Max. element front width	139
Max. node half band width	143
Number of elements	34288
Maximum element Id	34288
Number of nodes	17549
Maximum node Id	17549
Minimum Z value (m)	-18.4
Maximum Z value (m)	10.48
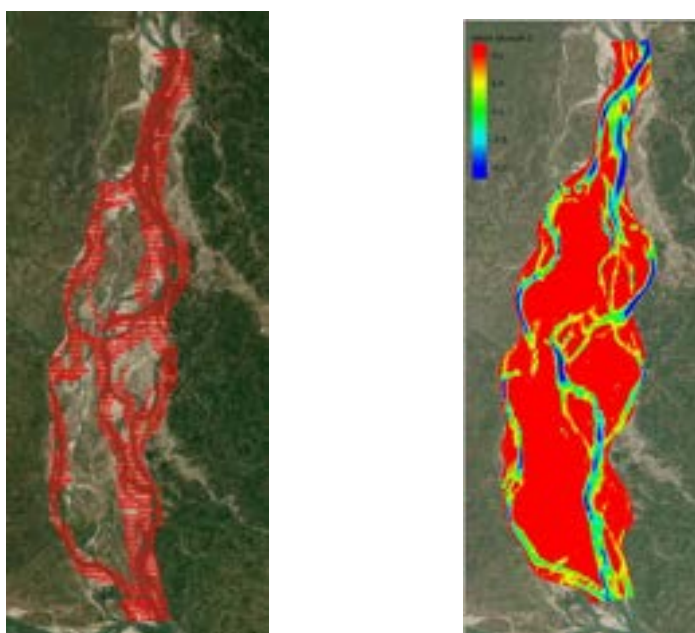
Figure 5.8 Mesh Generation SRH 2D
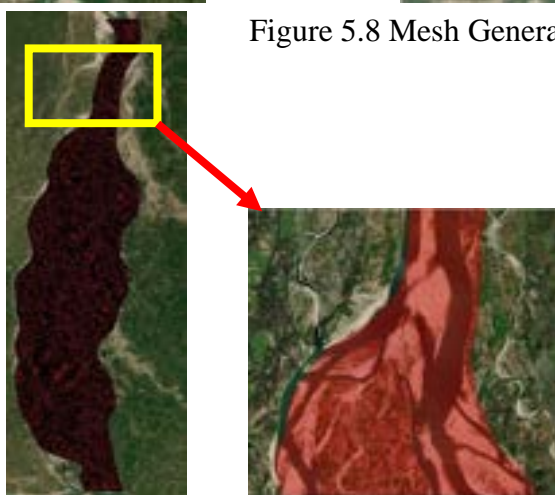
Figure 5.9 mesh elements of model

5.2.4 Boundary Data Definition

There was no discharge measuring station near model input boundary so, to generate inlet boundary condition discharge 1D Hecras was developed. In the hecras model discharge at Bahadurabad Transit was used as inlet boundary condition and water level at Mathura station as downstream boundary. As Hecras model was well calibrated and validated discharge at model inlet was derived with confidence. Figure below shows Upstream and downstream boundary condition for SRH 2D model. Figure 5-10 and 5-11 shows boundary data of Srh 2d model.
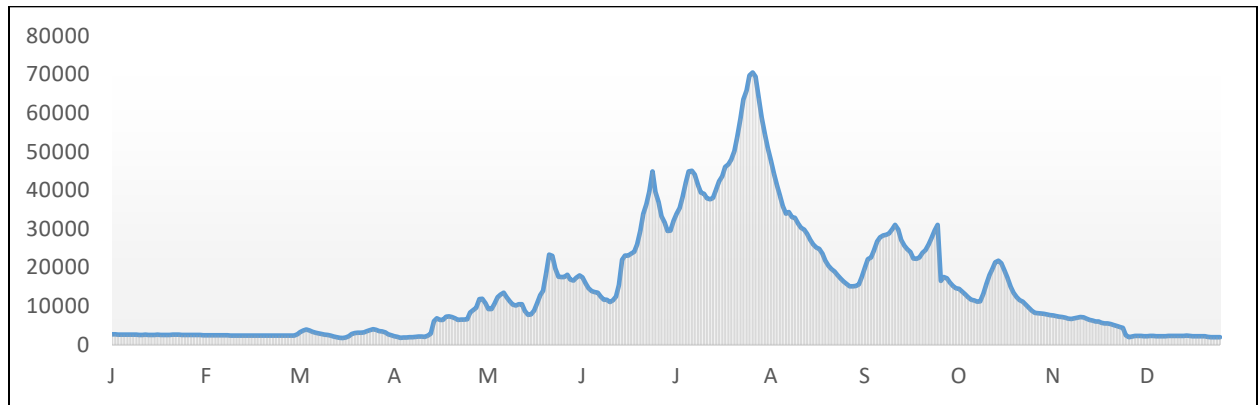
Figure 5.10 Discharge Just downstream of jamuan river
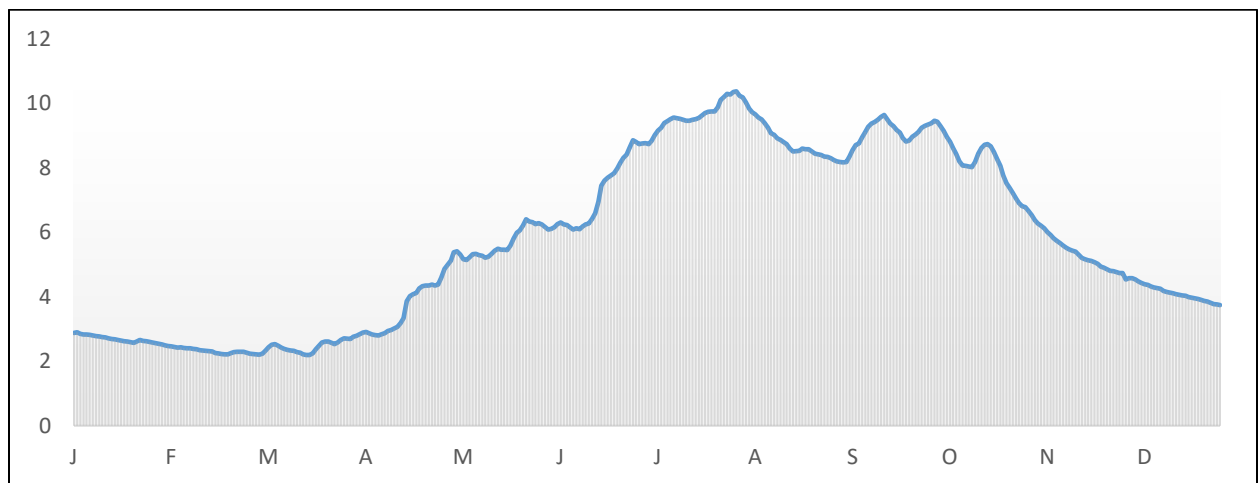
Figure 5.11 water level at Mathura station

5.2.5 Model Simulation

Model simulation has been performed for the wet period of 2018 (From May to October) using daily time series data of discharge and water level as described in the earlier section done on a daily basis. In this simulation, Manning's n was used 0.025 for river channel 0.03 for flood plain. Model result output interval was 24 hours.

5.2.6 Calibration and Validation

During model development, many uncertainties exists related to input as model geometry, boundary conditions, roughness, eddy viscosity etc. which can have momentous impact on model solutions. Once geometry and boundary conditions have been obtained with reasonable accuracy from the field, it is common practice to set them out of preview of the calibration process. Validation is a multi-step process of model adjustments and comparisons, leavened with careful consideration of both the model and the data. During validation, a new set of observed data have been incorporated to justify whether the calibrated parameters produces satisfactory result for a new condition

Figure 5.12 SRH 2D Calibration and Validation station

For hydrodynamic calibration, roughness is the parameter to play with to obtain an adequate match with the observed field conditions. For the present study, the water levels at HECRAS station 27688.92 were compared with the simulated water levels of the model for the same location Figure (5-12). The roughness parameter (Manning's n) was adjusted to get the best result. Calibration and validation were made in wet period (may to October).
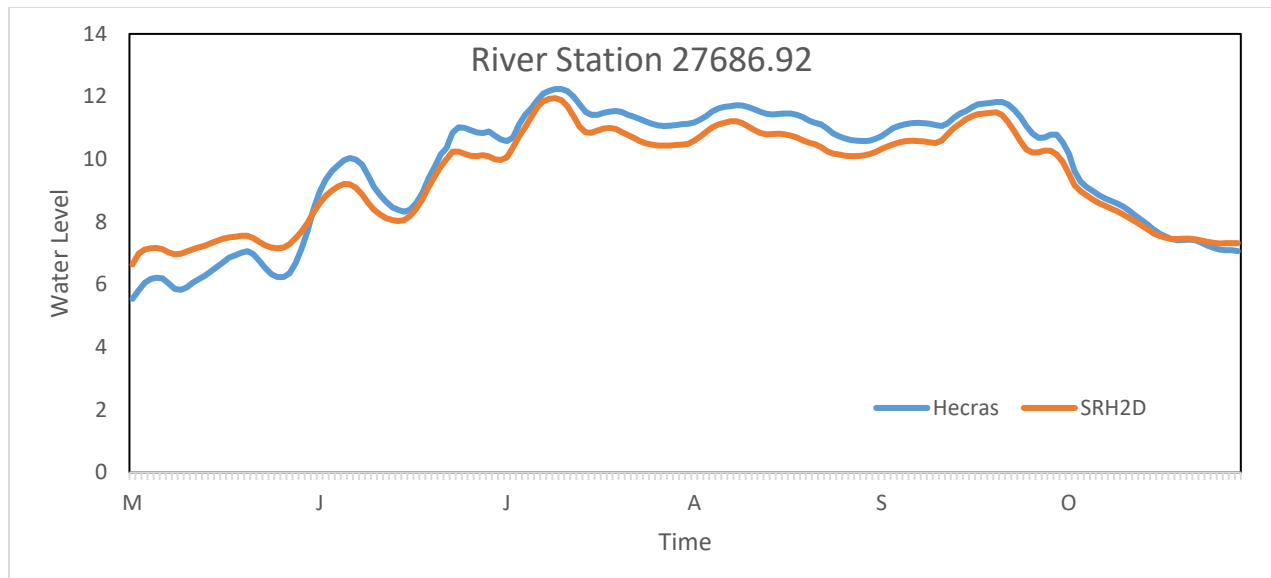
Figure 5.13 SRH 2D Calibration
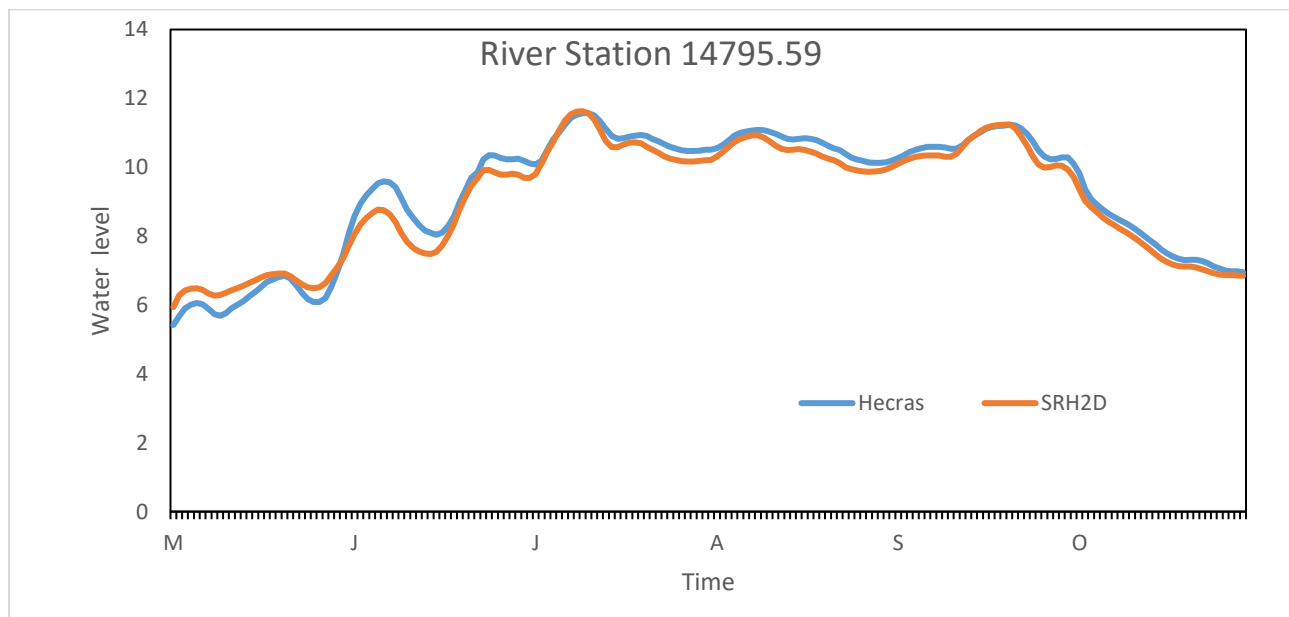
Figure 5.14 SRH2D validation

5.2.7 Results

Following figures show water elevation, flow direction, velocity magnitude. Figure 5-15 shows velocity contour and flow direction and water depth at the time of peak. Bed shear stress from the model shown in figure 5-16. Shear stress is higher in the main channel zone where most of the erosion and deposition take place. From the stress value along the model boundary, lateral stress on the river bank can be assessed. The higher the stress the higher the possibility of bank erosion. From the model velocity maximum velocity was found as 2.57 m/s and velocity is higher along the main or active channel and the velocity is relatively lower around the flood plain during high flood. The water depth output showing variation of water depth along the reach Bed shear stress output showing sheer stress is higher at the bottom of the active channel. Shear stress at the model boundary may indicate stress at the toe of the bank. Thus, if the stress is high enough it could erode the river bank.
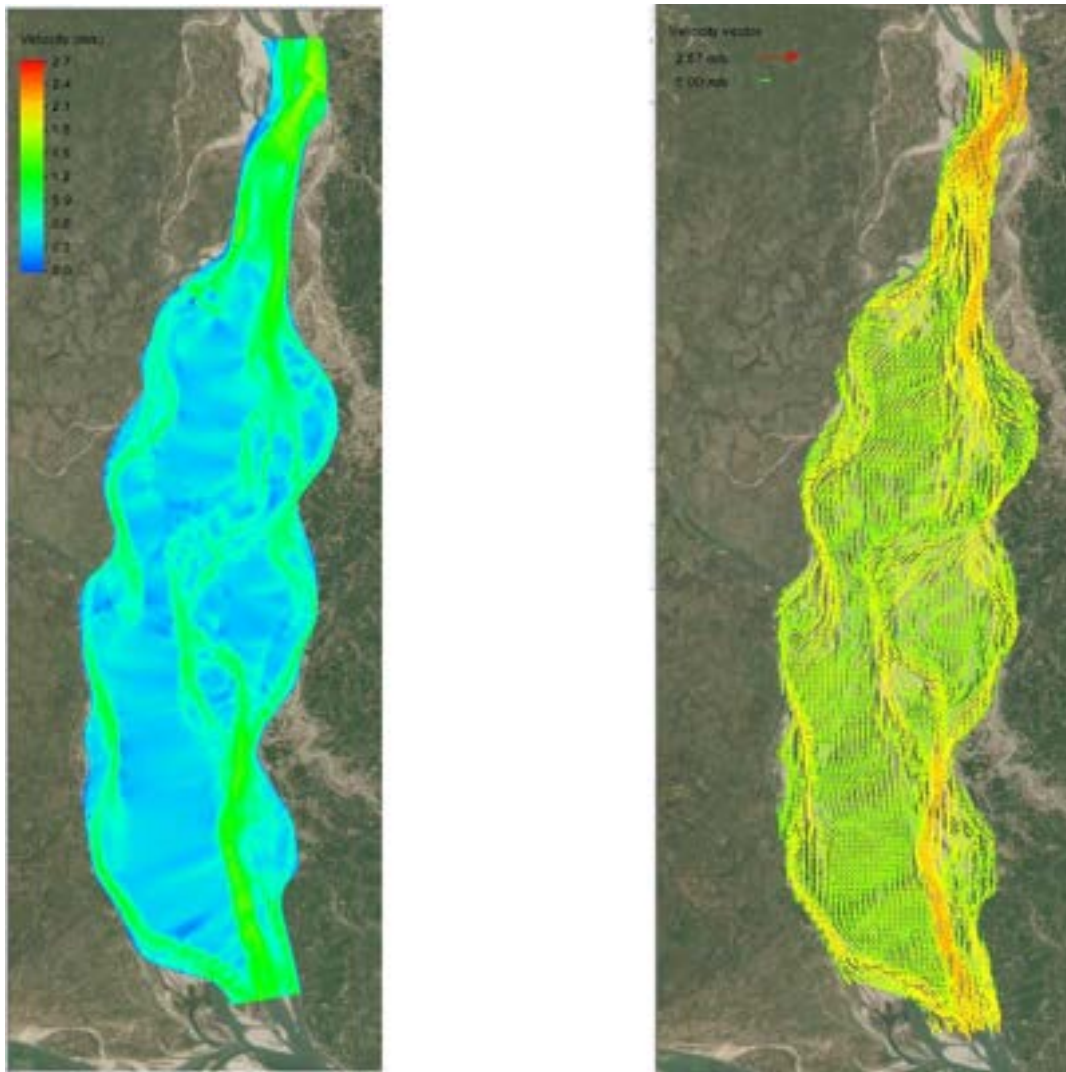
Figure 5.15 Velocity contour and flow direction
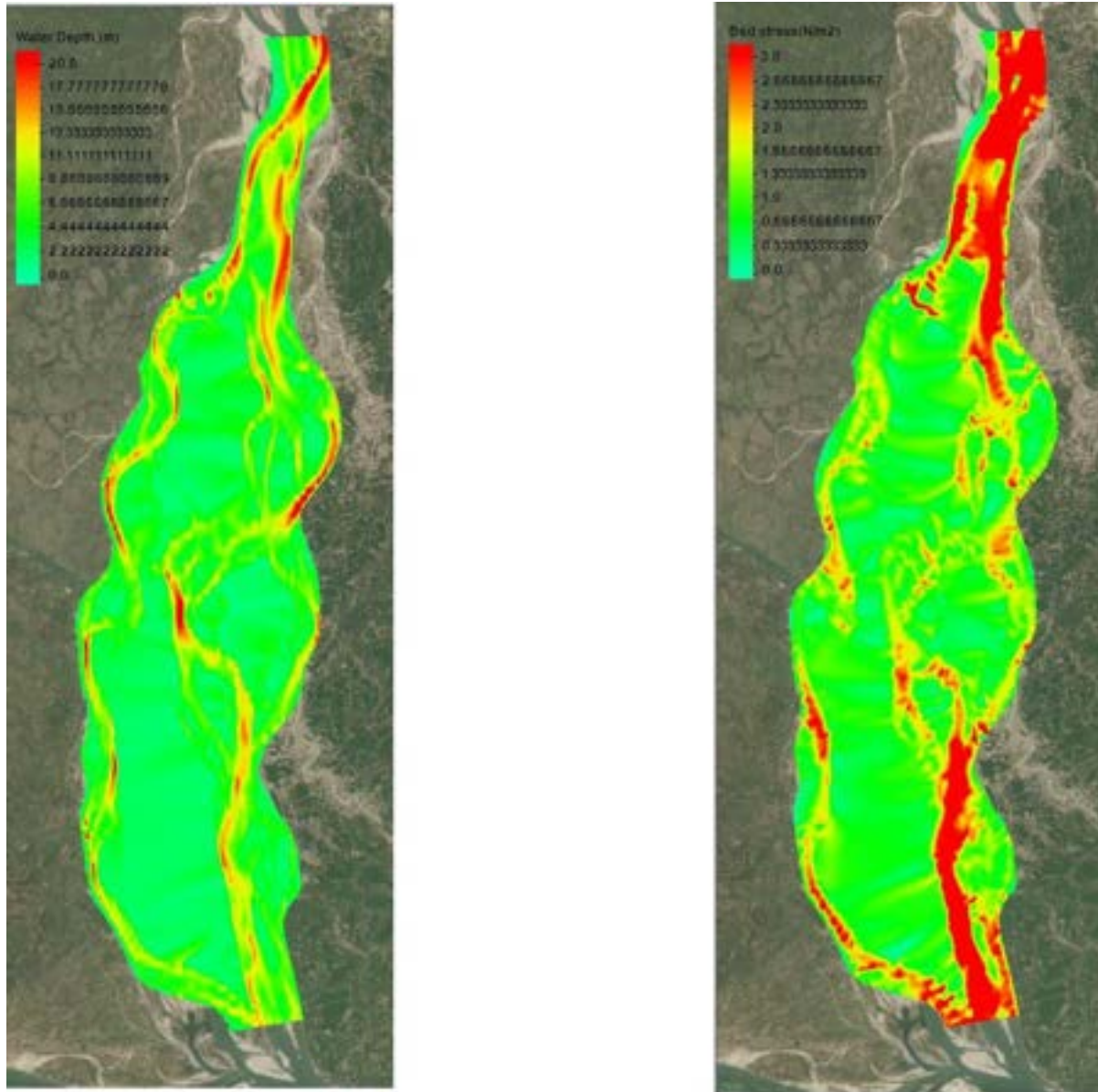
Figure 5.16 water depth and Bed shear stress at the time of peak.

5.3 Morphological Model Development and Simulation

SRH-2D is a two-dimensional, depth-averaged, hydraulic and sediment transport model for river systems under development at the Bureau of Reclamation. The hydraulic flow model, documented by Lai (2008; 2010), has been widely used by internal and external users. The sediment transport mobile-bed module is used to predict stream-bed vertical changes and has been described by Lai and Greimann (2008; 2010) and Lai et al. (2011). The sediment module tracks multi-size, non-equilibrium sediment transport for suspended, mixed, or bed load for both cohesive and non-cohesive materials.

5.3.1 Development of Morphological Model

Morphological model was developed with the mesh generated for 2D hydrodynamic model. Input and output boundary conditions were also similar to Hydrodynamic model except sediment size gradation, Governing equation, adaptation length, active layer thickness. These terms are described below.

Sediment size gradation

Along the length of Jamuna river the size and gradation of sediments changes and it varies from 0.14 mm to .20mm. In this study D50 was assumed to be 0.185 mm and three size class were used in simulation. Each size class is transported and tracked by the model (non-uniform representation). Cohesive sediments are lumped into one size class and represented by the size class number one.

Sediment transport equation

Among seven sediment transport equations available in SRH-2D "Engelund-Hansen" (1967) – A total load equation was used in this simulation. This sediment equation is suitable for sandy river bed and again size diameter 0.16mm to 0.93 mm. As in Jamuna average sediment particle size is about 0.2 mm , Engelund-Hansen(1967) was adopted in modeling.

For Adaption Coefficient of Suspended Load "Phillips-Sutherland Saltation Length Formula" was used. – this defines characteristic length for sediment to adjust from non-equilibrium to equilibrium transport conditions and active layer thickness was specified by 10 times of D90.

5.3.2 Limitations of Sediment Transport Modeling with SRH 2D

Due to the computational expense of sediment transport modeling, if the ultimate goal of a modeling project is to conduct a sediment transport study the number of elements should be limited to less than 40,000. For better result it is recommended that the number of elements be kept to less than 30,000. When converting an existing hydraulic model into a sediment transport model the same limits apply meaning the mesh may require coarsening. For almost 60 km long study area it was very challenging to keep mesh elements number with in the limit of the model. In this process selected mesh size become as long as 175m. Which is very coarse resolution to produce satisfactory results for the study needs of this project. On the other hand,

best fine resolution data available was of 500 m interval. In a very active river like Jamuna in 500 m bed form pattern may change multiple times due to these limitations Model results may not match the actual scenario of bedform change over the year.

5.4 Simulation

In this study a numerical model was simulated only for the wet period of the year 2018. The assumption worked behind this simulation was the major morphological changes are happened during the monsoon season. Simulation run period was from May 2018 to October 2018 with 30sec time step.

5.5 Result and Discussion

Morphological modeling of such an active river like Jamuna was very challenging. Moreover, there was limitation on fine resolution data, computational power etc. The beat available bathymetry data have a resolution of 500 m but in Jamuna river within 500 m the river bed may change several times. Including all these uncertainties it was very difficult to replicate the real scenario. As such SRH 2D has some limitation modeling morphological process. Figure (5-18) showing bathymetry before and after simulation of 2019. Figure 5-17 is showing a comparison between simulated and observed bed level at two cross sections. From the plot, it was evident that simulation of morphology did not give a good match with the observed data. This is due to the uncertainties involved in the process. Moreover, there limitation in sediment transport governing equations for these kinds of rivers. However, to address all these uncertainties in predicting river bank erosion, deep learning method has been incorporated in this study.
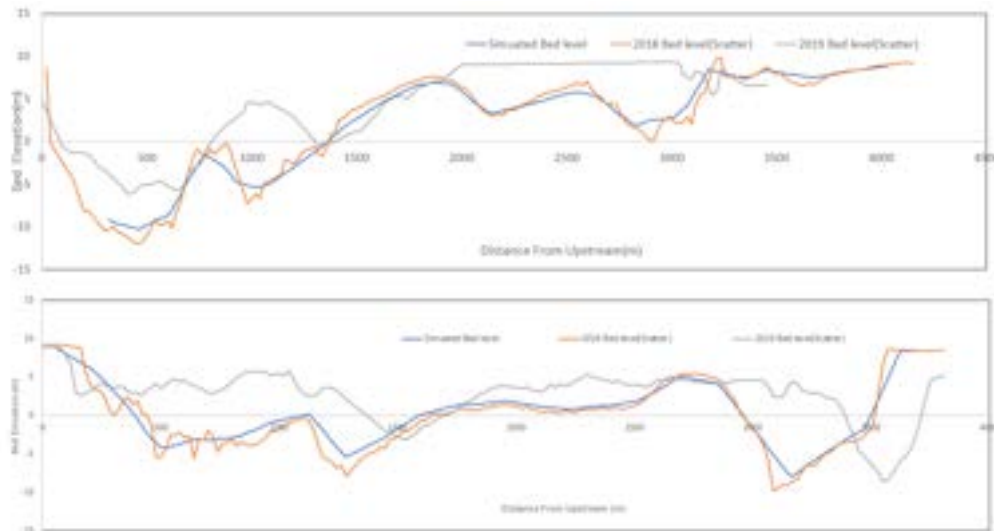
Figure 5.17 simulated and observed bed level
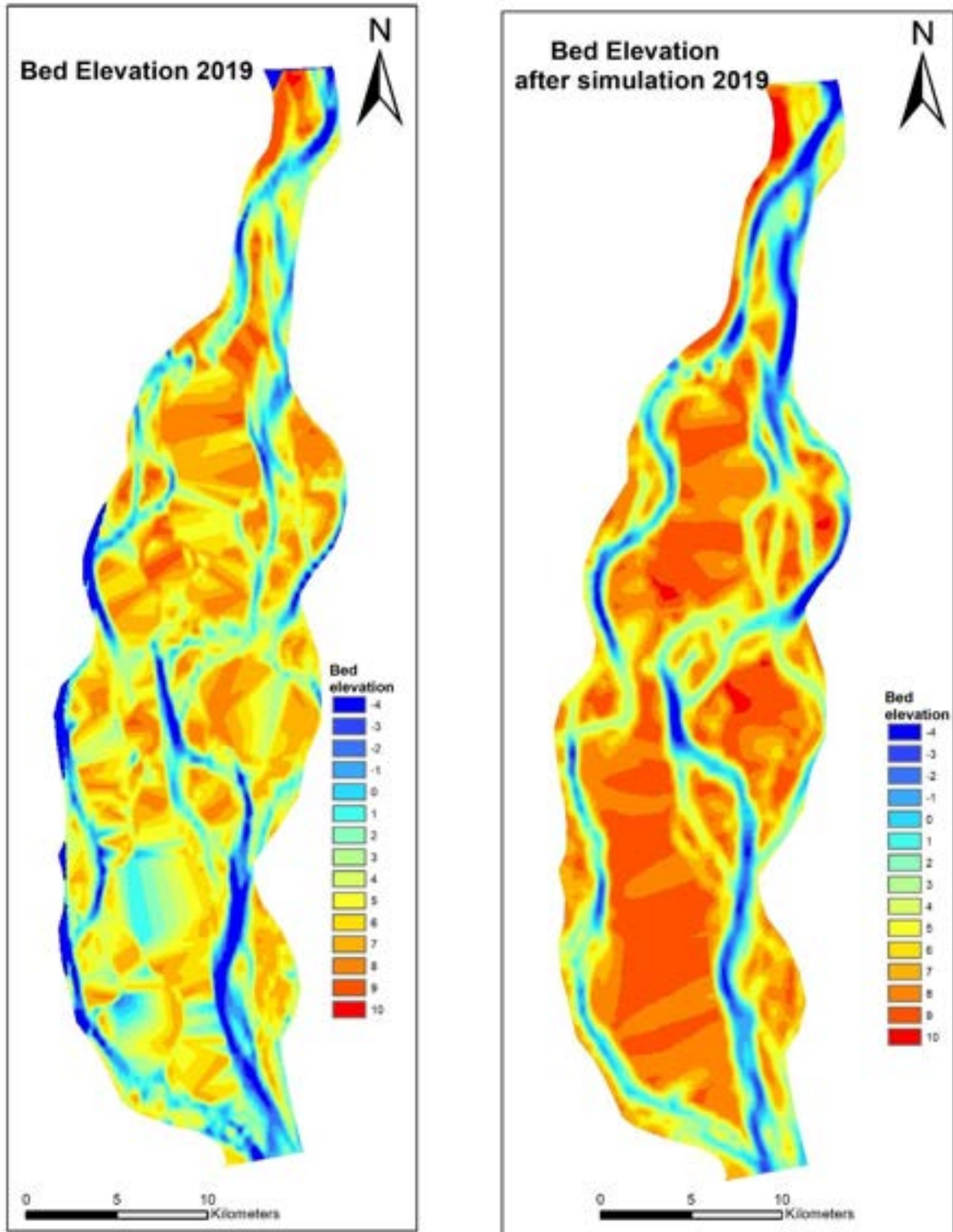
Figure 5.18 Bathymetry before and after simulation of 2019

5.6 Relation between Model result and Planform

The model results clearly do not agree with observed bedform change. Model may predict erosion or deposition correctly, but the extent of erosion and deposition was not obtained. This may be due to very coarse resolution data and mesh grid size. Although the model cannot predict the bed form change accurately for this grid size it could give some indication of bank erosion. To assess the probability of bank erosion bed shear stress along the bank was observed. It was found from the simulation that at the places where erosion took place in the year 2019, shear stress is higher and where the bank remained almost at the same position shear stress is relatively lower there. In erosion prone area 01,02,03 erosion took place in 2019 and from model result it can be found that shear stress is relatively higher in those areas. Similarly, in area 04,05 and 06 there was little to no erosion and bed shear stress along the bank ass relatively lower. (Figure5-19 to 5-24).
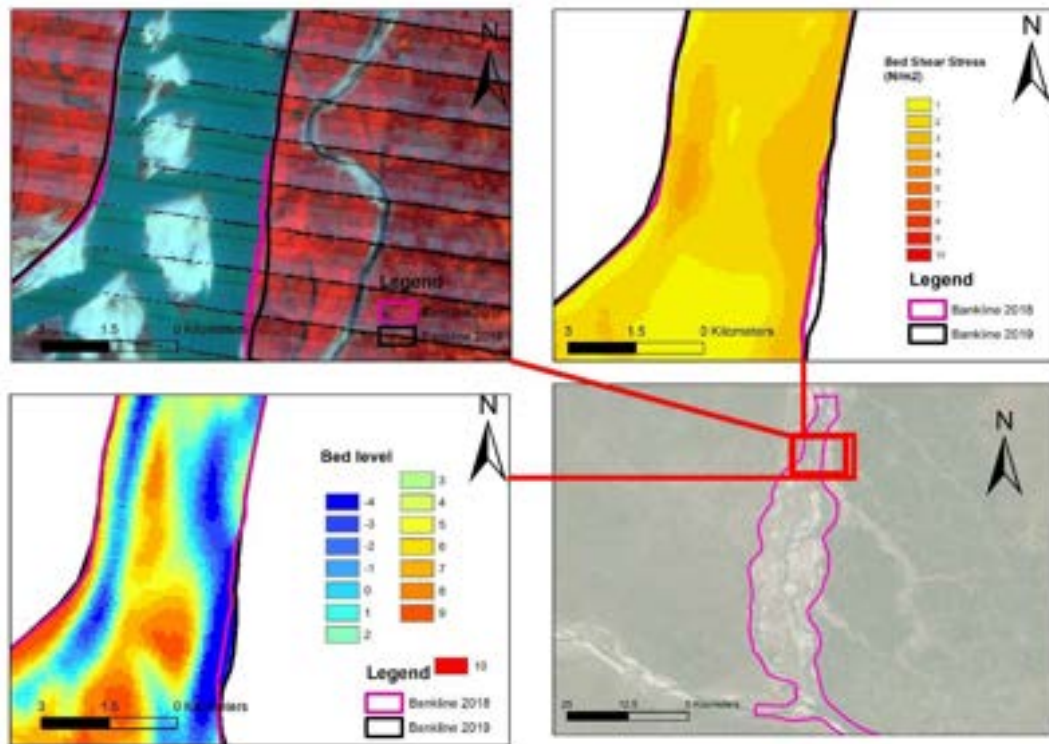
Figure 5.19 Bank erosion probability in Area 01
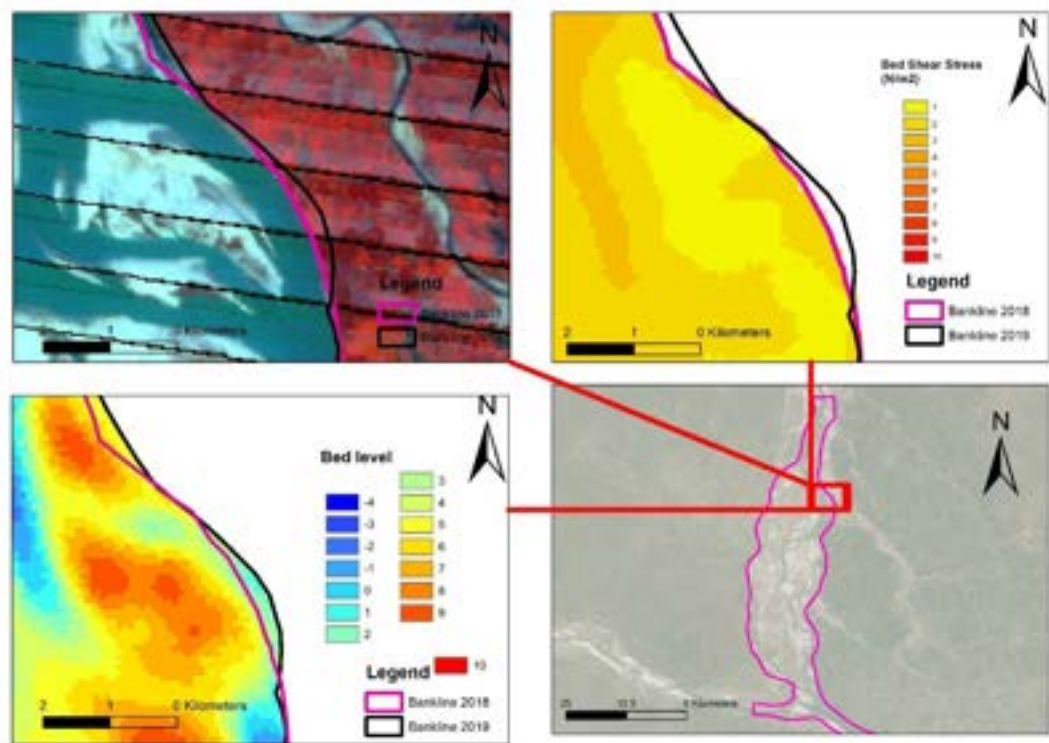
Figure 5.20 Bank erosion probability in Area 02
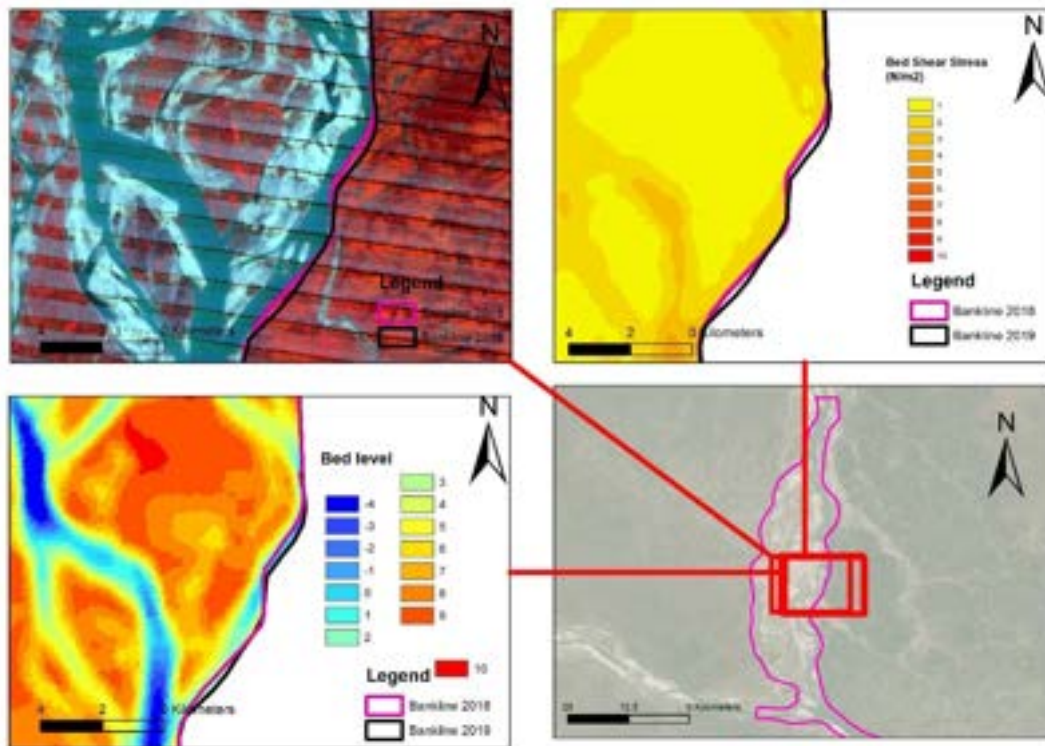
Figure 5.21 Bank erosion probability in area 03
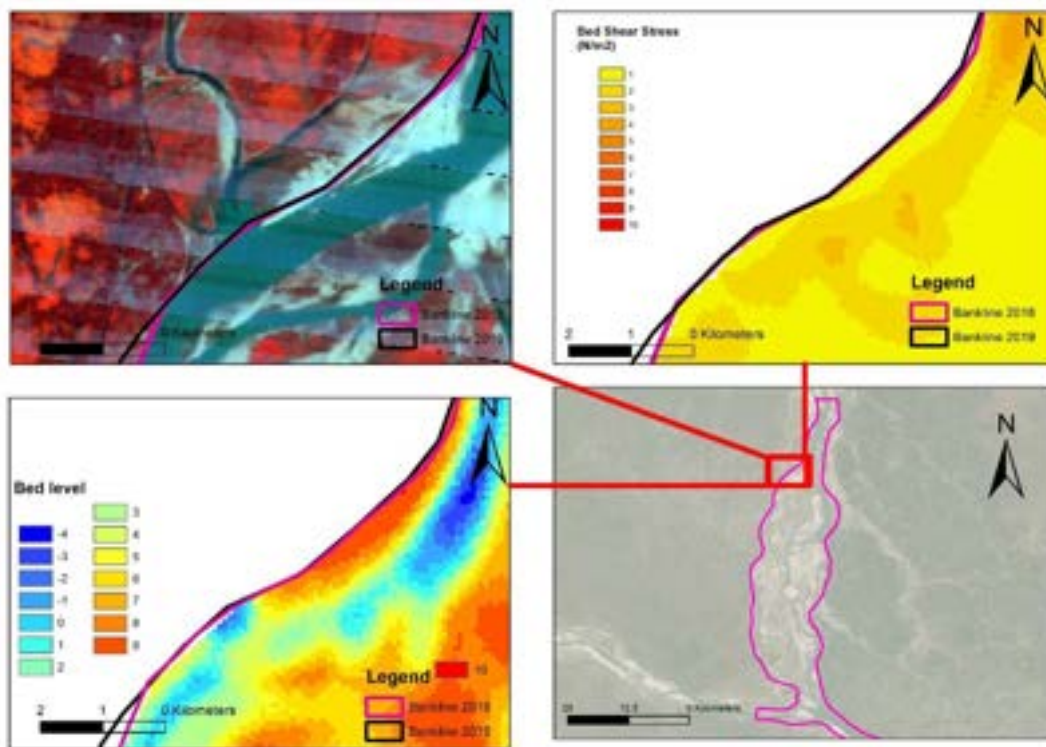
Figure 5.22 Bank erosion probability in area 04
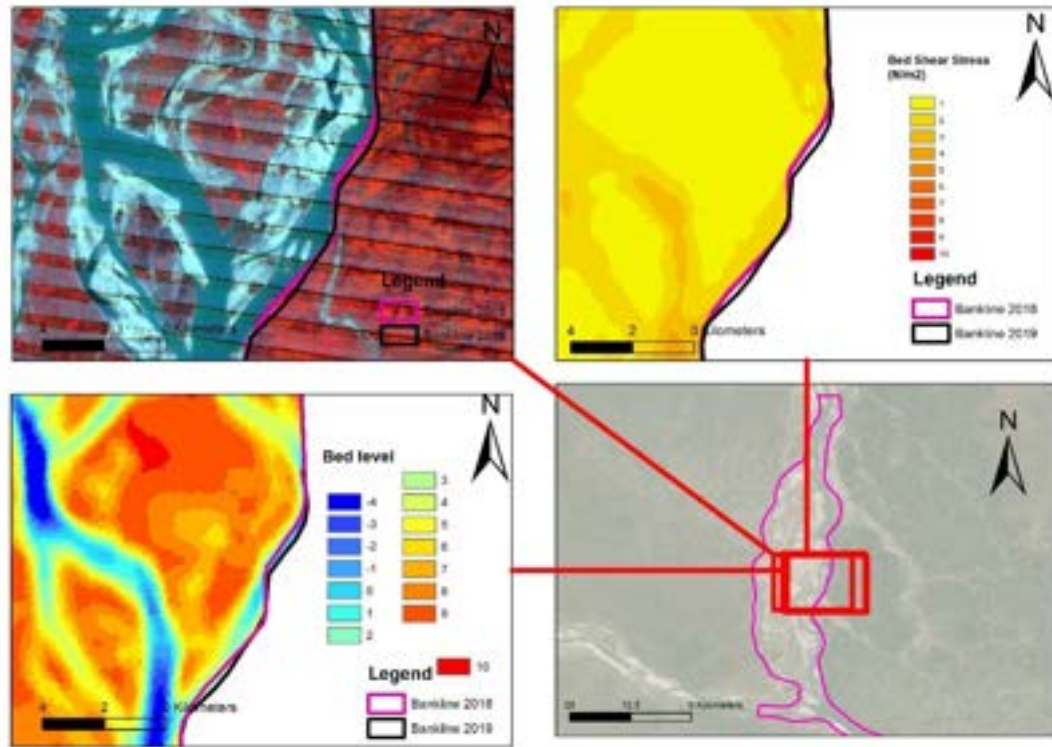
Figure 5.23 Bank erosion probability in area 05
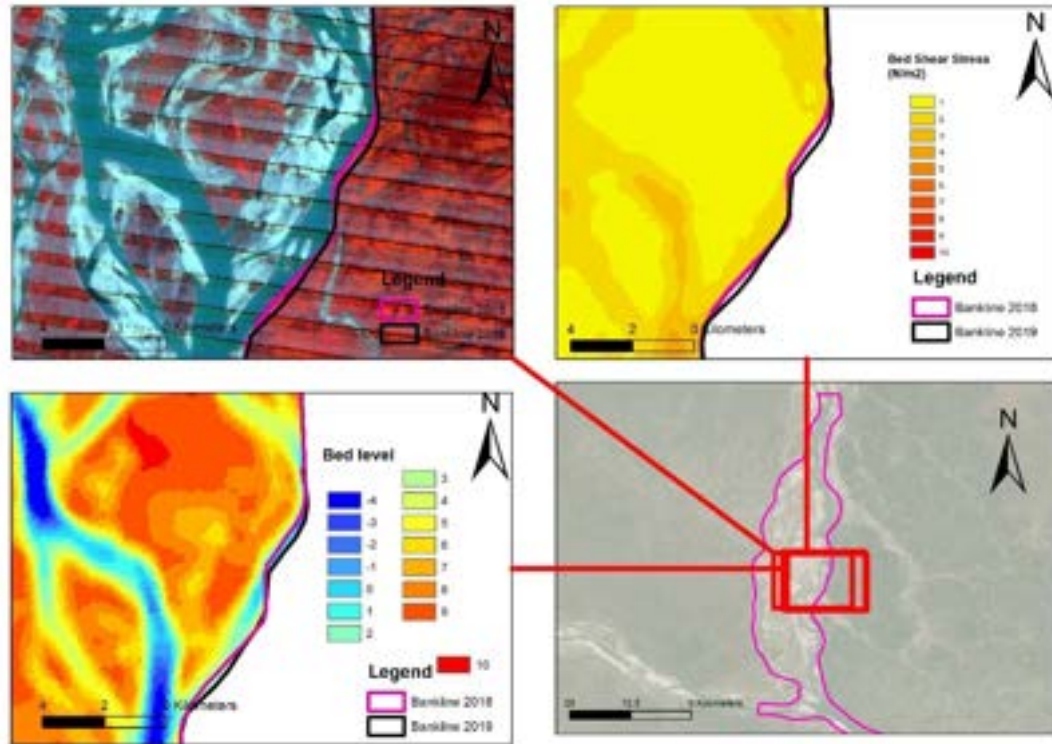
Figure 5.24 Bank erosion probability in area 06

5.7 Morphological modeling with primary data.

A Morphological model was developed with primary data of 50 m resolution. Due to lack of computational capabilities mesh element number was limited to 30000. For this model 50 m grid spacing was used. Though this grid size is finer than the large-scale model, it was still not fine enough to predict bed form change accurately.

For this model upstream and downstream boundary condition data were extracted from the large-scale mode with course resolution grid. The large scale model was simulated with 2019 discharge and water level. All other parameters are same as the large model.

5.9.1 Results and discussion

Figure 5-25 shows the simulated water depth and velocity in the model domain. Figure 5-26 shows erosion from observed data and model simulated data. Unlike large scale model a similarity can be found between these two maps. These tow map match spatially to some extent after a certain distance from upstream. Although there is a matching pattern, extent of erosion deposition is not the same for these maps. To quantify the extent of matching with bedform change an analysis was made for longitudinal and cross-sectional profiles. Figure showing (Figure 5-27 to 5-28) Three longitudinal profile and four cross sectional profiles. It can be seen model can predict erosion or deposition at some area but with no precision. This is may be due to coarse gird mesh data. These results can be improved with very fine resolution bathymetry data as well as with fine mesh grid.
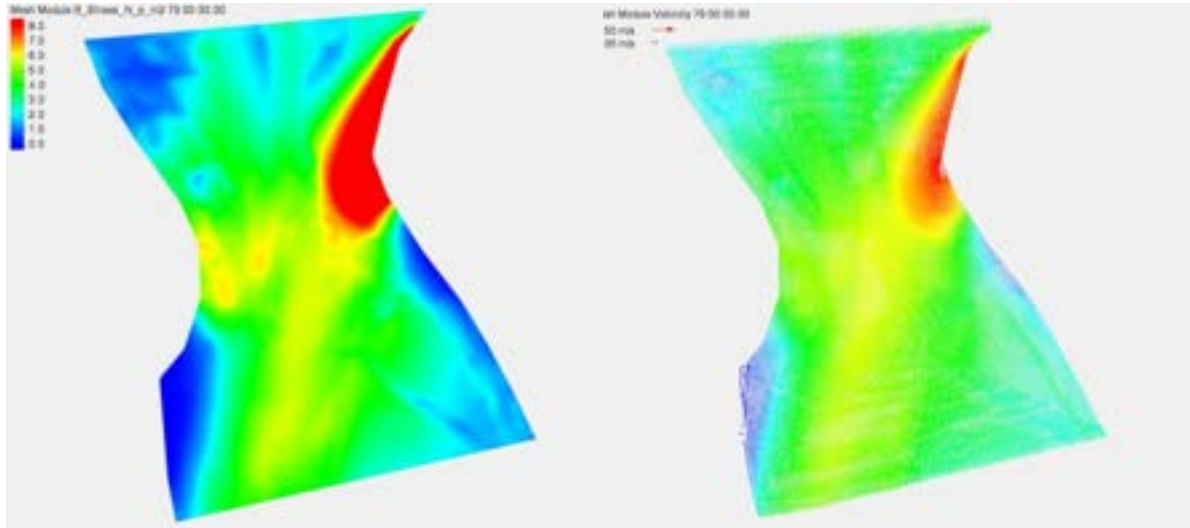
Figure 5.25 Simulated water depth and velocity in the model domain
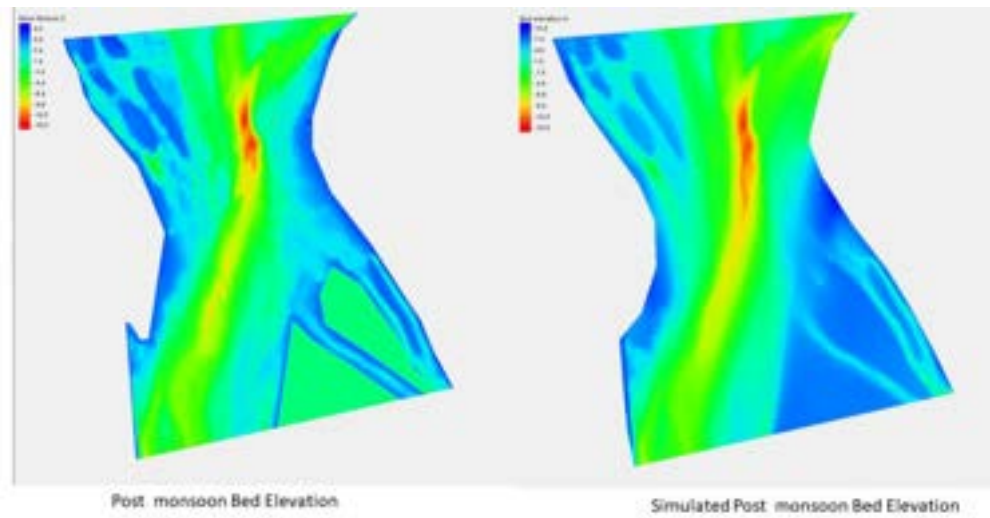
Figure 5-26 Comparison between surveyed and model simulated Bed level.
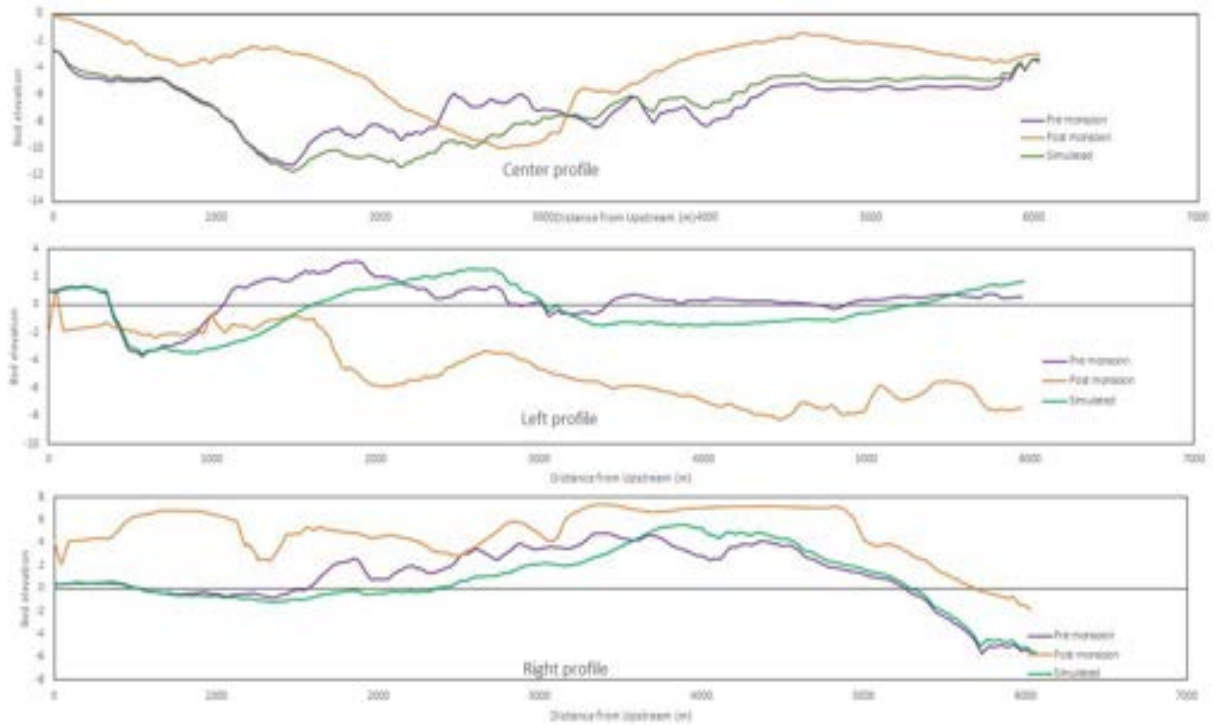
Figure 5-27 Change in Bed level along longitudinal profile.
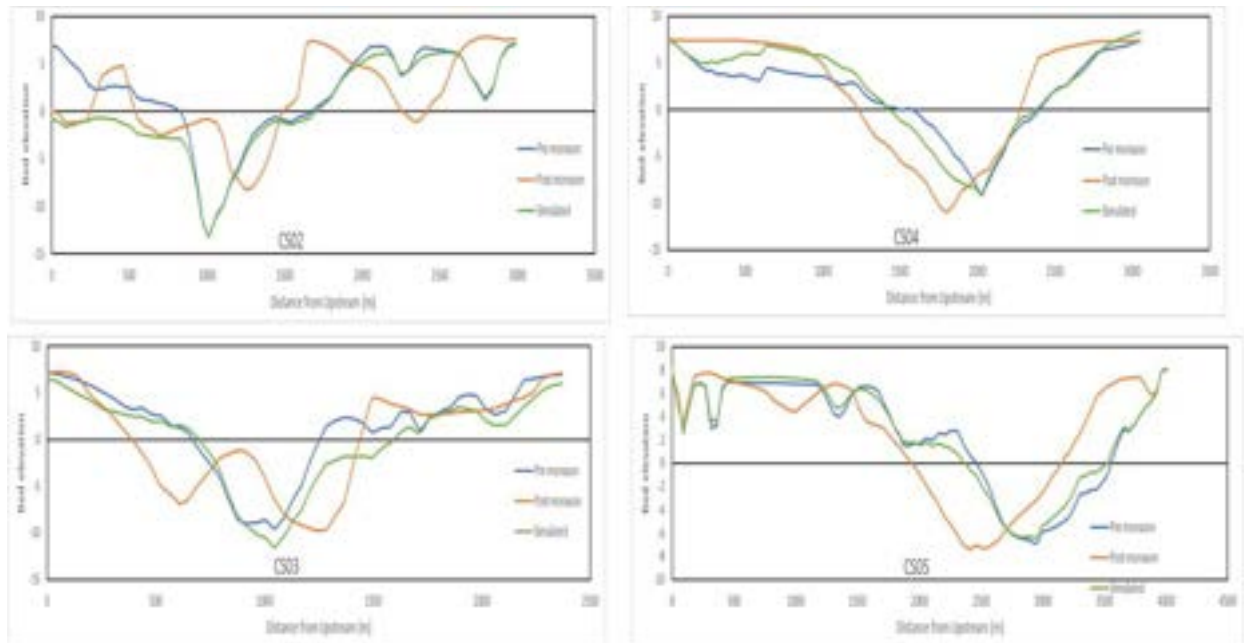
Figure 5-28 Change in Bed level along cross-sectional profile.

5.8 Conclusions

This chapter contains 3 mathematical model results: a) 1D hydrodynamic model, b) 2D hydrodynamic model and c) 2D morphological model. 1D hydrodynamic model was developed because there was no intermediate gauge station in the study domain. Using the 1D model, boundary conditions for 2D hydrodynamic model was extracted. 2D hydrodynamic model was also calibrated and validated using HecRas model results. 2D hydrodynamic model was developed to understand the flow characteristics of the model domain. Flow velocity, flow direction, and water depth was examined to get a better understanding of the situation. Using well calibrated 2D hydrodynamic model, 2D morphologic model was developed. Morphological model was developed to reproduce the morphological scenario of Jamuna river.

Morphological modeling of such active river like Jamuna was very challenging. Moreover, there was limitation on fine resolution data, computational power etc. The best available bathymetry data have a resolution of 500 m but in Jamuna river within 500 m the river bed may change several times. Again, there is constraints on model capacity, for morphological modeling SRH 2D can handle about thirty thousand to forty thousand. To accommodate this model cell size was coarse. Including all these uncertainties it was very difficult to replicate the real scenario. As such SRH 2D has some limitation modeling morphological process.

Model may predict erosion or deposition correctly but the extent of erosion and deposition was not obtained. This may be due to very coarse resolution data and mesh grid size. Although the model cannot predict the bed form change accurately for this grid size it could give some indication of bank erosion. To assess the probability of bank erosion bed shear stress along the bank was observed. It was found from the simulation that at the places where erosion took place in the year 2019, shear stress is higher and where the bank remained almost at the same position shear stress is relatively lower. In erosion prone areas, erosion took place in 2019 and from model result it can be found that shear stress is relatively higher in those areas. Similarly, in areas, where there was little to no erosion and bed shear stress along the bank are relatively lower.

Chapter 6: Deep Learning Modeling and Results

6.1 Introduction

For any deep learning task, the mapping from input to output is approximated by the deep learning model. So, in order to make accurate predictions using a certain model, it is necessary for the input data to inherently have relevant information that would be utilized by the model to make predictions. If input data do not have meaningful features that would help in making predictions then the unnecessary input data acts as noise and the model tries to map those noise information to the output. In summary, the input data needs to be somehow correlated to the output. Using domain knowledge, it is usually determined which data has meaningful correlations with the output. To tackle the bank erosion prediction problem, freely available historical satellite images and the historical trend of bankline locations were considered as data with meaningful correlations that influence future bank erosion events. These data were first explored and then a deep learning model was developed to verify the effectiveness of deep learning modeling approach in predicting future bank erosion regions.

6.2 Data Exploration and Processing

In order to explore freely available satellite data, all the major satellite image platforms were considered. It was found that the Google Earth Engine platform allows users to access all the Landsat images through their web-based Earth Engine JavaScript API. So, a script was written to visualize, explore and process all the Landsat images taken over the study area. The images captured by the Landsat Satellites in January of each year were filtered out and the median of those images was computed so that there was one image representing the month of January for each year. This filtering process resulted in a collection of 33 images starting from the year 1988 to 2020. Using Earth Engine, the images were further processed to have a dimension of 2222 by 745 pixels with six channels named Blue, Green, Red, Near Infrared, Shortwave Infrared 1, and Shortwave Infrared 2. These images were saved in individual tiff files. The 1988 January tiff file visualized using the Blue, Green and Red channels (BGR) in one image and visualized using the Near Infrared, Shortwave Infrared 1, and Shortwave Infrared 2 channels in another image, are given below.

Figure 6.1 1988 January Tiff file Visualized in QGIS
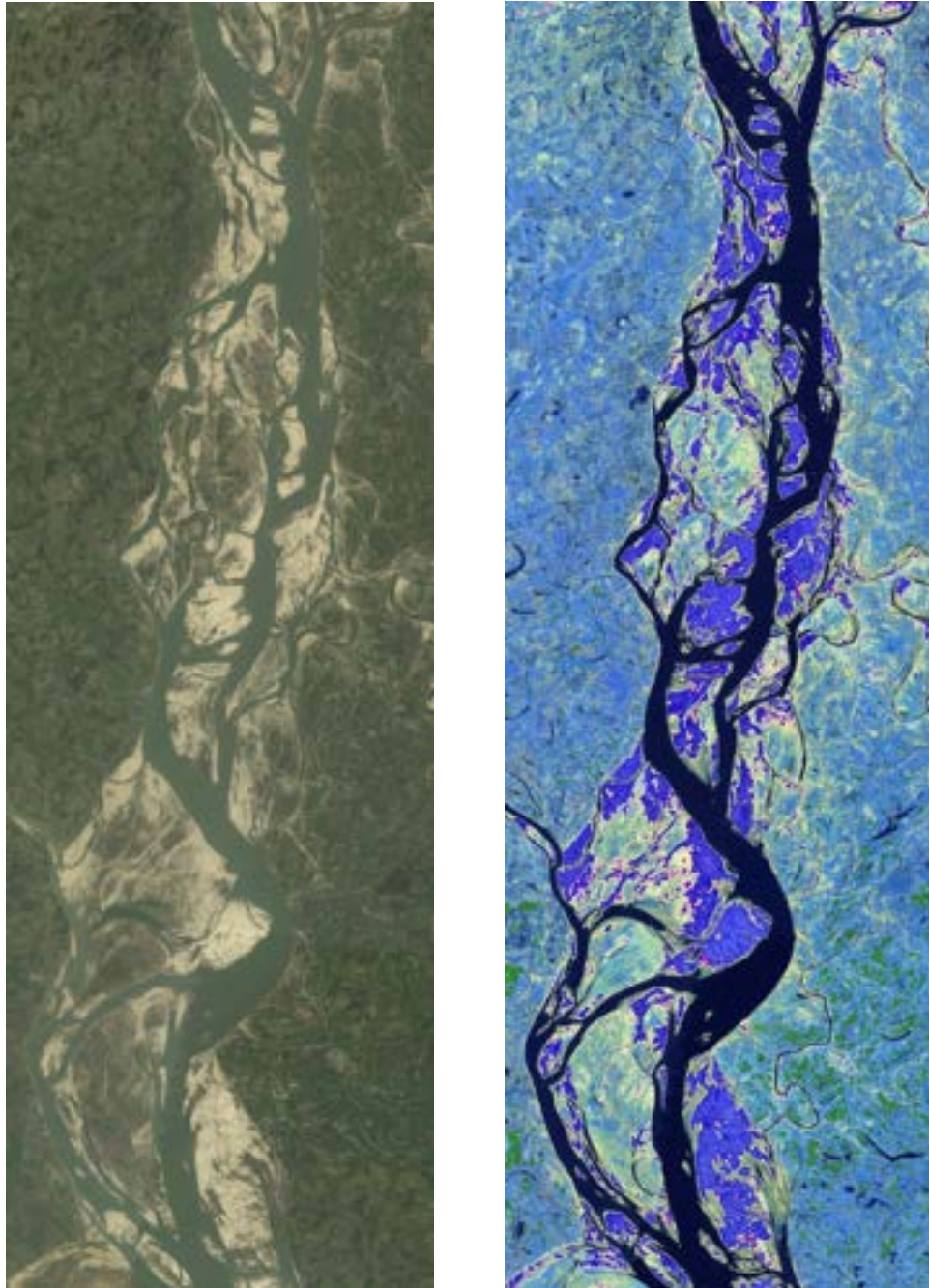
Figure 6.2 BGR and Infrared Channels visualized in two different images

Exploring the available historical data, it was evident that multi-channel satellite images had valuable features/information correlated to future river bank lines. Factors contributing to bank erosion like water body, river bars, and river bank lines etc. were all visually present in the satellite images as collections of raw pixel values. These important features or factors which influence bank erosion were not prominently visible or represented by each of the channels of multichannel satellite images. For example, the first three channels of the satellite data Blue Green Red did not draw major distinctions between the green pixel values of vegetation and

the green pixel values of water bodies; both features were represented by slightly green pixels. Instead it was found that when visualized, the distinction between water body and vegetation was much more prominent in the Infrared, Shortwave Infrared 1 and Shortwave Infrared 2 channels of the satellite images. This was important as it was necessary to draw distinctions between the color/pixel values representing two important factors of bank erosion: water body and vegetation. This observation and review of past deep learning literature led to the use of visual data from all the channels. After data collection and processing, an extensive analysis was performed to check for anomalies in images.

6.2.1 Exploratory Data Analysis

Machine learning models learn from data and so the performance of such models is highly dependent on the data that is used to develop the model. So, it's important to ensure that the model is trained on high-quality data with inherent patterns helpful for predicting bank erosion. After collecting image data from Google Earth Engine some analyses were carried out to understand the distribution and patterns within the data. This initial investigation on data so as to discover patterns, spot anomalies, test hypotheses, and check assumptions with the help of summary statistics and graphical representations is known as Exploratory Data Analysis (EDA). EDA also helps in making model development decisions like model architecture, model size, image down sampling method, etc. To explore the data, satellite images of the study area were first looked into.

6.2.2 Image Anomalies

The 33 images obtained from Google Earth Engine were not all of the same quality. Mainly three types of artifacts were noticed in the images. They were data gaps created by Landsat 7 SLC off failure, data gaps created by clouds and white artifacts created by mild haze. Each of the issues is discussed below.

6.2.3 Data Gaps by Landsat 7 SLC off failure:

Landsat 7 SLC-off data refers to all Landsat 7 images collected after May 31, 2003, when the Scan Line Corrector (SLC) component of the Landsat 7 satellite failed. Due to this satellite component failure, there are data gaps in the images collected over our study area. This issue was resolved by first taking the mean of available images close to January and then replacing the data gaps with values from the mean image. The results are given below.

Figure 6.3 SLC off image data gaps replaced by mean values (Before and After)

6.2.4 Data Occlusion by Clouds

In a lot of the images taken over January by the Landsat Programs, there were clouds. These clouds obstructed the study area and prevented the observation of part of the study area beneath them. With the help of native cloud masking algorithms from Google Earth Engine, the clouds were masked with null values, and furthermore, the null values were replaced by mean image values similar to the process of replacing null values for the SLC-off data gaps discussed above. There were also very few artifacts with abnormal color values. These were not treated by any process as they were very few in numbers. One of the regions with discolored artifacts is visualized below.

Figure 6.4 Artifacts of inconsistent color values

6.2.5 Data Artifacts by Haze

The images were produced by merging and taking the median from a number of images taken on different days. So, on the days when there was a mild haze, a bluish tint was observed in parts of the images. One of the haze artifacts is provided below.

Figure 6.5 Data Artifacts by Haze

After exploring the image data, identifying data gaps, and replacing them with meaningful values, the data labeling process was conducted in order to prepare data for deep learning model development.

6.3 Labeling the data

In the context of supervised deep learning - the type of deep learning being explored in this research - data labeling refers to the task of adding context to raw data so that models can learn from data. So for bank erosion prediction context, the task of data labeling meant defining the output of the model. As the desired output from the model was the location of future river bank lines so that erosion-prone areas and erosion magnitude could be predicted, river bank lines were considered as labels for this deep learning task. So, GIS Softwares like ArcGIS and QGIS were used to delineate the river bank lines. This delineation resulted in shape files for each of the images. This allowed the location of river bank lines to be represented by the geographical coordinates.

Figure 6.6 Data Labeling using QGIS and Python

The shape files were further processed so that the bank lines could be fed to the deep learning model. The type of deep learning model used in this research required labels represented as integers or floating-point numbers not as vector data. This meant, for representing the location of the river bank lines, the geographical coordinates saved as vector data in the shape file needed to be converted into integers or floating-point numbers.

6.3.1 Defining the coordinate system

A python script - by utilizing Raterio library - was written to use the coordinate information from the shapes files and draw the left and right river bank lines as white lines on BGR raster images of the study area. The river bank lines represented by these white lines helped to locate the banks in the local context where there was no geographic coordinate system like the one found embedded in tiff file format.

In this new paradigm, each white pixel represented a 30m length of river bank line, and predicting the future location of this white pixel meant predicting the next year location of the same 30m unit bank line. In order to express the location of each white pixel in the images in numbers, a coordinate system was defined by considering the left edge of the image as the origin. So, the position of the left and right river bank lines were expressed in terms of their distances from the left edge in units of number of pixels.

Figure 6.7 Coordinate System for defining Bank Line Locations

By following the above-mentioned process, the delineated river bank lines were converted into integer numbers so that the integer numbers could be fed as labels for the deep learning model. This conversion was done for all 33 images.
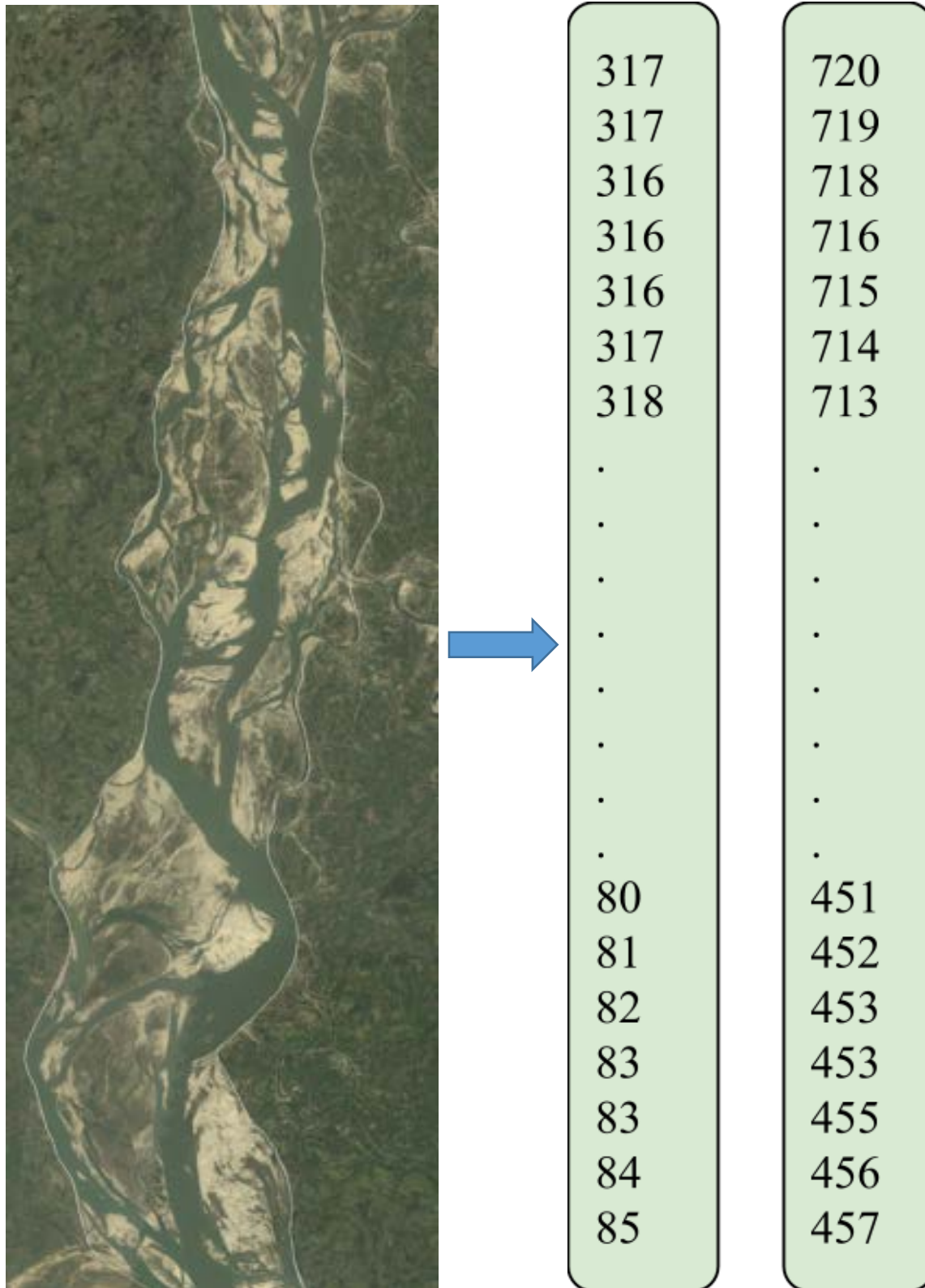
Figure 6.8 Converting Raster lines into Array Coordinates

6.4 Distribution of Coordinates Across Time

Similar to the image data, later on EDA was performed on the integer numbers representing river bank lines. The changes in bank lines over the years were observed by utilizing the integer numbers representing the bank lines. These values representing 30m units of bank lines changed from one year to another. The changes in values for left and right banks starting from 1988 are visualized below.
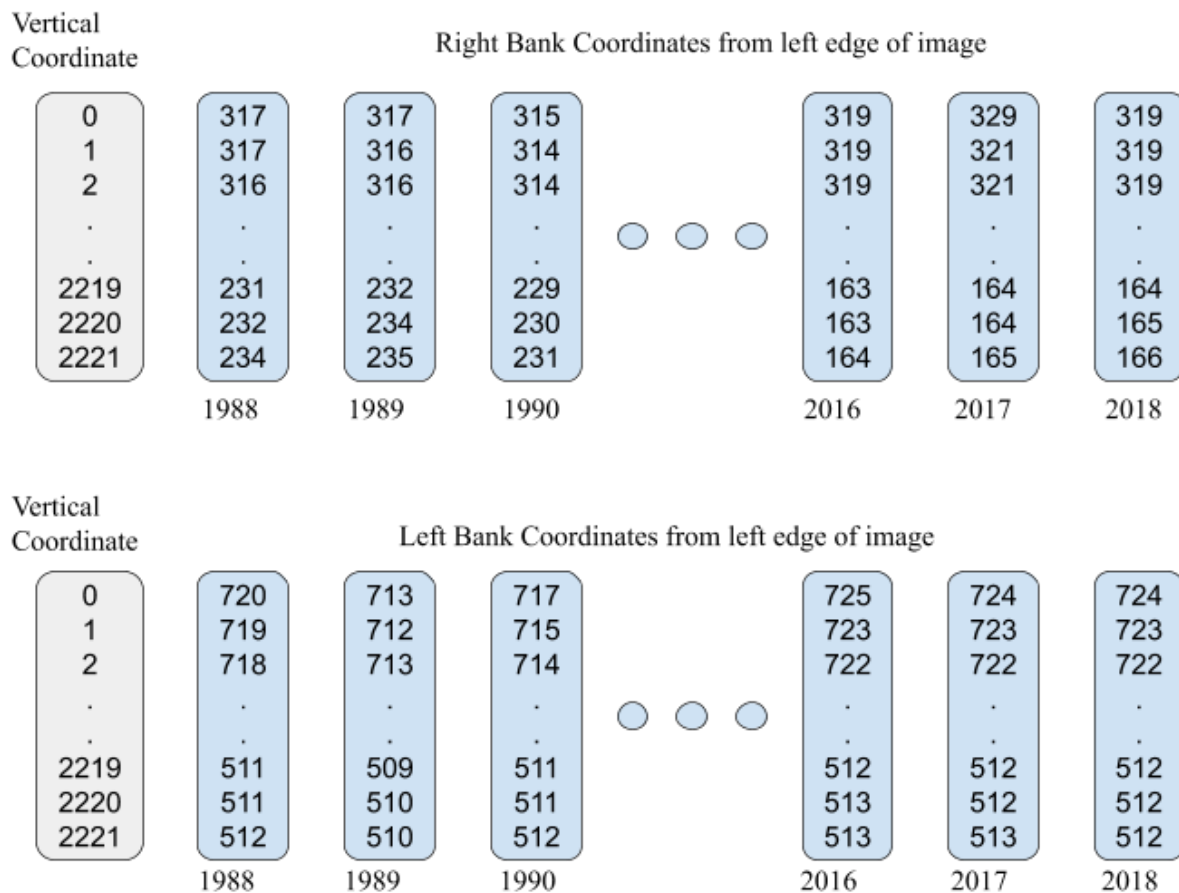
Figure 6.9 Change in Coordinate Distribution across time for both banks

The first value for each of these arrays represented the location of the first 30m left or right river bank line. To represent and identify all of these 30m units of bank lines for a particular year each of the 30m line portions were identified by an index starting from zero. So, using this coordinate system any bankline portion for a year was identified using two coordinates. One coordinate for locating the 30m portion from the upstream which started from zero and reached a maximum value of 2221 and the other coordinate for locating the portion from the left edge of the image which started from zero and reached a maximum value of 744.

The changes in coordinates of bank lines across the years contained the distribution of change of bankline shifting. To better understand the distribution of coordinates the change was visualized with the help of tensorboard library and python code.
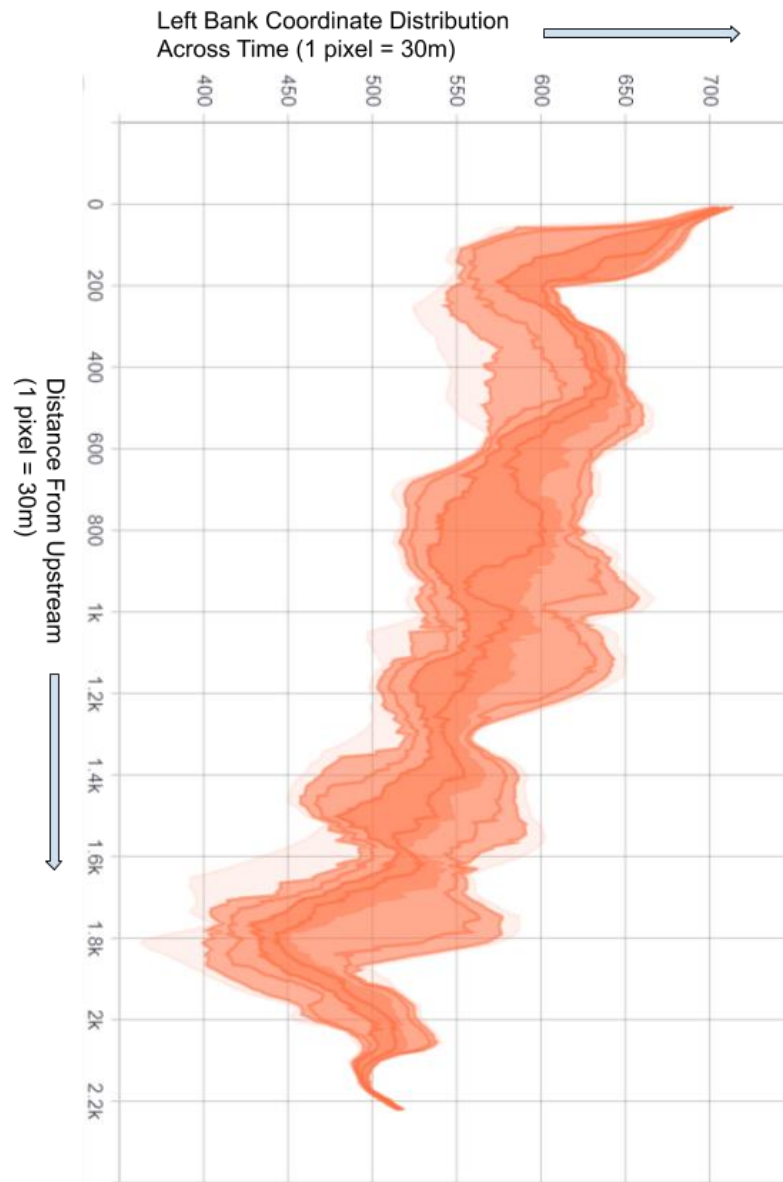
Figure 6.10 Left Bank Distribution Across Time

In the above visualization of the distribution of left bank coordinates for both x and y-axis 1 unit = 1 pixel = 30 meters. The darker the region the higher the probability was for left bank to assume the coordinate values stated across the horizontal axis. It was observed that that left bank coordinate values ranged from around 400 to 700 pixel distance from the left edge of the images. There were some regions with higher changes in coordinates than others. For example, around 600 to 1000 pixels from the upstream of our study area the coordinates had a high frequency region of values ranging from 550 to 600 pixels. Next, for each year, the difference

between that year's bank line coordinates and previous year's bankline coordinates was calculated. Then the distribution of these differences across the years was visualized.
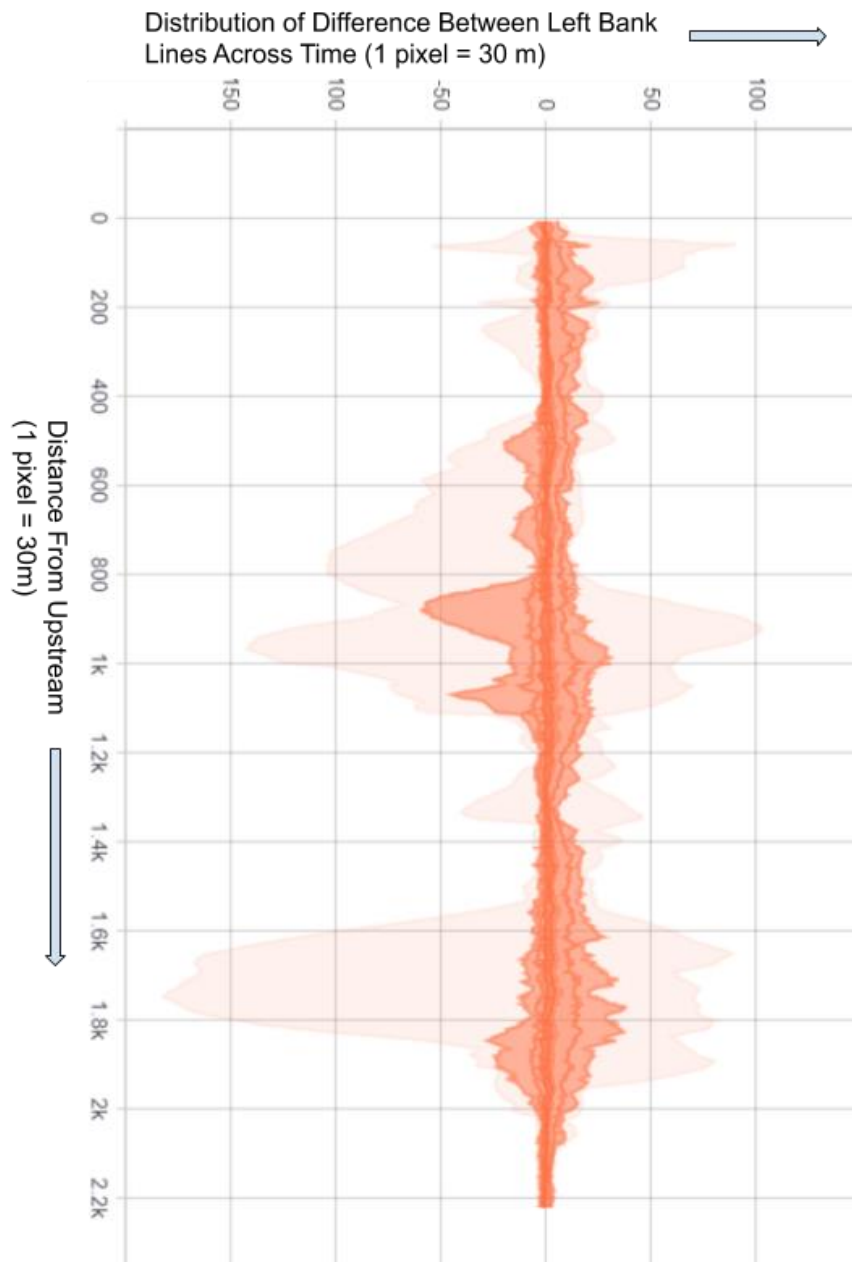
Figure 6.11 Distribution of Difference Between Left Bank Lines Across Time

The coordinates represented the distance from the left edge of the image. So, for the left bank, if the difference was negative and positive it meant deposition and erosion had occurred respectively. If the difference was zero it meant no change was observed from the previous year. From the visualization, it was observed that across the study area most of the erosion magnitude for the left bank assumed values ranging from 1 pixel to 10 pixels (1 pixel = 30

meters). There were also some outlier cases of erosion and deposition which were identified by the lightest region of the distribution. For example, 1600 to 1900 pixels from the upstream of the study area the erosion magnitude assumed values up to 75 pixels. After observing the distributions for the left bank, the right bank line shifting was visualized in a similar manner.
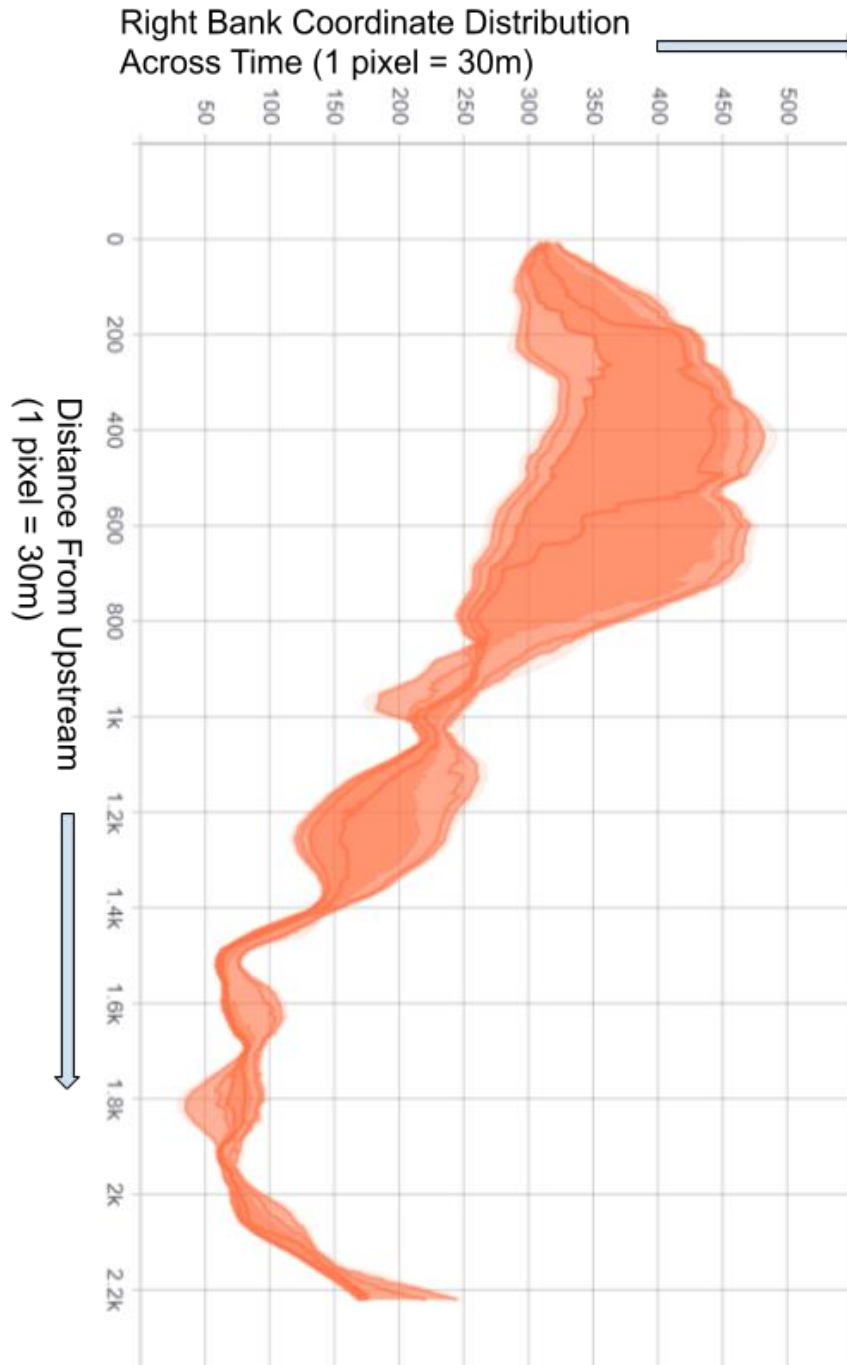
Figure 6.12 Right Bank Distribution across time

From visualization of the distribution of right bank line shifting across the years, it was evident most of the changes in bank line occurred in the top half of our study area and the bank line coordinates ranged from around 300 to 450. Similar to the distribution of difference with previous year for the left bank, the right bank difference distribution was also visualized.
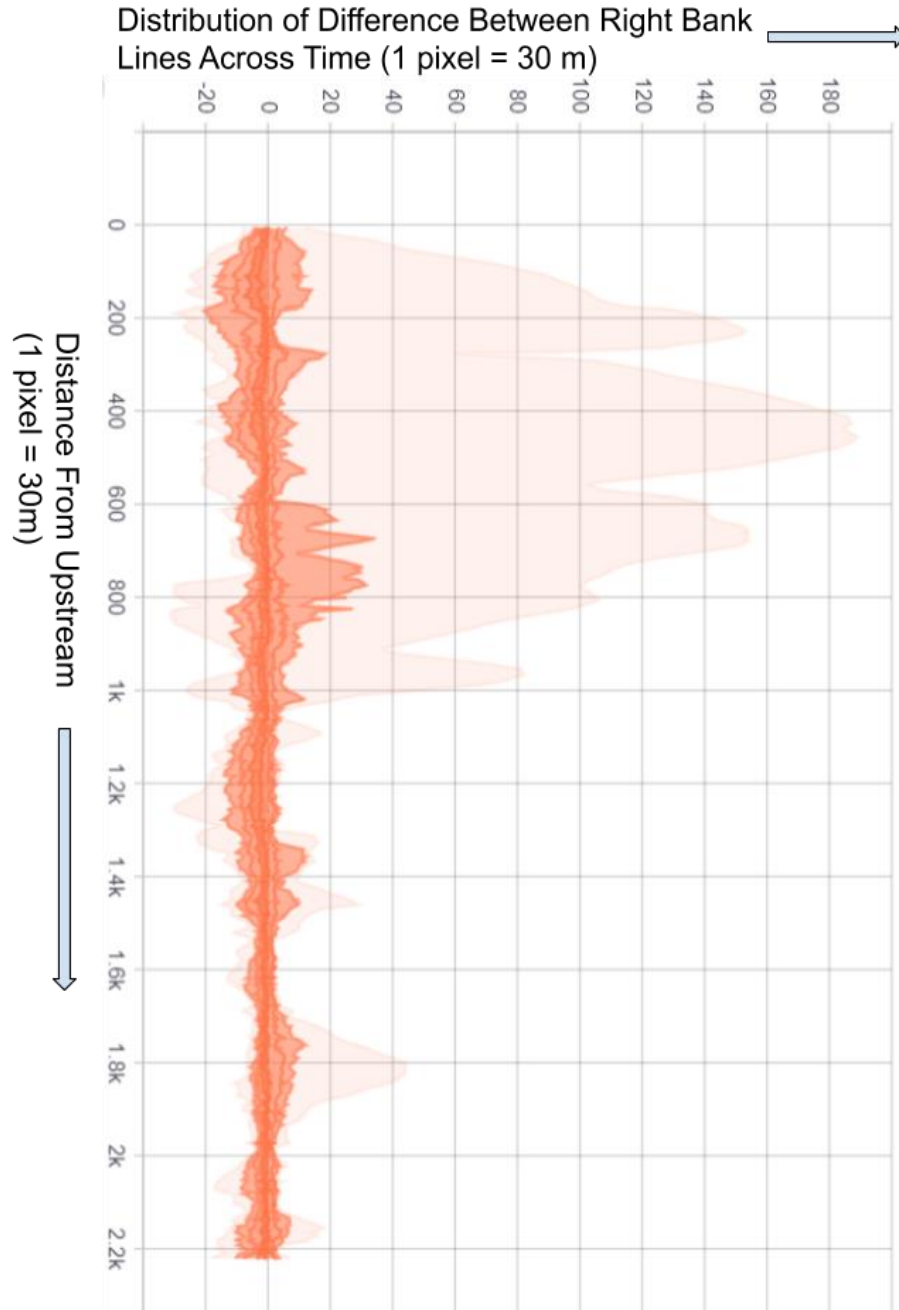
Figure 6.13 Distribution of Difference Between Right Bank Lines Across Time

Again, the coordinates represented the distance from the left edge of the image. So, for the right bank, if the difference was positive and negative it meant deposition and erosion had occurred respectively. If the difference was zero it meant no change was observed from the

previous year. It was evident that most of the erosion had occurred in the top half of the right bank and the erosion magnitude on average assumed values ranging from 1 pixel to 10 pixels (1 pixel = 30 meters).

After exploring the data for the deep learning task, the input and output for the deep learning model were defined. The performance of the approach depended on predicting bank erosion depended on what is defined as model input and output/label.

6.4.1 Use one extra channel and Bank Lines

One of the most important factors influencing future bank lines was the location of previous bank lines. In order to incorporate the previous year bank lines into the multichannel image data, an extra channel was generated. This extra channel was a binary mask that expressed river bank lines by setting pixel values inside and outside the banklines to ones and zeros respectively. The channel was generated from the BGR raster images with white lines as river banklines by writing a python script.

The extra binary channel resulted in raster data with 7 channel information. This multichannel raster data, previous year bank line location coordinates and, bank line vertical coordinates were used as input data. The raster data were passed through a feature extractor component of the model made of convolutional neural networks. The resulting features from raster data were then passed to a temporal feature learning component of the model comprised of LSTM layer to learn time dependencies.

Figure 6.14 Extracting Binary Mask channel

6.5 Train Validation and Test Dataset

In deep learning, a model is developed using training data to learn model parameters and then the model is validated on the validation dataset to find optimal model configuration. After training and validation, the trained model is finally deployed to make predictions on the testing dataset. For the bank erosion prediction task there were data starting from 1988 to 2020. Following standard deep learning methodology the entire dataset was first split into training, validation and testing dataset. Data until 2017 were used to train the model and model prediction of the year 2018 was used to validate the model performance. Further prediction of the year 2019 was also used to test model performance. After developing a model for this training-validation-testing dataset configuration where the 2018 data was used to validate the model, the same model configuration was used to train and compute predictions for dataset configuration where the last year data in the validation set was of 2015, 2016, 2017, 2019 and 2020.

6.5.1 Overall goal of the model development process

First, model development for the training-validation-testing dataset configuration where model prediction in 2018 had been used to validate performance, will be discussed. For the deep learning approach, a baseline model was first developed by following standard model training configurations. There were various model training configurations or factors that influence the model performance differently. The model configuration was iteratively changed so that improvement in model performance was observed and a final model configuration could be found that performs the best. In order to explain the complete deep learning model development process at first a broad overview will be provided on the development pipeline for a single model training configuration. Then the process of finding optimal model configuration through iterative experimentation will be explained. Lastly, the model configurations which were explored and experimented will be discussed in detail. Now the complete development loop for a single configuration will be discussed.

6.6 Overview of training loop

At first, the input data was batched into groups and each group of data was fed to the model one at a time. The model took the input data and processed it to make a prediction. The prediction from the model was then compared with the actual label/output by using a cost function. Based on the difference between predicted and actual output, the model was updated using an optimization algorithm. This loop consisting of input, prediction difference calculation, and update step was repeated several times. When the model was updated once for every available group of data, it was considered that the model had been trained over the entire training dataset once.

6.6.1 Training and validation error

After training the model over the dataset once, two important metrics were calculated and stored : training error and validation error. Training error and validation error is known as the average difference between predicted output and actual output over the training dataset and validation dataset, respectively. These two error values gave an idea about how well the model performed on training data and also the unseen validation data. It's considered that the lower the error values the better the model performance.

6.6.2 Evaluation metrics

Even though training error and validation error provided information about relative performance error on the training and validation dataset, these error metrics did not provide absolute model performance on bank erosion prediction. A singular evaluation metric was needed to understand the model accuracy. Mean absolute error (MAE) between predicted river bank lines and actual river bank lines, was considered to be the singular evaluation metric which provided information about the absolute performance of the trained model. So, apart from the training error and validation error, two additional evaluation metrics were also logged after each training loop; these were Mean Absolute Training Error and Mean Absolute Validation Error. These errors were expressed in terms of pixels where 1 pixel was equivalent to 30 meters. So, a MAE of 3 pixels meant on average the difference between the predicted bank line and the actual bank line was 90 meters.

6.6.3 Training one model configuration

The performance of a deep learning model improves as the model is trained over the entire dataset for several times. So, after each training loop over the entire dataset Training and Validation MAE were logged and it was observed that gradually the error was going down meaning the model was learning to make better predictions. After several training iterations the error metrics reached a stable value after which further training did not improve model performance. When such a stable state was reached it was considered that the model had been trained for the given model training configuration. So, a single model configuration was trained by following the above-mentioned process. One of the training errors charts - which visualizes decreasing training error - is provided below.
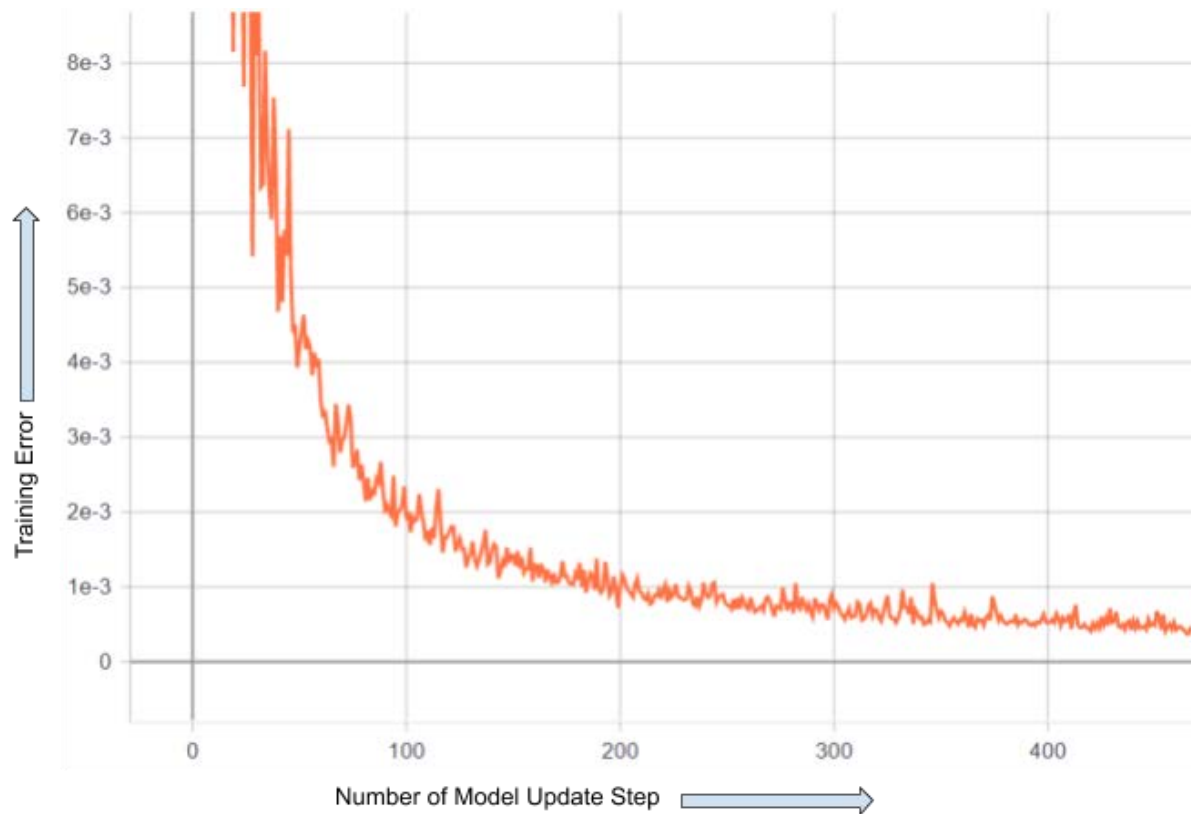
Figure 6.15 Training Error vs Number of model update steps

6.6.4 Bias and Variance

Different model training configurations for the same bank erosion prediction task gave different MAE values. The lower the MAE value the more suitable the model configuration would be for solving the problem. In order to search the best model training configuration different variables of the training process and model architecture were experimented and explored. To compare between different model configurations two values were used; bias and variance.

MAE on the training set expressed the absolute prediction performance of the model on the data it was trained on. This training MAE metric is also known as bias. The lowest bias value that could be achieved is zero. A zero bias would mean that the model could perfectly predict the next year river bank line for the data it was trained on. A low bias was desired as it ensured that the model was able to reasonably learn all the patterns in the training data. The difference between training MAE and validation MAE is known as variance. A lower variance value ensured that the model performance on unseen/new data was as good as it's performance on the training data.

6.7 Finding optimal model configuration

The overall goal in deep learning model development was to iteratively experiment with different model training configurations so that the configuration with the lowest bias and variance could be found. By doing so, an optimal model configuration was achieved for bank erosion prediction task.

Deep learning modeling is a very iterative process. In order to find the optimal model configuration different ideas were explored, then those ideas were implemented in code and experiments were performed to observe if the model could achieve a lower bias and variance value than before. Different model training configurations are different based on many factors from input data batch size, model weight initialization method to type of activation function, optimization algorithm, etc. Changing any of these factors of model configuration led to the development of a different model. These factors/decisions that influence the model configuration and thus model performance on bank erosion prediction, are known as hyperparameters of the modeling approach. These are called hyperparameters because they are defined before model training takes place by the people developing the model as opposed to the model parameters which are learned by the model itself during training time. Through this iterative process of idea generation, code implementation and experimentation an optimal model configuration was found for the bank erosion prediction problem as shown in Table 6-1.

Table 6-1 The final model training configuration

Hyperparameter Name	Hyperparameter Value
Data type	Images and Lines
Meters of reach across the channel provided as input for predicting 30 meters unit bank line	3840 meters
Number of past year information used to predict one year into the future	Last four years
Batch size	4
Number of convolutional layers	6
Use of Batch Normalization for all convolutional layers	True
Use of padding in convolutional layers	False
kernel size of convolutional layers	3
Convolutional Stride	1
Downsampling method of Pooling Layers	Average Pooling
Activation function for all layers	ReLu
Number of LSTM layers	1
Number of LSTM layer neurons	257 by 150

Number of fully connected layers	1 for each bank
Number of fully connected layer neurons	150 by 1, for each bank
Last layer activation function	Linear
Cost function	Weighted Huber Loss
Left bank loss weight	0.4
Right bank loss weight	0.6
Optimization Algorithm	Adam
Learning Rate	0.000031623
Number of epochs	28

6.7.1 Model Architecture
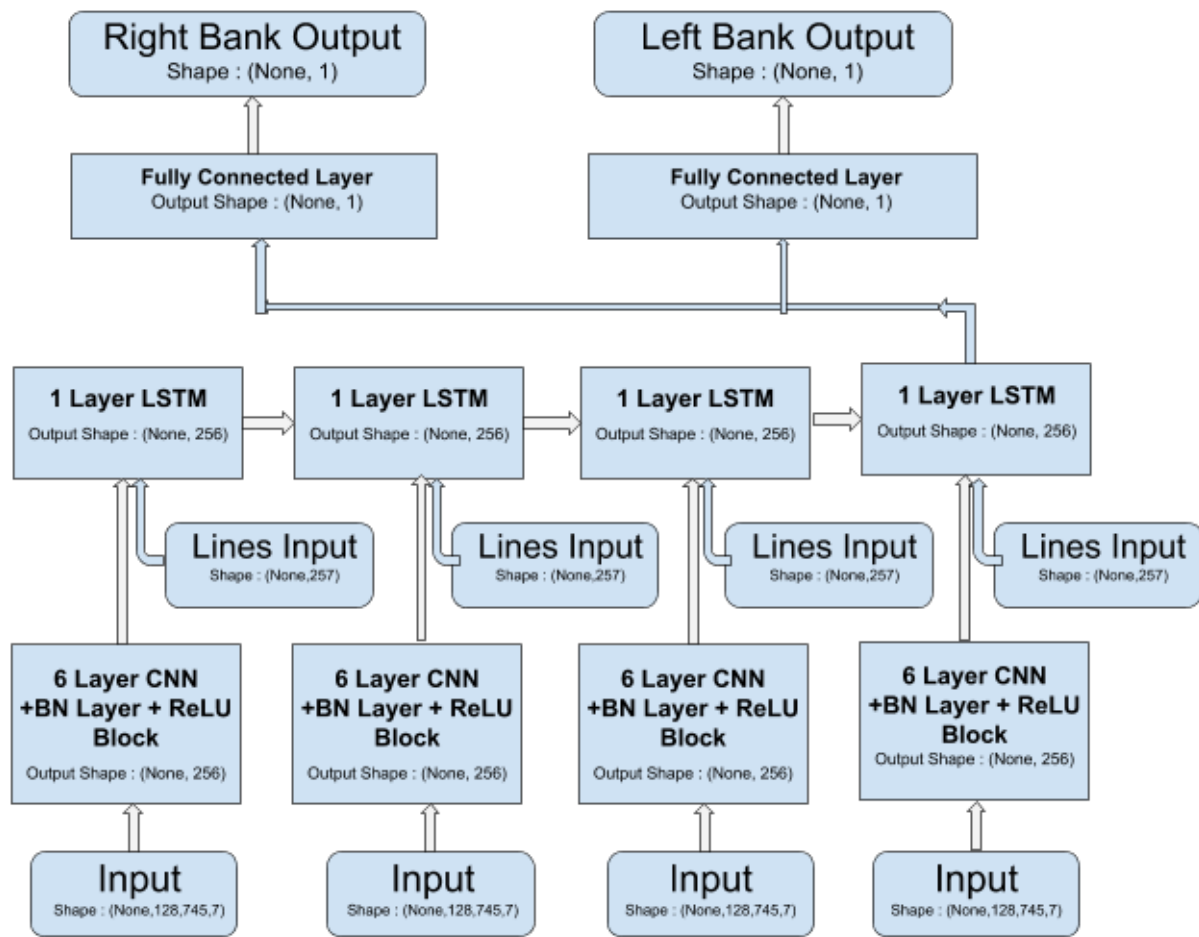
Figure 6.16 Multi Input-Both Bank output Lines Plus Images Model Architecture

6.8 Results and Discussion

The banklines of 2017-18, 2018-19 and 2019-20 were simulated using the final model configuration as shown in Table 6-1 and the model arichitechture shown in Fig 6-15. For predicting the banklines of a certain year, the model input of images and banklines of previous four years were provided. To understand the general difference between predicted and actual bank lines some numerical metrics were calculated for both banks of the last six years. For each year, Mean Absolute Error (MAE) and Standard Deviation of the Error in Pixels were calculated for both bank lines. For example, for the year 2019, an MAE of 2.67 pixels (1 pixel = 30 meters) means the difference between the predicted and actual left bank line for 2019 was on average (2.67X30) = 80.1 meters. The value of the model performance are shown in Table 6-2.

Table 6-2. Summary statistics of Deep learning training and prediction.

YEAR	TRAINING MAE (PIXEL)		PREDICTION MAE (PIXEL)		ST. DEVIATION (PIXEL)	
	Right Bank	Left Bank	Right Bank	Left Bank	Right Bank	Left Bank
2020	1.278	1.066	3.46	3.29	2.91	2.81
2019	0.898	0.729	3.82	2.67	4.31	1.89
2018	0.808	0.723	3.06	4.75	3.11	4.33

6.8.1 Prediction of Erosion Prone Areas

The banklines predicted by the Deep Learning Technique for different years are shown in Fig. 6-16 to Fig. 6-20. The bankline of previous year is marked by red line, current year by white line and prediction by green line. Fig. 6-18a shows the actual banklines of January 2019 and January 2020. A number of erosion prone regions have been selected to closely compare the model results which are shown in Fig. 6.18b. The regions of erosion have been selected based on visual inspection with a general principle of having erosion of more than 100-150 m as the average error in prediction is around 3 to 4 pixels equivalent to 90 to 120 meters. In 2019-2020, the model can predict 4 erosion areas more or less accurately in the left bank. However, in the right bank the model predicts erosion in 3 locations but cannot predict only at one location. In 2018-2019, the model can predict erosion in all five locations in the left bank and failed to predict the erosion at one location in the right bank. In 2017-2018 the model predicts erosion in 4 locations along left bank but failed to predict in two locations and in the right bank, the model predicts erosion in 3 locations and could not predict at one location. It is to be

noted that the bankline prediction by CEGIS model marked by blue line in 2018-2019 has also been compared in Fig. 6-17.

A summary of the model performance in predicting number of erosion prone areas is provided in Table 6-3. Out of 24 erosion locations during 2017 to 2020, the model could predict erosion in 79% of the locations. Although the model generally underpredicted the magnitude of the erosion, the prediction of location in the erosion prone area is very satisfactory.

One of the most erosion prone area on the left bank was Chowhali during 2015-2016. But during 2017 to 2020 there was no erosion as the region was protected by bank protection works. However, the model still predicts erosion in this region in 2017-2020 as marked by green circle in Fig. 6-19. The overprediction of the model is due to the fact that no information on the protection could be provided in the Deep Learning model. It means that had there been no erosion protection in this area, there would have been a significant erosion during 2017-2020.

Figure 6.17 Actual bankline of 2019 and 2020 and predicted bankline of 2020 with locations of selected regions.
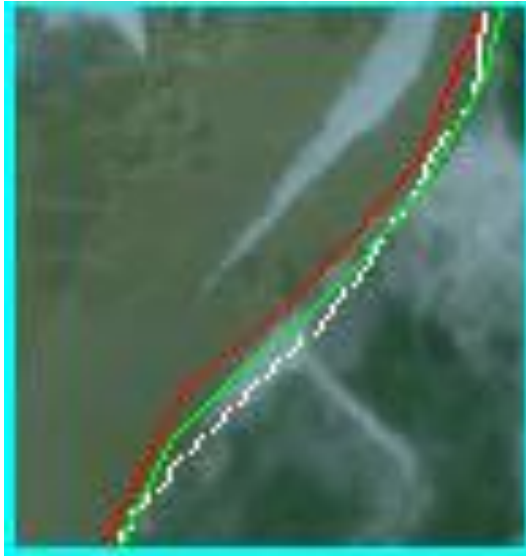
Predicted Regions

Region-1

Region-2

Region-3

Region-4

Figure 6.18 Actual bankline of 2019 and 2020 and predicted
bankline of 2020 at selected regions.
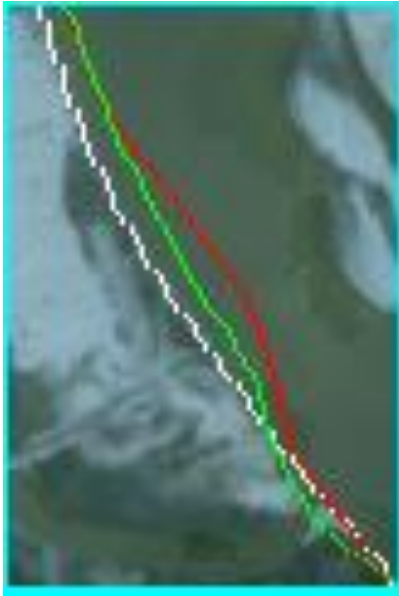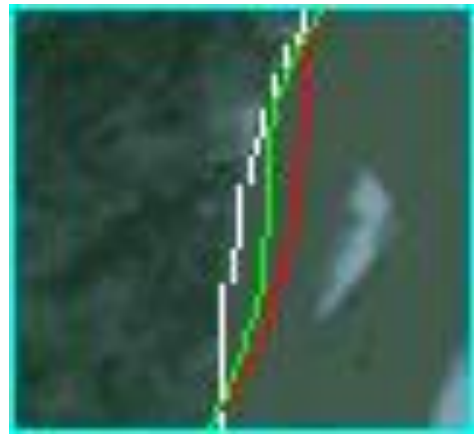
Region-5   Region-7

Not-Predicted Regions

Figure 6.19 Actual bankline of 2019 and 2020 and predicted
bankline of 2020 at selected regions.

Figure 6.20 Actual bankline of 2018 and 2019 and predicted bankline of 2019 with locations of selected regions.

Predicted Regions:
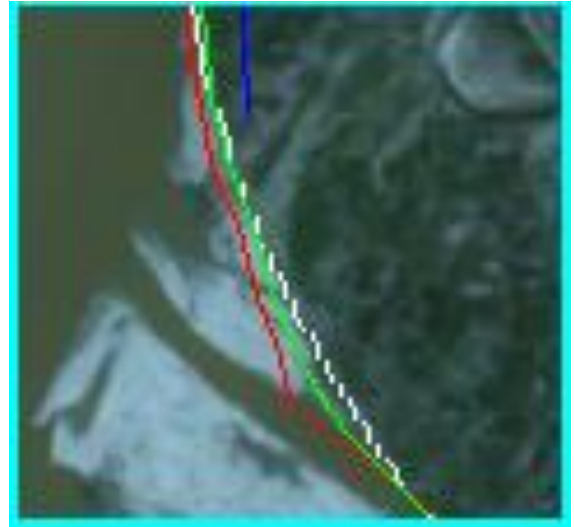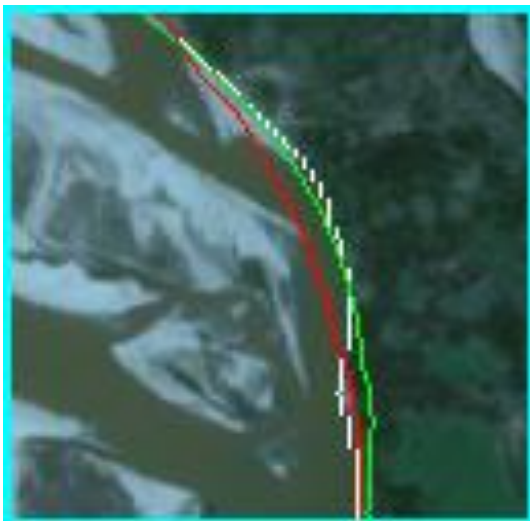
Region-1
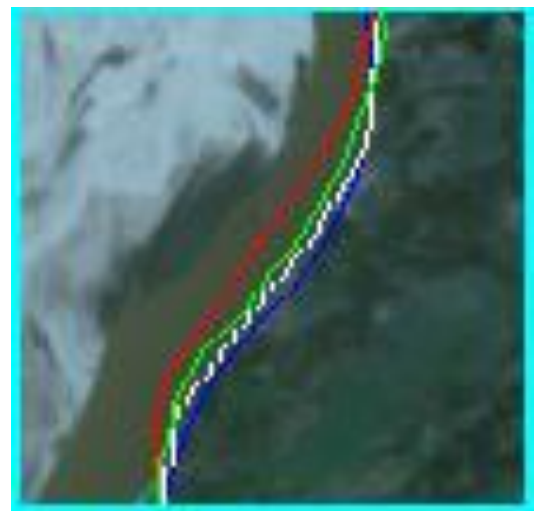
Region-2

Region-3

Region-4

N.B: Blue Lines Represent prediction results reproduced from CEGIS report

Figure 6.21 Actual bankline of 2018 and 2019 and predicted bankline of 2019 at selected regions.
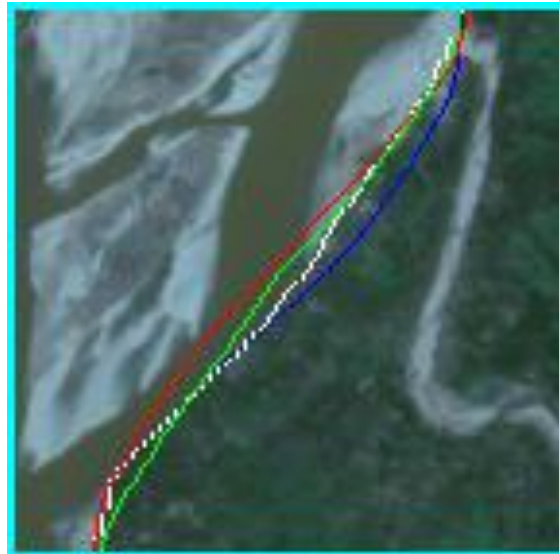
Region-5

Not-Predicted Regions:
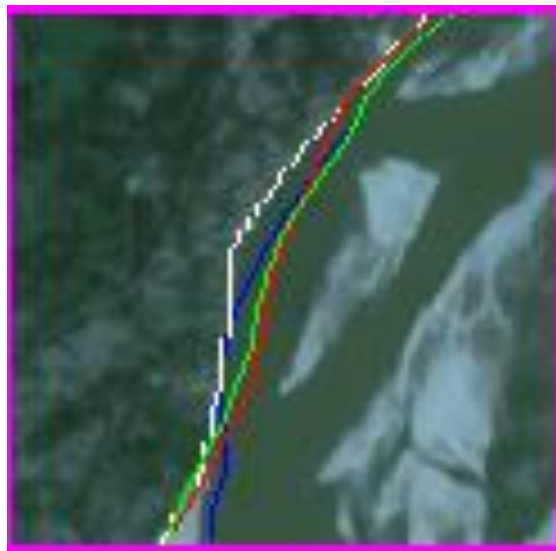
Region-6

N.B: Blue Lines Represent prediction results reproduced from CEGIS report

Figure 6.22 Actual bankline of 2018 and 2019 and predicted bankline of 2019 at selected regions

Figure 6.23 Actual bankline of 2017 and 2018 and predicted bankline of 2018 with locations of selected regions.

Predicted Regions:
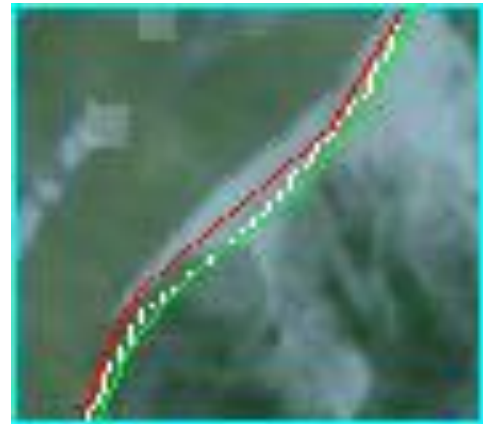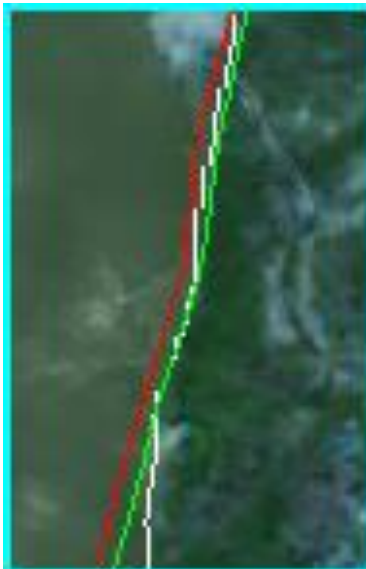
Region-1
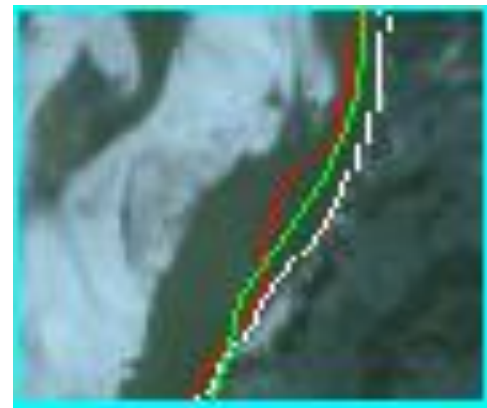
Region-2

Region-3

Region-6

Figure 6.24 Actual bankline of 2017 and 2018 and predicted bankline of 2018 at selected regions.
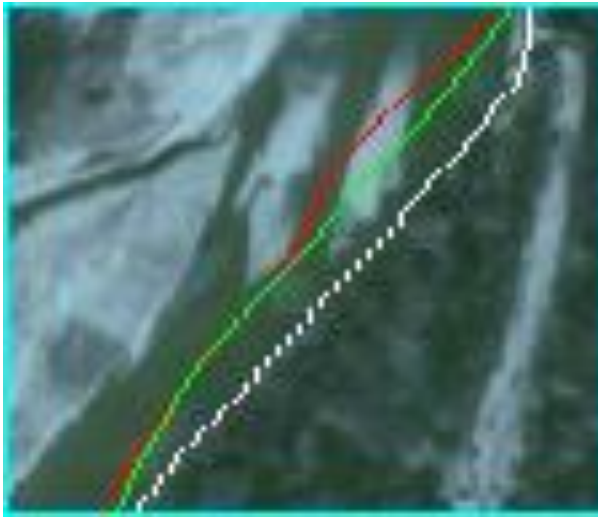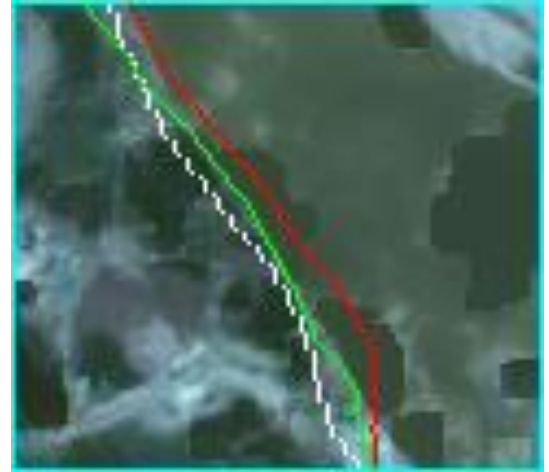
Region-7   Region-8
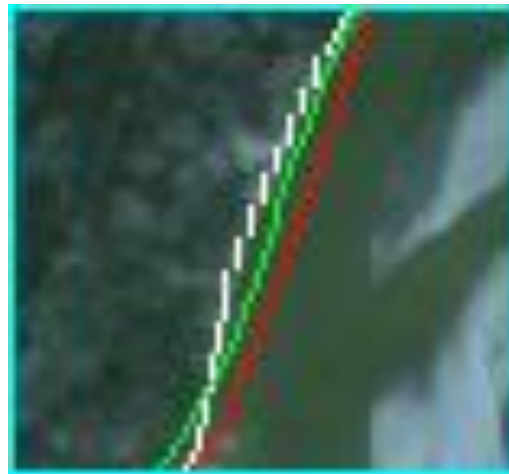
Region-10

Figure 6.25 Actual bankline of 2017 and 2018 and predicted bankline of 2018
at selected regions.

Not-Predicted Regions:
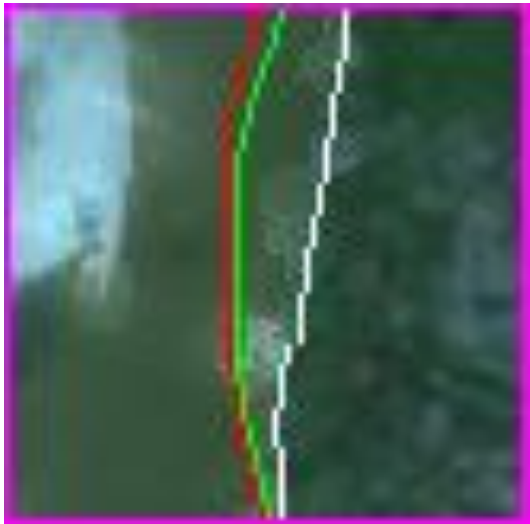
Region-4
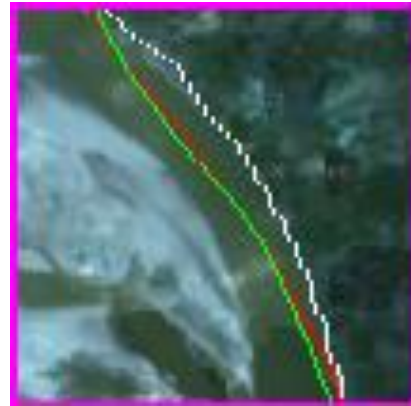
Region-5
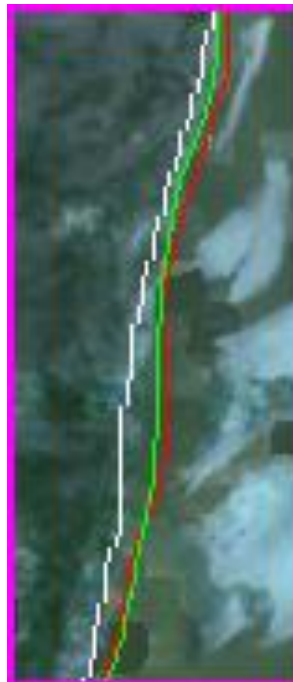
Region-9

Figure 6.26 Actual bankline of 2017 and 2018 and predicted
bankline of 2018 at selected regions.
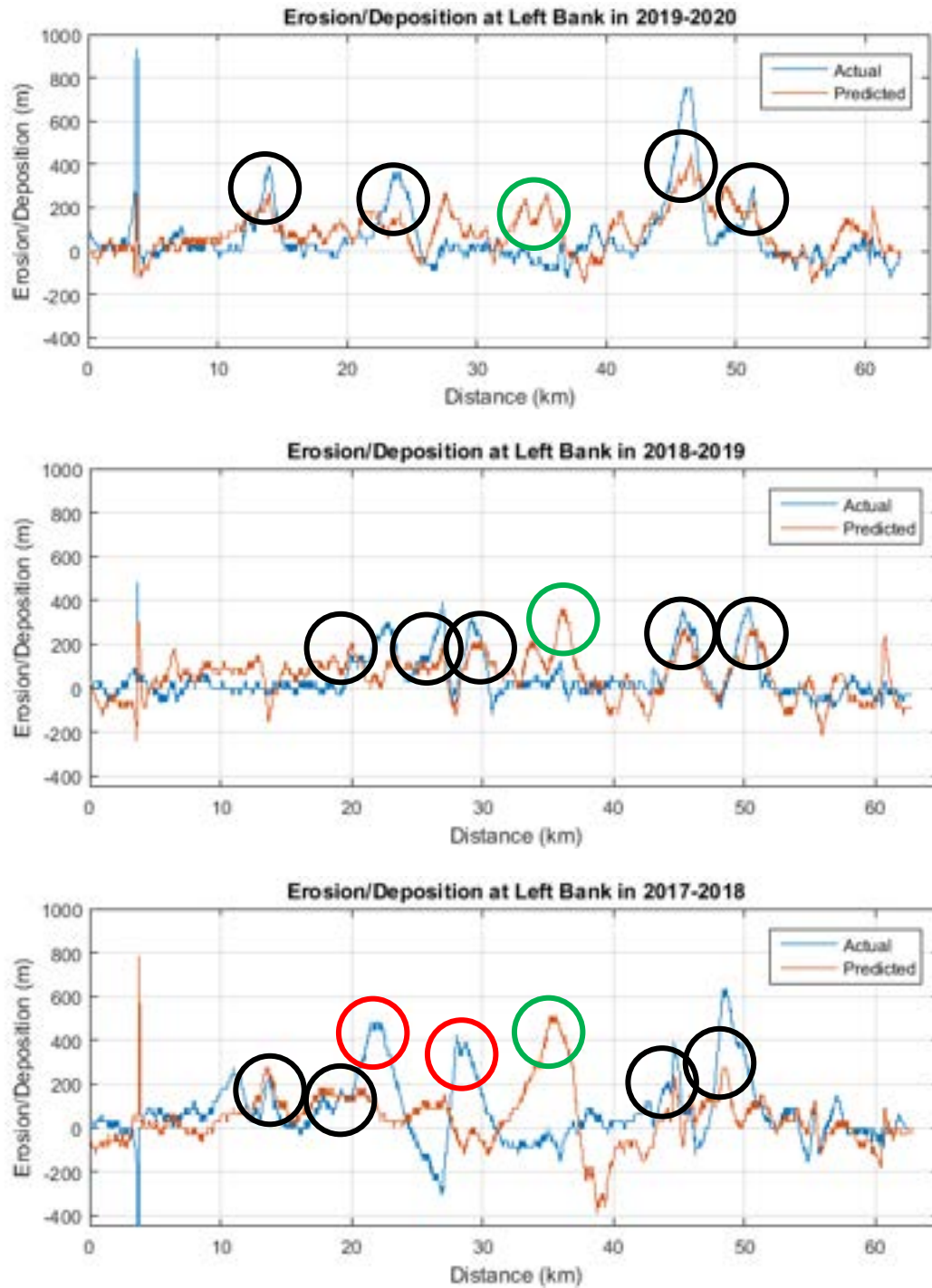
Figure 6.27 Actual and predicted erosion (+ve) and deposition (-ve) of left bank
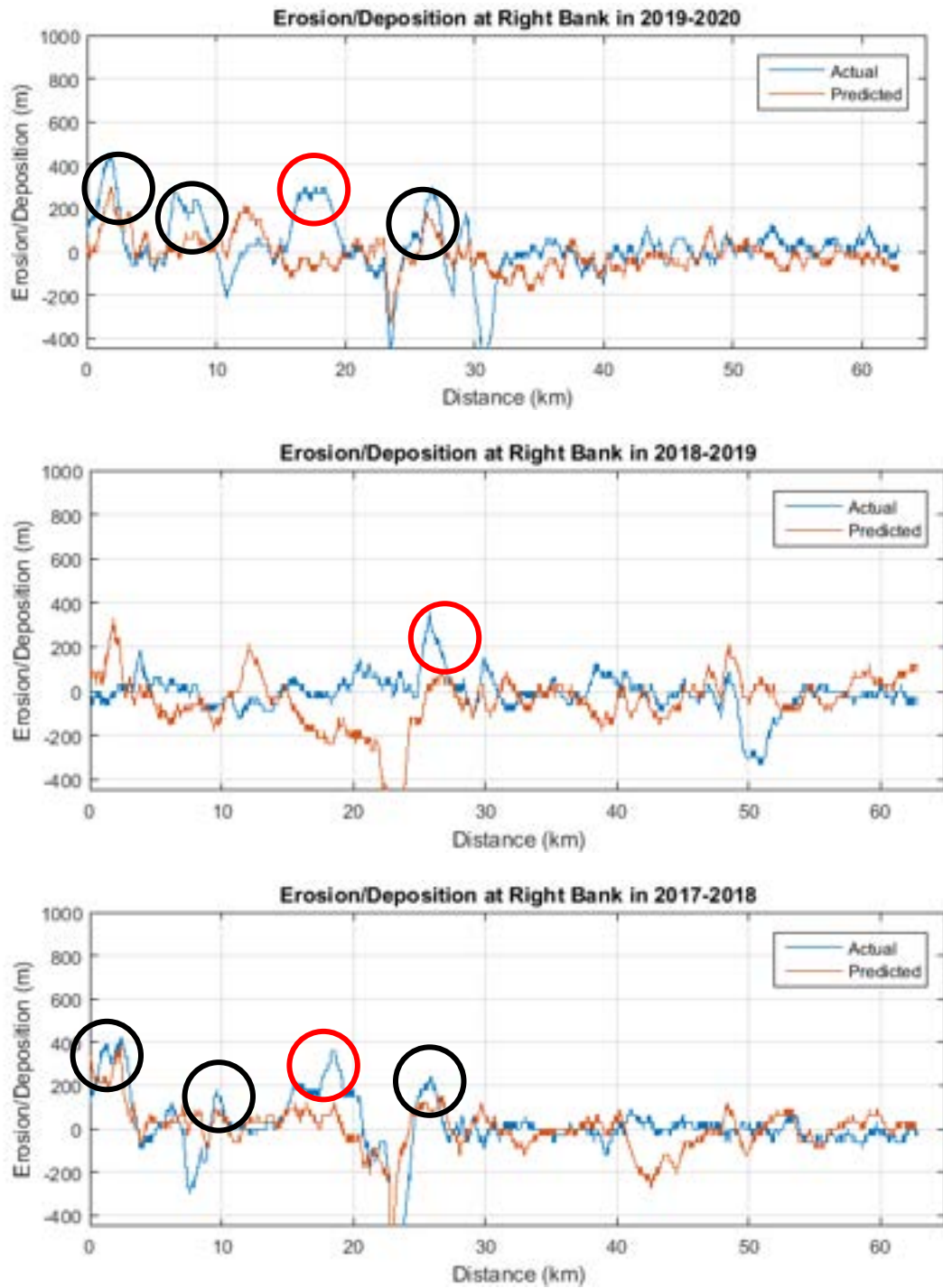
Figure 6.28 Actual and predicted erosion (+ve) and deposition (-ve) of right bank

Table 6-2. Performance of Deep Learning Model in Predicting Bankline during 2017-2020

Year	2019-2020	2018-2019	2017-2018	Total	%
Actual Erosion Events (Nos)	8	6	10	24	100
Predicted (Nos)	7	5	7	19	79
Not-Predicted (Nos)	1	1	3	5	21

N.B: 1 Pixel = 30 meters

6.9 Conclusions

Deep learning modeling technique has been applied to predict future banks using historical satellite images. Total thirty-two years of satellite images from 1988 to 2020 have been used in this modeling. Model architecture of neural network consists of six convolution layers, one LSTM layer and two fully connected layers. This trained and validated model has been used to predict river banks for the year of 2018, 2019 and 2020 and the predicted river banks have been compared with the actual river banks respectively. The mean absolute error (MAE) in training was found to vary between 2.1 m to 3.9 m while MAE in validation was found to vary between 80 m to 142 m. The performance of the model in predicting the bank erosion in selected erosion prone locations has been assessed for 3 years. Out of 24 erosion locations during 2017 to 2020, the model could predict erosion in 79% of the locations. Although the model generally underpredicted the magnitude of the erosion, the prediction of location in the erosion prone area is very satisfactory.

Chapter 7: Prediction Tool

7.1 Introduction

To use the deep learning modeling approach and make bank erosion predictions for future years, a software was developed using python script and PyQt5 library. The software will enable users to easily apply the full deep learning pipeline explained in this research by accessing the underlying Application Programming Interface (API) through an intuitive Graphical User Interface (GUI) (as shown in Figure 7.1). This will help people easily get reliable prediction results of future bank erosion events by following some easy-to-follow steps.

Figure 7.1 Prediction Tool Main Interface

7.2 Data Download

The first feature available is downloading previous satellite images from the project google drive repository. All the required images for running the software are made available to the user. The required images are filtered and preprocessed using Google Earth Engine beforehand so that the user can readily download the preprocessed file to train the model. To download the files the user will click on the "Download" button as shown in Figure 7.2.
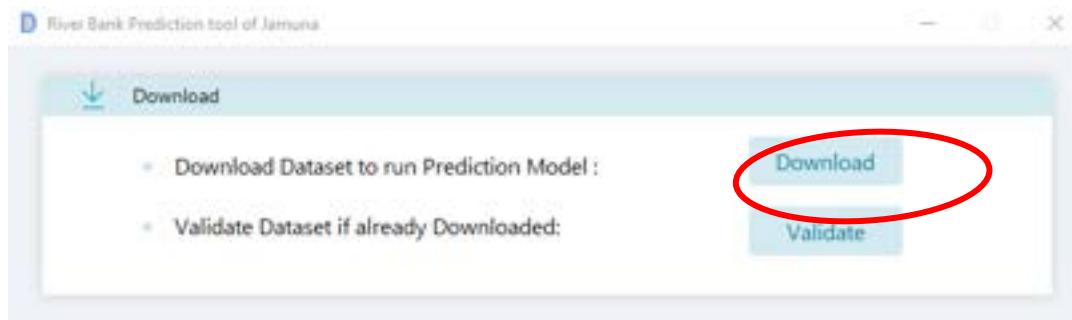
Figure 7.2 Data Download Features

The preprocessed images are stored in a project google drive repository that can only be accessed by authorized users. During the deep learning tool workshop, the potential users who were present there were added to the list of authorized users and so these users can access the required files to run the tool. If there is a new user then he or she can request access. If the user is already an authorized user, then a new page in the user's browser will appear with a download option. The user will click the button to download the files to a local machine as shown in Figure 7.3.
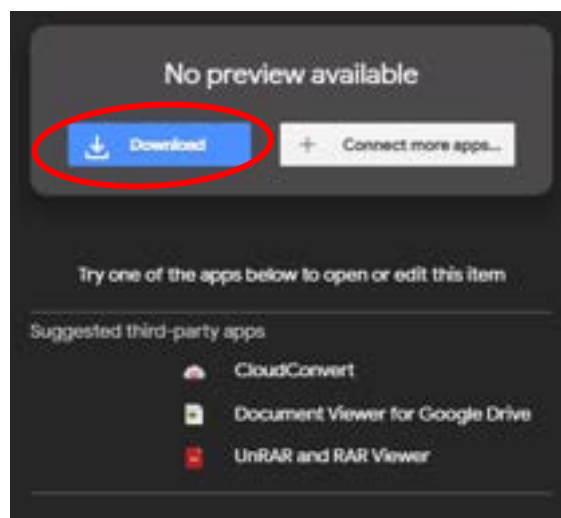
Figure 7.3 Data Download from Project Drive

Another window will pop up (as shown in Figure 7.4) so that user can select the location to save the compressed file. As there are a lot of satellite images and their corresponding bank line, all the files were compressed to a single file for better management of data. After navigating to the desired location, the user will click save to confirm the location of the downloaded compressed file.
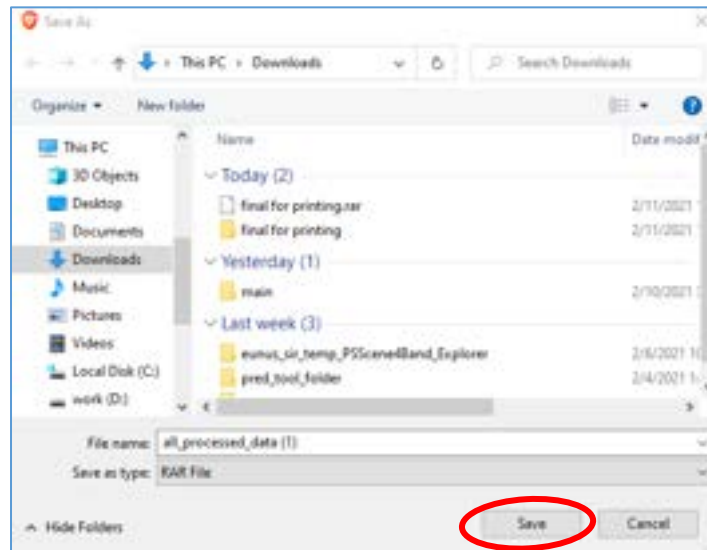
Figure 7.4 Save Downloaded Data

Another window within the tool will also pop up as shown in Figure 7.5. The downloaded compressed file will need to be extracted and the extracted files will need to be moved to the required location within the prediction tool folder. This will happen automatically once the user selects the file using the new window. There will be two options in the window: "Open File" and "Extract File". The user will first open the file which was just downloaded using the "Open File" button.
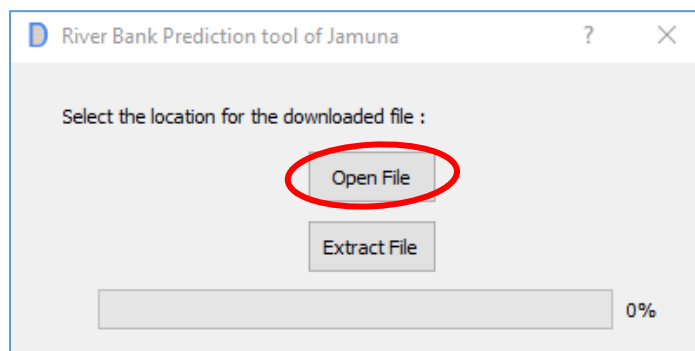
Figure 7.5 Select Downloaded File
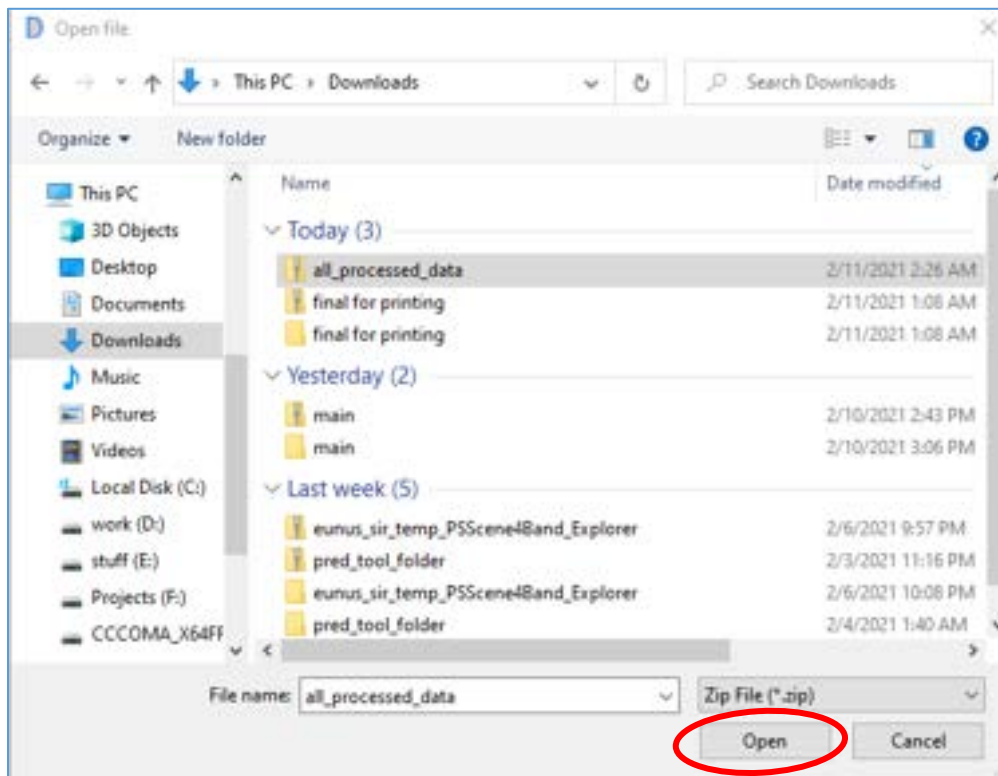
Figure 7.6 Select Downloaded File

After the compressed file is selected by the user, internally the tool will store the location of the file as shown in Figure 7.6. So, when the button to extract the file contents is selected the appropriate extraction and file management will be completed. To extract the compressed file contents to required location the user will select "Extract File" button as shown in Figure 7.7.
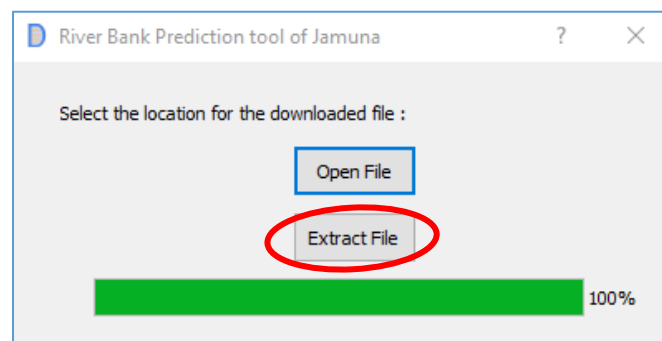
Figure 7.7 Extract Files to Required Location

Once all the above-mentioned steps are completed, all the required files for the tool will have been download to appropriate file location. The steps to download the files is a one-time operation. The user will need to follow these steps only once per year. Operations related to training and getting results can be performed subsequently once the above-mentioned steps have been performed. To check if all the data are available for predicting new bank lines, the user will be able to validate the available data. Through this step the tool will check and make sure that all the required images and shape files are present. The user will click the "Validate" button which will open a pop up with a message about the data validation process (as shown in Figure 7.8). If all data is present then the message will show " Successfully Validated. Your Data is Up to Date" or else it will provide information about the missing data.
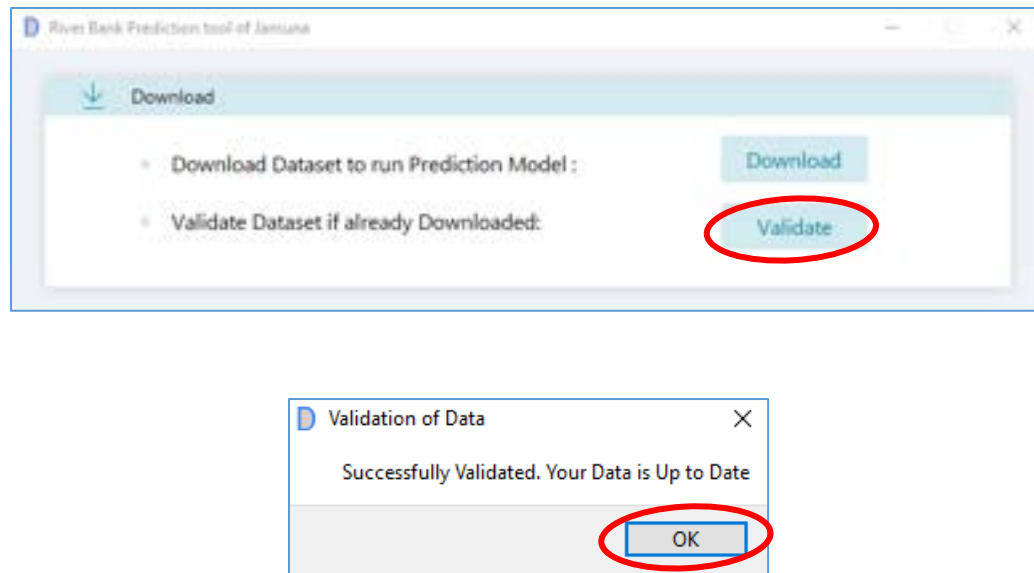
Figure 7.8 Validate Downloaded Data

7.3 Model Training

After the data download step, the user will have the option to use the recommended model training configurations or set custom configurations to train a deep learning model. The user only has to select the year he or she wants prediction of and the appropriated data along with the required operations will take place in the backend of the tool. Deep learning models are sensitive to the hyperparameters of the model. These hyperparameters determine the different configurations of the model and were selected based on experiments. The "Train Model" loads the recommended model configuration and starts the training process (as shown in Figure 7.9). It will take a lot of time for the training process to complete. In a modern-day computer, it will

take 3-4 days for the model to get fully trained and prepared to make prediction. This is also a one-time operation which will need to be performed once a year.
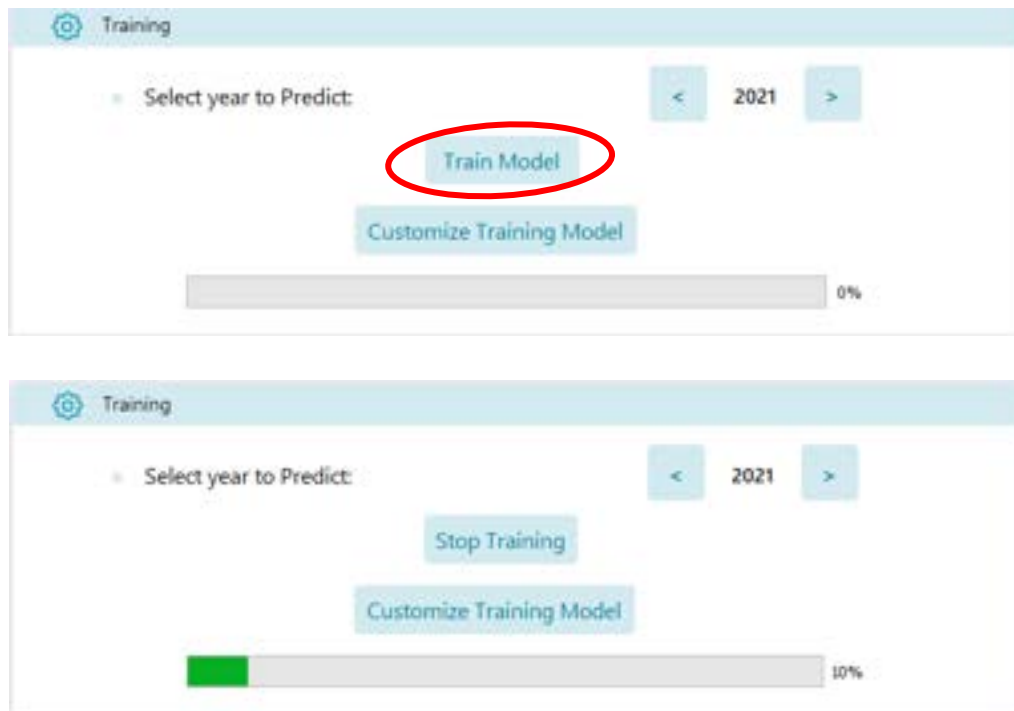
Figure 7.9 Train Default Model

The user can also choose to not use the recommended model and train a custom model. Training a custom model allows the user to further experiment with possible model configurations and observe the effect. This option for custom training was provided to allow the user to build a powerful custom deep learning model for bank erosion prediction problem. To train a custom model the user will click on "Customize Training Model" (as shown in Figure 7.10).
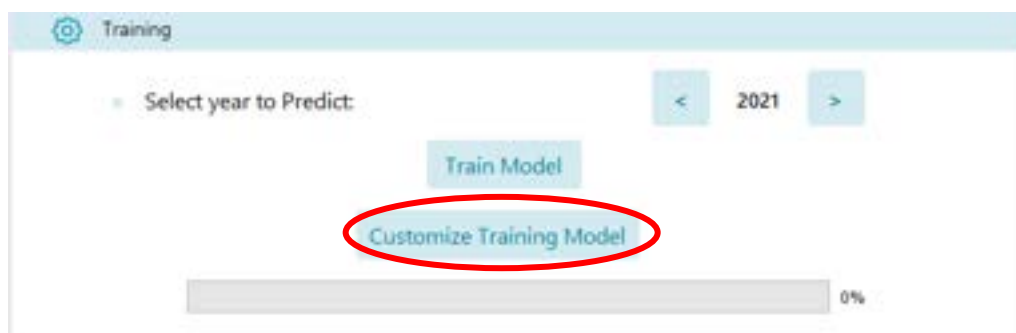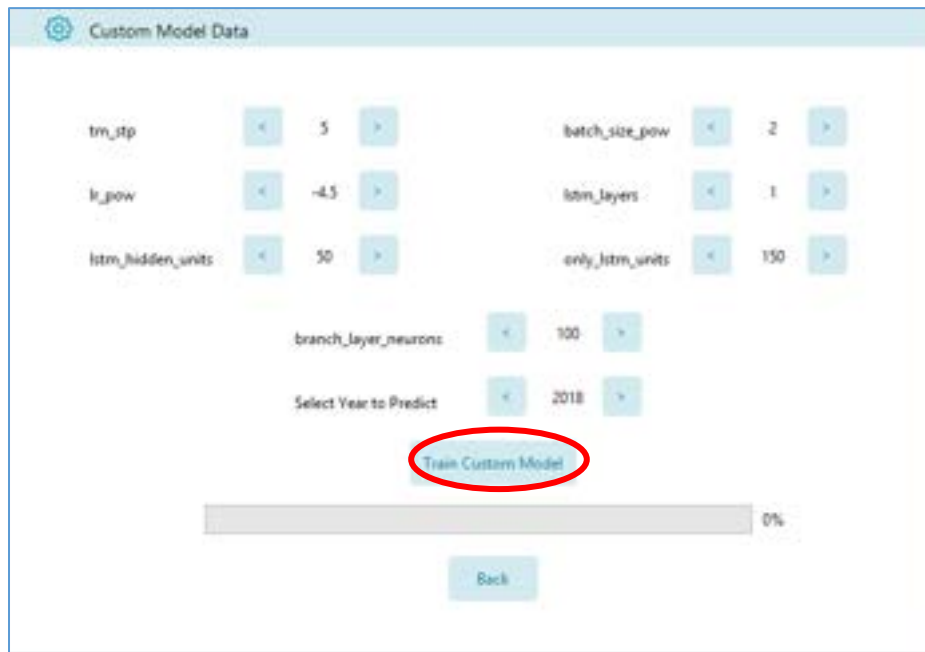
Figure 7.10 Train Custom Model

Selecting to train custom model will open a window with various hyperparameters and their range of possible values that can be modified (as shown in Figure 7.11). Hyperparameters cannot be chosen at random. So, the possible values provided here were selected so that the user does not end up trying to train a model configuration that breaks the software. As in the hyperparameters of a model dictate how much time will be required, it cannot be determined beforehand how much time it will take for a certain configuration of the model in a local machine.

Figure 7.11 Custom Model Hyperparameters

7.4 Model Prediction

After successful model training, the tool will store the prediction at a predefined location within the software directory. The user will be able to view the trained model prediction directly from the tool interface. The user will select "Show" to view the results as shown in Figure 7.12. The future bank line prediction along with left and right bank erosion deposition graph will be shown in a pop-up window as shown in Figure 7.13. The prediction for 2021 is shown in Figure 7.13.
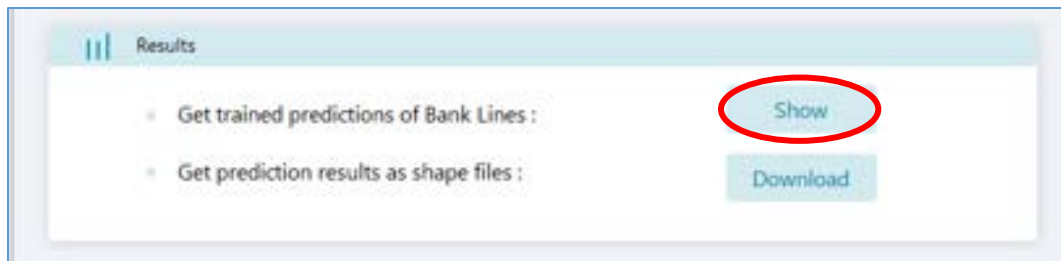
Figure 7.12 Show Prediction
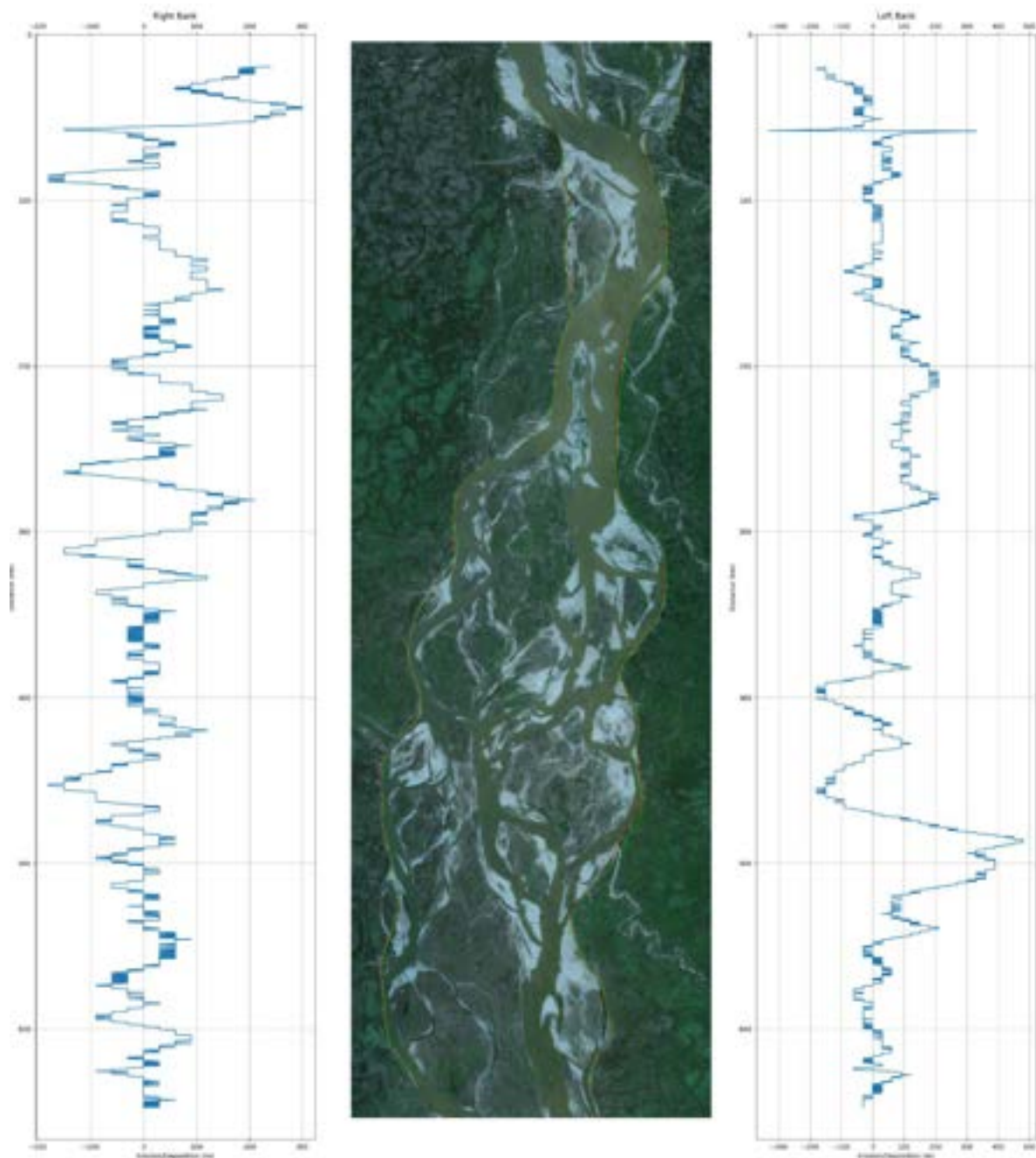
Figure 7.13 Model Prediction for 2021

The user can also get the prediction from the project google drive repository. Each year the prediction for next year will be made available through this repository. The user will click the "Download" button (as shown in Figure 7.14) to download the prediction image and the associated shape files. Only authorized people will be able to download these results from the project drive repository.
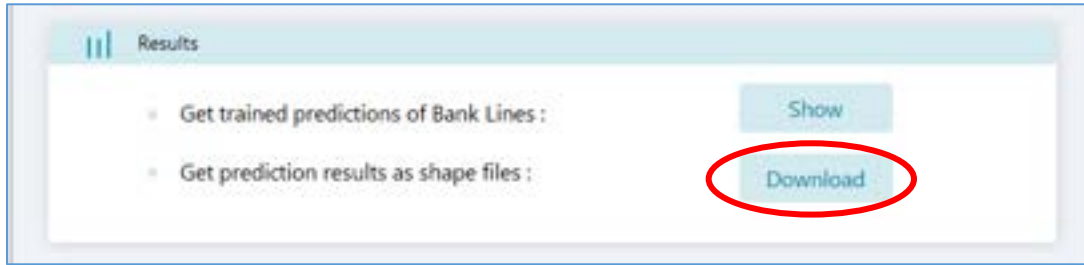
Figure 7.14 Download Prediction in Shape (.shp) file format

From the project drive folder, an user will download the previous year tiff file and the next year shape file prediction. Any GIS software like QGIS, ArcGIS can be used to import the tiff file and the shape file for further analysis of the prediction. A sample visualization of 2020 tiff file and 2021 prediction using shape file is shown in Figure 7.15.

Figure 7.15 Prediction for 2021, viewed in QGIS

Chapter 8: Capacity Building

8.1 Introduction

One of the key objectives of this project was to share technical knowledge to WARPO officials so as to develop their capacity in the field of river erosion prediction, mathematical modeling. To fulfill this objective four WARPO officials were directly involved in this study. Moreover, trainings on a 2D mathematical model, a GIS software and the river bank prediction tool, developed in this project, were arranged for the officials of WARPO.

8.2 Agreement Signing

The agreement between the Dept. of Water Resources Engineering, BUET and Water Resources Planning Organization (WARPO) to conduct the collaborative research project on *"Riverbank Erosion Dynamics using Numerical Modeling and Deep Learning Techniques"* was signed on 3rd February, 2019 (Figure 8.1) as per ToR shown in Appendix A-3. The Director General of WARPO along with senior scientific officers and other officials were present in this ceremony. Research team of Dept. of WRE consisting of the Principal Investigator, Dr. Md. Mostafa Ali, the Co-Principal Investigator, Dr. Hasan Zobeyer along with two research assistants were also present on this event. The ceremony was held in WARPO Bhaban, Green road, Dhaka.

Figure 8.1 Contract signing between WRE, BUET and WARPO

8.3 Office Setup

After contract signing, an office was setup in room no 734 in the dept. of WRE, BUET as shown in Figure 8.2. Sufficient accommodation along with logistic facilities had also been provided. Two workstations of specific configuration along with two table, two chair, one printer and necessary stationary were bought.

Figure 8.2 Project office in Dept. of WRE, BUET

8.4 Progress Meeting

Progress meetings of DWRE and WARPO research teams of the project were held in almost every month. In progress meeting the research team presented their progress report, discussed about the methodology, data collection process, and results of different analysis. Progress meeting was also held through zoom amidst corona situation. Total 21 progress meeting was held during the project run. Figure 8-3 below shows an online progress meeting via zoom. and participant list of the progress meeting is stated in the table 8-1.

Figure 8.3 Progress meeting via zoom .

Table 8-1 Participant list of progress meeting.

Team	Designation	Name
BUET TEAM	Principal Investigator	Prof. Dr. Md. Mostafa Ali
	Co-Principal Investigator	Prof. Dr. Hasan Zobeyer
	Research Assistant	A.S.M Julker Naem
	Research Assistant	Kazi Antor Hasan
WARPO TEAM	Senior Scientific Officer (Navigation)	Kazi Saidur Rahman
	Scientific Officer (Water)	Alamin Kabir
	Scientific Officer (Ground Water)	Jamal Haidar
	Scientific Officer (Soil)	Shuvro Bhoumick

8.5 Workshop and Training

8.5.1 Inception Workshop

Inception workshop was arranged on Saturday 04th May 2019 at International Training Network (ITN) center, BUET, Dhaka. Mr. S.M. Reazaul Mostafa Kamal, Joint Secretary, Ministry of Water Resources, Government of the People's republic of Bangladesh and Mr. Md. Mahmudul Hasan, Director General, Water Resources planning organization attended the event as special guest. Dr. A.T.M. Hasan Zobeyer, Professor, DWRE presented the project synopsis and Dr. Mostafa Ali, Professor, DWRE presided the Inception workshop. Officials from WARPO, CEGIS, IWM and faculty members of BUET and Dhaka University also attended the workshop.

The program started with a registration process and a welcome tea at 9.30 am, followed by a recitation from the Holy Quran by Dr. K. M. Ahtesham Hossain, Assistant Professor, DWRE. After the welcome remarks, Dr. Hasan Zobeyer presented the research objective and purposes of the project which was followed by an open discussion on Riverbank Erosion Dynamics using Numerical Modeling and Deep Learning Techniques. Everyone expressed innate interest and discussed how it could be beneficial to other sectors in Bangladesh. Sudipto Kumar Hore, Junior Specialist, CEGIS emphasized on how this model output could help BIWTA navigation. Aminul Islam, Executive engg, BWDB suggested that, protectiveness of right bank of Jamuna river should be considered in making erosion prediction. Director General of WARPO thanked everyone and praised that such research initiative had been undertaken.

After informative speeches from the special guests, the chair of the workshop, announced the closing of the program. Selected pictures from the inception workshop are shown in Figure 8.4.

Figure 8.4 Selected picture of Inception workshop

8.5.2 SRH 2D Training

A training on 2D hydrodynamic model (SRH 2D) use was arranged in 18th & 23rd September 2019 at WARPO to enhance the technical capacity of the scientific officers of WARPO in hydraulic modeling. Total 18 participants from WARPO have been attended in this training. In this two-day long program, a hydrodynamic model as well as a morphological model was developed with the primary data. The program was brought to a closing with the principal investigator Dr. Mostafa Ali, Co-principal investigator Dr. Hasan Zobeyer, Dr. Taufiqe Elahi and Mr. Md. Mahmudul Hasan, Director General of WARPO distributing certificates among the participants. Selected pictures from the training are shown in Figure 8.5.

Figure 8.5 SRH 2D Training program

8.5.3 QGIS Training

A Training on QGIS was held on January 14, 2020 at WARPO. This training was arranged beyond the scope of the project upon request of honorable DG of WARPO. Total 20 participants from WARPO have been attended in this training. In this training session principal investigator Dr. Mostafa Ali briefed about the use of QGIS and its application. At the end of the training session a short exam was taken to evaluate the performance of the participants. The program was brought to a closing with the principal investigator Dr. Mostafa Ali, Co-principal investigator Dr. Hasan Zobeyer, Dr. Taufiqe Elahi and Mr. Md. Mahmudul Hasan, Director General of WARPO distributing certificates among the participants. Selected pictures from the training are shown in Figure 8.6.

Figure 8.6 Training on QGIS.

8.5.4 Training on Prediction Tool

Training on prediction tool was held on 10th and 11th February, 2021 at WARPO. This Prediction tool has been developed from research outcome of the Research on River Bank Erosion Dynamics using Numerical Modeling and Deep Learning Techniques. Total 16 trainee from WARPO and 4 from BWDB participated in this training program. In this training session principal investigator Dr. Mostafa Ali briefed about the introduction and applications of deep learning technique. Then Kazi Antor Hasan, Research Assistant of this project, provided hands on training on the Prediction tool. The two days long program was brought to a closing with the principal investigator Dr. Mostafa Ali, Co-principal investigator Dr. Hasan Zobeyer, and Md. Delwar Hossain, Director General of WARPO distributing certificates among the participants. Selected pictures from the training are shown in Figure 8.7.
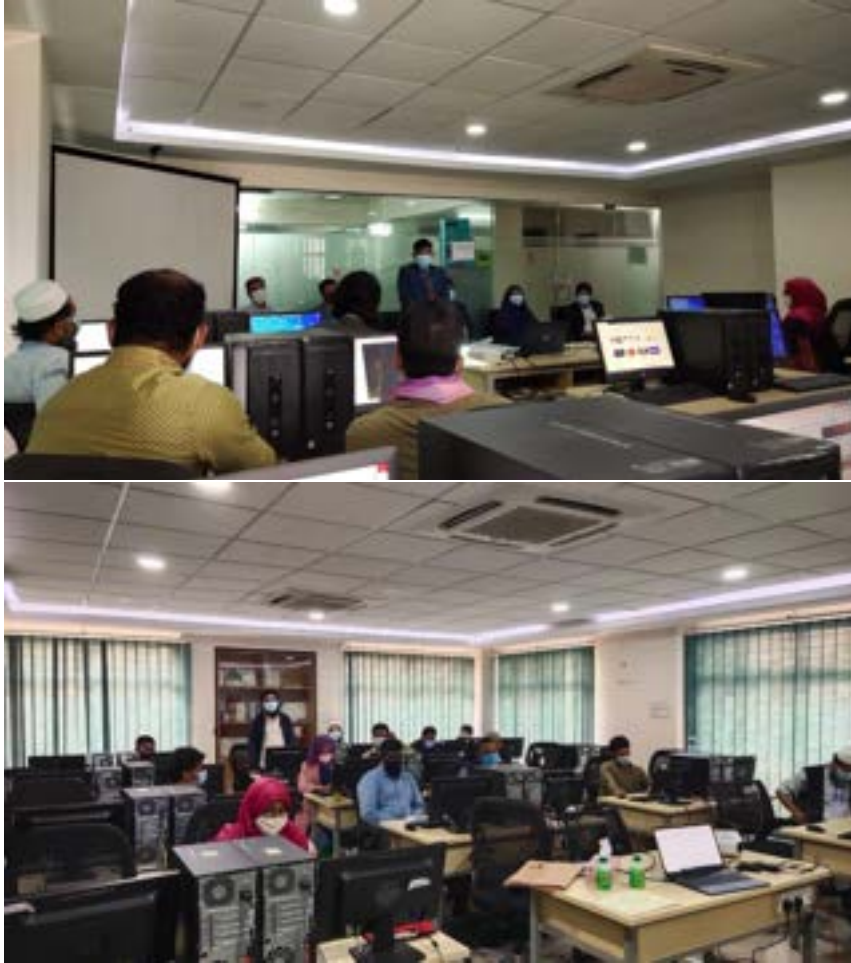
Figure 8.7 Training on prediction tool

8.5.5 Final Workshop

Final workshop was arranged on Wednesday 19th May 2019 through zoom video conference medium due to pandemic situation. Mr. Kabir Bin Anwar, Senior Secretary, Ministry of Water Resources, Government of the People's republic of Bangladesh, was the chief guest of the final workshop. Mr. Md. Rokon Ud-Doula, Additional Secretary, Ministry of Water Resources, and Mr. AKM Waheduddin Chowdhury, Director General, Bangladesh Water Development Board, attended the event as special guests. Mr. Md. Delwar Hossain, Director General , Water Resource Planning Organization, had conducted the session as the chairperson. Dr. Mostafa Ali, Professor, DWRE and Principal Investigator of the research project presented the research outcomes. Officials from WARPO, BWDB, Ministry of Water Resources, Planning commission, CEGIS, IWM and faculty members of BUET and Dhaka University also attended the workshop.

At first, the program was started with a registration process at 10.30 am and followed by a recitation from the Holy Quran. Then, DG, WARPO initiated the workshop with his introductory remarks. Engr. Kazi Sidur Rahman, Project Director of the research project, gave a short speech on background and motivation of the research project. After that, Dr. Mostafa Ali, Professor, DWRE and Principal investigator of the project, presented the research outcomes which was followed by an open discussion. Everyone expressed innate interest and discussed how it could be beneficial to other sectors in Bangladesh. Everyone appreciated this kind of research initiate and recommended this type of application in other major rivers of Bangladesh. Especially, the Chief Guest, Mr. Kabir Bin Anwar, praised the research outcome and requested BUET research team to develop similar type of prediction tool for other rivers, such as the part of lower Meghna estuary. Selected pictures from the final workshop are shown in Figure 8.8-8.10. A detailed minutes of the final workshop is attached in Appendix – 5. The following decisions were taken in the final workshop:

i)   Similar research needs to be caried out for the estuary region of Bangladesh to combat river bank erosion.

ii)   The developed erosion prediction tool needs to be improved and customized for other major rivers by conducting more similar kinds of research.

iii)   WARPO should initiate institutionalization of the erosion prediction tool through capacity development programs with the relevant stakeholders.
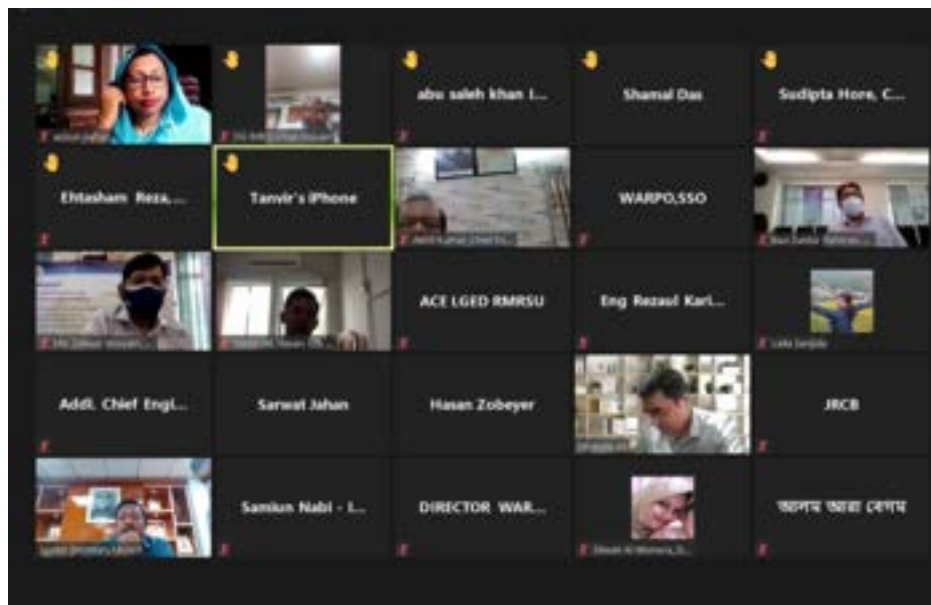
Figure 8.8: Final workshop Participants (Part 01)
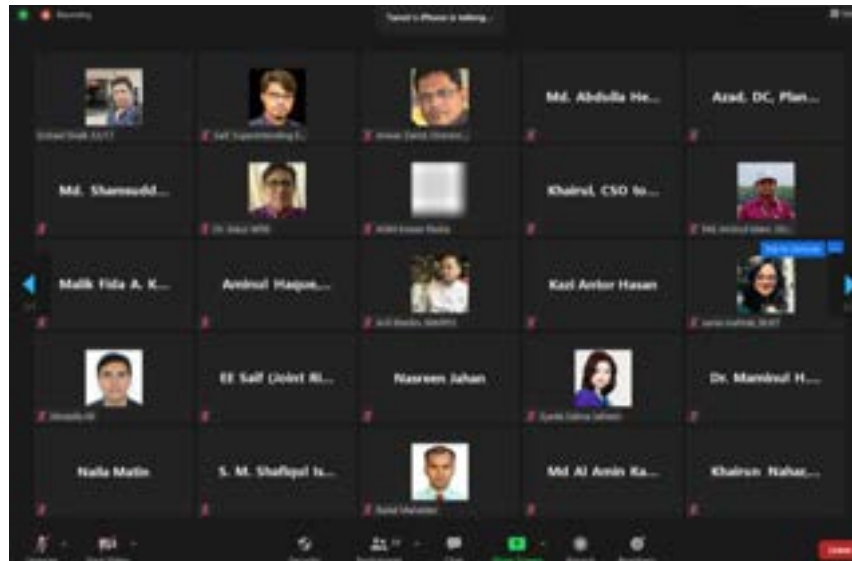
Figure 8.9: Final workshop Participants (Part 2)

Figure 8.10: Final workshop Participants (Part 3)

8.6 Field Visit

8.6.1 Field visit-01

According to the work plan the first field visit was conducted on 28th March 2019. The research team of the project participated (as shown in Table 8-2) in the field visit at Daulatpur Upazila, Manikganj (Figure 8-11). The purpose of the field visit was to observe the background condition and erosion pattern of Jamuna river.
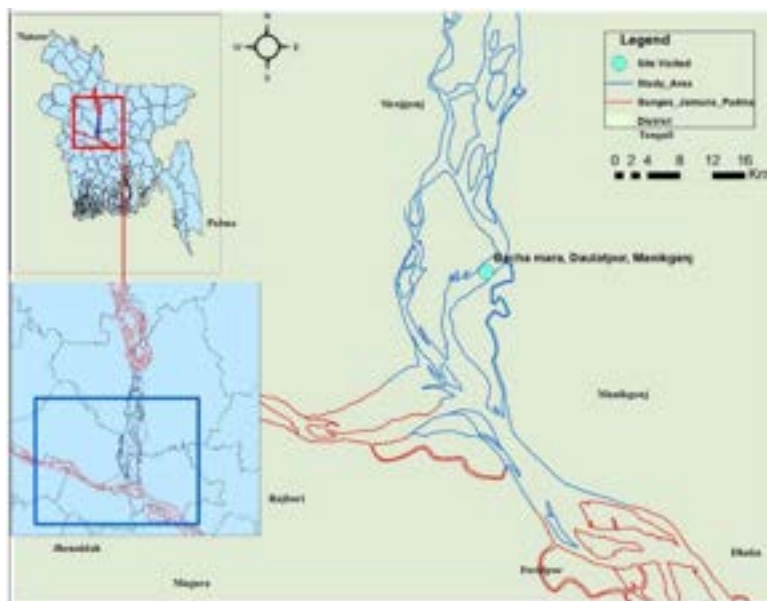
Figure 8.11 Field visit location

Table 8-2 Research Team members in field visit

Name	Designation
Prof. Dr. Md. Mostafa Ali	Principal Investigator
Prof. Dr. Hasan Zobeyer	Co-Principal Investigator
Md. Alifnur Salim	Research Assistant
Kazi Antor Hasan	Research Assistant
Kazi Saidur Rahman	Senior Scientific Officer (Navigation)
Alamin Kabir	Scientific Officer (Water)
Jamal Haidar	Scientific Officer (Ground Water)
Maimuna Qazi	Scientific Officer (Soil)
Abdulla Al Mahabub Zoraf	Scientific Officer (Assistant Programmer)

The primary destination was Daulatpur, Manikganj. The team started from BUET for Manikganj at 7:15 am and reached the Water Board office, Manikganj at 11:10 am. After arrival, a conversation was conducted with the Executive engineer and Sub-divisional engineer of Water Board, Manikganj about maximum erosion prone area of the locality. Then the team made their way to Bacha Mara village, Daulatpur Upazila. In this part of journey, they were unable to use their microbus and had to avail the local motorbike service to reach the destination. A meeting with the local BWDB officers and local union members was arranged to know about the details of bank erosion in the locality (Figure 8-12).

According to the member of 7 no Union Parishad, Adbur Rahim molla, the area of Char Katari had been severely damaged by the erosion process and currently the area of Bacha Mara is facing the same problem. Several union parishad members and social workers were present in the meeting. Executive engineer and Sub-divisional engineer of Manikganj were also present in the meeting. Table 8-3 represents the important persons we met during the field visit. Figure 8-13 shows the research team members with local people. A pictorial description of the field visit-01 is given in Appendix (A-6).

Table 8-3 People present in the meeting

Personnel	Name	Designation
BWDB	Mehedi Hasan	Executive Engineer
	Mamun Hawladar	Sub-Divisional Engineer
Locals	Abdur Rahim Molla	UP member
	Badrur Rahman	UP member
	Nazrul Islam	Social Worker
	Abdul Majid	Businessman
	Abdul Baten	Businessman
	Unus Ali Molla	School Committee Member
	Mrs Rahimon	Female UP member

Figure 8.132 Meeting with local correspondences in 7 no. Union Parishad Office, Bachamara, Daulatpur, Manikganj

Figure 8.123 Group Photo with local people.

8.6.2 Field visit-02

Another field visit was conducted on 4th November 2019. All the research team members of this project participated in this field visit at Jafarganj, Shibhalaya Upazila, Manikganj (Figure 8-14). The Director General of WARPO along with senior scientific officers and other officials also participated in this field visit (Figure 8-15). The purpose of this field visit was to observe the background condition of the Jamuna river and to observe the survey procedure.
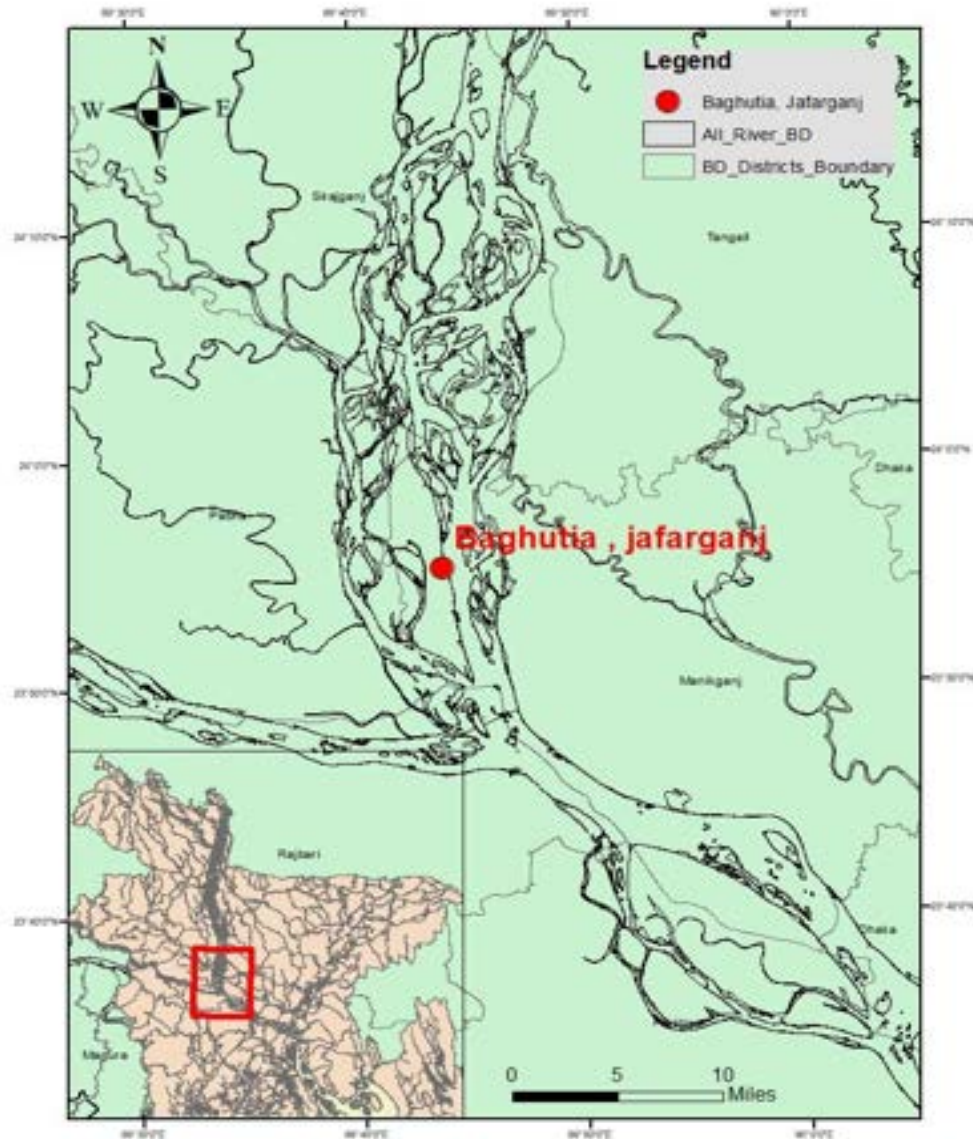
Figure 8.14 Field visit-02 location

A day before the field visit, a team of three members went to the site, talked to the surveyors, locals and collected information on how the river behaved during different seasons, how the local people predicted riverbank erosion by observing dunes etc. The next day the research team along with WARPO officials started from WARPO for Manikganj at 8:00 am and arrived Paturia ferry terminal at 11:30 am. After a short break the team went to Aricha ferry port where a boat was waiting for them.

On the way to the site severe bank erosion was observed in some places (Figure 8-16). There was some bank protection works along the riverbank but most of them were vulnerable. geo textile bags and concrete blocks had been displaced due to toe failure. Numerous numbers of Cracks had been observed and different layers of soil along the riverbank could also be identified. After one and a half hour of boat journey the team reached Baghutia. A pictorial description of the field visit-02 is given in Appendix (A-7).

Figure 8.15 Group photo of the research team with WARPO officials.

The survey team was ready with their equipment. They briefed (Figure 8-17) about the survey equipment such as GPS tracker, sounding machine, antenna, laptop and battery. They also described the software they were using to collect data. They had divided the survey area in several number of cross sections. They showed the full process of collecting hydrographic data in two of the cross sections.

Figure 8.16 Severe bank erosion

Figure 8.17Surveyor describing the survey procudeure

Chapter 9: Conclusion and Recommendation

The aim of this project is to understand river hydrodynamics and morphological processes including river bank erosion and to develop a riverbank erosion prediction tool using Deep Learning for a 80 km selected reach of Jamuna River starting from Bangabandhu Bridge. Based on various analyses, modeling and results and other activities following conclusions and recommendations can be made:

i.   A proper hydrologic analysis was made using discharge and water level data of Bahadurabad station and Mathura station. From historical hydrologic data it was observed that mean annual discharge was found to be around 17000 m^3/s. Maximum and minimum flood discharge was recorded as 102535 m^3/s and 3095 m^3/s respectively.

ii.   Erosion and deposition were calculated for both banks of Jamuna river using 32 years of satellite images to understand the erosion pattern during this period. From 1988 to 2019, total erosion along the Jamuna river left bank was 23800 ha with an average of 770 ha per year. Whereas for the right bank of the river total erosion was 11840 ha and 380 ha per year. It was evident from the data that erosion rate was higher for left bank of the Jamuna river. From the planform analysis it was found that width of the Jamuna river has an increasing trend and it is widening at the left bank side. Since the early 1980s, the Jamuna River in this study area widened from 14.2 km to 15 km in the 2020 and now the average width is 14.69 km.

iii.   Longitudinal profiles of Jamuna show a high spike of deposition, always followed by a steep crest erosion and a medium crest deposition is followed by medium to low crest erosion. Maximum erosion of 15.07m occurred along the center profile in 2017-2018 and Minimum erosion of 8.06 m occurred along the right profile in the year 2016-2017. Maximum deposition was observed as 20.81 m along the left profile in the year 2018-2019.

iv.   From these hydrological and erosion data a correlation between peak discharge and total erosion was found, with higher discharge erosion will be higher. It was observed from the figure that for peak discharge in the year 1996 and 1998, erosion was maximum and erosion was less in case of lower discharge.

v.   Morphological modeling of such active river like Jamuna was very challenging. Moreover, there was limitation on fine resolution data, computational power etc. The best available bathymetry data have a resolution of 500 m but in Jamuna river within 500 m the river bed may change several times. Again, there is constraints on model capacity, for morphological modeling SRH 2D can handle about thirty thousand to forty thousand. To accommodate this model cell size was coarse. Including all these uncertainties it was very difficult to replicate the real scenario.

vi.   Model may predict erosion or deposition correctly but the extent of erosion and deposition was not obtained. This may be due to very coarse resolution data and mesh grid size. Although the model cannot predict the bed form change accurately for this grid size it could give some indication of bank erosion. To assess the

probability of bank erosion bed shear stress along the bank was observed. It was found from the simulation that at the places where erosion took place in the year 2019, shear stress is higher and where the bank remained almost at the same position shear stress is relatively lower. In erosion prone areas, erosion took place in 2019 and from model result it can be found that shear stress is relatively higher in those areas. Similarly, in areas, where there was little to no erosion and bed shear stress along the bank are relatively lower.

vii.   Deep learning modeling is a very iterative process. In order to find the optimal model configuration different ideas were explored, then those ideas were implemented in code and experiments were performed to observe if the model could achieve a lower bias and variance value than before. Different model training configurations are different based on many factors from input data batch size, model weight initialization method to type of activation function, optimization algorithm, etc. Changing any of these factors of model configuration led to the development of a different model. Through this iterative process of idea generation, code implementation and experimentation an optimal model configuration was found for the bank erosion prediction problem.

viii.   The banklines of 2017-18, 2018-19 and 2019-20 were simulated using the final model configuration. For predicting the banklines of a certain year, the model input of images and banklines of previous four years were provided. To understand the general difference between predicted and actual bank lines some numerical metrics were calculated for both banks of the last six years. The mean absolute error (MAE) in training was found to vary between 2.1 m to 3.9 m while MAE in validation was found to vary between 80 m to 142 m.

ix.   A number of erosion prone regions have been selected to closely compare the model results. The regions of erosion have been selected based on visual inspection with a general principle of having erosion of more than 100-150 m as the average error in prediction is around 3 to 4 pixels equivalent to 90 to 120 meters. In 2019-2020, the model can predict 4 erosion areas accurately in the left bank. However, in the right bank the model predicts erosion in 3 locations but cannot predict only at one location. In 2018-2019, the model can predict erosion in all five locations in the left bank and failed to predict the erosion at one location in the right bank. In 2017-2018 the model predicts erosion in 4 locations along left bank but failed to predict in two locations and in the right bank, the model predicts erosion in 3 locations and could not predict at one location. It is to be noted that the bankline prediction by CEGIS model marked by blue line in 2018-2019 has also been compared.

x.   Out of 24 erosion locations during 2017 to 2020, the model could predict erosion in 79% of the locations. Although the model generally underpredicted the magnitude of the erosion, the prediction of location in the erosion prone area is very satisfactory.

xi.   Finally, a river-bank prediction tool for lower part of Jamuna starting from Bangabandhu bridge has been developed for use by WARPO. A graphical user

xii.   interface (GUI) has been developed for easy use of the model. All programming codes including the prediction tool have been handed over to WARPO. The official hand-over letter is attached in Appendix A-4.

xii.   Three trainings: a) on hydro-morphological model SRH-2D, b) on GIS software QGIS and c) on the prediction tool that has been developed in this research, have been provided to the officials of WARPO and selected officials of BWDB. Manuals for these trainings have been prepared and supplied during workshops.

xiii.   Furthermore, two workshops: an inception workshop and a final workshop, have been arranged to disseminate the outcomes of this research.

xiv.   Four selected scientific officers from WARPO have been involved throughout the research project. Through these collaborative works and trainings, capacity of WARPO officials has enriched their technical capabilities to develop and assess different water resources development project.

Recommendations

- Defining bank lines was found to be a hard problem given the versatile nature of river planform. But identifying prominent features like bars, vegetation, waterbody is an easier task and consensus can be reached. Future work can look into predicting all of these prominent features as a semantic segmentation mask. This is a promising avenue as a lot of recent deep learning works deal with semantic segmentation problems.

- Only January month data of every year was used to make predictions. Data from other months can be used with the hope of improved performance as deep learning models always perform better with more data.

- Bankline and satellite image have been used in predicting river bank erosion. As an extra parameter bathymetry data can be incorporated.

- Here Convolutional many to one LSTM algorithm has been used, different suitable algorithm can be tried. One of the recent sequence prediction algorithms known as Transforms can be a prime candidate for future work.

- Prediction tool can be also be developed for other major rivers, such as upper part of Jamuna river, Ganges, Padma, Teesta and Lowe Meghna.

References

Afrose, S., 2012. "Morphological Analysis of Teesta River", B. Sc. Engineering Thesis, Department of Water Resources Engineering, BUET.

Alex Graves, Abdel-rahman Mohamed, and Georey Hinton. Speech recognition with deep recurrent neural networks. In Acoustics, speech and signal processing (icassp), 2013 ieee international conference on, pages 6645{6649. IEEE, 2013.

Alex Graves. Generating sequences with recurrent neural networks. arXiv preprint arXiv:1308.0850, 2013.

Allen, Richard & Pereira, L & Raes, D & Smith, M. (1998). Crop evapotranspiration guidelines for computing crop requirements. FAO Irrig. Drain. Report modeling and application. J. Hydrol.. 285. 19-40.

Ashmore, P. E. (2000). Braiding phenomena: statics and kinetics. In: Gravel Bed Rivers V (Ed. by P.M. Mosley), pp. 95–114. New Zealand HydrologicalSociety, Wellington.

Ashworth, P.J., Best, J.L., Roden, J.E., Bristow, C.S. and Klaassen, G.J. (2000) Morphological evolution and dynamics of a large, sand braid-bar, Jamuna River, Bangladesh. Sedimentology, 47, 533–555.

B. Baharudin, L.H. Lee, K. Khan (2010). A review of machine learning algorithms for text documents classification, In: Journal of Advances in Information Technology 1:4âAS20.

Bagnold, R. A. (1956). "The flow of cohesionless grains in fluids." Philosophical Transactions of the Royal Society of London, Series A, 249, 315–319.

Baki, A.B.M., Gan, T.Y., 2012. Riverbank migration and island dynamics of the braided Jamuna River of the Ganges Brahmaputra basin using multi-temporal Landsat images. Quaternary International 263, 146-161.

Best, James & Ashworth, Philip & Sarker, Maminul & E. Roden, Julie. (2008). The Brahmaputra-Jamuna River, Bangladesh. 10.1002/9780470723722.ch19.

Blondeaux, P., and Seminara, G. (1985). "A unified bar-bend theory of river meanders." Journal of Fluid Mechanics, 157, 449–470.

Bridge, J. S. (2003). Rivers and floodplains: forms, processes, and sedimentary record. Blackwell, Oxford, United Kingdom.

Bristow, C.S. (1987) Brahmaputra River: channel migration and deposition. In: Recent Developments in Fluvial Sedimentology (Eds Ethridge, F.G., Flores, R.M. and Harvey, M.D.), Special Publication of the Society of Economic Palaeontologists and Mineralogists, No. 39, Tulsa, OK, 63–74.

Bristow, C.S. (1993a) Sedimentary structures in bar tops in the Brahmaputra River, Bangladesh. In: Braided Rivers (Eds Best, J.L. and Bristow, C.S.), Special Publication of the Geological Society of London, No. 75, London, 277–289.

Burger, J., Klaassen, G.J., Prins, A., 1991. Bank erosion and channel processes in the Jamuna River, Bangladesh. In: Elahi, K.M., Ahmed, K.S., Mofizuddin,M. (Eds.), Riverbank Erosion, Flood and Population Displacement in Bangladesh. Publ. by Riverbank Impact Study, Jahangirnagar University, Dhaka, pp. 13–29.

CEGIS, (2017). Prediction of riverbank erosion along the Jamuna, the Ganges and the Padma Rivers in 2017.

Christopher M. Bishop. Pattern Recognition and Machine Learning (Information Science and Statistics). Springer-Verlag, Berlin, Heidelberg, 2006. ISBN 0387310738.

Christopher Olah. Understanding lstm networks. http://colah.github.io/posts/2015-08-Understanding-LSTMs/, 2015. Accessed:2018-05-25.

Chu, Z.X., Sun, X.G., Zhai, S.K., Xu, K.H., 2006. Changing pattern of accretion/erosion of the modern Yellow River (Huanghe) subaerial delta, China: based on remote sensing images. Marine Geology 227, 13e30.

Coleman, J.M. (1969) Brahmaputra River: channel processes and sedimentation, Sedimentary Geology, 3, 129–239.

D. Lim, "Convolutional attention-based seq2seq neural network for end-to-end asr," mathesis, Korea University, 2017.

Darby, S. E., and Thorne, C. R. (1996). ''Numerical simulation of widening and bed deformation of straight sand-bed rivers. I: Model development.'' J. Hydr. Engrg., ASCE, 122(4), 184–193.

Datta, B.and Singh, V. P. (2004). Hydrology. In The Brahmaputra Basin Water Resources , ed. V.P. Singh, N.Sharma, C.Shekhar and P.Ojha. Boston:Kluwer Academic Publishers, pp.139– 95.

David E Rumelhart, Georey E Hinton, and Ronald J Williams. Learning representations by back-propagating errors. Nature, 323(6088):533, 1986.

Denny Britz. Recurrent neural networks tutorial. http://www.wildml.com/2015/09/recurrent-neural-networks-tutorial-part-1-introduction-to-rnns/, 2015. Accessed: 2018-05-25.

Duan, G., Jia, Y., and Wang, S. (1997). ''Meandering process simulation with a two dimensional numerical model.'' Proc., Conf. on Mgmt. of Landscapes Disturbed by Channel Incision, University of Mississippi, Miss., 389–394.

E. Racah, C. Beckham, T. Maharaj, Prabhat, and C. Pal, "Semi-supervised detection of extreme weather events in large climate datasets," arXiv preprint arXiv:1612.02095, 2016.

EGIS, 1997, Morphological dynamic of the Brahmaputra-Jamuna river, prepared for WARPO

Einstein, H. A. (1950). "The Bedload Function for Bedload Transportation in Open Channel Flows." Technical Bulletin No. 1026, U.S.D.A., Soil Conservation Service, 1–71.

Exner, F. M. (1925). "Uber die Wechselwirkung zwischen Wasser und Geschiebe in Flussen." Sitzber. Akad. Wiss Wien, Part IIa, Bd. 134 (in German). Falcon, M. A., and Kennedy,

FAP -24 River Survey

Faruque A. 2007. Resettlement Policy Resettlement Policy Development: The Case of Development: The Case of Bangladesh. Asian Development Bank Asian Development Bank . Bangladesh Bangladesh, Resident Mission, PowerPoint Presentation.

Fedele, J. J. (1995). "Dune velocity in sand bed rivers." XXVI International Association for Hydraulic Research Congress (IAHR), John F. Kennedy Student Paper Competition, London, U.K., 37–42.

Frank Rosenblatt. The perceptron: a probabilistic model for information storage and organization in the brain. Psychological review, 65(6):386, 1958.

Furbish, D.J. (2003). Using the dynamically coupled behaviour of land-surface geometry and soil thickness in developing and testing hillslope evolution models. In: Predictions in Geomorphology (Ed. P.R. Wilcock and R.M. Iverson), pp. 169–181. Monograph 135, American Geophysical Union, Washington, DC.

Garcia, 2000, Sedimentation Engineering, ASCE Manual.

Ghosh, S., & Dutta, S. (2012). Impact of climate change on flood characteristics in Brahmaputra basin using a macro-scale distributed hydrological model. Journal of Earth System Science, 121(3), 637-657.

Gomez, B. and Church, M. (1989). "An assessment of bed load sediment transport formulae for gravel bed rivers." Water Resources Research, 25, 1161–1186.

Hassan, A., Martin, T.C., Mosselman, E., 1999. Island Topography Mapping for the BrahmaputraeJamuna River Using Remote Sensing and GIS. In: Geological Society, London, Special Publications, vol. 163, 153e161 pp.

Hossain, M.A., Gan, T.Y., Baki, A.B.M., 2013. Assessing morphological changes of Ganges River using satellite images. Quaternary International 304, 142-155.

Howard, A., S.R. Raine, and G. Titmarsh, (1998). The contribution of stream bank erosion to sediment loads in Gowrie Creek, Toowoomba. ASSI National Soils Conference, Brisbane, volume 2004, pp.491-493.

I. Goodfellow, Y. Bengio, and A. Courville, Deep Learning. MIT Press, 2016, http://www.deeplearningbook.org.

I. Sutskever, O. Vinyals, and Q. V. Le, "Sequence to sequence learning with neural networks," in Advances in Neural Information Processing Systems, pp. 3104–3112, 2014.

Islam, M.R., Begum, S.F., Yamaguchi, Y., Ogawa, K., 1999. The Ganges and Brahmaputra Rivers in Bangladesh: basin denudation and sedimentation. Hydrological Processes 13, 2907e2923.

ISPAN, 1993. The Dynamic Physical and Human Environment of the Riverine Charlands: BrahmaputraeJamuna, Geographic Information System. Prepared for the Flood Plan Coordination Organization (FPCO), Dhaka, Bangladesh.

References

J. Chen, L. Yang, Y. Zhang, M. Alber, and D. Z. Chen, "Combining fully convolutional and recurrent neural networks for 3d biomedical image segmentation," Advances in Neural Information Processing Systems, pp. 3036–3044, 2016.

J. Chorowski, D. Bahdanau, D. Serdyuk, K. Cho, and Y. Bengio, "Attention-based models for speech recognition," in Advances in Neural Information Processing Systems, pp. 577–585, 2015.

J. Hagerty, D. (1991). Piping/Sapping Erosion. I: Basic Considerations. Journal of Hydraulic Engineering-asce - J HYDRAUL ENG-ASCE. 117. 10.1061/(ASCE)0733-9429(1991)117:8(991).

Jagers B.(2003). "Modeling Planform Changes of Braided Rivers", Ph.D.thesis, Delft University.

Jagers, H.R.A. (2003). Modelling planform changes of braided rivers, PhD thesis, University of Twente, The Netherlands, 313pp.

Jerey L Elman. Finding structure in time. Cognitive science, 14(2):179-211, 1990.

Jerey L Elman. Finding structure in time. Cognitive science, 14(2):179-211, 1990.

Jianpeng Cheng, Li Dong, and Mirella Lapata. Long short-term memory-networks for machine reading. arXiv preprint arXiv:1601.06733, 2016.

Junyoung Chung, Caglar Gulcehre, KyungHyun Cho, and Yoshua Bengio. Empirical evaluation of gated recurrent neural networks on sequence modeling. arXiv preprint arXiv:1412.3555, 2014.

Jurgen Schmidhuber. Deep learning in neural networks: An overview. Neural networks, 61:85-117, 2015.

K. Cho, B. van Merrienboer, C. Gulcehre, D. Bahdanau, F. Bougares, H. Schwenk, and Y. Bengio, "Learning phrase representations using rnn encoder-decoder for statistical machine translation," in Proceedings of the 2014 Conference on Empirical Methods in Natural Language Processing (EMNLP), pp. 1724–1734, 2014.

Kai Sheng Tai, Richard Socher, and Christopher D Manning. Improved semantic representations from tree-structured long short-term memory networks. arXiv preprint arXiv:1503.00075, 2015.

Karmaker, Tapas & Dutta, Subashisa. (2013). Modeling seepage erosion and bank retreat in a composite river bank. Journal of Hydrology. 476. 178–187. 10.1016/j.jhydrol.2012.10.032.

Karmaker, Tapas & Ramprasad, Y & Dutta, Subashisa. (2010). Sediment transport in an active erodible bend of Brahmaputra river. Shadhana. 35. 693-706. 10.1007/s12046-010-0052-7.

Kennedy, J. F. (1963). "The mechanics of dunes and antidunes in erodible- bed channels." Journal of Fluids Mechanics, 16, 521–544.

Kennedy, J. F. and Odgaard, A. J. (1991). "Informal monograph on riverine sand dunes." Contract Report CERC-91-2, Coastal Engineering Research Center, US Army Waterways Experiment Station, Vicksburg, Mississippi.

Kenneth R Foster, Robert Koprowski, and Joseph D Skufca. Machine learning, medical diagnosis, and biomedical engineering research-commentary. Biomedical engineering online, 13(1):94, 2014.

Kevin Gurney. An introduction to neural networks. CRC press, 2014.

Khan, M., and Ali, M. M., 2016, An approach to predict the yearly bank erosion rates of Jamuna river: An application of the correlation of bank shear stress and river discharge, International Journal of Engineering Development and Research, Vol. 4 (2) , pp. 1180-1185

Khan., 2014. "A study on River Bank Erosion of Jamuna River using GIS and Remote Sensing Technology." Volume-II, M. Sc. Thesis. Department of Water resources Engineering, BUET.

Klaassen, G.J. and Masselink, G. (1992) Planform Changes of a Braided River with Fine Sand as Bed and Bank Material.

Knighton, A.D. (1998), Fluvial Forms and Processes: A New Perspective. Arnold, London, UK. 383 pp.

Konstantina Kourou, Themis P Exarchos, Konstantinos P Exarchos, Michalis V Karamouzis, and Dimitrios I Fotiadis. Machine learning applications in cancer prognosis and prediction. Computational and structural biotechnology journal, 13:8{17, 2015.

Kotsiantis, S.B. (2007). Supervised Machine Learning: A Review of Classification Techniques. Informatica 31:249-268.

Kronvang, B., R. Grant and A.L. Laubel, (1997). Sediment and phosphorus export from a lowland catchment: Quantification of sources. Water Air and Soil Pollution, 99 (1-4), 465-476.

Kummu, M., Lu, X.X., Rasphone, A., Sarkkula, J., Koponen, J., 2008. Riverbank changes along the Mekong River: remote sensing detection in the Vientiane- Nog Khai area. Quaternary International 186, 100e112.

Lee, H-Y., Chen, Y-H., You, J-Y., and Lin, Y-T. (2000). "Investigations of continuous bed load saltating process." Journal of Hydraulic Engineering, ASCE, 126, 691–700.

M.A. Kon, L. Plaskota. Information complexity of neural networks. Neural Networks, 13 (2000), pp. 365-376.

Maryam M Najafabadi, Flavio Villanustre, Taghi M Khoshgoftaar, Naeem Seliya, Randall Wald, and Edin Muharemagic. Deep learning applications and challenges in big data analytics. Journal of Big Data, 2(1):1, 2015.

McLelland, S.J., Ashworth, P.J., Best, J.L., Roden, J.E. and Klaassen, G.J. (1999) Flow structure and transport of sandgrade suspended sediment around an evolving braid-bar, Jamuna River, Bangladesh.

Meyer-Peter, E., and Muller, R. (1948). "Formulas for Bedload Transport." Proceedings of the 2nd Congress, IAHR, Stockholm, 39–64.

Mirza, Monirul & A. Warrick, R & J. Ericksen, N. (2003). The Implications of Climate Change on Floods of the Ganges, Brahmaputra and Meghna Rivers in Bangladesh. Climatic Change. 57. 287-318. 10.1023/A:1022825915791.

Mitchell, T. (1997). Machine Learning. McGraw Hill.

Mosselman, Erik. (1995). A review of mathematical models of river planform changes. Earth Surface Processes and Landforms. 20. 661 - 670. 10.1002/esp.3290200708.

Murray, A. B., & Paola, C. (1997). Properties of a cellular braided-stream model. Earth Surface Processes and Landforms, 22(11), 1001-1025.

N. Srivastava, E. Mansimov, and R. Salakhutdinov, "Unsupervised learning of video representations using lstms," in International Conference on Machine Learning, pp. 843–852, 2015.

Nagata, N & Hosoda, T & Muramoto, Y. (2000). Numerical Analysis of River Channel Processes with Bank Erosion. Journal of Hydraulic Engineering. 126. 10.1061/(ASCE)0733-9429(2000)126:4(243).

Nemeth, A. A., Hulscher, S.J.M.H. and de Vriend, H. J. (2002). "Modelling sand wave migration in shallow shelf seas," Continental Shelf Research, 22 (18-19), 2795–2806.

Nicholas, A. P., Ashworth, P. J., Sambrook Smith, G. H., & Sandbach, S. D. (2013). Numerical simulation of bar and island morphodynamics in anabranching megarivers. Journal of Geophysical Research: Earth Surface, 118(4), 2019-2044.

P. Domingos, "A Few Useful Things to Know about Machine Learning," Communications of the ACM, vol. 55, no. 10, pp. 78–87, 2012.

Paul J Werbos. Backpropagation through time: what it does and how to do it. Proceedings of the IEEE, 78(10):1550{1560, 1990.

R. Bekkerman, M. Bilenko, J. Langford, Scaling Up Machine Learning, Cambridge University Press, January 2012.

Rahman, M.R., 2010. Impact of riverbank erosion hazard in the Jamuna floodplain areas in Bangladesh. Journal of Science Foundation, 8(1-2), pp.55-65.

Randall C. O'Reilly, Yuko Munakata, Michael J. Frank, Thomas E. Hazy, and Contributors. Computational Cognitive Neuroscience. Wiki Book, 1st Edition, URL: http://ccnbook.colorado.edu, 2012. 2-2.

Ranga Raju, K. G. and Soni, J. P. (1976). "Geometry of ripples and dunes in alluvial channels." Journal of Hydraulic Research, IAHR, 14, 77–100.

Razvan Pascanu, Tomas Mikolov, and Yoshua Bengio. On the difficulty of training recurrent neural networks. In International Conference on Machine Learning, pages 1310-1318, 2013.

Razvan Pascanu, Tomas Mikolov, and Yoshua Bengio. Understanding the exploding gradient problem. CoRR, abs/1211.5063, 2012

Rhoads, B. L. and Welford, M. R. (1991). "Initiation of River Meandering." Progress in Physical Geography, 15, 127–156.

Ronald J Williams and David Zipser. A learning algorithm for continually running fully recurrent neural networks. Neural computation, 1(2):270{280, 1989.

References

S. Hochreiter and J. Urgen Schmidhuber, "Long short-term memory," Neural Computation, vol. 9, no. 8, pp. 1735–1780, 1997.

S. Hong, S. Kim, M. Joh, and S.-k. Song, "Globenet: Convolutional neural networks for typhoon eye tracking from remote sensing imagery," Proceedings of the 7th International Workshop on Climate Informatics: CI 2017., Aug. 2017.

S. K. Kim, S. Ames, J. Lee, C. Zhang, A. Wilson C., and D. Williams, "Massive Scale Deep Learning for Detecting Extreme Climate Events," in Proceedings of the 7th International Workshop on Climate Informatics: CI 2017., 2017.

S. Ruder, "An Overview of Gradient Descent Optimization Algorithms," arXiv preprint arXiv:1609.04747, 2016.

Sarker, M.H., 2009. Morphological Response of the Brahmaputra–Jamuna–Padma–Lower Meghna River to the AssamEarthquake of 1950. PhD thesis University of Nottingham, UK (297 pp.).

Sarker, M.H., Huque, I., Alam, M., 2003. Rivers, chars and char dwellers of Bangladesh. International Journal of River Basin Management 1 (1), 61e80.

Sarker, M.H., Thorne, C.R., 2013. Morphological responses to passage of a sediment wave through the Jamuna–Padma–Lower Meghna River system. Earth Surface Processes and Landforms

Sarker, M.H.; Thorne, C.R.; Aktar, M.N.; and Ferdous, M.R., 2014. Morpho-dynamics of the Brahmaputra–Jamuna River, Bangladesh. Geomorphology 215:45–59. DOI: 10.1016/j.geomorph.2013.07.025.

Schuurman, F., Marra, W. A., & Kleinhans, M. G. (2013). Physics based modeling of large braided sandbed rivers: Bar pattern formation, dynamics, and sensitivity. Journal of Geophysical Research: Earth Surface, 118(4), 2509-2527.

Sepp Hochreiter and Jurgen Schmidhuber. Long short-term memory. Neural computation, 9(8):1735-1780, 1997.

Serra, S. G., and Vionnet, C. A. (2006). "Migration of large dunes during extreme floods of the Parana River, Argentina." River, coastal and estuarine morphodynamics: RCEM 2005, G. Parker and M. H. García, eds., Taylor & Francis/Balkema, Leiden, The Netherlands, 897–901.

Shampa, and Ali, M. M., 2018, Interaction between the braided bar and adjacent channel during flood: a case study of a sand-bed braided river, Brahmaputra-Jamuna, Journal of Sustainable Water Resources Management,

Shimizu, Y., and Itakura, T. (1989). ''Calculation of bed variation in alluvial channels.'' J. Hydr. Engrg., ASCE, 115(3), 367–384.

Siddique, Q.I., 2008. Impact of Climate Change on Water Related Disasters and Water Resources Management in Bangladesh, Presentation Delivered at Stockholm, World Water Week on 21 August, 2008.

Simon, A., M. Rinaldi, and G. Hadish, (1996). Channel evolution in the loess area of the Midwestern United States. Sixth Federal Interagency Sedimentation Conference, Las Vegas, pp III-86 to III-93.

Soulsby, R. L. (1997). Dynamics of marine sands, Thomas Telford, London, 249 pp.

Southard, J. B. (1989). "Synthesis of data on bed configurations in alluvial channels, and the effect of water temperature and suspended-load concentration." Taming the Yellow River: Silt and Floods." Proceedings of a Bilateral Seminar on problems in the Lower Reaches of the Yellow River, L. M. Brush, M. G. Wolman, and H. Bing-Wei, eds., Kluwer Academic Publishers, Boston, Mass.

Subhashini Venugopalan, Marcus Rohrbach, Jeff Donahue, Raymond Mooney, Trevor Darrell, and Kate Saenko. Sequence to sequence-video to text. Technical report, University of Texas at Austin Austin United States, 2015.

Takagi, T., Oguchi, T., Matsumoto, J., Grossman, M.J., Sarker, M.H. and Matin, M.A. (2007) Channel braiding and stability of the Brahmaputra River, Bangladesh, since 1967: GIS and remote sensing analyses, Geomorphology, 85, 294–305.

Takagi, T., Oguchi, T., Matsumoto, J., Grossman, M.J., Sarker, M.H., Matin, M.A., 2007. Channel braiding and stability of the Brahmaputra River, Bangladesh, since 1967: GIS and remote sensing analyses. Geomorphology 85, 294e305.

Thorne, C.R., Russell, A.P.G., 1993. Geomorphic study of bankline movement of the Brahmaputra River in Bangladesh. Proc. 5th Annual Seminar of Scottish Hydraulics Study Group on Sediment transport processes and phenomena, Edinburgh

Thorne, C.R., Russell, A.P.G., Alam, M.K. (1993) Planform pattern and channel evolution of the Brahmaputra River, Bangladesh. In: Braided Rivers (Eds Best, J.L. and Bristow, C.S.), Special Publication of the Geological Society of London, No. 75, 257–276.

Tim Rocktaschel, Edward Grefenstette, Karl Moritz Hermann, Tomas Kocisky, and Phil Blunsom. Reasoning about entailment with neural attention. arXiv preprint arXiv:1509.06664, 2015.

Tomas Mikolov, Martin Karafiat, Lukas Burget, Jan Cernocky, and Sanjeev Khudanpur. Recurrent neural network based language model. In Eleventh Annual Conference of the International Speech Communication Association, 2010.

V. Patraucean, A. Handa, and R. Cipolla, "Spatio-temporal video autoencoder with differentiable memory," arXiv preprint arXiv:1511.06309, 2015.

Valdiya, K. S. (1998). Dynamic Himalaya, Universities Press, Hyderabad, India.

Valliappa Lakshmanan, Eric Gilleland, Amy McGovern, and Martin Tingley. Machine learning and data mining approaches to climate science. In Proceedings of the 4th International Workshop on Climate Informatics. Springer, 2015.

Vanoni, V. A., ed. (1975). Sedimentation engineering. Manual 54, American Society of Civil Engineers, New York, 745 p.

Vionnet, C. A., Marti, C., Amsler, M. L., and Rodriguez, L. (1998). "The use of relative celerities of bedforms to compute sediment transport in the Paraná River" Modelling Soil Erosion, Sediment Transport and Closely Related Hydrological Processes, International Association of Hydrological Sciences Special Publication 249, 399–406.

Walling, D.E., P.N. Owens, and G.J.L. Leeks, (1999). Fingerprinting suspended sediment sources in the catchment of the River Ouse, Yorkshire, UK. Hydrol. Proc., 13(7), 955-975.

Wan, Z. and Z. Wang (1994). Hyperconcentrated Flow, Balkema, Rotterdam 290 pp.

Wang, J.J., Lu, X.X., 2010. Estimation of suspended sediment concentrations using Terra MODIS: an example from the Lower Yangtze River, China. Science of the Total Environment 408, 1131e1138

Watson, A.J. and L.R. Basher, (2006). Stream bank erosion: a review of processes of bank failure, measurement and assessment techniques, and modeling approaches, Landcare ICM Report No. 2005-2006/01, Landcare Research, Lincoln, Private Bag 6, Nelson, NEW ZEALAND.

Watson, A.J. and L.R. Basher, (2006). Stream bank erosion: a review of processes of bank failure, measurement and assessment techniques, and modeling approaches, Landcare ICM Report No. 2005-2006/01, Landcare Research, Lincoln, Private Bag 6, Nelson, NEW ZEALAND.

Wiberg, P. L., and Smith, D. (1991). "Velocity distribution and bed roughness in high gradient streams." Water Resources Research, 27, 825–838.

Wilkin, D.C. and S.J. Hebel, (1982). Erosion, redeposition, and delivery of sediment to Midwestern streams. Water Resour. Res. 18(4), 1278-1282.

X.-J. Mao, C. Shen, and Y.-B. Yang, "Image restoration using very deep convolutional encoderdecoder networks with symmetric skip connections," in Advances in Neural Information Processing Systems, 2016.

Yalin, M. S. (1964). "Geometrical properties of sand waves," Journal of the Hydraulics Division, ASCE, 90, 105–119.

Yan Xu, Lili Mou, Ge Li, Yunchuan Chen, Hao Peng, and Zhi Jin. Classifying relations via long short term memory networks along shortest dependency paths. In Proceedings of the 2015 Conference on Empirical Methods in Natural Language Processing, pages 1785-1794, 2015b.

Yann LeCun, Yoshua Bengio, and Georey Hinton. Deep learning. Nature, 521(7553):436, 2015.

Yann LeCun, Yoshua Bengio, et al. Convolutional networks for images, speech, and time series. The handbook of brain theory and neural networks, 3361(10):1995, 1995.

Zhiheng Huang, Wei Xu, and Kai Yu. Bidirectional lstm-crf models for sequence tagging. arXiv preprint arXiv:1508.01991, 2015.

Appendix

Appendix A-1: Research Proposal to DWRE, BUET from WARPO.

Figure A-1 Research Proposal to DWRE, BUET

Appendix A-2:

The Water level, discharge and cross section station, Id and name of the stations are tabulated below.

Table A-1 Water Level and Discharge Measuring Stations on the study area

Serial	Station ID	Type	River Name	Station Name
1	SW46.9L	Non Tidal WL	Brahmaputra-Jamuna	Bahadurabad (Tr)
2	SW90	Non Tidal WL	Ganges	Hardinge Bridge
3	SW91.9L	Non Tidal WL	Ganges	Baruria Transit
4	SW49	Non Tidal WL	Brahmaputra-Jamuna	Sirajganj
5	SW91	Non Tidal WL	Ganges	Talbaria
6	SW49A	Non Tidal WL	Brahmaputra-Jamuna	Kazipur
7	SW91.2	Non Tidal WL	Ganges	Mohendrapur
8	SW46.9R	Non Tidal WL	Brahmaputra-Jamuna	Fulchari (Tr)
9	SW15J	Non Tidal WL	Brahmaputra-Jamuna	Mathurpara (Milanpur)
10	SW50.6	Non Tidal WL	Brahmaputra-Jamuna	Aricha
11	SW50.3	Non Tidal WL	Brahmaputra-Jamuna	Mathura
12	SW91.1	Non Tidal WL	Ganges	Sengram
13	SW93.5L	Tidal WL	Ganges	Mawa
14	SW46.9L	Non-Tidal Q	Brahmaputra-Jamuna	Bahadurabad (Tr)
15	SW90	Non Tidal Q	Ganges	Hardinge Bridge
16	SW91.9L	Non Tidal Q	Ganges	Baruria Transit
17	SW4A	Tidal Q	Arial Khan	Chowdhury Char
18	SW93.5L	Tidal Q	Ganges	Mawa

Table A-2 Cross-section Measuring stations on the study area

Serial No	Station ID	River Name
1	P2	Padma
2	P2.1	Padma
3	P3	Padma
4	P3.1	Padma
5	P4	Padma
6	P4.1	Padma
7	P5	Padma
8	P5.1	Padma
9	P6	Padma
10	P6.1	Padma
11	P7	Padma
12	G1	Ganges
13	G1.1	Ganges
14	G2	Ganges
15	G3	Ganges
18	G5	Ganges
19	G6	Ganges
20	G7	Ganges
21	G8	Ganges
22	G9	Ganges
23	G10	Ganges
24	G11	Ganges
25	G12	Ganges
26	G13	Ganges
27	G12.1	Ganges
28	G4	Ganges
30	J6.1	Brahmaputra- Jamuna
31	J6	Brahmaputra- Jamuna
32	J5.1	Brahmaputra- Jamuna
33	J5	Brahmaputra- Jamuna
34	J4.1	Brahmaputra- Jamuna
35	J4	Brahmaputra- Jamuna

36	J3.1	Brahmaputra- Jamuna
37	J3	Brahmaputra- Jamuna
38	J2.1	Brahmaputra- Jamuna
39	J1.1	Brahmaputra- Jamuna
40	J1	Brahmaputra- Jamuna
41	J2	Brahmaputra- Jamuna
42	J7	Brahmaputra- Jamuna
43	J7.1	Brahmaputra- Jamuna
44	J8	Brahmaputra- Jamuna
45	J8.1	Brahmaputra- Jamuna
46	J9	Brahmaputra- Jamuna
47	J9.1	Brahmaputra- Jamuna
48	J10	Brahmaputra- Jamuna
49	J10.1	Brahmaputra- Jamuna
50	J11	Brahmaputra- Jamuna
51	J11.1	Brahmaputra- Jamuna
52	J12	Brahmaputra- Jamuna
53	J13	Brahmaputra- Jamuna
60	J13.1	Brahmaputra- Jamuna
61	J14	Brahmaputra- Jamuna

Appendix A-3:

Terms of References (ToR) for

"Research on River Bank Erosion Dynamics using Numerical Modeling and Deep Learning Techniques"

Water Resources Planning Organization (WARPO), Ministry of Water Resources, Government of Bangladesh and Bureau of Research, Testing and Consultation (BRTC) represented by the Department of Water Resources Engineering (DWRE), Bangladesh University of Engineering and Technology (BUET), BUET join in the following agreement in order to conduct the above mentioned collaborative research project:

1. To collect all necessary secondary data including satellite images, historical hydrological data and bathymetric data from different sources
2. To conduct hydrographic survey in a selected region of the study area to obtain high resolution bathymetry data
3. To analyze the historical trend of river bank erosion in the selected study area using satellite images
4. To apply deep learning techniques to predict bank erosion rate for the selected study area
5. To analyze measured bathymetric data of different years to understand the morphological characteristics of the selected study area
6. To develop a 2D hydrodynamic model to understand the flow hydraulics in the selected study area
7. To develop a 2D morphological model to understand the general morphodynamics and bank erosion processes for the selected study area
8. To develop a tool to predict riverbank erosion for the selected study area combining deep learning and numerical model results
9. To arrange workshops to disseminate research progress and findings
10. To provide technical support to WARPO professionals on river bank erosion process, modeling and prediction
11. The basic methodology and approach of the 1.5-year collaborative research project is given in Annexure-I;
12. WARPO will supply necessary data free of cost from the NWRD for the development and implementation of the model. The data will be used only for this project.
13. DWRE will install the tools at WARPO and provide training to the WARPO personnel.
14. The Principal Investigator of the project from DWRE (as mentioned in Annexure-I) and the designated Research Coordinator from WARPO will be responsible for planning the project activities.
15. Outcome of this collaborative project will be published jointly by DWRE and WARPO in the conferences and peer reviewed journals.
16. DWRE and WARPO will be the owner of the model software to be developed (if any) under this project; future improvements and modifications of the model may be made

by DWRE and WARPO, if necessary. If any party modifies the model, it will be transferred along with source code to the other party free of cost.

17. The cost of this research project including tax is 84.28 lac Taka and the amount of VAT is 10.42 lac Taka. Therefore, total cost of the project is 94.70 lac Taka. The breakdown of this cost estimate is provided in Annexure-I.

18. Director, BRTC, BUET will submit bill(s) to WARPO for the installment payment according to the schedule described in Annexure-I. All payments for the services shall have to be made through account payee cheques drawn in favor of Director, BRTC, BUET. If VAT and Tax are deducted at source, the copies of challans of deposited VAT & Tax shall have to be submitted to BRTC office along with the payment.

19. The duration of this research project is 18 (Eighteen) months starting from the date of signing the contract. However, the project duration can be extended, if necessary, upon agreement between two parties.

20. Reporting and activities will be carried out as per the work plan shown in Annexure-I.

This agreement is signed on 27th January, 2019.

-------------------------------------   --

Md. Mahmudul Hasan   Professor Dr. Md. Shamsul Hoque

Director General   Director

Water Resources Planning Organization   Bureau of Research, Testing and Consultation

Ministry of Water Resources   Bangladesh University of Engineering and Technology (BUET), Dhaka, Bangladesh

72 Green Road, Dhaka-1215, Bangladesh

Witness:

------------------------------   -------------------------------------
Kazi Saidur Rahman
Senior Scientific Officer   Dr. Md. Mostafa Ali
Water Resources Planning Organization
                                                          Professor and Head
Ministry of Water Resources
                                                          Department of Water Resources Engineering
72 Green Road, Dhaka-1215, Bangladesh
                                                          Bangladesh University of Engineering and Technology (BUET), Dhaka, Bangladesh

Appendix A-4 : Submission letter of the River Bank Erosion Prediction Tool

DEPARTMENT OF WATER RESOURCES ENGINEERING
Bangladesh University of Engineering and
Technology, Dhaka – 1000, Bangladesh

Head of the Department
Professor Dr. Anika Yunus

পানিসম্পদ কৌশল বিভাগ
বাংলাদেশ প্রকৌশল বিশ্ববিদ্যালয়, ঢাকা-১০০০
Tel: Direct (880 2) 9665631
PABX: (880 2) 55167100, 55167228-57 / Ext. 7290
Fax: (880 2) 9665631
E-mail: headwre@wre.buet.ac.bd

Memo No. WRE-129/BRTC/WARPO/2021 (02)   Date: 13.02.2021

To
Mr. Md. Delwar Hossain
Director General
Water Resources Planning Organization
Ministry of Water Resources
WARPO Bhaban 72 Green Road, Dhaka-1215

Subject: Submission of the River Bank Erosion Prediction Tool

Reference No: 42.02.0000.004.14.002.19.5 Dated: 24-01-2019

Project: Research on River Bank Erosion Dynamics using Numerical Modeling and
Deep Learning Techniques.

Dear Mr. Hossain,

We have the pleasure to submit herewith one soft copy (attached USB pen drive) of the
installer of the River Bank Erosion Prediction Tool of Jamuna river for the above-
mentioned project for your kind perusal. We are pleased with the opportunity to work
with WARPO.

Thanking you for the cooperation.

 Yours sincerely,

Dr. Anika Yunus
Professor and Head
Dept. of Water Resources Engineering
BUET, Dhaka.

Copy to: Director, BRTC, BUET, Dhaka

Minutes of the Final Workshop of "Research on River Bank Erosion Dynamics Using Numerical Modeling and Deep Learning Techniques"

Chief Guest: Kabir Bin Anwar, Senior Secretary, Ministry of Water Resources
Chairperson: Md. Delwar Hossain, Director General (Additional Secretary), WARPO
Date: 19 May, 2021 (10:30 am)
Venue: WARPO Conference Room, WARPO, Dhaka

The Chairperson of the Workshop **Mr. Md. Delwar Hossain,** Director General (Additional Secretary), WARPO inaugurated the program with welcoming the esteemed guests and participants of the Workshop. He gave a brief overview of the research activities at the outset and thanked the research team for this event. He added that the findings and methodology from this research on the Jamuna River could be used in other major rivers of Bangladesh in future. The welcome address was given by **Mr. Kazi Saidur Rahman,** Senior Scientific Officer, WARPO and Research Coordinator for this research program. According to him, once the floods were a catastrophe for Bangladesh, but with technical advancement and non-structural measures such as flood forecasting as well as early warning system, improved flood management has been achieved. But no such advanced techniques were applied to fight against river bank erosion. That is why, WARPO and BUET initiated this research using Deep Learning Techniques to predict the river bank erosion rate in the 80 km reach of the Jamuna River.

Dr. Mostafal Ali, Professor, Department of Water Resources, BUET and Principal Investigator of the Research Team gave a power-point presentation and presented the main finding of the research. He briefly showed how river bank erosion prediction has been made using the historical satellite images as well as applying deep learning techniques. He also briefly demonstrated the riverbank prediction tool which was developed during this research, and suggested that such prediction tools can also be customized for other major rivers to predict bank erosion. After the presentation, the Chairperson opened the floor for discussion.

Mr. Abu Saleh Khan, Executive Director, IWM thanked the research team for carrying out such kind of application-based research. He said that river bank erosion prediction with deep learning techniques will not be easier with numerous interventions in the river. He also mentioned that the submerged islands play an important role in riverbank erosion and the satellite images have no information about these islands. Therefore, he suggested to make the prediction tool more purposive to deal with such continuous interventions and submerged islands. **Dr. Shamal Chandra Das,** Superintending Engineer, BWDB also suggested to incorporated the localized effects such as submerged islands, bridge piers and channel bifurcation into the prediction tool. However, he expressed that the developed prediction tool seems more comprehensive to him, and being BWDB is the direct user of this tool, he suggested to take steps for capacity building at the institutional level.

Dr. Tanvir Ahmed, Professor, Department of Civil Engineering, BUET said that the prediction tool performed satisfactorily as the 80% of the erosion locations were identified by using this tool. However, he recommended to evaluate the difference in the results between the traditional method used by CEGIS and the application of deep learning techniques. He also suggested that the prediction tool developed as part of this research activity should now be used as institutional application by relevant organizations like BWDB. **Mr. Adil Mohammad Khan**, Associate Professor, Jahangirnagar University said that the findings of this excellent research will be extremely helpful for the planning of riverine areas in Bangladesh.

Mr. Md. Afzal Hossain, Director General (Sector 6), IMED thanked the presenter for explaining such critical technical issues easily understandable even for non-technical person. He wanted to know whether there was any opportunity to do river bed level analysis using satellite images in this research. **Mr. Ehtasham Reza**, Deputy Secretary, MoWR asked whether the soil structure data was used in this river bank erosion prediction process; as it can be seen that island with dense vegetative cover are less prone to erosion than that of island with less vegetative cover. **Mr. S M Sadik Tanveer**, Senior Assistant Secretary, MoWR suggested to improve the efficiency of the prediction tool with careful choice of calibration and validation parameters so that a much larger error in the model could be reduced. **Ms. Azizun Nahar**, Deputy Secretary, ERD recommended to address the correlation between the extent of bank erosion and displacement in future. She also discussed the importance of such collaborative and impactful research between universities and government agencies.

Dr. Mominul Haque Sarker, Senior Adviser, CEGIS said that he has been working on the bank erosion of the Jamuna River for more than 18 years, and he believed that the results of the prediction tool would improve with time and more collaboration with other agencies. **Mr. Sudipta Hore**, Associate Specialist, CEGIS suggested to evaluate the performance of the prediction tool in the reach upstream of Bangabandhu Bridge where the course of the Jamuna River is more changeable and variable. **Ms. Sarwat Jahan**, Principal Specialist, IWM said that deep learning and artificial intelligence are going to be the tools of the future and thanked the research team for using this tool for such a sophisticated issue like river bank erosion.

Finally **Mr. Kabir Bin Anwar**, Senior Secretary, MoWR and the Chief Guest of this program thanked the research team and said that the use of technology can bring benefits of people's lives and the works become much easier by using updated information along with IT. He said that there were already many consultations on the river Jamuna and it is possible to carry out development work by taking new recommendations from this research. He further said that we need to implement Bangladesh Delta Plan 2100 by preventing river bank erosion through holistic approach, so that not only the water-induced problem would be eliminated, but also agricultural sector, fisheries, shipping and navigation sector would benefit. He recommended to use this approach applying deep learning techniques in the estuary region of Bangladesh. He also suggested

A-9

to take necessary steps to protect the eastern bank of the Jamuna River which is constantly eroding, and create and economic corridor by keeping the floodplain in order. Finally, he suggested BWDB Hydrology and Design division to work together with WARPO, BUET, IWM and CEGIS as a team to fight against the threat of river bank erosion in Bangladesh.

In his concluding remarks, the Chairperson of the Workshop said that WARPO will continue to upgrade the erosion prediction tool time to time, and would implement this approach to other major rivers where river bank erosion problems are severe. He thanked all the participants of the Workshop and drew conclusion to the session.

The following decisions are taken in the Workshop:

i)   Similar research need to be carried out for the estuary region of Bangladesh to combat river bank erosion.
ii)   The developed erosion prediction tool needs to be improved and customized for other major rivers by conducting more similar kinds of research.
iii) WARPO should initiate institutionalization of the erosion prediction tool through capacity development programs with the relevant stakeholders.

(Md. Delwar Hossain)
Director General (Additional Secretary)
WARPO

Appendix A-5:

Field visit:01

Figure A-2: Meeting with BWDB, Manikganj officials

Figure A-3 Discussion with Executive Engineer, BWDB

Figure A-4 Co-Discussion with Local People

Figure A-5 Bank Erosion in Bachamara, Daulatpur, Manikganj.

Figure A-6 Bank erosion at Bachamara, Dauatpur, Manikganj.

Figure A-7 Eroded Bank with bamboo tree

Figure A-8 Crack near the bank

Appendix A-6:

Field visit 02

Figure A-1:Field visit Team on the way to Baghutia.

Figure A-2 River bank protection work

Figure A-3 : River bank protection work-2

Figure A-4: River bank of Jamuna